RL-TR-91-422
Final Technical Report
December 1991

EFFECT OF NONLINEARITY ON RECEIVER SIGNAL TO DISTURBANCE RATIO IN HIGH SUBCLUTTER VISIBILITY

Syracuse University

Donald D. Weiner and Mohamed Adel Slamani

APPROVED FOR PUBLIC RELEASE; DISTRIBUTION UNLIMITED.

Rome Laboratory
Air Force Systems Command
Griffiss Air Force Base, NY 13441-5700

This report has been reviewed by the Rome Laboratory Public Affairs Office (PA) and is releasable to the National Technical Information Service (NTIS). At NTIS it will be releasable to the general public, including foreign nations.

RL-TR-91-422 has been reviewed and is approved for publication.

APPROVED: Vincent C. Vannicola

VINCENT C. VANNICOLA
Project Engineer

FOR THE COMMANDER:

JAMES W. YOUNGBERG, Lt Col, USAF
Deputy Director
Surveillance & Photonics Directorate

If your address has changed or if you wish to be removed from the Rome Laboratory mailing list, or if the addressee is no longer employed by your organization, please notify RL(OCTS) Griffiss AFB, NY 13441-5700. This will assist us in maintaining a current mailing list.

Do not return copies of this report unless contractual obligations or notices on a specific document require that it be returned.

REPORT DOCUMENTATION PAGE

Form Approved
OMB No. 0704-0188

1. AGENCY USE ONLY (Leave Blank)	2. REPORT DATE	3. REPORT TYPE AND DATES COVERED
	December 1991	Final Sep 90 - Jun 91

4. TITLE AND SUBTITLE
EFFECT OF NONLINEARITY ON RECEIVER SIGNAL TO DISTURBANCE RATIO IN HIGH SUBCLUTTER VISIBILITY

5. FUNDING NUMBERS
C - F30602-88-D-0027,
Task A-9-1126
PE - 62702F
PR - 4506
TA - 11
WU - P4

6. AUTHOR(S)
Donald D. Weiner
Mohamed Adel Slamani*

7. PERFORMING ORGANIZATION NAME(S) AND ADDRESS(ES)
Syracuse University
111 Link Hall
Syracuse NY 13244-1240

8. PERFORMING ORGANIZATION REPORT NUMBER
N/A

9. SPONSORING/MONITORING AGENCY NAME(S) AND ADDRESS(ES)
Rome Laboratory (OCTS)
Griffiss AFB NY 13441-5700

10. SPONSORING/MONITORING AGENCY REPORT NUMBER
RL-TR-91-422

11. SUPPLEMENTARY NOTES
Rome Laboratory Project Engineer: Vincent C. Vannicola/OCTS/(315) 330-4437
*Submitted for the partial fulfillment of the requirements for the degree of Master of Science in Electrical Engineering in the Graduate school of Syracuse University

12a. DISTRIBUTION/AVAILABILITY STATEMENT
Approved for public release; distribution unlimited.

12b. DISTRIBUTION CODE

13. ABSTRACT (Maximum 200 words)
Analyses of radar performance usually proceed by assuming a linear receiver. In presence of strong signals, however, actual receivers are subject to saturation effects. This nonlinear behavior can cause a significant change in the statistics of the disturbance. The purpose of this work is to study the effects of the non-linearity of the radar receiver on the signal-to-disturbance ratio for the case of high subclutter visibility. The signal-to-disturbance ratio (SDR) is maximized using a transversal filter with adaptive weights. Three cases are considered in our research: Case I: The receiver is linear and the weights of the transversal filter are computed so as to maximize the SDR. This case serves as a baseline against which the others are compared. Case II: The receive is nonlinear. The weights of Case I are used for the transversal filter. Case III: The receiver is nonlinear and the weights of the transversal filter are computed so as to maximize the SDR taking into account the effect of the nonlinearity. For all three cases, studies are made to determine how the SDR is affected when the following parameters are varied: 1) shape of the nonlinearity, 2) Doppler frequency, 3) clutter correlation, 4) thermal noise level, 5) clutter power level, and 6) number of pulses.

14. SUBJECT TERMS	15. NUMBER OF PAGES
Sensor Fusion, Signal Processing, Algorithms	186
	16. PRICE CODE

17. SECURITY CLASSIFICATION OF REPORT	18. SECURITY CLASSIFICATION OF THIS PAGE	19. SECURITY CLASSIFICATION OF ABSTRACT	20. LIMITATION OF ABSTRACT
UNCLASSIFIED	UNCLASSIFIED	UNCLASSIFIED	UL

ACKNOWLEDGEMENT

I wish to express my very special appreciation to my advisor professor Donald D. Weiner for the guidance he provided during this research. His interest, advice, and effort were essential for the completion of this thesis.

I am extremely grateful to my entire family for the continuous support they have given me, for the values they have taught me and for the sacrifices they have made for the sake of my education. I dedicate this thesis to my mother, my father, my two brothers Ahmed and Mounir and my loving wife.

TABLE OF CONTENTS

LIST OF SYMBOLS

(In the Order Referenced in the Chapter Cited)

CHAPTER 1

LRT	likelihood ratio test
SDR	signal-to-disturbance ratio

CHAPTER 2

$r_k(t)$, k=1,2...,5	signal at node k of Fig. 2.1
L	saturation level of the nonlinear amplifier
G	linear gain of the RF amplifier
σ_g	standard deviation of Gaussian distribution function assumed for the nonlinearity
f_c	carrier frequency of the received signal
f_s	sampling frequency
T_s	sampling period
B_{RF}	bandwidth of the RF amplifier bandpass filter
$H_{RF}(f)$	transfer function of the RF amplifier bandpass filter
B_L	bandwidth of the lowpass filter
$H_L(f)$	transfer function of the lowpass filter
N	number of samples
$\tilde{w}_k$, k=1,2...,N	weights of the transversal filter

CHAPTER 3

E	amplitude of the emitted pulse
τ_e	width of the emitted pulse
e(t)	transmitted signal
f_D	Doppler frequency
V_r	radial velocity of target
$a_s(t)$	envelope of the received desired signal
θ_s	random phase of the received desired signal
$a_d(t)$	envelope of the received disturbance

θ_d	random phase of the received disturbance
s(t)	received signal
c(t)	received clutter
n(t)	received thermal noise
d(t)	received disturbance
Δr_2	terms in $r_2(t)$ corresponding to the spectral zones other than those centered at $\pm f_c$

CHAPTER 4

$R_k(\tau)$, k=1,2...,5	autocorrelation function ot the signal $r_k(t)$
$P_k(r_k)$, k=1,2	probability density function of the signal $r_k(t)$
σ_1^2	variance of $r_1(t)$
α	measure of the degree of nonlinearity
M(ju,jv)	joint characteristic function of two random variables
$\rho_1(\tau)$	correlation function

CHAPTER 5

$R_s(\tau)$	autocorrelation function of the signal s(t)
$R_c(\tau)$	autocorrelation function of the clutter c(t)
$R_n(\tau)$	autocorrelation function of the noise n(t)
A	random Rayleigh amplitude of the signal s(t)
σ_s^2	variance of the signal s(t)
σ_c^2	variance of the clutter c(t)
σ_w^2	variance of the Gaussian shaped clutter autocorrelation function envelope
σ_n^2	variance of the noise n(t)
$S_c(f)$	power spectral density of the clutter c(t)
$S_n(f)$	power spectral density of the noise n(t)
$\Delta R_2(\tau)$	terms in $R_2(\tau)$ corresponding to the spectral zones other than those centered at $\pm f_c$

CHAPTER 6

M	covariance matrix of the total signal at node 5 of Fig.2.1
M_s	covariance matrix of the desired signal at node 5 of Fig.2.1
M_d	covariance matrix of the disturbance at node 5 of Fig.2.1
$(SDR)_i$,i=I,II,III	SDR for case i
S	signal power

D	disturbance power
$\underline{a}$	signal vector defined by Eqs. (6.52) and (6.53)

CHAPTER 7

Ω	normalized frequency variable
$H_{TF}(f)$	transfer function of the transversal filter
ρ_c	clutter correlation coefficient
U_N	ratio of the smallest to the largest values of $\bar{R}_{cT}(kT_s)$
A_1	amplitude of the first sidelobe in the power spectral density of the truncated desired signal
r	ratio of A_1 to the amplitude of the mainlobe of the power spectral density of the truncated desired signal

CHAPTER 8

$(SNR)_{in}$	signal-to-noise ratio at receiver input
$(SCR)_{in}$	signal-to-clutter ratio at receiver input
$(NCR)_{in}$	noisel-to-clutter ratio at receiver input
$(SDR)_{in}$	signal-to-disturbance ratio at receiver input
$(PG)_i, i=I,II,III$	processing gain for case i relative to input
$(NLL)_i, i=I,II$	nonlinear loss for case i relative to case I
J	improvement factor for case III relative to case II

SUBSCRIPTS

s	signal
d	disturbance
c	clutter
n	noise
T	truncated
D	Doppler
in	receiver input
o	transversal filter output

SUPERSCRIPTS

*	complex conjuguate
T	transpose
H	Hermitian (complex conjugate transpose)
L	linear RF amplifier

NL nonlinear RF amplifier

OTHER

All vectors are denoted by an underline (e.g., $\underline{a}$)
All complex quantities are denoted by a tilde (e.g., $\tilde{w}_k$)

Chapter 1

INTRODUCTION

Assuming a Gaussian input signal, design of the optimum radar processor is well known. Specifically, consider a coherent train of N received pulses, with random initial phase and amplitude, embedded in clutter plus noise. Let the clutter plus noise be referred to as the disturbance process. For Gaussian inputs, it is known that the probability of detection is maximized for a constant false alarm probability by maximizing the signal-to-disturbance ratio (SDR) [1]. To maximize SDR, a transversal filter is placed before the likelihood ratio test (LRT) detector. The optimum transversal filter is completely described by a set of N complex weights whose values depend upon the disturbance statistics and the target signal model [2].

Analyses of radar performance usually proceed by assuming a linear receiver [3]. In the presence of strong signals, however, actual receivers are subject to saturation effects. This nonlinear behavior can cause a significant change in the statistics of the disturbance. The goal of this study is to determine the amount of degradation in the signal-to-disturbance ratio at the transversal filter output when a nonlinearity, whose input-output characteristic models the receiver saturation curve, is included within the RF amplifier.

Three different situations are investigated as indicated below:

Case I - The radar receiver is modeled as being linear and the weights of the transversal filter are chosen so as to maximize the SDR.

Case II - The radar receiver is modeled as being nonlinear. Even so, the weights of the transversal filter are set equal to those used in case I. This case can arise when the design engineer is either unaware of the nonlinearity or elects not to compensate for it.

Case III - The radar receiver is modeled as being nonlinear. However, now the weights of the transversal filter are selected to maximize the SDR taking into

account the receiver nonlinearity.

The amount of degradation in SDR caused by ignoring the nonlinearity is obtained by comparing cases I and II. Comparison of cases II and III reveals the improvement to be gained by accounting for the nonlinearity . Finally, the loss due to the nonlinearity even with the optimum transversal filter is evaluated by comparing cases I and III.

In chapter 2 the analytical model used to analyze the radar receiver is presented. Analytical expressions are derived in chapter 3 for the nonlinear responses at each point of the receiver model. The relations between autocorrelation functions at the various receiver stages are presented in chapter 4. The autocorrelation function at the transversal filter input is derived in chapter 5 for the Gaussian case where specific models are assumed for the target signal, clutter, and noise. Expressions for the signal-to-disturbance ratio at the transversal filter output are obtained in chapter 6 for cases I, II, and III. Up to this point, all of the analysis is carried out in the time domain. A frequency domain interpretation is given in chapter 7. Finally, computer generated results are presented in chapter 8.

Chapter 2

RECEIVER MODEL

The model used to analyse the receiver is illustrated in Fig. 2.1. Only the signal processing stages before the LRT detector are included in the figure. let $r_k(t)$ denote the signal at a point k.

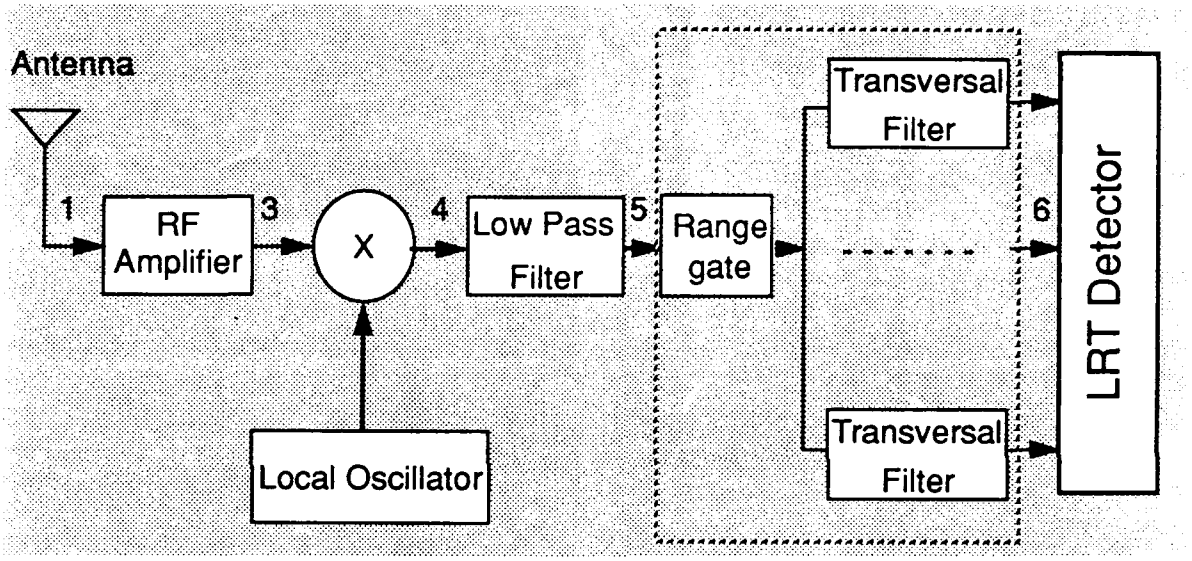

Figure 2.1 - Receiver Model.

As shown in Fig. 2.1, the received signal $r_1(t)$ is first amplified and filtered by the RF amplifier. The output $r_3(t)$ is then multiplied by the local oscillator signal and low pass filtered to produce the baseband signal $r_5(t)$. The range gate selects the successive pulse returns from a particular range cell. These, in turn, are processed by a bank of transversal filters so as to maximize the signal-to-disturbance ratio at the input of the LRT detector. Each transversal filter is tuned to a different Doppler frequency. The transversal filter whose Doppler frequency coincides with that of the desired signal yields the maximum output in the absence of disturbance and is the only one analyzed in this work. In this chapter the analytical model for each block is discussed in detail.

2.1 The RF Amplifier:

For simplicity of analysis, the receiver nonlinear behavior is assumed to be confined to the RF amplifier. As seen in Fig. 2.2, the RF amplifier is modeled as a zero-memory nonlinear amplifier cascaded with an ideal bandpass filter having unity gain. Observe that the nonlinear amplifier output is denoted by $r_2(t)$.

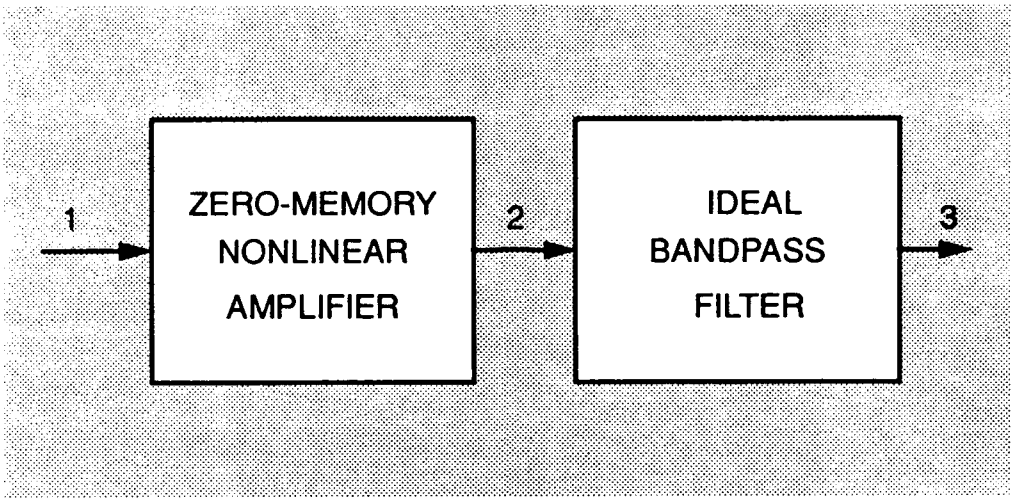

Figure 2.2 - Block Diagram of the RF Amplifier.

2.1.1 The Nonlinear Amplifier:

Receiver saturation effects are accounted for by the zero-memory nonlinear amplifier whose input-output characteristic is given by

$$r_2(t) = \frac{2L}{\sqrt{2\pi\sigma_g^2}} \int_0^{r_1(t)} \exp\left(-\frac{Z^2}{2\sigma_g^2}\right) dZ \quad . \tag{2.1}$$

Thus, $r_2(t)$ is propotional to the integral of a zero-mean Gaussian density function with variance σ_g^2. A sketch of $r_2(t)$ versus $r_1(t)$ is shown in Fig. 2.3. The amplifier has zero memory in the sense that the present value of the output is determined only by the present value of the input. Observe that L represents the saturation level of the non-linearity.

The slope of the input-output characteristic is

$$\frac{dr_2(t)}{dr_1(t)} = \frac{2L}{\sqrt{2\pi\sigma_g^2}} \cdot \exp\left(-\frac{r_1^2(t)}{2\sigma_g^2}\right) . \qquad (2.2)$$

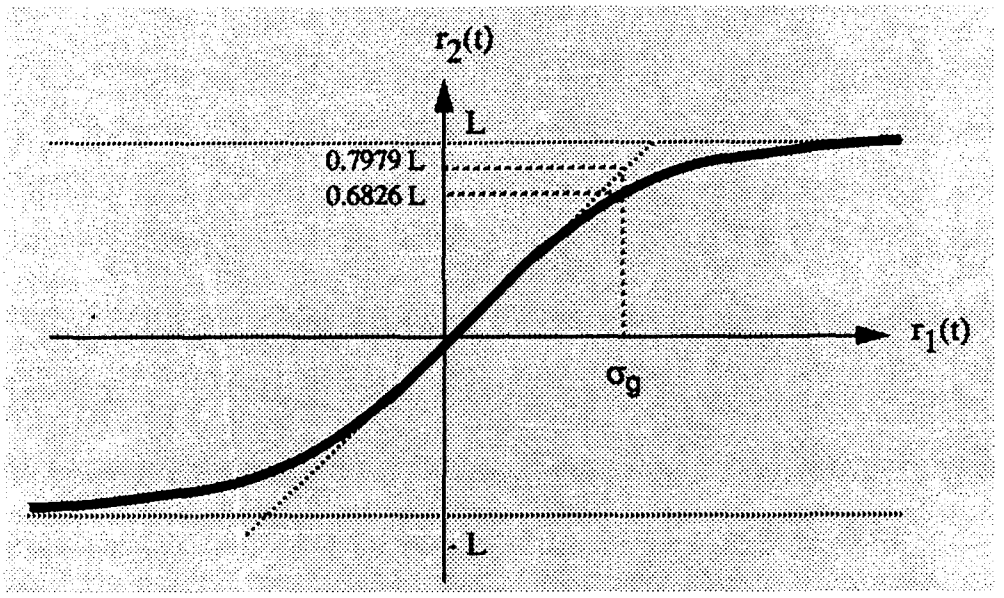

Figure 2.3 - Input-Output Characteristic of Zero- Memory Nonlinear Amplifier.

Let the linear gain of the RF amplifier, denoted by G, be defined as the slope of the input-output characteristic evaluated at the origin. It follows that

$$G = \left.\frac{dr_2(t)}{dr_1(t)}\right|_{r_1(t)=0} = \frac{2L}{\sqrt{2\pi\sigma_g^2}} = \sqrt{\frac{2}{\pi}} \cdot \frac{L}{\sigma_g} . \qquad (2.3)$$

For small enough inputs, the nonlinear amplifier output can be determined from the linear characteristic

$$r_2(t) = G \cdot r_1(t) . \qquad (2.4)$$

Note that the linear gain involves the ratio of L to σ_g . When $r_1=\sigma_g$, Equations (2.1) and (2.4) yield

$$r_2 = \begin{cases} 0.6826L & ; \text{Eq(2.1)} \\ 0.7979L & ; \text{Eq(2.4)} \end{cases} \cdot \tag{2.5}$$

Hence, when $r_1=\sigma_g$, the ratio (in dB) of the outputs from the nonlinear and linear characteristic is

$$20\text{Log}_{10}\left(\frac{0.6826}{0.7979}\right) = -1.355\text{dB} \cdot \tag{2.6}$$

Conventionally, the 1 dB compression point determines the linear region of a non-linear amplifier. It follows that the nonlinearity of Eq.(2.1) can be considered to be approximately linear over the range

$$-\sigma_g \le r_1 \le \sigma_g \cdot \tag{2.7}$$

2.1.2 The Bandpass Filter

Let f_c denote the carrier frequency, in Hertz, of the received signal. The magnitude of the ideal bandpass filter transfer function is shown in Fig.2.4. Note

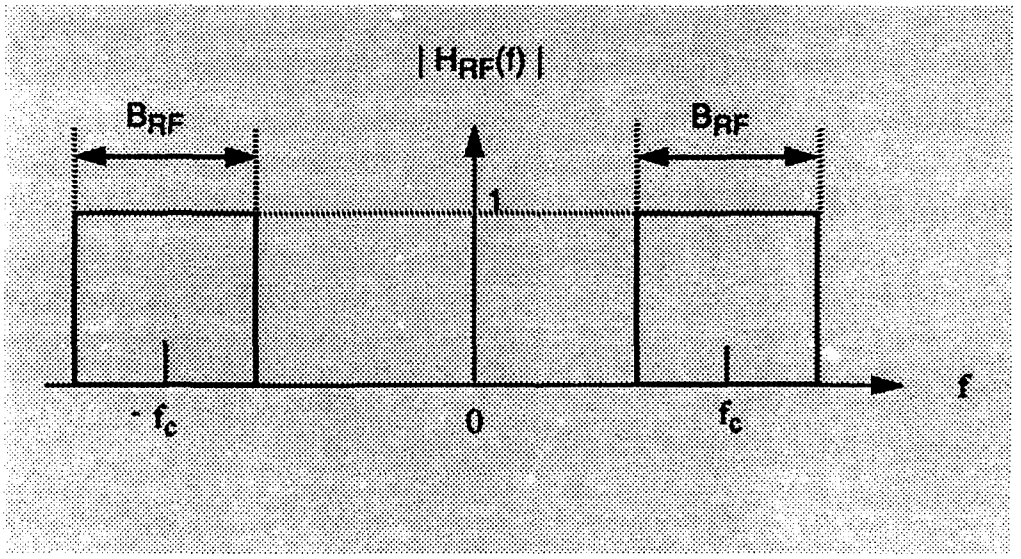

Figure 2.4 - Transfer Function Magnitude of Ideal Bandpass Filter.

that the filter has unity gain over the entire bandpass region and zero gain otherwise. The filter bandwidth B_{RF} is the smallest bandwidth required to pass undistorted the desired signal portion of $r_2(t)$. Note that the filter removes the nonlinear products in $r_2(t)$ centered at harmonics of the carrier frequency along with components of the noise which fall outside of the desired signal bandwidth.

2.2 The Mixer

The mixer consists of the multiplier, local oscillator, and lowpass filter. It serves to translate the spectrum of $r_3(t)$ from $\pm f_c$ to dc. Assuming the local oscillator signal is a unit amplitude sinusoid at the carrier frequency f_c, the input to the lowpass filter is

$$r_4(t) = r_3(t)\cos(2\pi f_c t) \quad . \tag{2.8}$$

The lowpass filter is assumed to be ideal with a transfer function magnitude as shown in Fig. 2.5. Once again, the filter gain is unity over the passband and zero otherwise.The filter bandwidth B_L is the smallest bandwidth required to pass undistorted the desired signal portion of $r_4(t)$. Note that $r_5(t)$ is a baseband signal.

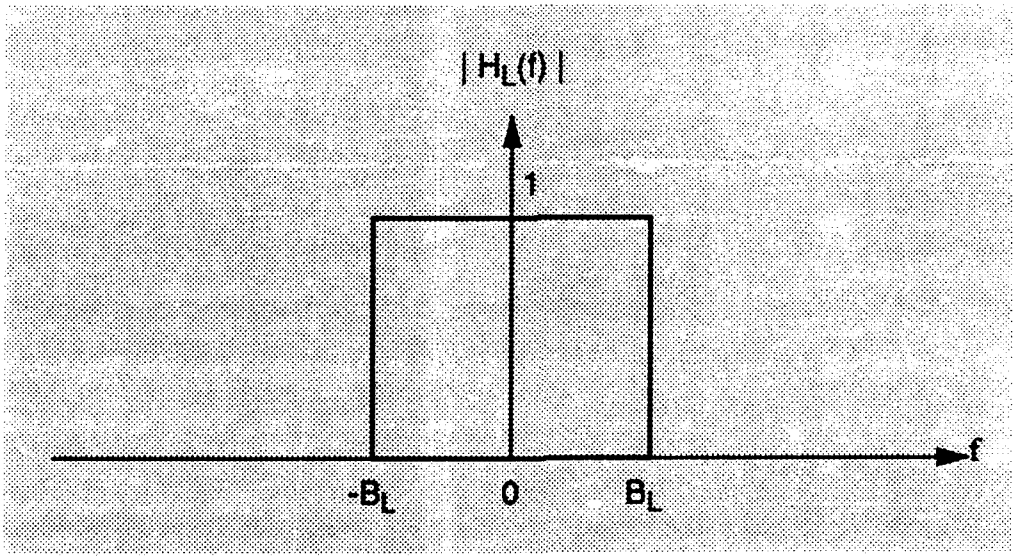

Figure 2.5 - Transfer Function Magnitude of Ideal Lowpass Filter.

2.3 The Range Gate and Transversal Filter

Analysis of the transversal filter is most readily carried out in terms of the complex envelopes of the modulated signals. As developed in section 3.3, let $\tilde{r}_5(t)$ denote the complex envelope associated with $r_5(t)$. The range gate serves to select successive pulse returns from a particular range cell. Let T_s denote the length of the pulse repitition interval (i.e.; the time duration between consecutive pulses). If $r_5(t)$ represents the current pulse return from a particular range cell, then the $(k-1)^{th}$ previous return from the same range cell is given by $r_5[t-(k-1)T_s]$. The corresponding complex envelope is denoted by $\tilde{r}_5[t-(k-1)T_s]$.

Assume N pulses are received from a particular range cell. The transversal filter sums the weighted returns to produce the complex envelope output

$$\tilde{r}_6(t) = \sum_{k=1}^{N} \tilde{w}_k^* \cdot \tilde{r}_5[t-(k-1)T_s] \quad . \tag{2.9}$$

$\tilde{w}_k$ represents the k^{th} weight where the tilde denotes a complex quantity and the asterisk denotes the complex conjugate. A block diagram of the transversal filter is presented Fig.2.6. When $t = NT_s$, the output is given by

$$\tilde{r}_6(NT_s) = \sum_{k=1}^{N} \tilde{w}_k^* \cdot \tilde{r}_5[(N-k+1)T_s] \quad . \tag{2.10}$$

Let

$$\tilde{r}_{5k} = \tilde{r}_5[(N-k+1)T_s] \qquad ; k = 1,2,...,N \tag{2.11}$$

and define the vectors

$$\begin{aligned} (\underline{\tilde{w}}^*)^T &= \left[\tilde{w}_1^* \;\; \tilde{w}_2^* \;\; .....\tilde{w}_N^*\right] \\ (\underline{\tilde{r}}_5^*)^T &= \left[\tilde{r}_{51}^* \;\; \tilde{r}_{52}^* \;\; .....\tilde{r}_{5N}^*\right] \end{aligned} \tag{2.12}$$

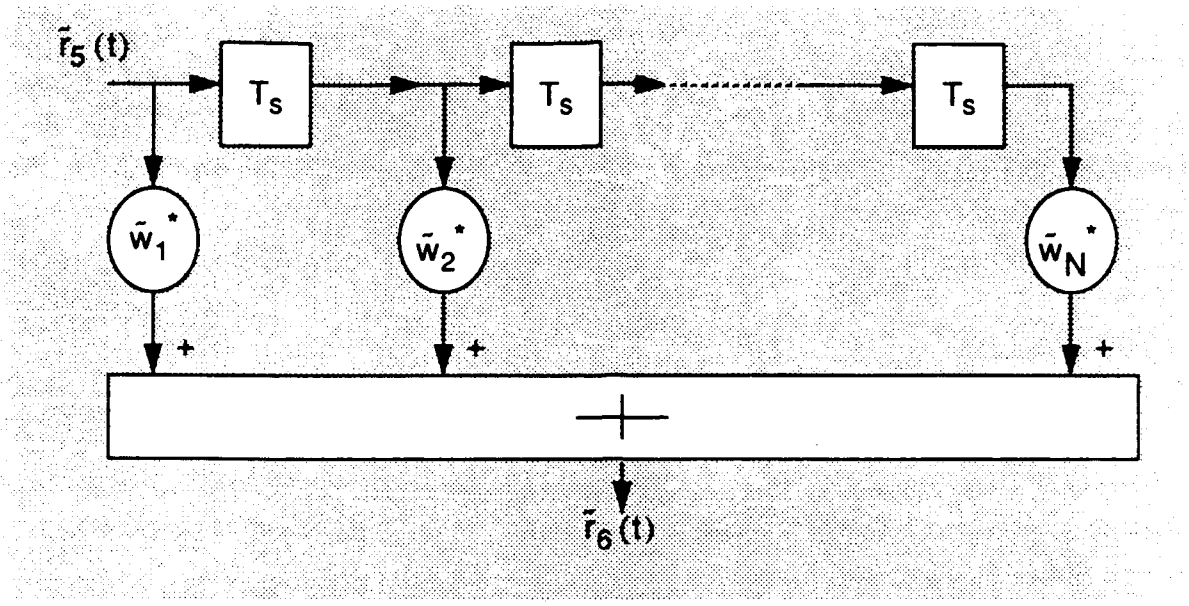

Figure 2.6 - Block Diagram of Transversal Filter .

where T denotes transpose. Eq.(2.10) can then be expressed as the inner product

$$\tilde{r}_6(NT_s) = (\underline{\tilde{w}}^*)^T \cdot \underline{\tilde{r}}_5 \quad . \tag{2.13}$$

Chapter 3

NONLINEAR RECEIVER ANALYSIS

The transmitted radar waveform is a periodic signal composed of a series of sinusoidal bursts, whose envelope is shown in Fig. 3.1. Note that

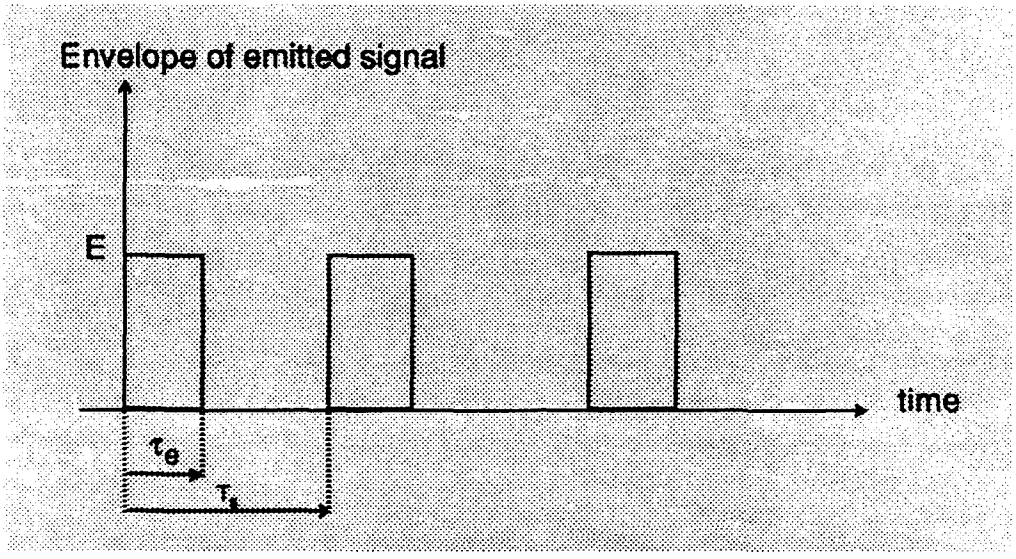

Figure 3.1 - Transmitted Radar Signal.

E = pulse amplitude

f_c = sinusoidal carrier frequency

τ_e = pulse width

T_s = pulse repitition interval.

An analytic expression for the transmitted signal is

$$e(t) = \begin{cases} E.\cos(2\pi f_c t) & nT_s < t < nT_s+\tau_e \\ 0 & nT_s+\tau_e < t < (n+1)T_s \end{cases} \qquad (3.1)$$

where n = ...,-2,-1,0,1,2,... .

3.1 Signal at Receiver Input (node 1)

Consider a received signal which is reflected from a moving target with velocity vector v, as illustrated in Fig. 3.2. Let v_r and v_n denote the radial and normal

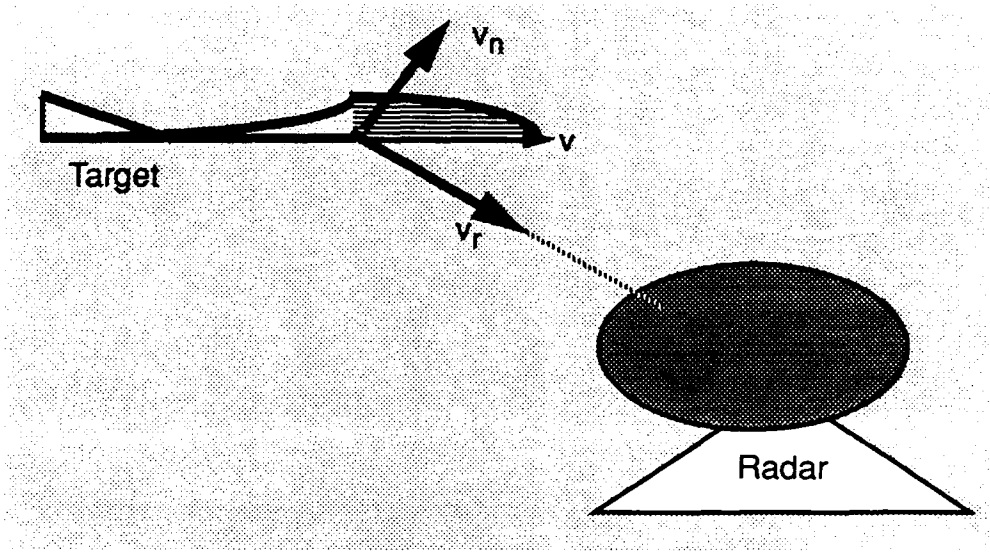

Figure 3.2 - Signal Received from Moving Target.

components of v, respectively. The carrier frequency of the received signal is (f_c+f_D) where the Doppler frequency shift due to the radial motion of the target is given by [4]

$$f_D = \frac{2v_r f_c}{c} \quad . \tag{3.2}$$

In Eq. (3.2) c denotes the speed of light which is the velocity of propagation of the electromagnetic wave. The doppler shift plays an important role in the detection of weak signals embedded in strong clutter returns.

Assuming that the delay between a transmitted and received pulse is known, there is no loss in generality by omitting the delay and expressing the received signal at the input to the RF ampifier as

$$r_1(t) = a_s(t)\cos[2\pi(f_c+f_D)t+\theta_s] + a_d(t)\cos[2\pi f_c t+\theta_d] \quad . \tag{3.3}$$

The envelope and phase of the desired signal are denoted by $a_s(t)$ and θ_s while those of the additive disturbance are denoted by $a_d(t)$ and θ_d. In terms of complex signals, $r_1(t)$ can be written as

$$r_1(t) = \mathrm{Re}\{a_s(t)\,e^{j[2\pi(f_c+f_D)t+\theta_s]}\} + \mathrm{Re}\{a_d(t)\,e^{j[2\pi f_c t+\theta_d]}\}$$

$$= \mathrm{Re}\left(\{a_s(t)\,e^{j(2\pi f_D t+\theta_s)} + a_d(t)\,e^{j\theta_d}\}\,e^{j(2\pi f_c t)}\right)$$

$$= \mathrm{Re}\{\tilde{r}_1(t)\,e^{j(2\pi f_c t)}\} \qquad (3.4)$$

where Re{.} denotes the real part operator. The complex envelopes of the desired signal, disturbance, and received signal, respectively, are

$$\tilde{s}(t) = a_s(t)\,e^{j(2\pi f_D t+\theta_s)}$$

$$\tilde{d}(t) = a_d(t)\,e^{j\theta_d} \qquad (3.5)$$

$$\tilde{r}_1(t) = \tilde{s}(t) + \tilde{d}(t).$$

The disturbance consists of clutter plus thermal noise. Hence,

$$\tilde{d}(t) = \tilde{c}(t) + \tilde{n}(t) \qquad (3.6)$$

where $\tilde{c}(t)$ and $\tilde{n}(t)$, respectively, denote the complex envelopes of the clutter and noise. $\tilde{s}(t)$, $\tilde{c}(t)$, and $\tilde{n}(t)$ are each modeled as statistically independent zero mean stationary complex Gaussian random processes. Because a sum of jointly Gaussian random processes is Gaussian, $\tilde{d}(t)$ and $\tilde{r}_1(t)$ are also zero mean stationary complex Gaussian processes. Hence, at a specified instant of time, their magnitudes and phases are Rayleigh and uniformly distributed random

variables, respectively. In addition, each phase random variable is statistically independent of the corresponding magnitude random variable. $r_1(t)$ is assumed to be a bandpass signal with a spectrum as shown in Fig. 3.3.

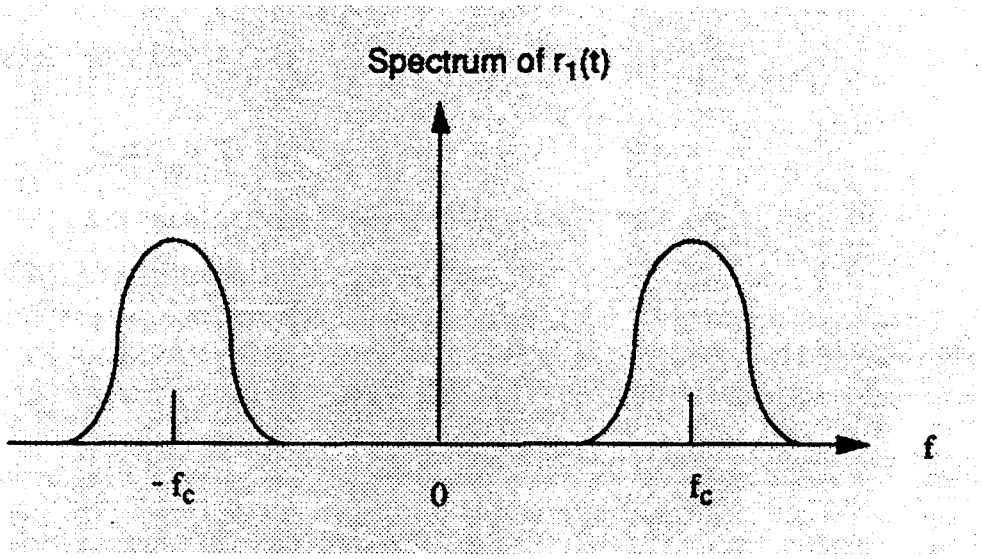

Figure 3.3 - Power Spectral Density of $r_1(t)$.

3.2 Signal at RF Amplifier Output (node 3)

As shown in Fig. 2.2, the RF amplifier is modeled as a zero-memory nonlinear amplifier in cascade with an ideal bandpass filter. The output of the nonlinear amplifier is determined first.

3.2.1 Output of Nonlinear Amplifier (node 2)

As given in Eq.(2.1), the input-output characteristic of the nonlinear amplifier is

$$r_2(t) = \frac{2L}{\sqrt{2\pi\sigma_g^2}} \int_0^{r_1(t)} \exp\left(-\frac{Z^2}{2\sigma_g^2}\right) dZ \quad . \qquad (3.7)$$

Since the nonlinearity is continuous and single-valued and has all derivatives on an interval including $r_1 = 0$, it can be expanded in a Mac Laurin's series at $r_1 = 0$.

Let the nonlinearity be denoted by

$$r_2 = g(r_1) \quad . \tag{3.8}$$

The Mac Laurin's series is then given by

$$r_2 = \sum_{p=0}^{\infty} a_p \cdot r^p{}_1 \tag{3.9}$$

where the p^{th} coefficient is

$$a_p = \frac{1}{p!} \frac{d^p}{dr^p{}_1} g(r_1) \Big|_{r_1 = 0}$$

$$= \begin{cases} 1 & ; p=1 \\ \dfrac{2L}{\sqrt{2\pi\sigma_g^2}} \cdot \left(\dfrac{-1}{\sigma_g^2}\right)^{\frac{p-1}{2}} \dfrac{1 \cdot 3 \cdot 5 \ldots (p-4)\,(p-2)}{p!} & ; p=3,5,7,.. \\ 0 & ; p=0,2,4,6,.. \end{cases} \quad . \tag{3.10}$$

Letting p = 2k+1, it follows that

$$r_2 = \frac{2L}{\sqrt{2\pi\sigma_g^2}} \cdot \left[r_1 + \sum_{k=1}^{\infty} \left(\frac{-1}{\sigma_g^2}\right)^k \cdot \frac{(2k-1)!!}{(2k+1)!} \cdot r_1^{2k+1} \right] \tag{3.11}$$

where the double factorial is defined to be

$$(2k-1)!! = 1 \cdot 3 \cdot 5 \ldots\ldots (2k-3)\,(2k-1) \quad . \tag{3.12}$$

Eq.(3.11) is now expressed in terms of the complex envelope of $r_1(t)$. Recall that

$$r_1(t) = \mathrm{Re}\{\tilde{r}_1(t)\, e^{j2\pi f_c t}\}$$

$$= \frac{\tilde{r}_1(t)\, e^{j2\pi f_c t} + \tilde{r}_1^{\,*}(t)\, e^{-j2\pi f_c t}}{2} \qquad (3.13)$$

where the asterisk denotes complex conjugate. It follows that

$$r_1^{2k+1} = \frac{1}{2^{2k+1}} \cdot \left[\tilde{r}_1 e^{j2\pi f_c t} + \tilde{r}_1^{\,*} e^{-j2\pi f_c t}\right]^{2k+1} . \qquad (3.14)$$

Application of the binomial expansion to Eq.(3.14) results in

$$r_1^{2k+1} = \frac{1}{2^{2k+1}} \cdot \sum_{m=0}^{2k+1} C_m^{2k+1} \cdot \left[\tilde{r}_1 e^{j2\pi f_c t}\right]^{2k+1-m} \cdot \left[\tilde{r}_1^{\,*} e^{-j2\pi f_c t}\right]^{m} \qquad (3.15)$$

where the binomial coefficient is

$$C_m^{2k+1} = \frac{(2k+1)!}{m! \cdot (2k+1-m)!} . \qquad (3.16)$$

Combining the exponentials, Eq.(3.15) becomes

$$r_1^{2k+1} = \frac{1}{2^{2k+1}} \cdot \sum_{m=0}^{2k+1} C_m^{2k+1} \cdot [\tilde{r}_1]^{2k+1-m} \cdot [\tilde{r}_1^{\,*}]^{m} \cdot e^{j2\pi f_c t(2k+1-2m)} . \qquad (3.17)$$

It is seen that raising r_1 to the power (2k+1) creates spectral zones located at the frequencies $(2k+1-2m)f_c$ where m is an integer ranging from 0 to (2k+1). The spectral zones are referred to as even or odd, respectively, depending upon whether the factor multiplying f_c is even or odd.

The following observations are now made with respect to the various spectral zones :

1) As m varies from 0 to (2k+1), the locations of the spectral zones range from $(2k+1)f_c$ to $-(2k+1)f_c$.

2) All of the spectral zones are odd because (2k+1-2m) is always an odd integer.

3) An odd spectral zone occurs at the positive frequency $(2p+1)f_c$ when

$$(2k+1-2m) = (2p+1)$$

$$m = k-p \quad . \tag{3.18}$$

4) An odd spectral zone occurs at the negative frequency $-(2p+1)f_c$ when

$$(2k+1-2m) = -(2p+1)$$

$$m = k+p+1 \quad . \tag{3.19}$$

5) Zones located at positive frequencies result when (2k+1-2m) > 0. This will be the case provided

$$0 \le m \le k \quad . \tag{3.20}$$

Substituting Eq.(3.18) into Eq.(3.20) and simplfying produces the inequality

$$0 \le p \le k \quad . \tag{3.21}$$

6) Zones located at negative frequencies result when (2k+1-2m) <0. This will be the case provided

$$k+1 \le m \le 2k+1 \quad . \tag{3.22}$$

Substituting Eq.(3.19) into Eq.(3.22) and simplifying also produces the inequality

$$0 \le p \le k \quad . \tag{3.23}$$

Using the above observations, Eq.(3.17) is readily expressed as two summations where the first sum is over negative frequencies and the second sum is over positive frequencies. In particular,

$$\begin{aligned} r_1^{2k+1} &= \frac{1}{2^{2k+1}} \Bigg\{ \sum_{p=0}^{k} C_{k+p+1}^{2k+1} \cdot [\tilde{r}_1]^{k-p} \cdot [\tilde{r}_1^{\,*}]^{k+p+1} \\ &\quad \cdot e^{-j2\pi(2p+1)f_c t} + \sum_{p=0}^{k} C_{k-p}^{2k+1} \cdot [\tilde{r}_1]^{k+p+1} \cdot [\tilde{r}_1^{\,*}]^{k-p} \\ &\quad \cdot e^{j2\pi(2p+1)f_c t} \Bigg\} \\ &= \frac{1}{2^{2k+1}} \Bigg\{ \sum_{p=0}^{k} C_{k+p+1}^{2k+1} \cdot [\tilde{r}_1]^{k-p} \cdot [\tilde{r}_1^{\,*}]^{k-p} \cdot [\tilde{r}_1^{\,*}]^{2p+1} \cdot \\ &\quad \cdot e^{-j2\pi(2p+1)f_c t} + \sum_{p=0}^{k} C_{k-p}^{2k+1} \cdot [\tilde{r}_1]^{k-p} \cdot [\tilde{r}_1^{\,*}]^{k-p} \\ &\quad \cdot [\tilde{r}_1]^{2p+1} \cdot e^{j2\pi(2p+1)f_c t} \Bigg\} \\ &= \frac{1}{2^{2k+1}} \Bigg\{ \sum_{p=0}^{k} C_{k+p+1}^{2k+1} \cdot |\tilde{r}_1|^{2(k-p)} \cdot [\tilde{r}_1^{\,*}]^{2p+1} \\ &\quad \cdot e^{-j2\pi(2p+1)f_c t} + \sum_{p=0}^{k} C_{k-p}^{2k+1} \cdot |\tilde{r}_1|^{2(k-p)} \\ &\quad + [\tilde{r}_1]^{2p+1} \cdot e^{j2\pi(2p+1)f_c t} \Bigg\} \quad . \end{aligned} \tag{3.24}$$

Evaluation of the binomial coefficients results in

$$C_{k+p+1}^{2k+1} = \frac{(2k+1)!}{(k+p+1)!\cdot(2k+1-k-p-1)!} = \frac{(2k+1)!}{(k+p+1)!\cdot(k-p)!}$$

$$C_{k-p}^{2k+1} = \frac{(2k+1)!}{(k-p)!\cdot(2k+1-k+p)!} = \frac{(2k+1)!}{(k-p)!\cdot(k+p+1)!} \quad \bullet \quad (3.25)$$

It is concluded that

$$C_{k+p+1}^{2k+1} = C_{k-p}^{2k+1} \quad \bullet \quad (3.26)$$

Eq.(3.24), therefore, simplifies to

$$r_1^{2k+1} = \frac{1}{2^{2k+1}}\left\{ \sum_{p=0}^{k} C_{k-p}^{2k+1} \cdot |\tilde{r}_1|^{2(k-p)} \cdot \left[[\tilde{r}_1^{\,*}]^{2p+1} \cdot e^{-j2\pi(2p+1)f_c t} + [\tilde{r}_1]^{2p+1} \cdot e^{j2\pi(2p+1)f_c t} \right] \right\}$$

$$= \frac{1}{2^{2k}} \cdot \sum_{p=0}^{k} C_{k-p}^{2k+1} \cdot |\tilde{r}_1|^{2(k-p)} \cdot \mathrm{Re}\left\{ \left[\tilde{r}_1 e^{j2\pi f_c t} \right]^{2p+1} \right\} \quad \bullet \quad (3.27)$$

Substituting Eq.(3.27) into Eq.(3.11), the expression for the nonlinear amplifier output becomes

$$r_2 = \frac{2L}{\sqrt{2\pi\sigma_g^2}} \cdot \left[r_1 + \sum_{k=1}^{\infty} \left(\frac{-1}{\sigma_g^2} \right)^k \cdot \frac{(2k-1)!!}{(2k+1)!} \cdot \sum_{p=0}^{k} \frac{C_{k-p}^{2k+1}}{2^{2k}} \cdot |\tilde{r}_1|^{2(k-p)} \cdot \mathrm{Re}\left\{ \left[\tilde{r}_1 e^{j2\pi f_c t} \right]^{2p+1} \right\} \right] \quad \bullet \quad (3.28)$$

Separating out the spectral zones located at $\pm f_c$, the above expression can be re-written as

$$r_2 = \frac{2L}{\sqrt{2\pi\sigma_g^2}}\left[1 + \sum_{k=1}^{\infty}\left(\frac{-1}{\sigma_g^2}\right)^k \cdot \frac{C_k^{2k+1}}{2^{2k}} \cdot \frac{(2k-1)!!}{(2k+1)!} \cdot |\tilde{r}_1|^{2k}\right] \mathrm{Re}\{\tilde{r}_1 e^{j2\pi f_c t}\}$$

$$+ \quad \frac{2L}{\sqrt{2\pi\sigma_g^2}} \cdot \left[\sum_{k=1}^{\infty}\left(\frac{-1}{\sigma_g^2}\right)^k \cdot \frac{(2k-1)!!}{(2k+1)!} \cdot \sum_{p=1}^{k} \frac{C_{k-p}^{2k+1}}{2^{2k}} \cdot |\tilde{r}_1|^{2(k-p)}\right.$$

$$\left. \cdot \ \mathrm{Re}\left\{\left[\tilde{r}_1 e^{j2\pi f_c t}\right]^{2p+1}\right\}\right] . \qquad (3.29)$$

Let Δr_2 denote the terms in r_2 corresponding to the spectral zones other than those centered at $\pm f_c$. In addition, define the complex envelope

$$\tilde{r}_2\big|_{f_c} = \frac{2L}{\sqrt{2\pi\sigma_g^2}} \cdot \left[1 + \sum_{k=1}^{\infty}\left(\frac{-1}{\sigma_g^2}\right)^k \cdot \frac{C_k^{2k+1}}{2^{2k}} \cdot \frac{(2k-1)!!}{(2k+1)!} \cdot |\tilde{r}_1|^{2k}\right] \cdot \tilde{r}_1 \quad . \qquad (3.30)$$

It is then possible to express the nonlinear amplifier output as

$$r_2 = \mathrm{Re}\left\{\tilde{r}_2\big|_{f_c} \cdot e^{j2\pi f_c t}\right\} + \Delta r_2 \, . \qquad (3.31)$$

The spectrum of $r_2(t)$ is illustrated in Fig.3.4. The spectral zones at $\pm 3f_c$, $\pm 5f_c$,... arise from terms in Δr_2. The spectral zones at $\pm f_c$ are due to the first term in Eq.(3.31).

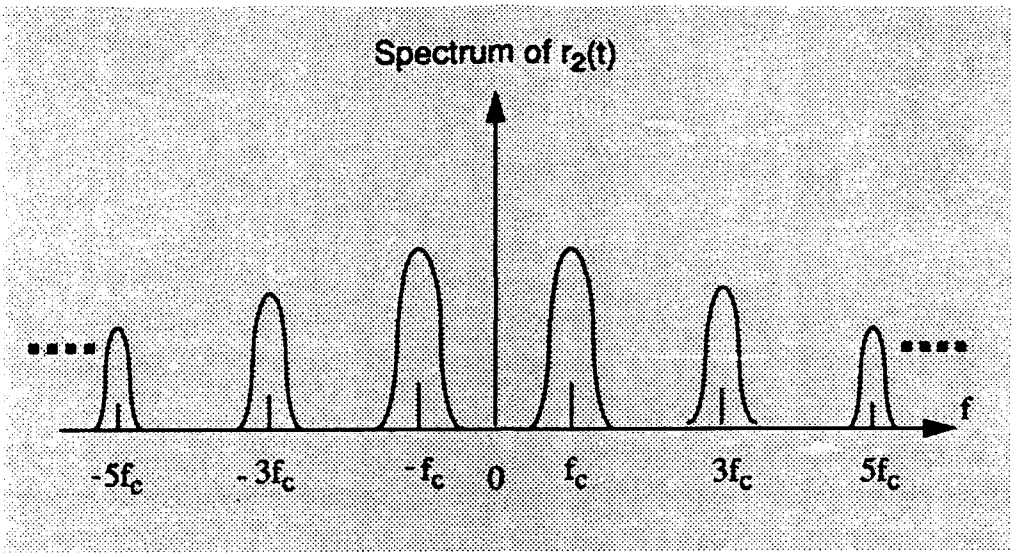

Figure 3.4 - Power Spectral Density of $r_2(t)$.

3.2.2 Output of Bandpass Filter (node 3)

The bandpass filter is assumed to have the ideal transfer function whose magnitude is shown in Fig.2.4. The bandwidth B_{RF} is assumed to be narrow enough such that only the spectral zones at $\pm f_c$ are passed with negligible distortion. The remaining spectral zones are assumed to be perfectly attenuated. It follows that the output of the RF amplifier is given by

$$r_3(t) = \mathrm{Re}\left\{\tilde{r}_2\Big|_{f_c} \cdot e^{j2\pi f_c t}\right\} . \qquad (3.32)$$

where the complex envelope $\tilde{r}_2\Big|_{f_c}$ is defined in Eq.(3.30). The spectrum of $r_3(t)$ is shown in Fig.3.5.

3.3 Signal at Mixer Output (node 5)

As discussed in Section 2.2, the mixer consists of the multiplier, local oscillator, and lowpass filter. The input to the lowpass filter is

$$r_4(t) = r_3(t) \cdot \cos(2\pi f_c t) . \qquad (3.33)$$

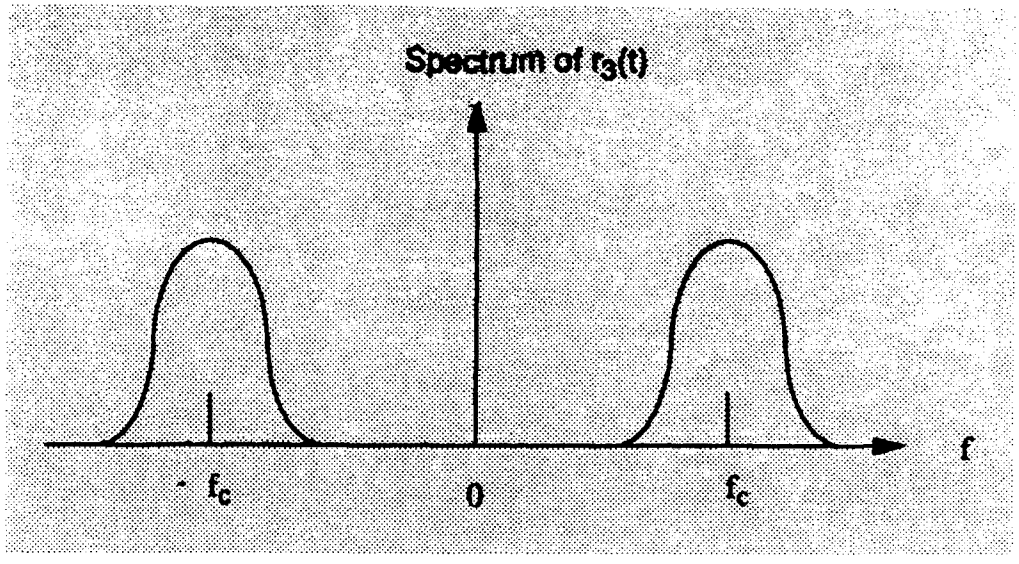

Figure 3.5 - Power Spectral Density of $r_3(t)$.

From Eq.(3.32)

$$r_3(t) = \frac{1}{2} \cdot \left[\tilde{r}_2\Big|_{f_c} \cdot e^{j2\pi f_c t} + \tilde{r}_2^{*}\Big|_{f_c} \cdot e^{-j2\pi f_c t} \right] \quad . \tag{3.34}$$

In addition,

$$\cos(2\pi f_c t) = \frac{1}{2} \cdot \left[e^{j2\pi f_c t} + e^{-j2\pi f_c t} \right] \quad . \tag{3.35}$$

It follows that

$$r_4(t) = \frac{1}{4} \cdot \left[\tilde{r}_2\Big|_{f_c} \cdot e^{j2\pi f_c t} + \tilde{r}_2^{*}\Big|_{f_c} \cdot e^{-j2\pi f_c t} \right] \cdot \left[e^{j2\pi f_c t} + e^{-j2\pi f_c t} \right]$$

$$= \frac{1}{4} \cdot \left[\tilde{r}_2\Big|_{f_c} + \tilde{r}_2^{*}\Big|_{f_c} \right] + \frac{1}{4} \cdot \left[\tilde{r}_2\Big|_{f_c} \cdot e^{j2\pi(2f_c)t} + \tilde{r}_2^{*}\Big|_{f_c} \cdot e^{-j2\pi(2f_c)t} \right]$$

$$= \frac{1}{2} \cdot \mathrm{Re}\{\tilde{r}_2\Big|_{f_c}\} + \frac{1}{2} \cdot \mathrm{Re}\left\{ \tilde{r}_2\Big|_{f_c} \cdot e^{j2\pi(2f_c)t} \right\} \quad . \tag{3.36}$$

Observe that the spectral zones of $r_4(t)$ are located at dc and $\pm 2f_c$. The spectrum of $r_4(t)$ is shown in Fig.3.6.

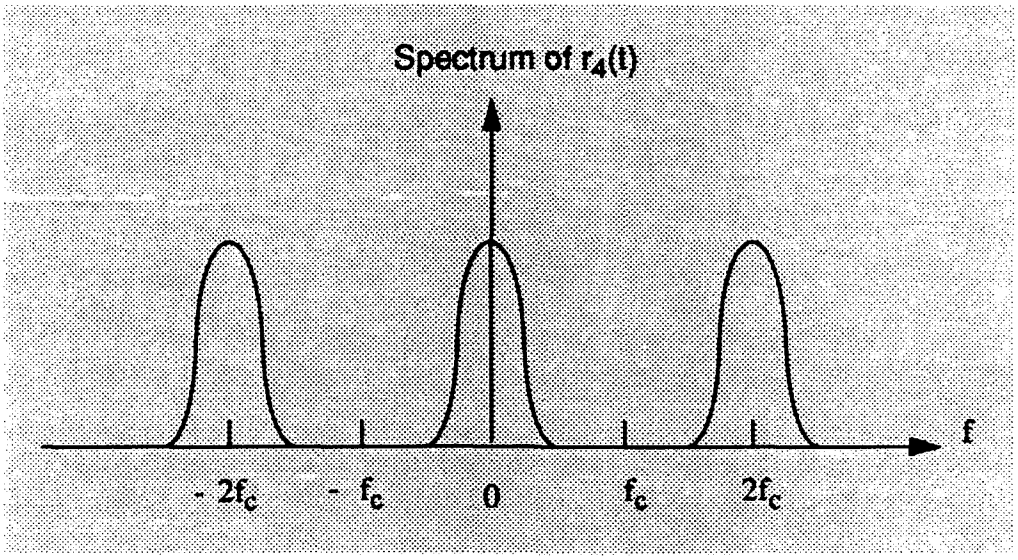

Figure 3.6 - Power Spectral density of $r_4(t)$.

The lowpass filter is assumed to have the ideal transfer function whose magnitude is shown in Fig.2.5. The bandwidth B_L is assumed to be wide enough to pass with negligible distortion the spectral zone at dc but small enough such that the spectral zones at $\pm 2f_c$ are perfectly attenuated. It follows that the signal at the mixer output is

$$r_5(t) = \frac{1}{2} \cdot \mathrm{Re}\{\tilde{r}_2|_{f_c}\} \,. \tag{3.37}$$

Define the complex signal

$$\tilde{r}_5(t) = \frac{1}{2} \cdot \tilde{r}_2|_{f_c} \,. \tag{3.38}$$

where $\tilde{r}_2|_{f_c}$ is defined in Eq.(3.30). Then

$$r_5(t) = \mathrm{Re}\{\tilde{r}_5(t)\} \,. \tag{3.39}$$

The spectrum of $r_5(t)$ is illustrated in Fig.3.7. Note that $r_5(t)$ is a base-band signal which serves as the input to the range gate and transversal filter.

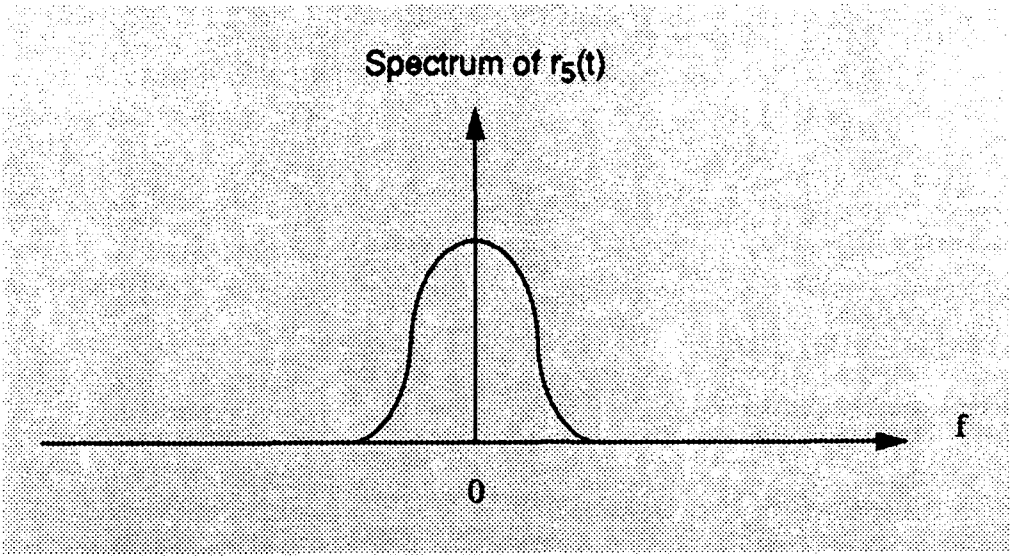

Figure 3.7 - Power Spectral Density of $r_5(t)$.

Chapter 4

RELATIONS BETWEEN AUTOCORRELATION FUNCTIONS AT VARIOUS POINTS OF THE RECEIVER

In this chapter the general form of the complex autocorrelation function at the input to the transversal filter (node 5 of Fig.2.1) is derived as a function of the complex autocorrelation function at the output of the zero-memory nonlinear amplifier (node 2 of Fig.2.2).

4.1 Autocorrelation Function at the Input to the RF Amplifier (node 1 of Fig.2.1)

The autocorrelation function of the signal $r_1(t)$ at the input to the RF amplifier is defined as

$$R_1(t,\tau) = E[r_1(t) \cdot r_1(t-\tau)] \quad . \tag{4.1}$$

In terms of the complex envelope $\tilde{r}_1(t)$ introduced in Eq.(3.4), the autocorrelation function becomes

$$R_1(t,\tau) = E\left[\mathrm{Re}\{\tilde{r}_1(t)\, e^{j2\pi f_c t}\} \cdot \mathrm{Re}\{\tilde{r}_1(t-\tau)\, e^{j2\pi f_c (t-\tau)}\} \right]$$

$$= E\left[\frac{\tilde{r}_1(t)\, e^{j2\pi f_c t} + \tilde{r}_1^{*}(t)\, e^{-j2\pi f_c t}}{2} \cdot \right.$$

$$\left. \frac{\tilde{r}_1(t-\tau)\, e^{j2\pi f_c (t-\tau)} + \tilde{r}_1^{*}(t-\tau)\, e^{-j2\pi f_c (t-\tau)}}{2} \right]$$

$$R_1(t,\tau) = \frac{1}{2}\left\{E\left[\frac{\tilde{r}_1(t)\tilde{r}_1(t-\tau)e^{j2\pi f_c(2t-\tau)} + \tilde{r}_1^{*}(t)\tilde{r}_1^{*}(t-\tau)e^{-j2\pi f_c(2t-\tau)}}{2}\right.\right.$$

$$\left.\left. + \frac{\tilde{r}_1(t)\cdot\tilde{r}_1^{*}(t-\tau)\cdot e^{j2\pi f_c\tau} + \tilde{r}_1^{*}(t)\cdot\tilde{r}_1(t-\tau)\cdot e^{-j2\pi f_c\tau}}{2}\right]\right\} \quad .$$

Interchange of the real part and expectation operators results in

$$R_1(t,\tau) = \frac{1}{2}\cdot \mathrm{Re}\{E[\tilde{r}_1(t)\cdot\tilde{r}_1(t-\tau)]\cdot e^{j2\pi f_c(2t-\tau)}\}$$

$$+ \frac{1}{2}\cdot \mathrm{Re}\{E[\tilde{r}_1(t)\cdot\tilde{r}_1^{*}(t-\tau)]\cdot e^{j2\pi f_c\tau}\} \quad . \qquad (4.2)$$

Assuming stationarity of $r_1(t)$ within the gating window, it is shown in Appendix A that

$$E[\tilde{r}_1(t)\cdot\tilde{r}_1(t-\tau)] = 0 \quad . \qquad (4.3)$$

In addition, stationarity implies that $E[\tilde{r}_1(t)\cdot\tilde{r}_1^{*}(t-\tau)]$ is a function of the difference between the arguments. Hence, we define

$$\tilde{R}_1(\tau) = E[\tilde{r}_1(t)\cdot\tilde{r}_1^{*}(t-\tau)] \quad . \qquad (4.4)$$

It follows that

$$R_1(t,\tau) = R_1(\tau) = \frac{1}{2}\cdot \mathrm{Re}\left[\tilde{R}_1(\tau)\cdot e^{j2\pi f_c\tau}\right] \quad . \qquad (4.5)$$

4.2 Autocorrelation Function at the Output of the Zero-memory Nonlinear Amplifier (node 2 of Fig.2.2)

4.2.1 Transformation of the probability Density Function Due to the Nonlinearity [5]

As pointed out in section 2.1.1, the nonlinear amplifier is modeled as a soft nonlinearity with saturation levels at ±L. In particular, as given by Eq.(2.1), the input-output characteristic is described by

$$r_2(t) = \frac{2L}{\sqrt{2\pi\sigma_g^2}} \int_0^{r_1(t)} \exp\left(-\frac{Z^2}{2\sigma_g^2}\right) dZ \quad . \tag{4.6}$$

Let the probability density function of $r_1(t)$ and $r_2(t)$ be denoted by $p_1(r_1)$ and $p_2(r_2)$, respectively. These two densities are related by the transformation

$$p_2(r_2) = p_1(r_1) \cdot \left|\frac{dr_1}{dr_2}\right|_{r_1 = g^{-1}(r_2)} \quad . \tag{4.7}$$

From Eq.(2.2),

$$\frac{dr_1}{dr_2} = \frac{\sqrt{2\pi\sigma_g^2}}{2L} \cdot e^{\frac{r_1^2}{2\sigma_g^2}} \quad . \tag{4.8}$$

Because the slope is nonnegative,

$$p_2(r_2) = \frac{\sqrt{2\pi\sigma_g^2}}{2L} \cdot p_1(r_1) \cdot e^{\frac{r_1^2}{2\sigma_g^2}}\Bigg|_{r_1 = g^{-1}(r_2)} \quad . \tag{4.9}$$

Consider the case for which $r_1(t)$ is a zero-mean Gaussian random variable with variance σ_1^2. Then

$$p_1(r_1) = \frac{1}{\sqrt{2\pi\sigma_1^2}} \cdot e^{-\frac{r_1^2}{2\sigma_1^2}} \quad . \tag{4.10}$$

It follows that

$$p_2(r_2) = \frac{1}{\sqrt{2\pi\sigma_1^2}} \cdot \frac{\sqrt{2\pi\sigma_g^2}}{2L} \cdot e^{\left(\frac{r_1^2}{2\sigma_g^2} - \frac{r_1^2}{2\sigma_1^2}\right)}\Bigg|_{r_1 = g^{-1}(r_2)}$$

$$= \frac{\sigma_g/\sigma_1}{2L} \cdot e^{-\frac{r_1^2}{2\sigma_g^2}\left[\frac{\sigma_g^2}{\sigma_1^2} - 1\right]}\Bigg|_{r_1 = g^{-1}(r_2)} \quad . \tag{4.11}$$

Recall from Eq.(2.7) that the nonlinearity can be approximated by a linear characteristic over the range $(-\sigma_g, +\sigma_g)$. Also, note that σ_1 is the rms value of the input $r_1(t)$. Hence, the ratio

$$\alpha = \frac{\sigma_g}{\sigma_1} \tag{4.12}$$

is a measure of how weakly the nonlinearity is being driven by the input signal. The larger is the value of α, the more likely it is that the input will be in the linear region of the nonlinearity. In terms of α, the density function at the output of the nonlinearity is given by

$$p_2(r_2) = \frac{\alpha}{2L} \cdot e^{-\frac{\alpha^2 - 1}{2\sigma_g^2}\left[g^{-1}(r_2)\right]^2} \quad . \tag{4.13}$$

The nature of this density function is now discussed for various values of α. When $\alpha = 1$,

$$p_2(r_2) = \begin{cases} \frac{1}{2L} & ; -L \le r_2 \le L \\ 0 & ; \text{otherwise} \end{cases} . \qquad (4.14)$$

A plot of Eq.(4.14) is shown in Fig.4.1. We conclude that the nonlinear amplifier

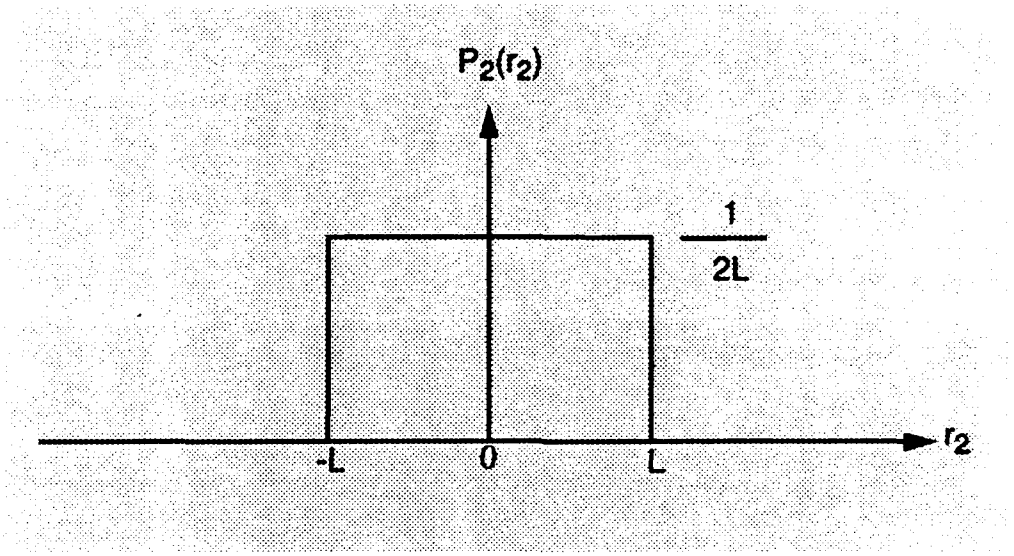

Figure 4.1 - Plot of $P_2(r_2)$ when $\alpha = 1$.

output is uniformly distributed when $\sigma_1 = \sigma_g$. For $\alpha > 1$, the exponent in $p_2(r_2)$ is negative.From Fig.2.3, it is obvious that

$$g^{-1}(-L) = -\infty \quad \text{and} \quad g^{-1}(L) = \infty \quad .$$

Consequently, $P_2(r_2)$ is a bell-shaped curve whose value asymptotes to zero for $r_2 = \pm L$. For $\alpha >> 1$, the nonlinearity is exercised primarily in its linear region. It is not suprising, therefore, that the corresponding density function is closely Gaussian. However, $p_2(r_2)$ cannot be strictly Gaussian because r_2 is constrained to the interval (-L,L) whereas a Gaussian random variable can assume values over the infinite interval $(-\infty,+\infty)$. For $\alpha < 1$, the exponent in $p_2(r_2)$ is positive. It follows that

the density function becomes infinite for $r_2 = \pm L$. In the limit, as $\alpha \rightarrow 0$, the density function approaches two impulses located at $r_2 = \pm L$, as shown in Fig.4.2. This is

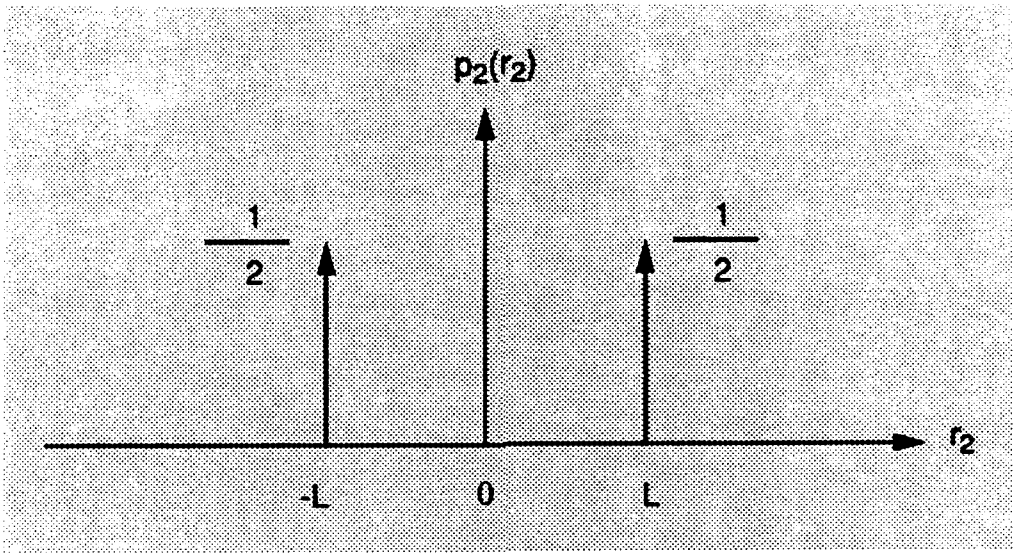

Figure 4.2 - Plot of $p_2(r_2)$ in the limit as $\alpha \rightarrow 0$.

consistent with the fact that the input-output characteristic approaches that of the hard limiter, illustrated in Fig.4.3, as $\sigma_g \rightarrow 0$. Even if $\sigma_g \neq 0$, the nonlinearity is driven into saturation most of the time when $\sigma_1 >> \sigma_g$ or, equivalently, $\alpha << 1$. The discrete density function of Fig.4.2 is then applicable.Sketches of $p_2(r_2)$ for various values of α are shown in Fig.4.4. From Fig.2.3, note that

$$g^{-1}(0) = 0 \quad .$$

Consequently, the curves in Fig.4.4 obey the property that

$$p_2(0) = \frac{\alpha}{2L} \quad . \tag{4.15}$$

Also, as pointed out previously,

$$p_2(\pm L) = \begin{cases} 0 & \text{if } \alpha > 1 \\ \infty & \text{if } \alpha < 1 \end{cases} \quad . \tag{4.16}$$

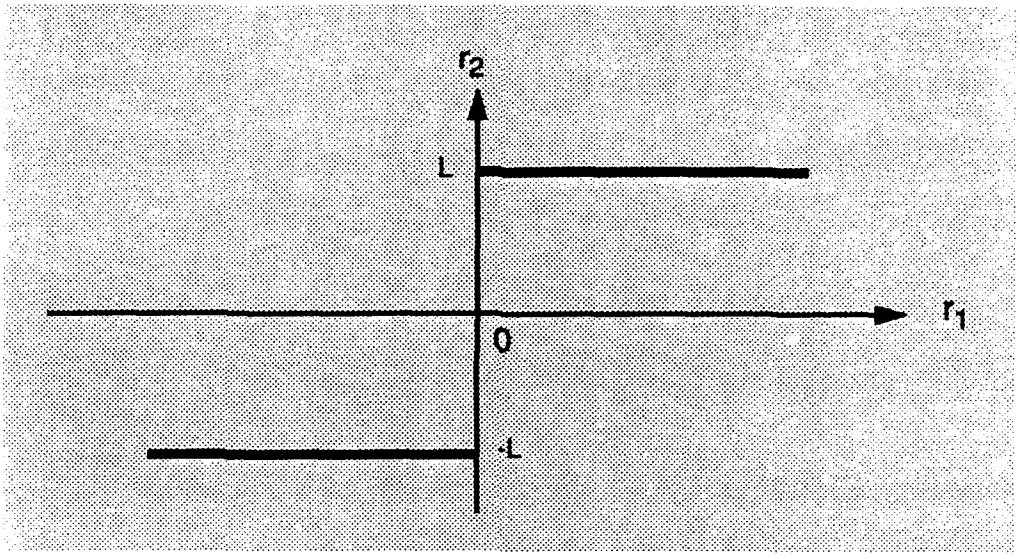

Figure 4.3 - Input-output characteristic of hard limiter.

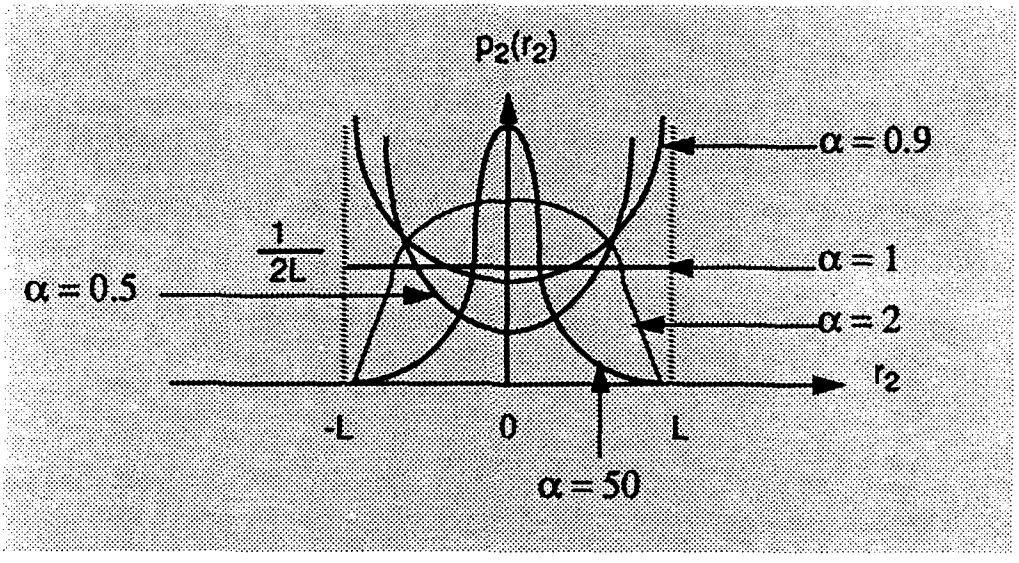

Figure 4.4 - Sketches of $p_2(r_2)$ for various values of α.

4.2.2 Transformation of the Correlation Function Due to the Nonlinearity [5]

Define the Fourier transform of the input-output characteristic to be

$$G(ju) = \int_{-\infty}^{\infty} g[r_1(t)] \cdot e^{-jur_1(t)} dr_1(t) \quad . \qquad (4.17)$$

Assuming stationarity, the output correlation function is given by

$$R_2(\tau) = E[r_2(t) \cdot r_2(t-\tau)] \quad . \tag{4.18}$$

The output voltages can be expressed in terms of the Fourier transform of the input-output characteristic according to the relations

$$r_2(t) = g[r_1(t)] = \frac{1}{2\pi} \int_{-\infty}^{\infty} G(ju) \cdot e^{jur_1(t)} du \tag{4.19}$$

and

$$r_2(t-\tau) = g[r_1(t-\tau)] = \frac{1}{2\pi} \int_{-\infty}^{\infty} G(jv) \cdot e^{jvr_1(t-\tau)} dv \quad . \tag{4.20}$$

It follows that

$$R_2(\tau) = E\left[\frac{1}{4\pi^2} \int_{-\infty}^{\infty} \int_{-\infty}^{\infty} G(ju) \cdot G(jv) \cdot e^{jur_1(t)} \cdot e^{jvr_1(t-\tau)} dudv \right]$$

$$= \frac{1}{4\pi^2} \int_{-\infty}^{\infty} \int_{-\infty}^{\infty} G(ju) \cdot G(jv) \cdot E\left[e^{jur_1(t)} \cdot e^{jvr_1(t-\tau)} \right] dudv \quad . \tag{4.21}$$

The quantity,

$$M(ju, jv) = E\left[e^{jur_1(t)} \cdot e^{jvr_1(t-\tau)} \right] \tag{4.22}$$

is recognized as the joint characteristic function of the random variables $r_1(t)$ and $r_1(t-\tau)$. Hence,

$$R_2(\tau) = \frac{1}{4\pi^2} \int_{-\infty}^{\infty} \int_{-\infty}^{\infty} G(ju) \cdot G(jv) \cdot M(ju, jv)\, dudv \quad . \tag{4.23}$$

It is now assumed that $r_1(t)$ and $r_1(t-\tau)$ are jointly Gaussian zero-mean random variables with variance σ_1^2 and correlation function

$$R_1(\tau) = E[r_1(t) \cdot r_1(t-\tau)] \quad .$$

Their joint characteristic function is then given by

$$M(ju, jv) = e^{-\frac{1}{2} \cdot \left[\sigma_1^2 u^2 + 2R_1(\tau)uv + \sigma_1^2 v^2\right]}$$

$$= e^{-\frac{\sigma_1^2}{2} \cdot \left[u^2 + 2\rho_1(\tau) + v^2\right]} \qquad (4.24)$$

where

$$\rho_1(\tau) = \frac{R_1(\tau)}{\sigma_1^2} \qquad (4.25)$$

is the correlation function relating $r_1(t)$ and $r_1(t-\tau)$. As a result, the output correlation function can be expressed as

$$R_2(\tau) = \frac{1}{4\pi^2} \int_{-\infty}^{\infty} \int_{-\infty}^{\infty} G(ju) \cdot G(jv) \cdot e^{-\frac{\sigma_1^2}{2} \cdot [u^2 + v^2] - R_1(\tau)uv} \cdot dudv \quad . \qquad (4.26)$$

To evaluate G(ju), use is made of the differentiation property of the Fourier transform. To begin with, we have the Fourier transform pair

$$g[r_1(t)] = \frac{2L}{\sqrt{2\pi\sigma_g^2}} \int_0^{r_1(t)} \exp\left(-\frac{Z^2}{2\sigma_g^2}\right) dZ \leftrightarrow G(ju) \quad . \qquad (4.27)$$

Applying the differentiation property to Eq.(4.27), there results

$$\frac{dg(r_1(t))}{dr_1(t)} = \frac{2L}{\sqrt{2\pi\sigma_g^2}} \cdot \exp\left(-\frac{r_1^2(t)}{2\sigma_g^2}\right) \leftrightarrow ju \cdot G(ju) \quad . \tag{4.28}$$

However, it is well known that the Fourier transform of a Gaussian waveform is a Gaussian waveform, as indicated below:

$$\exp\left(-\frac{r_1^2(t)}{2\sigma_g^2}\right) \leftrightarrow \sqrt{2\pi\sigma_g^2} \cdot e^{-\frac{\sigma_g^2 u^2}{2}} \quad . \tag{4.29}$$

It follows that

$$ju \cdot G(ju) = \frac{2L}{\sqrt{2\pi\sigma_g^2}} \cdot \sqrt{2\pi\sigma_g^2} \cdot e^{-\frac{\sigma_g^2 u^2}{2}} \quad . \tag{4.30}$$

Thus,

$$G(ju) = \frac{2L}{ju} \cdot e^{-\frac{\sigma_g^2 u^2}{2}} \quad . \tag{4.31}$$

Substituting Eq.(4.31) into the expression for $R_2(\tau)$, we have

$$R_2(\tau) = \frac{(2L)^2}{4\pi^2} \int_{-\infty}^{\infty}\int_{-\infty}^{\infty} \frac{-1}{uv} \cdot e^{-\frac{\sigma_g^2}{2} \cdot [u^2+v^2]} \cdot e^{-\frac{\sigma_1^2}{2} \cdot [u^2+v^2] - R_1(\tau)uv} \, dudv \quad . \tag{4.32}$$

Combining terms in the exponent of the integrand,

$$R_2(\tau) = \frac{(2L)^2}{4\pi^2} \int_{-\infty}^{\infty}\int_{-\infty}^{\infty} \frac{-1}{uv} \cdot e^{-\left(\frac{\sigma_g^2+\sigma_1^2}{2}\right)\cdot[u^2+v^2]-R_1(\tau)uv} \, dudv \quad . \tag{4.33}$$

To obtain an integrand without the factor $\frac{1}{u \cdot v}$, we differentiate $R_2(\tau)$ with respect to $R_1(\tau)$. Specifically,

$$\frac{dR_2(\tau)}{dR_1(\tau)} = \frac{(2L)^2}{4\pi^2} \int_{-\infty}^{\infty}\int_{-\infty}^{\infty} e^{-\left(\frac{\sigma_g^2+\sigma_1^2}{2}\right)\cdot[u^2+v^2]-R_1(\tau)uv} \, dudv \quad . \tag{4.34}$$

At this point, it is convenient to make the change of variables

$$x = \sqrt{\frac{\sigma_g^2+\sigma_1^2}{2}} \cdot u \qquad \text{and} \qquad y = \sqrt{\frac{\sigma_g^2+\sigma_1^2}{2}} \cdot v \quad . \tag{4.35}$$

This results in

$$\frac{dR_2(\tau)}{dR_1(\tau)} = \frac{(2L)^2}{4\pi^2} \frac{2}{\sigma_g^2+\sigma_1^2} \int_{-\infty}^{\infty}\int_{-\infty}^{\infty} e^{-(x^2+y^2)-\frac{2R_1(\tau)}{\sigma_g^2+\sigma_1^2}xy} \, dxdy \quad . \tag{4.36}$$

To further simplify the integrand, introduce the variable υ and γ such that

$$\begin{aligned} x = h(\upsilon,\gamma) &= \upsilon - \frac{a}{\sqrt{1-a^2}}\gamma \\ y = k(\upsilon,\gamma) &= \frac{1}{\sqrt{1-a^2}}\gamma \end{aligned} \tag{4.37}$$

where

$$a = \frac{R_1(\tau)}{\sigma_g^2 + \sigma_1^2} \cdot \tag{4.38}$$

Observe that

$$\upsilon = x + ay$$

$$\gamma = \sqrt{1-a^2}\cdot y \ . \tag{4.39}$$

The Jacobian of this transformation is given by

$$J(\upsilon,\gamma) = \begin{bmatrix} \frac{\partial h}{\partial \upsilon} & \frac{\partial h}{\partial \gamma} \\ \frac{\partial k}{\partial \upsilon} & \frac{\partial k}{\partial \gamma} \end{bmatrix} = \begin{bmatrix} 1 & \frac{-a}{\sqrt{1-a^2}} \\ 0 & \frac{1}{\sqrt{1-a^2}} \end{bmatrix} = \frac{1}{\sqrt{1-a^2}} \ . \tag{4.40}$$

Hence,

$$dxdy = \frac{1}{\sqrt{1-a^2}} d\upsilon d\gamma \ . \tag{4.41}$$

Utilizing the transformation of Eq.(4.37), the exponent of the integrand in Eq.(4.36) becomes

$$-[x^2+y^2+2axy] = -\left[\upsilon^2 - \frac{2a}{\sqrt{1-a^2}}\upsilon\gamma + \frac{a^2}{1-a^2}\gamma^2 + \frac{2a}{\sqrt{1-a^2}}\upsilon\gamma\right.$$

$$\left. + \frac{1}{1-a^2}\gamma^2 - \frac{2a^2}{1-a^2}\gamma^2\right] = -\left[\upsilon^2 + \frac{a^2+1-2a^2}{1-a^2}\gamma^2\right]$$

$$= -[\upsilon^2+\gamma^2] \ . \tag{4.42}$$

Thus, the expression for $\frac{dR_2(\tau)}{dR_1(\tau)}$ becomes

$$\frac{dR_2(\tau)}{dR_i(\tau)} = \frac{(2L)^2}{4\pi^2} \cdot \frac{2}{\sigma_g^2 + \sigma_1^2} \cdot \frac{1}{\sqrt{1-a^2}} \int_{-\infty}^{\infty}\int_{-\infty}^{\infty} e^{-[\upsilon^2+\gamma^2]} d\upsilon d\gamma \quad . \tag{4.43}$$

The double integral is readily evaluated to yield

$$\int_{-\infty}^{\infty}\int_{-\infty}^{\infty} e^{-[\upsilon^2+\gamma^2]} d\upsilon d\gamma = \pi \quad . \tag{4.44}$$

Consequently,

$$\frac{dR_2(\tau)}{dR_1(\tau)} = \frac{(2L)^2}{2\pi} \cdot \frac{1}{\sigma_g^2 + \sigma_1^2} \cdot \frac{1}{\sqrt{1-\left(\frac{R_1(\tau)}{\sigma_g^2+\sigma_1^2}\right)^2}} \quad . \tag{4.45}$$

Recalling that

$$\frac{d[\sin^{-1}u]}{dx} = \frac{1}{\sqrt{1-u^2}} \frac{du}{dx} \tag{4.46}$$

it follows that

$$R_2(\tau) = \frac{(2L)^2}{2\pi} \cdot \sin^{-1}\left[\frac{R_1(\tau)}{\sigma_g^2+\sigma_1^2}\right] + C \tag{4.47}$$

where C is a constant of integration. To evaluate C, consider the special case for which

$$\sigma_g^2 = \sigma_1^2 \quad \text{and} \quad \tau = 0 \; . \tag{4.48}$$

Then

$$R_1(0) = \sigma_1^2$$

and

$$R_2(0) = \frac{(2L)^2}{2\pi} \cdot \sin^{-1}\left[\frac{1}{2}\right] + C$$

$$= \frac{4L^2}{2\pi} \cdot \frac{\pi}{6} + C = \frac{L^2}{3} + C \quad . \tag{4.49}$$

Because $\sigma_g^2 = \sigma_1^2$, $\alpha = 1$. It follows that $p_2(r_2)$ is the uniform density function given by Eq.(4.14). As a result,

$$R_2(0) = E\left[r_2^2\right] = \int_{-L}^{L} \frac{r_2^2}{2L} dr_2 = \frac{1}{2L} \cdot \frac{r_2^3}{3}\Bigg|_{-L}^{L} = \frac{L^2}{3} \quad . \tag{4.50}$$

By comparison of Eqs.(4.49) and (4.50), it is concluded that C = 0. The output correlation function, therefore, is given by

$$R_2(\tau) = \frac{(2L)^2}{2\pi} \cdot \sin^{-1}\left[\frac{R_1(\tau)}{\sigma_g^2 + \sigma_1^2}\right] \quad . \tag{4.51}$$

Recalling that

$$\rho_1(\tau) = \frac{R_1(\tau)}{\sigma_1^2} \qquad \text{and} \qquad \alpha = \frac{\sigma_g}{\sigma_1}$$

$R_2(\tau)$ can also be expressed as

$$R_2(\tau) = \frac{(2L)^2}{2\pi} \cdot \sin^{-1}\left[\frac{\rho_1(\tau)}{1 + \alpha^2}\right] \quad . \tag{4.52}$$

4.3 Autocorrelation Function at the Output of the RF Amplifier (node 3 of Fig.2.1)

From Eq.(3.32) the RF amplifier output is

$$r_3(t) = \mathrm{Re}\left\{\tilde{r}_2(t)\Big|_{f_c} \cdot e^{j2\pi f_c t}\right\} \tag{4.53}$$

where $\hat{r}_2(t)\Big|_{f_c}$ is given by Eq.(3.30). By definition, the autocorrelation function of $r_3(t)$ is

$$R_3(t,\tau) = E[r_3(t) \cdot r_3(t-\tau)] \quad . \tag{4.54}$$

Following a development analogous to that which resulted in Eq.(4.2),

$$R_3(t,\tau) = \frac{1}{2} \cdot \mathrm{Re}\left\{E\left[\tilde{r}_2(t)\Big|_{f_c} \cdot \tilde{r}_2(t-\tau)\Big|_{f_c}\right] \cdot e^{j2\pi f_c(2t-\tau)}\right\}$$

$$+ \frac{1}{2} \cdot \mathrm{Re}\left\{E\left[\tilde{r}_2(t)\Big|_{f_c} \cdot \tilde{r}_2^{\,*}(t-\tau)\Big|_{f_c}\right] \cdot e^{j2\pi f_c \tau}\right\} \quad . \tag{4.55}$$

In Appendix B it is shown that

$$E\left[\tilde{r}_2(t)\Big|_{f_c} \cdot \tilde{r}_2(t-\tau)\Big|_{f_c}\right] = 0 \tag{4.56}$$

and $E\left[\tilde{r}_2(t)\Big|_{f_c} \cdot \tilde{r}_2^{\,*}(t-\tau)\Big|_{f_c}\right]$ is a function only of τ. Define

$$\tilde{R}_2(\tau)\Big|_{f_c} = E\left[\tilde{r}_2(t)\Big|_{f_c} \cdot \tilde{r}_2^{\,*}(t-\tau)\Big|_{f_c}\right] . \tag{4.57}$$

The expression for $R_3(t,\tau)$ then simplifies to

$$R_3(t,\tau) = R_3(\tau) = \frac{1}{2} \cdot \mathrm{Re}\{\tilde{R}_2(\tau)\big|_{f_c} e^{j2\pi f_c \tau}\} \quad . \tag{4.58}$$

4.4 Autocorrelation Function at the Mixer Output (node 5 of Fig.2.1)

As pointed out in section 3.3, the signal at the mixer output is a baseband signal given by

$$r_5(t) = \mathrm{Re}\{\tilde{r}_5(t)\} \tag{4.59}$$

where

$$\tilde{r}_5(t) = \frac{1}{2} \cdot \tilde{r}_2(t)\big|_{f_c} \quad . \tag{4.60}$$

The autocorrelation function of $r_5(t)$ is

$$R_5(t,\tau) = E[r_5(t) \cdot r_5(t-\tau)] = E\left[\mathrm{Re}\left\{\frac{\tilde{r}_2(t)\big|_{f_c}}{2}\right\} \cdot \mathrm{Re}\left\{\frac{\tilde{r}_2(t-\tau)\big|_{f_c}}{2}\right\}\right]$$

$$= \frac{1}{16} E\left\{\left[\tilde{r}_2(t)\big|_{f_c} + \tilde{r}_2^{\,*}(t)\big|_{f_c}\right]\left[\tilde{r}_2(t-\tau)\big|_{f_c} + \tilde{r}_2^{\,*}(t-\tau)\big|_{f_c}\right]\right\}$$

$$= \frac{1}{8} E\left\{\frac{\tilde{r}_2(t)\big|_{f_c}\tilde{r}_2(t-\tau)\big|_{f_c} + \tilde{r}_2^{\,*}(t)\big|_{f_c}\tilde{r}_2^{\,*}(t-\tau)\big|_{f_c}}{2}\right.$$

$$\left. + \frac{\tilde{r}_2(t)\big|_{f_c}\tilde{r}_2^{\,*}(t-\tau)\big|_{f_c} + \tilde{r}_2^{\,*}(t)\big|_{f_c}\tilde{r}_2(t-\tau)\big|_{f_c}}{2}\right\}$$

$$= \frac{1}{8}E\{Re\left[\tilde{r}_2(t)\Big|_{f_c}\tilde{r}_2(t-\tau)\Big|_{f_c}\right] + Re\left[\tilde{r}_2(t)\Big|_{f_c}\tilde{r}_2^{*}(t-\tau)\Big|_{f_c}\right]\}$$

$$= \frac{1}{8}Re\{E\left[\tilde{r}_2(t)\Big|_{f_c}\tilde{r}_2(t-\tau)\Big|_{f_c}\right] + E\left[\tilde{r}_2(t)\Big|_{f_c}\tilde{r}_2^{*}(t-\tau)\Big|_{f_c}\right]\} \quad . \tag{4.61}$$

As noted in section 4.3,

$$E\left[\tilde{r}_2(t)\Big|_{f_c}\cdot\tilde{r}_2(t-\tau)\Big|_{f_c}\right] = 0 \tag{4.62}$$

and $E\left[\tilde{r}_2(t)\Big|_{f_c}\cdot\tilde{r}_2^{*}(t-\tau)\Big|_{f_c}\right]$ is a function only of τ. With reference to Eq.(4.57), define

$$\tilde{R}_5(\tau) = \frac{1}{4}E\left[\tilde{r}_2(t)\Big|_{f_c}\cdot\tilde{r}_2^{*}(t-\tau)\Big|_{f_c}\right] = \frac{\tilde{R}_2(\tau)\Big|_{f_c}}{4} \quad . \tag{4.63}$$

It follows that

$$R_5(t,\tau) = R_5(\tau) = \frac{1}{2}Re\{\tilde{R}_5(\tau)\} = \frac{1}{8}Re\{\tilde{R}_2(\tau)\Big|_{f_c}\} \quad . \tag{4.64}$$

Equation (4.63) gives a direct relationship between the complex autocorrelation functions at the outputs of the mixer and zero-memory nonlinear amplifier.

Chapter 5

AUTOCORRELATION FUNCTION AT THE TRANSVERSAL FILTER INPUT FOR THE GAUSSIAN CASE

The results of Chapter 4 are used in this chapter to derive an expression for the complex autocorrelation function at the input to the transversal filter. If s(t), c(t) and n(t) denote the desired signal, clutter and noise, respectively, the received signal is given by

$$r_1(t) = s(t) + c(t) + n(t) \quad \bullet \tag{5.1}$$

The sum of clutter and noise is referred to as the disturbance, d(t). Thus,

$$d(t) = c(t) + n(t) \quad \bullet \tag{5.2}$$

The desired signal, clutter and noise are assumed to be statistically independent zero-mean Gaussian random processes. As a result, $r_1(t)$ is also a zero-mean Gaussian random process.

5.1 Autocorrelation Function at Receiver Input

Assuming stationarity, the autocorrelation function of the received signal is

$$R_1(\tau) = E[r_1(t) \cdot r_1(t-\tau)]$$

$$= E\{[s(t) + c(t) + n(t)] \cdot [s(t-\tau) + c(t-\tau) + n(t-\tau)]\} \quad \bullet \tag{5.3}$$

Because of statistical independence and zero-means, the expectations involving cross terms are zero. Therefore,

$$R_1(\tau) = R_s(\tau) + R_c(\tau) + R_n(\tau) \tag{5.4}$$

where

$$R_s(\tau) = E[s(t) \cdot s(t-\tau)]$$

$$R_c(\tau) = E[c(t) \cdot c(t-\tau)] \qquad (5.5)$$

$$R_n(\tau) = E[n(t) \cdot n(t-\tau)] \quad .$$

The desired signal, clutter and noise can be expressed in terms of their complex envelopes as

$$s(t) = Re\{\tilde{s}(t) \cdot e^{j2\pi f_c t}\}$$

$$c(t) = Re\{\tilde{c}(t) \cdot e^{j2\pi f_c t}\} \qquad (5.6)$$

$$n(t) = Re\{\tilde{n}(t) \cdot e^{j2\pi f_c t}\} \quad .$$

Following the same derivation which was used to obtain Eq.(4.5) from Eq.(4.1), the various autocorrelation functions are related to their complex autocorrelation functions by

$$R_s(\tau) = \frac{1}{2} \cdot Re\{\tilde{R}_s(\tau) \cdot e^{j2\pi f_c \tau}\}$$

$$R_c(\tau) = \frac{1}{2} \cdot Re\{\tilde{R}_c(\tau) \cdot e^{j2\pi f_c \tau}\} \qquad (5.7)$$

$$R_n(\tau) = \frac{1}{2} \cdot Re\{\tilde{R}_n(\tau) \cdot e^{j2\pi f_c \tau}\}$$

where

$$\tilde{R}_s(\tau) = E[\tilde{s}(t) \cdot \tilde{s}^*(t-\tau)]$$

$$\tilde{R}_c(\tau) = E[\tilde{c}(t) \cdot \tilde{c}^*(t-\tau)] \qquad (5.8)$$

$$\tilde{R}_n(\tau) = E[\tilde{n}(t) \cdot \tilde{n}^*(t-\tau)] \quad .$$

Substitution of Eqs (5.7) into (5.4) results in

$$R_1(\tau) = \frac{1}{2} \cdot Re\{\tilde{R}_1(\tau) \cdot e^{j2\pi f_c t}\}$$

$$= \frac{1}{2} \cdot Re\{[\tilde{R}_s(\tau) + \tilde{R}_c(\tau) + \tilde{R}_n(\tau)] \cdot e^{j2\pi f_c t}\} \quad . \qquad (5.9)$$

It follows that

$$\tilde{R}_1(\tau) = \tilde{R}_s(\tau) + \tilde{R}_c(\tau) + \tilde{R}_n(\tau) \quad . \qquad (5.10)$$

From Eq.(3.5) the complex envelope of the desired signal is

$$\tilde{s}(t) = a_s(t) \cdot e^{j(2\pi f_D t + \theta_s)} \quad .$$

Thus, the complex autocorrelation function of $\tilde{s}(t)$ is

$$\tilde{R}_s(\tau) = E\{a_s(t) \cdot e^{j(2\pi f_D t + \theta_s)} \cdot a_s(t-\tau) \cdot e^{-j[2\pi f_D (t-\tau) + \theta_s]}\}$$

$$= E[a_s(t) \cdot a_s(t-\tau)] e^{j2\pi f_D \tau} \quad . \qquad (5.11)$$

Assuming the fading to be constant during the interval over which the N pulses from a given range cell are received, $a_s(t)$ can be approximated by a random constant A which is Rayleigh distributed. Hence,

$$E[a_s(t) \cdot a_s(t-\tau)] = E[A^2] \quad . \tag{5.12}$$

Use of Eq.(5.12) in Eq.(5.11) results in

$$\tilde{R}_s(\tau) = E[A^2] \cdot e^{j2\pi f_D \tau} \quad . \tag{5.13}$$

Let σ_s^2 denote the variance of s(t). From Eqs (5.7) and (5.13) note that

$$R_s(0) = \sigma_s^2 = \frac{1}{2} Re\{\tilde{R}_s(0)\} = \frac{E[A^2]}{2} \quad . \tag{5.14}$$

Therefore,

$$E[A^2] = 2\sigma_s^2 \quad . \tag{5.15}$$

Consequently, the complex autocorrelation function of s(t) becomes

$$\tilde{R}_s(\tau) = 2\sigma_s^2 \cdot e^{j2\pi f_D \tau} \quad . \tag{5.16}$$

Substitution of Eq.(5.16) into Eq.(5.7) results in

$$R_s(\tau) = 2\sigma_s^2 \cdot \cos[2\pi (f_c + f_D)\tau] \quad . \tag{5.17}$$

As shown in Fig.5.1, the clutter power spectral density is assumed to be Gaussian shaped around the carrier frequency. Consequently, the autocorrelation function of the clutter is modeled as

$$R_c(\tau) = \sigma_c^2 \cdot e^{-\frac{\tau^2}{2\sigma_w^2}} \cdot \cos(2\pi f_c \tau) \quad . \tag{5.18}$$

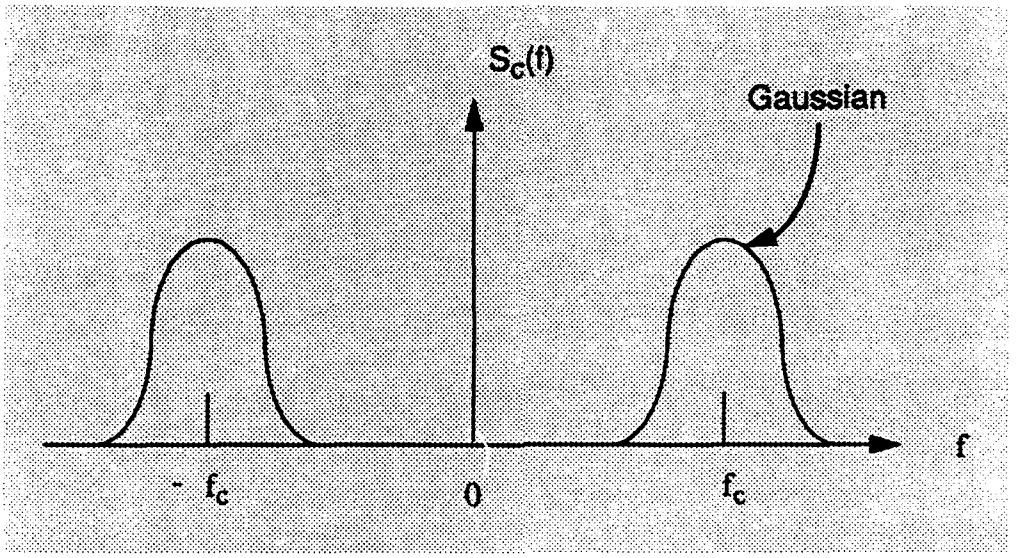

Figure 5.1 - Gaussian shaped clutter spectrum.

The corresponding power spectral density is

$$S_c(f) = \begin{cases} \sigma_c^2 \cdot \sqrt{2\pi\sigma_w^2} \cdot e^{-2\left[\pi\sigma_w (f - f_c)\right]^2} & ; f \geq 0 \\ \sigma_c^2 \cdot \sqrt{2\pi\sigma_w^2} \cdot e^{-2\left[\pi\sigma_w (f + f_c)\right]^2} & ; f \leq 0 \end{cases} \quad \text{(5.19)}$$

Note that

$$\sigma_c^2 = R_c(0) \quad \text{(5.20)}$$

is the variance of c(t). Also, σ_w^2 is the variance of the Gaussian function used to model the clutter autocorrelation function envelope. As such, it is a measure of the width of the clutter autocorrelation function. The larger is σ_w^2, the wider is the clutter autocorrelation function and the narrower is the clutter power spectral density. $R_c(\tau)$ can be expressed as

$$R_c(\tau) = Re\left\{\sigma_c^2 \cdot e^{-\frac{\tau^2}{2\sigma_w^2}} \cdot e^{j2\pi f_c \tau}\right\} . \quad \text{(5.21)}$$

Comparison of Eq.(5.21) with Eq.(5.7) results in

$$\tilde{R}_c(\tau) = 2\sigma_c^2 \cdot e^{-\frac{\tau^2}{2\sigma_w^2}} \quad . \tag{5.22}$$

The additive noise is assumed to be bandlimited white noise. Hence, its power spectral density is a constant over a band of frequencies of width W centered at $\pm f_c$, as seen in Fig.5.2. The corresponding autocorrelation function is

$$R_n(\tau) = \int_{-\infty}^{\infty} S_n(f) \cdot e^{j2\pi f\tau} df = \sigma_n^2 \cdot \frac{\sin(\pi W\tau)}{\pi W\tau} \cdot \cos(2\pi f_c\tau) \quad . \tag{5.23}$$

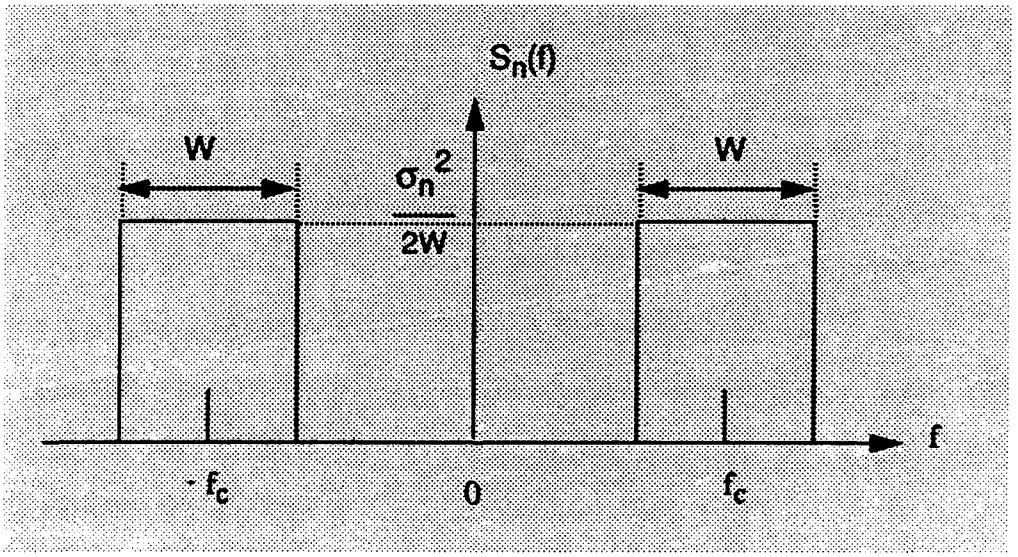

Figure 5.2 - Constant noise spectrum.

This can be rewritten as

$$R_n(\tau) = Re\{\sigma_n^2 \cdot \frac{\sin(\pi W\tau)}{\pi W\tau} \cdot e^{j2\pi f_c\tau}\} \quad . \tag{5.24}$$

By comparing Eqs(5.7) and (5.24), it follows that

$$\tilde{R}_n(\tau) = 2\sigma_n^2 \cdot \frac{\sin(\pi W\tau)}{\pi W\tau} \quad . \tag{5.25}$$

Combining the expressions for $\tilde{R}_s(\tau)$, $\tilde{R}_c(\tau)$ and $\tilde{R}_n(\tau)$, we obtain

$$\tilde{R}_1(\tau) = 2\sigma_s^2 \cdot e^{j2\pi f_D \tau} + 2\sigma_c^2 \cdot e^{-\frac{\tau^2}{2\sigma_w^2}} + 2\sigma_n^2 \cdot \frac{\sin(\pi W\tau)}{\pi W\tau} \quad . \tag{5.26}$$

5.2 Autocorrelation Function at the RF Amplifier Output

The autocorrelation function at the nonlinear amplifier output (node 2 of Fig.2.2) was derived in section 4.2. It is expressed in Eq.(4.52) as

$$R_2(\tau) = \frac{(2L)^2}{2\pi} \cdot \sin^{-1}\left[\frac{\rho_1(\tau)}{1+\alpha^2}\right] \tag{5.27}$$

where

$$\rho_1(\tau) = \frac{R_1(\tau)}{\sigma_1^2} \tag{5.28}$$

and

$$\alpha = \frac{\sigma_g}{\sigma_1} \quad . \tag{5.29}$$

Since $\sin^{-1}(x)$ is continuous and single-valued and has all derivatives on an interval including $x = 0$, it can be expanded in a Mac Laurin's series at $x = 0$. The

series expansion of Eq.(5.27) is

$$R_2(\tau) = \frac{(2L)^2}{2\pi} \sum_{k=0}^{\infty} b_k \cdot \left[\frac{\rho_1(\tau)}{1+\alpha^2}\right]^{2k+1} \tag{5.30}$$

where the k^{th} coefficient is

$$b_k = \begin{cases} 1 & ; k = 0 \\ \dfrac{1 \cdot 3 \cdot 5 \ldots\ldots (2k-1)}{2 \cdot 4 \cdot 6 \ldots\ldots (2k)\,(2k+1)} & ; k > o \end{cases} . \tag{5.31}$$

Substitution of Eq.(5.9) into (5.28) results in

$$\rho_1(\tau) = \frac{1}{2\sigma_1^2} \mathrm{Re}\{\tilde{R}_1(\tau) \cdot e^{j2\pi f_c \tau}\}$$

$$= \frac{1}{2\sigma_1^2} \cdot \frac{\tilde{R}_1(\tau) \cdot e^{j2\pi f_c \tau} + \tilde{R}_1^{*}(\tau) \cdot e^{-j2\pi f_c \tau}}{2} . \tag{5.32}$$

Consequently, the series expansion for $R_2(\tau)$ becomes

$$R_2(\tau) = \frac{(2L)^2}{2\pi} \sum_{k=0}^{\infty} b_k \cdot \left[\frac{1/(2\sigma_1^2)}{1+\alpha^2}\right]^{2k+1} \cdot$$

$$\left[\frac{\tilde{R}_1(\tau) \cdot e^{j2\pi f_c \tau} + \tilde{R}_1^{*}(\tau) \cdot e^{-j2\pi f_c \tau}}{2}\right]^{2k+1} . \tag{5.33}$$

Following the same development used to obtain Eq.(3.29) from Eqs (3.11) and (3.14), it follows that

$$R_2(\tau) = \frac{(2L)^2}{2\pi} \sum_{k=0}^{\infty} b_k \cdot \frac{C_k^{2k+1}}{2^{2k}} \cdot \left[\frac{1/(2\sigma_1^2)}{1+\alpha^2} \right]^{2k+1} \cdot \left| \tilde{R}_1(\tau) \right|^{2k}$$

$$\cdot \ \mathrm{Re}\{\tilde{R}_1(\tau) \cdot e^{j2\pi f_c \tau}\} + \Delta R_2(\tau) \qquad (5.34)$$

where $\Delta R_2(\tau)$ denotes the terms in $R_2(\tau)$ corresponding to the spectral zones other than those centered at $\pm f_c$. Define the complex envelope

$$\tilde{R}_2(\tau)\Big|_{f_c} = \frac{(2L)^2}{\pi} \sum_{k=0}^{\infty} b_k \cdot \frac{C_k^{2k+1}}{2^{2k}} \cdot \left[\frac{1/(2\sigma_1^2)}{1+\alpha^2} \right]^{2k+1}$$

$$\cdot \ \left| \tilde{R}_1(\tau) \right|^{2k} \cdot \tilde{R}_1(\tau) \ . \qquad (5.35)$$

It is then possible to express the autocorrelation function at the nonlinear amplifier output as

$$R_2(\tau) = \frac{1}{2} \mathrm{Re}\{\tilde{R}_2(\tau)\Big|_{f_c} \cdot e^{j2\pi f_c \tau}\} + \Delta R_2(\tau) \ . \qquad (5.36)$$

The bandpass filter following the nonlinear amplifier is assumed to have the ideal transfer function whose magnitude is shown in Fig.2.4. The bandwidth B_{RF} is assumed to be narrow enough such that only the spectral zones at $\pm f_c$ are passed with negligible distortion. The remaining spectral zones are assumed to be perfectly attenuated. It follows that the autocorrelation function at the RF amplifier output is given by

$$R_3(\tau) = \frac{1}{2} \mathrm{Re}\{\tilde{R}_2(\tau)\Big|_{f_c} \cdot e^{j2\pi f_c \tau}\} \ . \qquad (5.37)$$

5.3 Autocorrelation Function at the Transversal Filter Input

From Eq.(4.63) the complex autocorrelation function at the transversal filter input is

$$\tilde{R}_5(\tau) = \frac{\tilde{R}_2(\tau)\big|_{f_c}}{4} \cdot \tag{5.38}$$

Substitution of Eq.(5.35) into Eq.(5.38) yields

$$\tilde{R}_5(\tau) = \frac{(2L)^2}{2\pi} \sum_{k=0}^{\infty} b_k \cdot \frac{C_k^{2k+1}}{2^{2k+1}} \cdot \left[\frac{1/(2\sigma_1^2)}{1+\alpha^2}\right]^{2k+1} \cdot \left|\tilde{R}_1(\tau)\right|^{2k} \cdot \tilde{R}_1(\tau) \cdot \tag{5.39}$$

It should be recalled that the above result is valid only for the case of Gaussian signals at the receiver input.

5.4 Autocorrelation Function Considerations for the Ideal Linear Receiver

The ideal linear receiver provides a basis of comparison for performance of the nonlinear receiver. As explained in Chapter 2, the receiver nonlinear behavior is assumed to be confined to the RF amplifier. For small enough inputs the nonlinear amplifier behaves in a linear fashion. As given by Eq.(2.3), the linear gain of the RF amplifier is

$$G = \sqrt{\frac{2}{\pi}} \cdot \frac{L}{\sigma_g} \tag{5.40}$$

where G is the slope of the nonlinear input-output characteristic evaluated at the origin. Consequently, the RF amplifier output in the equivalent ideal linear receiver

is modeled as

$$r_3(t) = r_2(t) = G \cdot r_1(t) = \mathrm{Re}\{G \cdot \tilde{r}_1(t) \cdot e^{j2\pi f_c t}\} \quad . \qquad (5.41)$$

It follows that the complex envelopes of $r_3(t)$ and $r_2(t)$ are given by

$$\tilde{r}_3(t) = \tilde{r}_2(t) = G \cdot \tilde{r}_1(t) \quad . \qquad (5.42)$$

The complex autocorrelation function at the RF amplifier output is

$$\tilde{R}_3(\tau) = \tilde{R}_2(\tau) = E[\tilde{r}_3(t) \cdot \tilde{r}_3^{*}(t-\tau)]$$

$$= G^2 \cdot E[\tilde{r}_1(t) \cdot \tilde{r}_1^{*}(t-\tau)] = G^2 \cdot \tilde{R}_1(\tau) \quad . \qquad (5.43)$$

Using the result of Eq.(5.26), we obtain

$$\tilde{R}_3(\tau) = \tilde{R}_2(\tau)$$

$$= 2G^2 \cdot \left[\sigma_s^2 \cdot e^{j2\pi f_D \tau} + \sigma_c^2 \cdot e^{-\frac{\tau^2}{2\sigma_w^2}} + \sigma_n^2 \cdot \frac{\sin(\pi W \tau)}{\pi W \tau} \right] \quad . \qquad (5.44)$$

When the RF amplifier is linear, the only spectral zones in Fig.3.4 occur at $\pm f_c$. Hence,

$$\tilde{R}_2(\tau)\Big|_{f_c} = \tilde{R}_2(\tau) \quad . \qquad (5.45)$$

With reference to Eqs (4.63), (5.44), and (5.45), it is concluded that the complex

auto-correlation function at the transversal filter input is given by

$$\tilde{R}_5(\tau) = \frac{\tilde{R}_2(\tau)}{4}$$

$$= \frac{G^2}{2} \cdot \left[\sigma_s^2 \cdot e^{j2\pi f_D \tau} + \sigma_c^2 \cdot e^{-\frac{\tau^2}{2\sigma_w^2}} + \sigma_n^2 \cdot \frac{\sin(\pi W \tau)}{\pi W \tau} \right] . \qquad (5.46)$$

Chapter 6

SIGNAL-TO-DISTURBANCE RATIO AT THE TRANSVERSAL FILTER OUTPUT

One means for assessing radar performance degradation due to the nonlinear receiver behavior is to evaluate the signal-to-disturbance ratio at the transversal filter output. Analytical expressions for the signal-to-disturbance ratio are obtained in this chapter for both the linear and nonlinear receivers modeled previously. The transversal filter weights are then optimized to maximize the signal-to-disturbance ratios for the following cases :

Case I - an ideal linear receiver,

Case II - a nonlinear receiver having the same transversal filter as was used with the ideal linear receiver,

Case III - a nonlinear receiver with the transversal filter optimized to account for the receiver nonlinearity.

Case II can arise when the design engineer either does not know of the nonlinearities within the receiver or does not care to compensate for these nonlinearities.

6.1 Output Signal-to-Disturbance Ratio for the Ideal Linear Receiver

Consider the ideal linear receiver of section 5.4. A block diagram of the transversal filter is shown in Fig.2.6. Let the transpose of the transversal filter weight vector be

$$\underline{\tilde{w}}^T = [\tilde{w}_1 \tilde{w}_2 \ldots\ldots \tilde{w}_N] \quad . \tag{6.1}$$

The complex envelope of the transversal filter input is denoted by $\tilde{r}_5(t)$. Let

$$\tilde{r}_5[(N-k+1)T_s] = \tilde{r}_{5k} \quad ; k = 1,2, \ldots\ldots\ldots, N \; . \tag{6.2}$$

At time t = NTs, the complex envelope of the transversal filter output is then given by

$$\tilde{r}_6(NT_s) = (\underline{\tilde{w}}^*)^T \underline{\tilde{r}}_5 \tag{6.3}$$

where

$$\underline{\tilde{r}}_5 = [\tilde{r}_{51}\tilde{r}_{52}.....\tilde{r}_{5N}] \quad \bullet \tag{6.4}$$

Noting that $\tilde{r}_6(NT_s)$ is a scalar quantity, its transpose is equal to itself. Hence, the average power in $\tilde{r}_6(NT_s)$ can be expressed as

$$\begin{aligned} E\left[\left|\tilde{r}_6(NT_s)\right|^2\right] &= E[\tilde{r}_6(NT_s)\cdot\tilde{r}_6^*(NT_s)] \\ &= E\left[\tilde{r}_6(NT_s)\cdot(\underline{\tilde{r}}_6^*(NT_s))^T\right] \\ &= E\left[(\underline{\tilde{w}}^*)^T\underline{\tilde{r}}_5\cdot(\underline{\tilde{r}}_5^*)^T\underline{\tilde{w}}\right] \\ &= (\underline{\tilde{w}}^*)^T E\left[\underline{\tilde{r}}_5\cdot(\underline{\tilde{r}}_5^*)^T\right]\underline{\tilde{w}} \\ &= (\underline{\tilde{w}}^*)^T\cdot M^L\cdot\underline{\tilde{w}} \end{aligned} \tag{6.5}$$

where the correlation matrix

$$M^L = E\left[\underline{\tilde{r}}_5\cdot(\underline{\tilde{r}}_5^*)^T\right] \tag{6.6}$$

is an (N x N) Hermitian matrix. The superscript L is used to indicate that the analysis in this section is for the ideal linear receiver.

The entries in the matrix M^L are readily determined from the complex autocorrelation function $\tilde{R}_5(\tau)$, as is shown next. By definition,

$$M^L = E\left[\tilde{r}_5 \cdot (\tilde{r}_5^*)^T\right] = E\left\{\begin{bmatrix}\tilde{r}_{51}\\ \vdots \\ \tilde{r}_{5N}\end{bmatrix}\left[\tilde{r}_{51} \ldots \tilde{r}_{5N}\right]\right\}$$

$$= \begin{bmatrix} E(|\tilde{r}_{51}|^2) & E(\tilde{r}_{51}\tilde{r}_{52}^*) \cdots\cdots\cdots E(\tilde{r}_{51}\tilde{r}_{5N}^*) \\ E(\tilde{r}_{52}\tilde{r}_{51}^*) & E(|\tilde{r}_{52}|^2) \cdots\cdots\cdots E(\tilde{r}_{52}\tilde{r}_{5N}^*) \\ \cdots\cdots\cdots\cdots\cdots\cdots\cdots\cdots\cdots\cdots\cdots\cdots\cdots\cdots\cdots\cdots \\ E(\tilde{r}_{5N}\tilde{r}_{51}^*) & E(\tilde{r}_{5N}\tilde{r}_{52}^*) \cdots\cdots\cdots E(|\tilde{r}_{5N}|^2) \end{bmatrix} . \quad (6.7)$$

The uv^{th} element in M^L is given by

$$(M^L)_{uv} = E(\tilde{r}_{5u}\tilde{r}_{5v}^*) = E\{\tilde{r}_5[(N-u+1)T_s] \cdot \tilde{r}_5^*[(N-v+1)T_s]\}$$

$$= \tilde{R}_5[(v-u)T_s] . \quad (6.8)$$

Recognizing that

$$\tilde{R}_5[(u-v)T_s] = \tilde{R}_5^*[(v-u)T_s] , \quad (6.9)$$

it follows that

$$M^L = \begin{bmatrix} \tilde{R}_5(0) & \tilde{R}_5(T_s) & \cdots\cdots\cdots \tilde{R}_5[(N-1)T_s] \\ \tilde{R}_5^*(T_s) & \tilde{R}_5(0) & \cdots\cdots\cdots \tilde{R}_5[(N-2)T_s] \\ & \cdots\cdots\cdots\cdots\cdots\cdots\cdots\cdots\cdots\cdots\cdots\cdots\cdots\cdots & \\ \tilde{R}_5^*[(N-1)T_s] & \tilde{R}_5^*[(N-2)T_s] \cdots\cdots\cdots & \tilde{R}_5(0) \end{bmatrix} . \quad (6.10)$$

With reference to Eq.(5.46), note that

$$(M^L)_{uv} = \tilde{R}_5[(v-u)T_s] = \frac{G^2}{2}\cdot\left[\sigma_s^2\cdot e^{j2\pi f_D(v-u)T_s}\right.$$

$$\left. + \sigma_c^2\cdot e^{-\frac{((v-u)T_s)^2}{2\sigma_w^2}} + \sigma_n^2\cdot\frac{\sin(\pi W(v-u)T_s)}{\pi W(v-u)T_s}\right] . \quad (6.11)$$

The desired signal term in $(M^L)_{uv}$ is readily recognized to be

$$(M_s^L)_{uv} = \frac{G^2\sigma_s^2}{2}\cdot e^{j2\pi f_D(v-u)T_s} \quad (6.12)$$

whereas the disturbance term is

$$(M_d^L)_{uv} = \frac{G^2}{2}\left[\sigma_c^2\cdot e^{-\frac{((v-u)T_s)^2}{2\sigma_w^2}} + \sigma_n^2\cdot\frac{\sin(\pi W(v-u)T_s)}{\pi W(v-u)T_s}\right] . \quad (6.13)$$

Consequently, the matrix M^L can be decomposed as

$$M^L = M_s^L + M_d^L \quad (6.14)$$

where $(M^L{}_s)_{uv}$ and $(M^L{}_d)_{uv}$ are the uv^{th} elements of $M^L{}_s$ and $M^L{}_d$, respectively. When Eq.(6.14) is substituted into Eq.(6.5), the average power in $\tilde{r}_6(NT_s)$ becomes

$$E\left[\left|\tilde{r}_6(NT_s)\right|^2\right] = (\tilde{\underline{w}}^*)^T M_s^L \tilde{\underline{w}} + (\tilde{\underline{w}}^*)^T M_d^L \tilde{\underline{w}} \quad . \tag{6.15}$$

The signal power is defined to be

$$S = (\tilde{\underline{w}}^*)^T M_s^L \tilde{\underline{w}} \quad . \tag{6.16}$$

Also, by definition, the disturbance power is given by

$$D = (\tilde{\underline{w}}^*)^T M_d^L \tilde{\underline{w}} \quad . \tag{6.17}$$

As a result, the output signal-to-disturbance ratio for the ideal linear receiver is

$$(SDR)_I = \frac{(\tilde{\underline{w}}^*)^T M_s^L \tilde{\underline{w}}}{(\tilde{\underline{w}}^*)^T M_d^L \tilde{\underline{w}}} \quad . \tag{6.18}$$

6.2 Output Signal-to-Disturbance Ratio for the Nonlinear Receiver

Having determined the output signal-to-disturbance ratio for the ideal linear receiver, the nonlinear receiver is treated next. Following the same development as in section 6.1, the average power in the complex envelope of the transversal filter output, sampled at time $t = NT_s$, is

$$E\left[\left|\tilde{r}_6(NT_s)\right|^2\right] = (\tilde{\underline{w}}^*)^T M^{NL} \tilde{\underline{w}} \tag{6.19}$$

where

$$M^{NL} = E\left[\tilde{r}_5 \cdot (\tilde{r}_5^*)^T\right] \tag{6.20}$$

is an (N x N) Hermitian matrix. The superscript NL is used to indicate that the analysis in this section is for the nonlinear receiver. The uv^{th} element in the matrix M^{NL} is

$$(M^{NL})_{uv} = \tilde{R}_5[(v-u)T_s] \tag{6.21}$$

where $\tilde{R}_5(\tau)$ is the complex autocorrelation function at the transversal filter input. From Eq.(5.39)

$$\tilde{R}_5(\tau) = \frac{(2L)^2}{2\pi} \sum_{k=0}^{\infty} b_k \cdot \frac{C_k^{2k+1}}{2^{2k+1}} \cdot \left[\frac{1/(2\sigma_1^2)}{1+\alpha^2}\right]^{2k+1} \cdot \left|\tilde{R}_1(\tau)\right|^{2k} \cdot \tilde{R}_1(\tau) \quad . \tag{6.22}$$

In terms of the linear gain of the RF amplifier, note that

$$\frac{(2L)^2}{2\pi} = G^2\sigma_g^2 \quad . \tag{6.23}$$

Hence, $\tilde{R}_5(\tau)$ can be written as

$$\tilde{R}_5(\tau) = G^2\sigma_g^2 \sum_{k=0}^{\infty} b_k \cdot \frac{C_k^{2k+1}}{2^{2k+1}} \cdot \left[\frac{1/(2\sigma_1^2)}{1+\alpha^2}\right]^{2k+1} \cdot \left|\tilde{R}_1(\tau)\right|^{2k} \cdot \tilde{R}_1(\tau) \quad . \tag{6.24}$$

From Eq.(5.26)

$$\tilde{R}_1(\tau) = 2\left[\sigma_s^2 \cdot e^{j2\pi f_D \tau} + \sigma_c^2 \cdot e^{-\frac{\tau^2}{2\sigma_w^2}} + \sigma_n^2 \cdot \frac{\sin(\pi W\tau)}{\pi W\tau}\right] \quad . \tag{6.25}$$

The desired signal term in $\tilde{R}_5(\tau)$ is obtained by retaining only the desired signal term in $\tilde{R}_1(\tau)$. This is equivalent to evaluating $\tilde{R}_1(\tau)$ when the disturbance is absent. In particular, the desired signal term in $\tilde{R}_1(\tau)$ is

$$\tilde{R}_1(\tau)\Big|_{d(t)=0} = 2\sigma_s^2 \cdot e^{j2\pi f_D \tau} \quad . \tag{6.26}$$

Note that

$$\left|\tilde{R}_1(\tau)\Big|_{d(t)=0}\right|^{2k} = (2\sigma_s^2)^{2k} \quad . \tag{6.27}$$

It follows that the desired signal term in $\tilde{R}_5(\tau)$ is given by

$$\tilde{R}_5(\tau)\Big|_{d(t)=0} = G^2\sigma_g^2 \sum_{k=0}^{\infty} b_k \cdot \frac{C_k^{2k+1}}{2^{2k+1}} \cdot \left[\frac{1/(2\sigma_1^2)}{1+\alpha^2}\right]^{2k+1}$$

$$\cdot (2\sigma_s^2)^{2k+1} \cdot e^{j2\pi f_D \tau} \quad . \tag{6.28}$$

As a result, the desired signal term in $(M^{NL})_{uv}$ is

$$(M_s^{NL})_{uv} = G^2\sigma_g^2 \sum_{k=0}^{\infty} b_k \cdot \frac{C_k^{2k+1}}{2^{2k+1}} \cdot \left[\frac{1/(2\sigma_1^2)}{1+\alpha^2}\right]^{2k+1}$$

$$(2\sigma_s^2)^{2k+1} \cdot e^{j2\pi f_D (v-u) T_s} \quad . \tag{6.29}$$

With this approach, observe that (signal x signal) cross terms which arise due to the nonlinearity are treated as desired signal components since they all contribute to the Doppler component evaluated at $\tau = (v-u)T_s$.

As a check, it is now shown that the k = 0 term reduces to Eq.(6.12) for the linear receiver. From Eqs.(3.16) and (5.31) note that

$$C_0^1 = b_0 = 1 \quad . \tag{6.30}$$

Hence, the k = 0 term in Eq.(6.29) is

$$(M_s^{NL})_{uv}\Big|_{k=0} = \frac{G^2\sigma_g^2}{2} \cdot \left[\frac{1/(2\sigma_1^2)}{1+\alpha^2}\right] \cdot 2\sigma_s^2 \cdot e^{j2\pi f_D (v-u) T_s} \quad . \tag{6.31}$$

However, α is defined in Eq.(4.12) as the ratio of σ_g to σ_1. Therefore,

$$(M_s^{NL})_{uv}\Big|_{k=0} = \frac{G^2\sigma_g^2}{2} \cdot \frac{1}{2\sigma_1^2} \cdot \frac{\sigma_1^2}{\sigma_1^2+\sigma_g^2} \cdot 2\sigma_s^2 \cdot e^{j2\pi f_D (v-u) T_s} \quad . \tag{6.32}$$

The receiver behaves in a linear fashion when $\sigma_1^2 \ll \sigma_g^2$. Using this inequality, it follows that

$$(M_s^{NL})_{uv}\Big|_{k=0} = \frac{G^2\sigma_s^2}{2} \cdot e^{j2\pi f_D (v-u) T_s} = (M_s^L)_{uv} \quad . \tag{6.33}$$

As expected, the linear result is a special case of the nonlinear result.

The disturbance term in $(M_d^{NL})_{uv}$ is simply obtained by substracting $(M_s^{NL})_{uv}$ from $(M^{NL})_{uv}$. This is valid because $(M^{NL})_{uv}$ is composed of (signal x signal) cross terms plus (signal x disturbance) cross terms plus (disturbance x disturbance) cross terms. By subtracting the (signal x signal) cross terms,we are left

with the disturbance terms which are given by

$$(M_d^{NL})_{uv} = (M^{NL})_{uv} - (M_s^{NL})_{uv} \quad . \tag{6.34}$$

Let $(M_s^{NL})_{uv}$ and $(M_d^{NL})_{uv}$ be the uv^{th} elements of the matrices M_s^{NL} and M_d^{NL}, respectively. Then

$$M^{NL} = M_s^{NL} + M_d^{NL} \quad . \tag{6.35}$$

Substitution of Eq.(6.35) into Eq.(6.19) results in

$$E\left[\left|\tilde{r}_6(NT_s)\right|^2\right] = (\tilde{\underline{w}}^*)^T M_s^{NL} \tilde{\underline{w}} + (\tilde{\underline{w}}^*)^T M_d^{NL} \tilde{\underline{w}} \quad . \tag{6.36}$$

The signal and disturbance powers are defined to be

$$S = (\tilde{\underline{w}}^*)^T M_s^{NL} \tilde{\underline{w}} \tag{6.37}$$

and

$$D = (\tilde{\underline{w}}^*)^T M_d^{NL} \tilde{\underline{w}} \quad . \tag{6.38}$$

Consequently, the output signal-to-disturbance ratio for the nonlinear receiver is

$$(SDR)_{NL} = \frac{(\tilde{\underline{w}}^*)^T M_s^{NL} \tilde{\underline{w}}}{(\tilde{\underline{w}}^*)^T M_d^{NL} \tilde{\underline{w}}} \quad . \tag{6.39}$$

The uv^{th} elements in the matrices M^{NL},M_s^{NL} and M_d^{NL} consist of infinite series. Evaluation of these elements raises the question of how many terms should be summed in order to obtain an adequate approximation. From Eqs (6.21) and (6.24)

$$(M^{NL})_{uv} = G^2\sigma_g^2 \sum_{k=0}^{\infty} b_k \cdot \frac{C_k^{2k+1}}{2^{2k+1}} \cdot \left[\frac{1/(2\sigma_1^2)}{1+\alpha^2}\right]^{2k+1}$$

$$\cdot \left|\tilde{R}_1[(v-u)T_s]\right|^{2k} \cdot \tilde{R}_1[(v-u)T_s] \quad . \quad (6.40)$$

Since the magnitude of a sum is less than or equal to the sum of the magnitudes,

$$\left|(M^{NL})_{uv}\right| \le G^2\sigma_g^2 \sum_{k=0}^{\infty} b_k \cdot \frac{C_k^{2k+1}}{2^{2k+1}} \cdot \left[\frac{1/(2\sigma_1^2)}{1+\alpha^2}\right]^{2k+1}$$

$$\cdot \left|\tilde{R}_1[(v-u)T_s]\right|^{2k+1} . \quad (6.41)$$

In addition, with reference to Eq.(5.26),

$$\left|\tilde{R}_1[(v-u)T_s]\right| \le 2\left[\sigma_s^2 + \sigma_c^2 + \sigma_n^2\right] . \quad (6.42)$$

Because the desired signal, clutter and noise are assumed to have zero means, their variances are given by

$$R_s(0) = \sigma_s^2, R_c(0) = \sigma_c^2, R_n(0) = \sigma_n^2 \quad . \quad (6.43)$$

From Eq.(5.4) it follows that the variance of the input signal $r_1(t)$ is

$$\sigma_1^2 = R_1(0) = \sigma_s^2 + \sigma_c^2 + \sigma_n^2 \quad . \quad (6.44)$$

Consequently, the inequality in Eq.(6.42) becomes

$$\left|\tilde{R}_1 [(v-u) T_s]\right| \le 2\sigma_1^2 \quad . \tag{6.45}$$

Use of Eq.(6.45) in Eq.(6.41) results in

$$\left|(M^{NL})_{uv}\right| \le G^2 \sigma_g^2 \sum_{k=0}^{\infty} b_k \cdot \frac{C_k^{2k+1}}{2^{2k+1}} \cdot \left[\frac{1}{1+\alpha^2}\right]^{2k+1} \quad . \tag{6.46}$$

Relative to the infinite series in Eq.(6.46), define the finite series

$$T(M) = \sum_{k=0}^{M} b_k \cdot \frac{C_k^{2k+1}}{2^{2k+1}} \cdot \left[\frac{1}{1+\alpha^2}\right]^{2k+1} \quad . \tag{6.47}$$

Values of T(M) are tabulated in Table 6.1 as a function of α and M. $\alpha = 0.05$ corresponds to the situation where the rms value of the input equals twenty times the linear range of the nonlinearity, as determined in Eq.(2.7). Assuming it is unlikely that the nonlinearity will be driven harder, we only consider

$$\alpha \ge 0.05 \quad . \tag{6.48}$$

Because the k^{th} term in T(M) decreases with increasing values for α, the rate of convergence of T(M) is most severe for $\alpha = 0.05$. When $\alpha = 0.05$, it is seen from Table 6.1 that T(M) has almost converged for M = 11. The relative change that results when the next term is added is

$$\left.\frac{T(12) - T(11)}{T(11)}\right|_{\alpha = 0.05} = 1.5 \times 10^{-3} \quad . \tag{6.49}$$

M	$\alpha = 0$	$\alpha = 0.05$	$\alpha = 0.1$	$\alpha = 0.5$	$\alpha = 1$
0	0.50000	0.498753	0.495049	0.400000	0.250000
1	0.56250	0.560786	0.555710	0.432000	0.257810
2	0.58590	0.583896	0.577974	0.439667	0.258541
3	0.59810	0.595884	0.589353	0.442225	0.258636
4	0.60557	0.603188	0.596184	0.443227	0.258650
5	0.61061	0.608098	0.600706	0.443660	0.258653
6	0.61425	0.611616	0.60390	0.443860	0.258653
7	0.61699	0.614258	0.606262	0.443956	0.258653
8	0.61913	0.616311	0.608071	0.444005	
9	0.62085	0.617951	0.609495	0.444029	
10	0.62226	0.619290	0.610640	0.444042	
11	0.62344	0.620403	0.611577	0.444049	
12	0.62444	0.621342	0.612356	0.444053	
13	0.62530	0.622144	0.613012	0.444055	
14	0.62604	0.622836	0.613570	0.444056	
15	0.62669	0.623440	0.614049	0.444057	
16	0.62727	0.623970	0.614464	0.444057	

Table 6.1 - Values of T(M) as a Function of α and M

A plot of T(M) as a function of M for values of α ranging from 0.05 to 1 is shown in Fig.6.1. It is concluded that 12 terms are adequate for evaluating the elements in M^{NL}. It is readily shown that this conclusion also holds for calculating the terms in M_s^{NL} and M_d^{NL}.

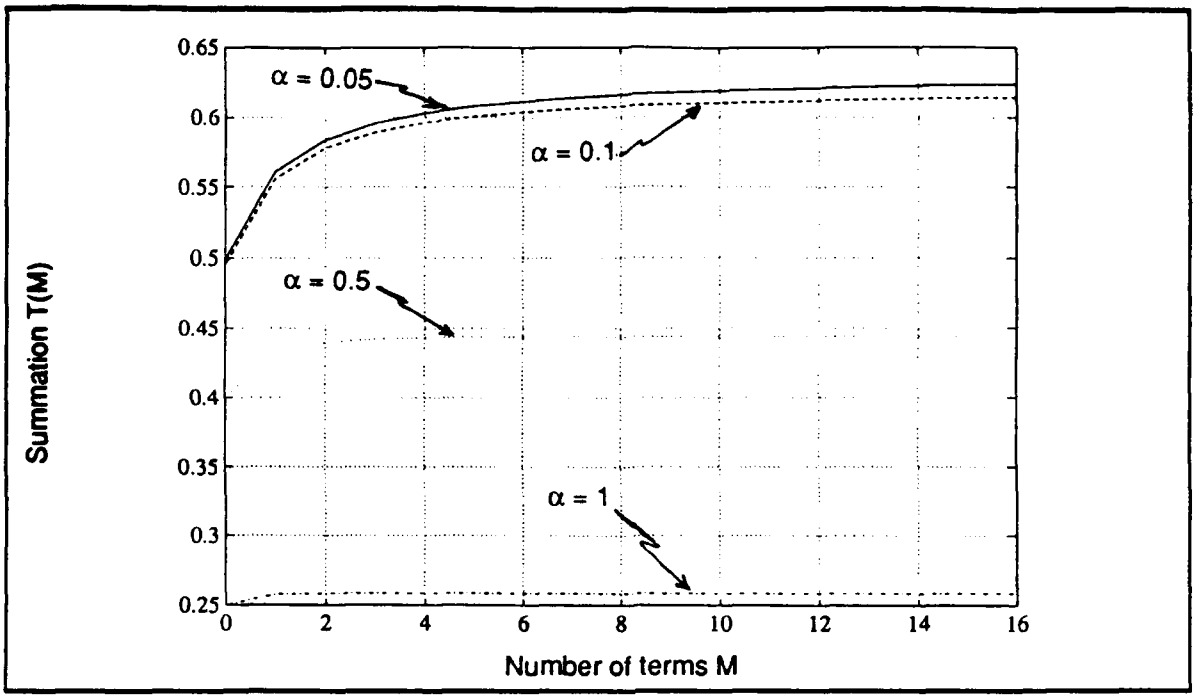

Figure 6.1 - Plot of T(M) as a function of M for values of α ranging from 0.05 to 1.

6.3 Determination of the Transversal Filter Weights

The weights of the transversal filter are selected so as to maximize the signal-to-disturbance ratio at the transversal filter output. As mentioned previously, there are three cases to consider. Each is discussed separately.

Case I

This case deals with the ideal linear receiver. From Eqs (6.18) and (6.12) the output signal-to-disturbance ratio is

$$(SDR)_I = \frac{\underline{\tilde{w}}^H M_s^L \underline{\tilde{w}}}{\underline{\tilde{w}}^H M_d^L \underline{\tilde{w}}} \qquad (6.50)$$

where the superscript H denotes conjugate transpose and the uv^{th} element of M_s^L is

$$(M_s^L)_{uv} = \frac{G^2\sigma_s^2}{2} \cdot e^{j2\pi f_D (v-u) T_s} \quad . \tag{6.51}$$

For convenience, let

$$a_k = e^{j2\pi f_D k T_s} \quad ; k = 1,2,.....,N \quad . \tag{6.52}$$

Define the vector $\underline{a}$ such that

$$\underline{a}^T = [a_1 a_2 ..... a_N] \quad . \tag{6.53}$$

Note that the matrix M_s^L can be expressed as

$$M_s^L = \frac{G^2\sigma_s^2}{2} \cdot \underline{a}^* \underline{a}^T \quad . \tag{6.54}$$

If follows that

$$(SDR)_I = \frac{G^2\sigma_s^2}{2} \cdot \frac{\tilde{\underline{w}}^H \underline{a}^* \underline{a}^T \tilde{\underline{w}}}{\tilde{\underline{w}}^H M_d^L \tilde{\underline{w}}} = \frac{G^2\sigma_s^2}{2} \cdot \frac{|\tilde{\underline{w}}^H \underline{a}^*|^2}{\tilde{\underline{w}}^H M_d^L \tilde{\underline{w}}} \quad . \tag{6.55}$$

Let $\tilde{\underline{x}}$ and $\tilde{\underline{y}}$ denote two N-component complex vectors. Because M_d^L is a positive definite (N x N) Hermitian matrix, it can be shown that

$$(\tilde{\underline{x}}, \tilde{\underline{y}}) = \tilde{\underline{x}}^H M_d^L \tilde{\underline{y}} \tag{6.56}$$

is an inner product of the vector space of N-component complex vectors. An important property of the inner product is the Schwartz inequality

$$|(\tilde{\underline{x}}, \tilde{\underline{y}})|^2 \leq (\tilde{\underline{x}}, \tilde{\underline{x}}) \, (\tilde{\underline{y}}, \tilde{\underline{y}}) \tag{6.57}$$

where equality holds if and only if

$$\tilde{\underline{x}} = k \cdot \tilde{\underline{y}} \tag{6.58}$$

and k is an arbitrary complex constant [2]. In terms of the inner product, note that

$$\tilde{\underline{w}}^H \underline{a}^* = \tilde{\underline{w}}^H M_d^L (M_d^L)^{-1} \underline{a}^* = (\tilde{\underline{w}}, (M_d^L)^{-1} \underline{a}^*) \quad . \tag{6.59}$$

Also,

$$\tilde{\underline{w}}^H M_d^L \tilde{\underline{w}} = (\tilde{\underline{w}}, \tilde{\underline{w}}) \quad . \tag{6.60}$$

As a result, the output signal-to-disturbance ratio can be written as

$$(SDR)_I = \frac{G^2 \sigma_s^2}{2} \cdot \frac{\left| (\tilde{\underline{w}}, (M_d^L)^{-1} \underline{a}^*) \right|^2}{\tilde{\underline{w}}^H M_d^L \tilde{\underline{w}}} \quad . \tag{6.61}$$

Application of the Schwartz inequality yields)

$$(SDR)_I \leq \frac{G^2 \sigma_s^2}{2} \cdot \frac{(\tilde{\underline{w}}, \tilde{\underline{w}}) \, ((M_d^L)^{-1} \underline{a}^*, (M_d^L)^{-1} \underline{a}^*)}{(\tilde{\underline{w}}, \tilde{\underline{w}})}$$

$$\leq \frac{G^2 \sigma_s^2}{2} \cdot ((M_d^L)^{-1} \underline{a}^*, (M_d^L)^{-1} \underline{a}^*) \quad . \tag{6.62}$$

Equality holds when

$$\tilde{\underline{w}} = k \cdot (M_d^L)^{-1} \underline{a}^* \quad . \tag{6.63}$$

Because

$$((M_d^L)^{-1})^H = (M_d^L)^{-1}, \tag{6.64}$$

the maximum signal-to-disturbance ratio, which is obtained when the weight vector is chosen according to Eq.(6.63), is given by

$$(SDR)_I = \frac{G^2\sigma_s^2}{2} \cdot ((M_d^L)^{-1}\underline{a}^*, (M_d^L)^{-1}\underline{a}^*)$$

$$= \frac{G^2\sigma_s^2}{2} \cdot \underline{a}^T((M_d^L)^{-1})^H M_d^L (M_d^L)^{-1}\underline{a}^*$$

$$= \frac{G^2\sigma_s^2}{2} \cdot \underline{a}^T(M_d^L)^{-1}\underline{a}^* \quad . \tag{6.65}$$

To verify that this is, indeed, the signal-to-disturbance ratio when Eq.(6.63) is valid, the weight vector is substituted into Eq.(6.55).This yields

$$(SDR)_I = \frac{G^2\sigma_s^2}{2} \cdot \frac{k^*\underline{a}^T((M_d^L)^{-1})^H \underline{a}^*\underline{a}^T k(M_d^L)^{-1}\underline{a}^*}{k^*\underline{a}^T((M_d^L)^{-1})^H M_d^L k(M_d^L)^{-1}\underline{a}^*}$$

$$= \frac{G^2\sigma_s^2}{2} \cdot \underline{a}^T(M_d^L)^{-1}\underline{a}^* \quad . \tag{6.66}$$

The result obtained in Eq.(6.66) is consistent with Eq.(6.65).

Case II

In this case the receiver is assumed to be nonlinear. However, the presence of the nonlinearity is unknown to the system designer. Hence, the "optimum" weight vector is chosen as though the receiver is linear. With reference to Eq.(6.39), the signal-to-disturbance ratio is given by

$$(SDR)_{II} = \frac{\underline{\tilde{w}}^H M_s^{NL} \underline{\tilde{w}}}{\underline{\tilde{w}}^H M_d^{NL} \underline{\tilde{w}}} \tag{6.67}$$

where the weight vector is determined according to Eq.(6.63). This weight vector does not result in a maximum signal-to-disturbance ratio because it depends upon the disturbance covariance matrix of the linear receiver instead of the disturbance covariance matrix of the nonlinear receiver.

Case III

Once again, the receiver is assumed to be nonlinear. The weight vector for this case is chosen to maximize the signal-to-disturbance ratio. From Eqs (6.39) and (6.29) the output signal-to-disturbance ratio is

$$(SDR)_{III} = \frac{\underline{\tilde{w}}^H M_s^{NL} \underline{\tilde{w}}}{\underline{\tilde{w}}^H M_d^{NL} \underline{\tilde{w}}} \tag{6.68}$$

where the uv^{th} element of M_s^L is

$$(M_s^{NL})_{uv} = G^2 \sigma_g^2 \sum_{k=0}^{\infty} b_k \cdot \frac{C_k^{2k+1}}{2^{2k+1}} \cdot \left[\frac{1/(2\sigma_1^2)}{1+\alpha^2}\right]^{2k+1}$$

$$\cdot (2\sigma_s^2)^{2k+1} \cdot e^{j2\pi f_D (v-u) T_s} . \tag{6.69}$$

Let A denote the constant

$$A = G^2\sigma_g^2 \sum_{k=0}^{\infty} b_k \cdot \frac{C_k^{2k+1}}{2^{2k+1}} \cdot \left[\frac{1/(2\sigma_1^2)}{1+\alpha^2}\right]^{2k+1} (2\sigma_s^2)^{2k+1} . \qquad (6.70)$$

In terms of the vector $\underline{a}$ defined by Eqs (6.52) and (6.53) the matrix M_s^{NL} can be expressed as

$$M_s^{NL} = A \cdot \underline{a}^* \underline{a}^T . \qquad (6.71)$$

Hence, the signal-to-disturbance ratio becomes

$$(SDR)_{III} = A \cdot \frac{\tilde{\underline{w}}^H \underline{a}^* \underline{a}^T \tilde{\underline{w}}}{\tilde{\underline{w}}^H M_d^{NL} \tilde{\underline{w}}} = A \cdot \frac{|\tilde{\underline{w}}^H \underline{a}^*|^2}{\tilde{\underline{w}}^H M_d^{NL} \tilde{\underline{w}}} . \qquad (6.72)$$

Because M_d^{NL} is a positive definite Hermitian matrix, it is possible to define the inner product by

$$(\tilde{\underline{x}}, \tilde{\underline{y}}) = \tilde{\underline{x}}^H M_d^{NL} \tilde{\underline{y}} . \qquad (6.73)$$

Following the same procedure as in Case I, it can be shown that the optimal weight vector is given by

$$\tilde{\underline{w}} = k \cdot (M_d^{NL})^{-1} \underline{a}^* \qquad (6.74)$$

where k is an arbitrary complex constant. The maximum signal-to-disturbance ratio is

$$(SDR)_{III} = A \cdot \underline{a}^T (M_d^L)^{-1} \underline{a}^* . \qquad (6.75)$$

The analytical results provided in this chapter are used in the following chapters to calculate the signal-to-disturbance ratios for the three cases considered.

Chapter 7

FREQUENCY DOMAIN ANALYSIS

The previous chapters utilized a time-domain approach to develop the signal-to-disturbance ratio at the transversal filter output. However, much physical insight can be gained by interpreting the results in the frequency domain. Assuming that the input signals are sampled in time, the continous Fourier transform of a discrete-time series is first discussed. This leads to development of the transversal filter transfer function. With respect to the power spectral densities of the clutter, thermal noise, and transmitted signal, the effect of processing a finite number of samples is considered. Finally, a relation is derived for the power spectral density at the transversal filter output.

7.1 Continuous Fourier Transform of Discrete Time Series

Let $\tilde{x}[nT_s]$ denote a complex valued discrete time sequence. Its continuous Fourier transform is defined [8] to be

$$\tilde{X}(f) = \sum_{n=-\infty}^{\infty} \tilde{x}[nT_s]\, e^{-j2\pi nfT_s}. \qquad (7.1)$$

Note that

$$\tilde{X}\left(f \pm \frac{k}{T_s}\right) = \sum_{n=-\infty}^{\infty} \tilde{x}[nT_s]\, e^{-j2\pi n\left(f \pm \frac{k}{T_s}\right)T_s}$$

$$= \sum_{n=-\infty}^{\infty} \tilde{x}[nT_s]\, e^{-j2\pi nfT_s} \underbrace{e^{\mp j2\pi nk}}_{1} = \tilde{X}(f). \qquad (7.2)$$

Hence, $\tilde{X}(f)$ is periodic with period $1/T_s$. The inverse Fourier transform is given by

$$\tilde{x}[nT_s] = T_s \int_{-\frac{1}{2T_s}}^{\frac{1}{2T_s}} \tilde{X}(f)\, e^{j2\pi nfT_s} df \ . \qquad (7.3)$$

It is convenient to suppress dependence on the sampling interval T_s by introducing the normalized frequency variable

$$\Omega = 2\pi \frac{f}{1/T_s} = 2\pi f T_s \ . \qquad (7.4)$$

Note that Ω is in radians/second whereas f is in Hertz. In terms of Ω, Eqs (7.1) and (7.3) become

$$\tilde{X}(\Omega) = \sum_{n=-\infty}^{\infty} \tilde{x}[nT_s]\, e^{-jn\Omega} \qquad (7.5)$$

and

$$\tilde{x}[nT_s] = \frac{1}{2\pi} \int_{-\pi}^{\pi} \tilde{X}(\Omega)\, e^{jn\Omega} d\Omega \ . \qquad (7.6)$$

Observe that

$$\tilde{X}(\Omega \pm 2\pi k) = \sum_{n=-\infty}^{\infty} \tilde{x}[nT_s]\, e^{-jn(\Omega \pm 2\pi k)}$$

$$= \sum_{n=-\infty}^{\infty} \tilde{x}[nT_s]\, e^{-jn\Omega} \underbrace{e^{\mp j2\pi nk}}_{1} = \tilde{X}(\Omega) \ . \qquad (7.7)$$

Consequently, $\tilde{X}(\Omega)$ is periodic with period 2π.

7.2 Transfer Function of the Transversal Filter

As given by Eq.(2.9), the transversal filter output is determined by

$$\tilde{r}_6(t) = \sum_{k=1}^{N} \tilde{w}_k^* \tilde{r}_5[t-(k-1)T_s] \tag{7.8}$$

where $\tilde{r}_5(t)$ denotes the transversal filter input. Assuming that the signals are uniformly sampled with sampling interval T_s, the filter output at the n^{th} sampling instant is

$$\tilde{r}_6[nT_s] = \sum_{k=1}^{N} \tilde{w}_k^* \tilde{r}_5[(n-k+1)T_s] \quad . \tag{7.9}$$

Let $\tilde{X}_5(\Omega)$ and $\tilde{X}_6(\Omega)$ denote the continuous Fourier transforms of $\tilde{r}_5(nT_s)$ and $\tilde{r}_6(nT_s)$, respectively. Using Eq.(7.9) in Eq.(7.5) and interchanging the order of summation results in

$$\tilde{X}_6(\Omega) = \sum_{n=-\infty}^{\infty} \tilde{r}_6[nT_s] e^{-jn\Omega} = \sum_{n=-\infty}^{\infty} \left\{ \sum_{k=1}^{N} \tilde{w}_k^* \tilde{r}_5[(n-k+1)T_s] \right\} e^{-jn\Omega}$$

$$= \sum_{k=1}^{N} \tilde{w}_k^* \left\{ \sum_{n=-\infty}^{\infty} \tilde{r}_5[(n-k+1)T_s] e^{-jn\Omega} \right\} \quad . \tag{7.10}$$

Introduce the change of variables

$$l = n-k+1 \quad . \tag{7.11}$$

It follows that

$$\tilde{X}_6(\Omega) = \sum_{k=1}^{N} \tilde{w}_k^* e^{-j(k-1)\Omega} \left\{ \sum_{l=-\infty}^{\infty} \tilde{r}_5[lT_s] e^{-jl\Omega} \right\}$$

$$= \tilde{X}_5(\Omega) \sum_{k=1}^{N} \tilde{w}_k^{*} e^{-j(k-1)\Omega} \quad . \tag{7.12}$$

By definition, the transversal filter transfer function is

$$\tilde{H}_{TF}(\Omega) = \frac{\tilde{X}_6(\Omega)}{\tilde{X}_5(\Omega)} = \sum_{k=1}^{N} \tilde{w}_k^{*} e^{-j(k-1)\Omega} \quad . \tag{7.13}$$

As explained in Chapter 6, the weights $\tilde{w}_k$ are determined so as to maximize the signal-to-disturbance ratio at the filter output.

7.3 Power Spectral Density of Complex Envelope at Receiver Input

Assuming wide-sense stationarity, consider the continuous autocorrelation function $\tilde{R}(\tau)$ where τ denotes the difference between two time instants. For uniform sampling, with a sampling interval T_s, the time difference is an integer multiple of T_s. Consequently, we let

$$\tau = kT_s \tag{7.14}$$

where k is an integer. The associated power spectral density $\tilde{S}(\Omega)$ is the continuous Fourier transform of the sequence $\tilde{R}(kT_s)$. With reference to Eqs.(7.5) and (7.6), this results in the Fourier transform pair

$$\tilde{S}(\Omega) = \sum_{k=-\infty}^{\infty} \tilde{R}[kT_s] e^{-jk\Omega} \tag{7.15}$$

and

$$\tilde{R}[kT_s] = \frac{1}{2\pi} \int_{-\pi}^{\pi} \tilde{S}(\Omega) e^{jk\Omega} d\Omega \quad . \tag{7.16}$$

Given that a target is present, the received signal consists of the sum of the signal reflected from the target , clutter and thermal noise. Because the transver-

sal filter processes N samples at a time, the target, clutter, and thermal noise sequences are effectively truncated to N samples. In this section, we study the effect of this truncation on the corresponding power spectral densities.

7.3.1 Effect of Truncation on the Clutter Power Spectral Denity

The autocorrelation function of the clutter complex envelope is given by Eq.(5.22) as

$$\tilde{R}_C(\tau) = 2\sigma_C^2 \cdot e^{-\frac{\tau^2}{2\sigma_W^2}} \quad . \tag{7.17}$$

For the sampled clutter, the corresponding correlation sequence is

$$\tilde{R}_C[kT_S] = 2\sigma_C^2 \cdot e^{-\frac{k^2T_S^2}{2\sigma_W^2}} \quad . \tag{7.18}$$

For convenience, define the clutter correlation parameter ρ_C to be

$$\rho_C = \frac{\tilde{R}_C[T_S]}{\tilde{R}_C[0]} = \frac{2\sigma_C^2 \cdot e^{-\frac{T_S^2}{2\sigma_W^2}}}{2\sigma_C^2} = e^{-\frac{T_S^2}{2\sigma_W^2}} \quad . \tag{7.19}$$

Observe that

$$0 \le \rho_C \le 1 \quad . \tag{7.20}$$

In terms of ρ_C and $\tilde{R}_C[0]$, the clutter correlation sequence becomes

$$\tilde{R}_C[kT_S] = \tilde{R}_C[0] \cdot \rho_C^{k^2} \quad . \tag{7.21}$$

The clutter samples are said to be highly correlated when $\rho_c \approx 1$ and are said to be uncorrelated when $\rho_c = 0$.

A sketch of the complete correlation sequence is shown in Fig.7.1. When N clutter samples are processed, the maximum time displacement between the

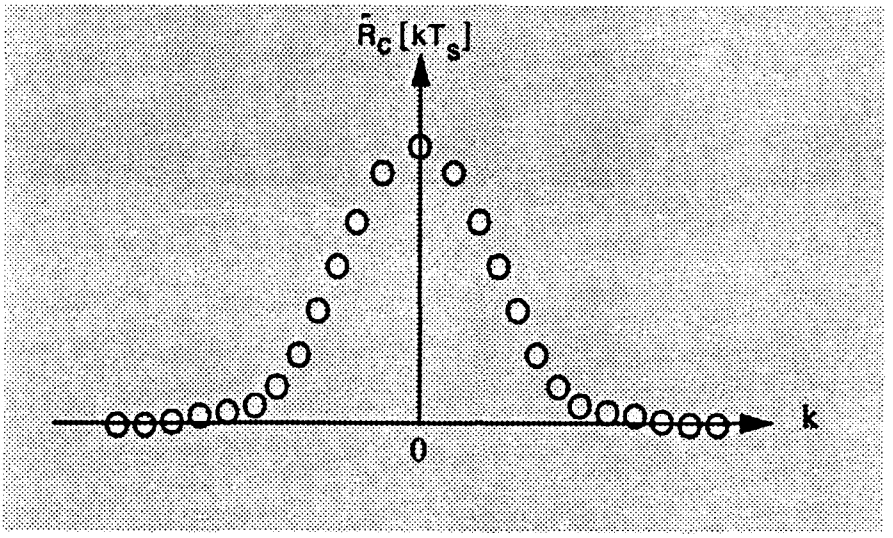

Figure 7.1 - Sketch of the complete correlation sequence $\tilde{R}_c[kT_s]$.

samples is (N-1)Ts. Hence, the allowable values for k are $k=0,\pm1,\pm2,.....,\pm(N-1)$. The effect is to truncate the correlation sequence, as is shown in Fig.7.2. The truncated correlation sequence is defined to be

$$\tilde{R}_{CT}[kT_s] = \begin{cases} \tilde{R}_c[kT_s] & ; -(N-1) \le k \le (N-1) \\ 0 & ; \text{otherwise} \end{cases} . \qquad (7.22)$$

The power spectral density corresponding to the truncated correlation sequence is given by

$$\tilde{S}_{CT}(\Omega) = \sum_{k=-(N-1)}^{(N-1)} \tilde{R}_c[kT_s]\, e^{-jk\Omega} . \qquad (7.23)$$

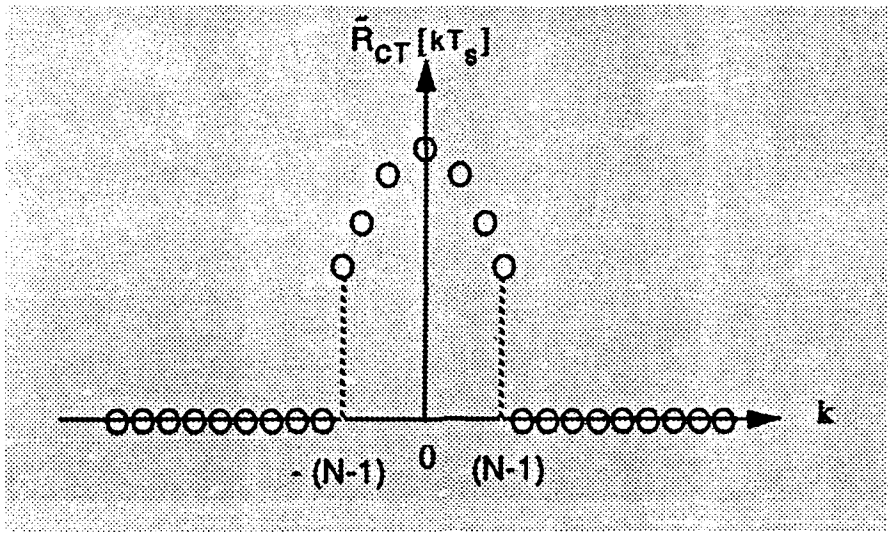

Figure7.2 - Sketch of the truncated correlation sequence $\tilde{R}_{CT}[kT_s]$.

The truncated correlation sequence may no longer be a valid correlation sequence in the sense that the corresponding power spectral density may assume negative values. This is illustrated in Fig.7.3 where $\tilde{S}_{CT}(\Omega)$ is plotted for various values of ρ_c and N. For convenience, the frequency axis is normalized by π so that the variation in Ω from - π to π is transformed into a variation of Ω/π from -1 to 1. When ρ_c=0

$$\tilde{R}_{CT}[kT_s] = \begin{cases} 2\sigma_c^2 & ;k=0 \\ 0 & ;k\neq 0 \end{cases} . \qquad (7.24)$$

Hence,

$$\tilde{S}_{CT}(\Omega) = 2\sigma_c^2 \qquad (7.25)$$

independent of the choice of N. This constant power spectral density is shown in Fig. 7.3.(a). For ρ_c=0.8 and N=5, $\tilde{S}_{CT}(\Omega)$ is essentially Gaussian shaped and nonnegative, as is shown in Fig.7.3.(b). However for ρ_c=0.9 and N=5, negative side lobes are observed in $\tilde{S}_{CT}(\Omega)$. This is shown in Fig.7.3.(c). As seen in

Fig.7.3.(d), the negative side lobes disappear when N is increased to 10 and ρ_c=0.9.

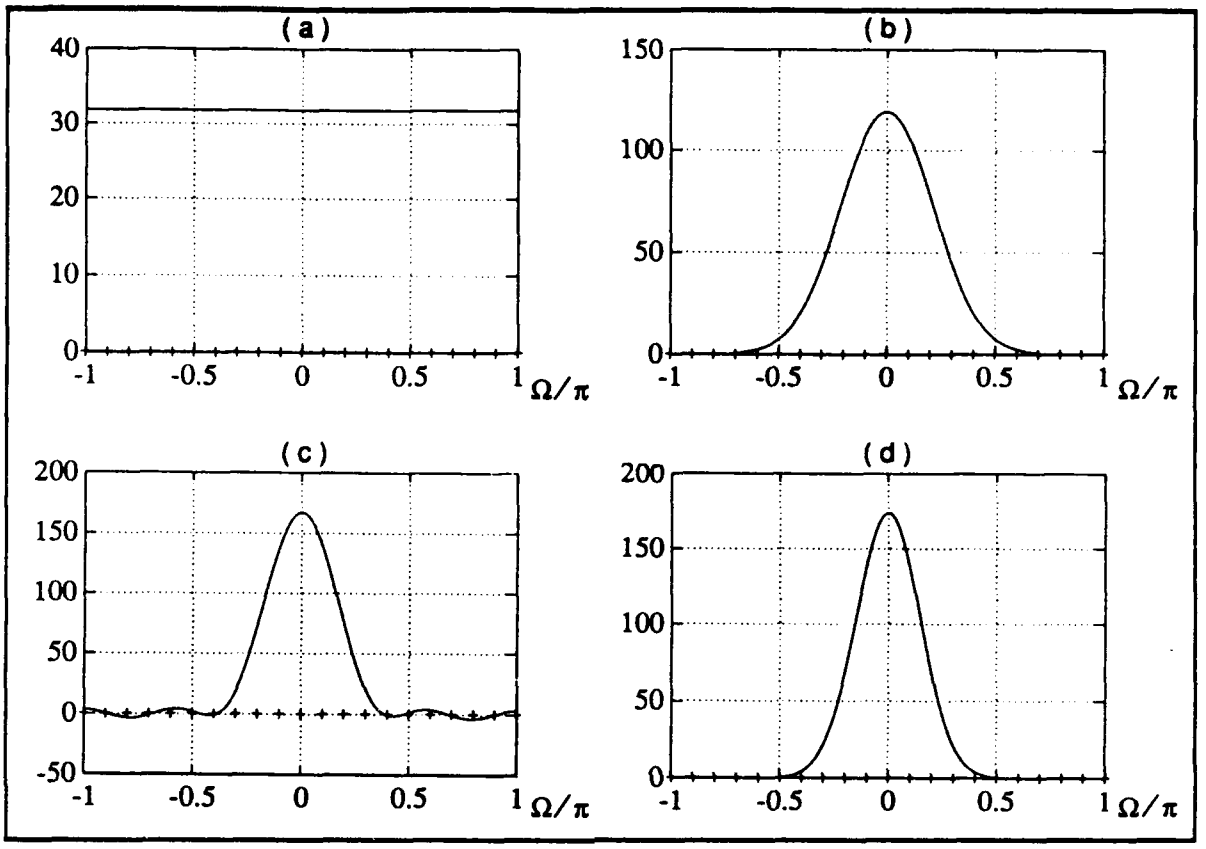

Figure 7.3 - Plots of $\tilde{S}_{CT}(\Omega)$ vs Ω/π.
(a) ρ_c=0 and N=5, (b) ρ_c=0.8 and N=5, (c) ρ_c=0.9 and N=5,
(d) ρ_c=0.9 and N=10.

Because we are interested in those cases for which the clutter is much larger than both the signal reflected from the target and the additive thermal noise, the clutter spectrum dominates and N is chosen large enough so as to avoid negative side lobes in $\tilde{S}_{CT}(\Omega)$. By choosing N large, the edge effects of the truncated correlation sequence are minimized. Define the ratio of the smallest to largest values of $\tilde{R}_{CT}(kT_s)$ to be

$$U_N = \frac{\tilde{R}_{CT}[(N-1)T_s]}{\tilde{R}_{CT}[0]} = \frac{2\sigma_c^2 \cdot \rho_c^{(N-1)^2}}{2\sigma_c^2} = \rho_c^{(N-1)^2} \quad . \qquad (7.26)$$

Solution for N results in

$$N = 1 + \sqrt{\frac{\log (U_N)}{\log (\rho_c)}} \quad . \tag{7.27}$$

In order to approximate $\tilde{R}_c(kT_s)$ as closely as possible, U_N is chosen equal to 10^{-9}. The values of N needed for $U_N = 10^{-9}$ are plotted in Figures 7.4 through 7.6 for various values of ρ_c. In Figure 7.4, $0 \le \rho_c \le 1$. Because of the large range of N, expanded plots are shown for $0 \le \rho_c \le 0.9$ in Fig.7.5 and for $0.9 \le \rho_c \le 1$ in Fig.7.6. In our analysis the maximum values allowed for ρ_c is $\rho_c = 0.9$. From Fig.7.5, the required value of N is N=15. As a result, it is assumed in our analysis that the transversal filter processes no fewer than 15 samples.

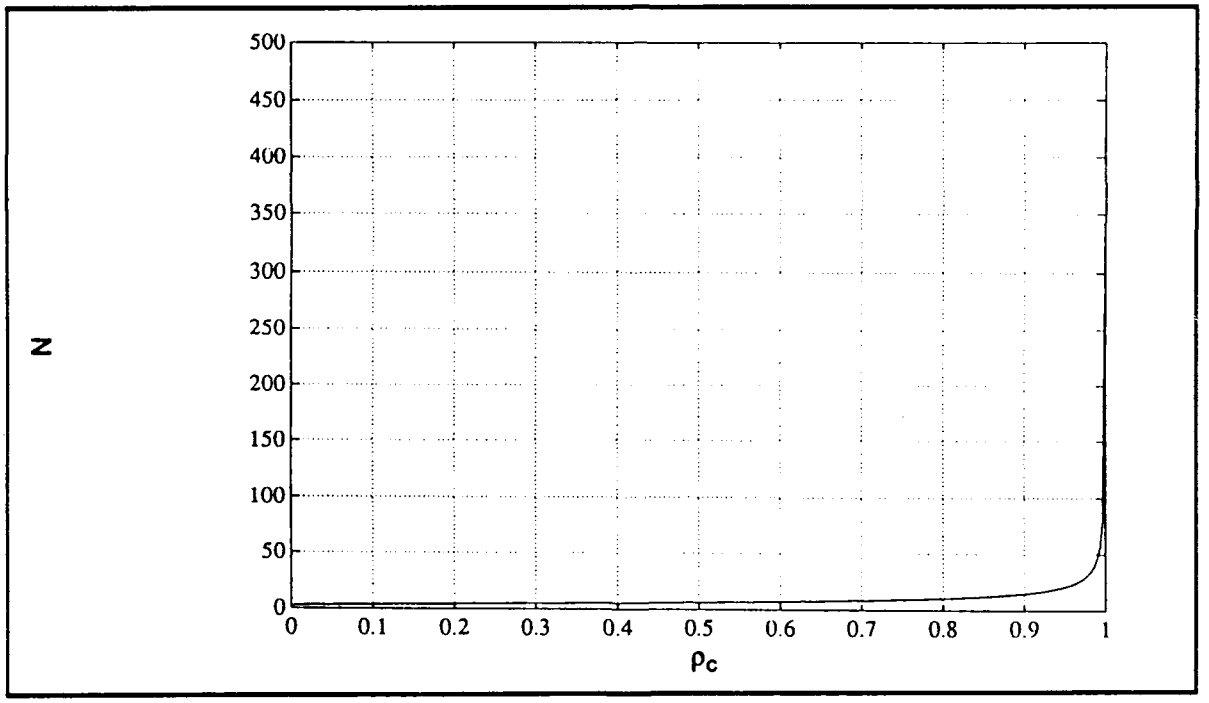

Figure 7.4 - Values of N needed for $U_N = 10^{-9}$, $0 \le \rho_c \le 1$.

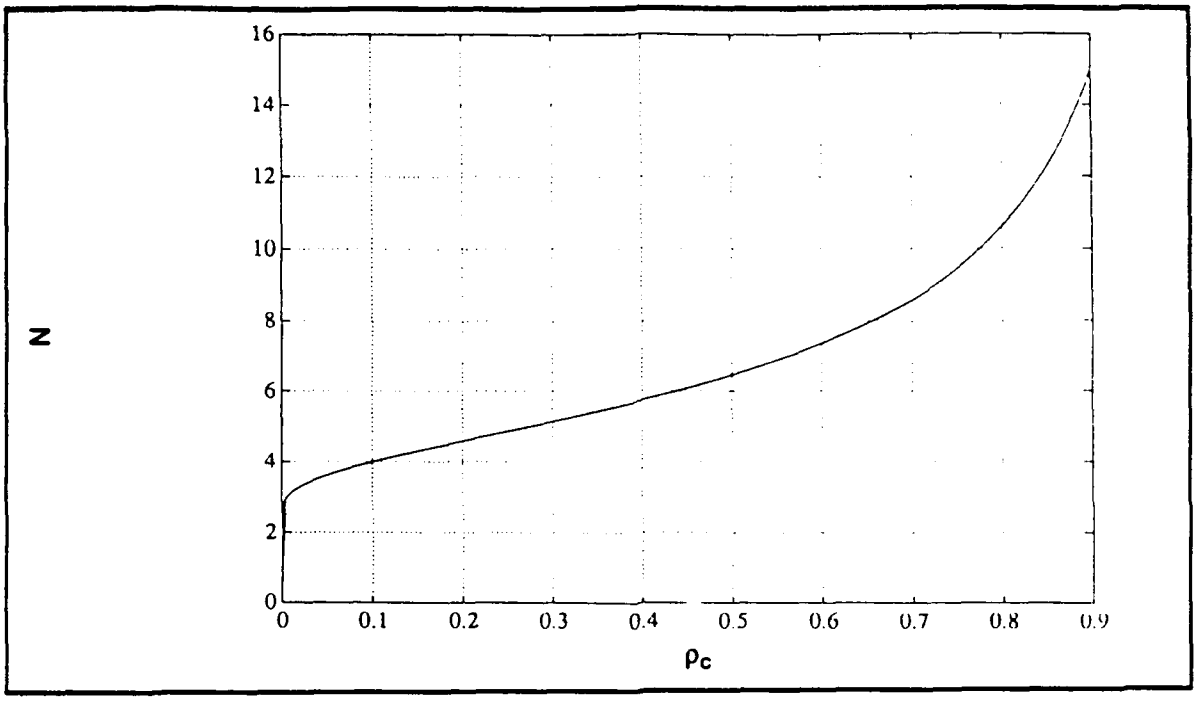

Figure 7.5 - Values of N needed for $U_N=10^{-9}$, $0 \leq \rho_c \leq 0.9$.

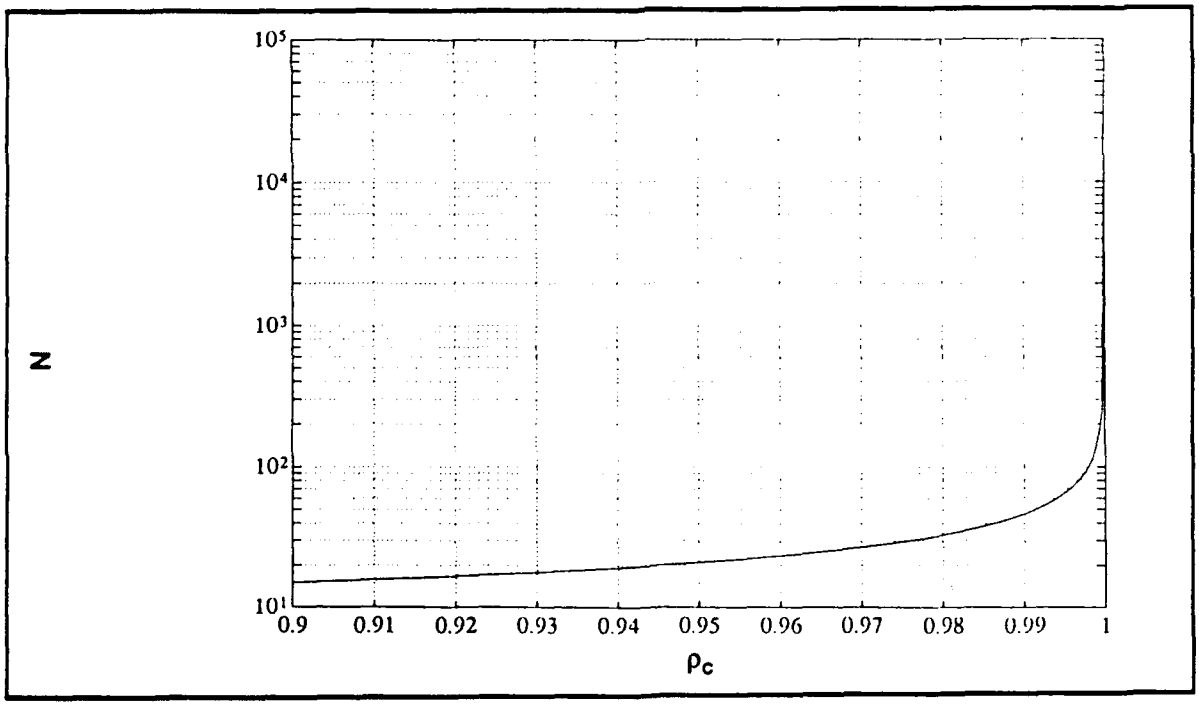

Figure 7.6 - Values of N needed for $U_N=10^{-9}$, $0.9 \leq \rho_c \leq 1$.

7.3.2 Effect of Truncation on the Thermal Noise Power Spectral Density

From Eq.(5.25), the power spectral density of the thermal noise complex envelope is

$$\tilde{R}_n(\tau) = 2\sigma_n^2 \cdot \frac{\sin(\pi W\tau)}{\pi W\tau} \tag{7.28}$$

where W is the bandpass bandwidth. Assuming uniform sampling of the noise, with the sampling interval Ts, the corresponding correlation sequence is

$$\tilde{R}_n[kT_s] = 2\sigma_n^2 \cdot \frac{\sin(\pi WkT_s)}{\pi WkT_s} \; . \tag{7.29}$$

Because the magnitude of $\sin(\pi WkT_s)$ is bounded by unity, the bound on the magnitude of $\tilde{R}_n(kT_s)$ for $k \neq 0$ is

$$\left|\tilde{R}_n[kT_s]\right| \leq \frac{2\sigma_n^2}{\left|\pi WkT_s\right|} \; . \tag{7.30}$$

Recall that T_s is equal to the time interval between consecutive pulses of the transmitted pulse train. Since this is typically on the order of milliseconds while W is on the order of Megahertz, it is assumed that

$$\left|\pi WkT_s\right| \gg 2\sigma_n^2 \quad ; k = \pm 1, \pm 2, \ldots\ldots \; . \tag{7.31}$$

Thus, $\tilde{R}_n(kT_s)$ is approximated by

$$\tilde{R}_n[kT_s] \approx \begin{cases} 2\sigma_n^2 & ; k=0 \\ 0 & ; k \neq 0 \; . \end{cases} \tag{7.32}$$

A sketch of the approximate autocorrelation sequence of the sampled thermal noise is shown in Figure 7.7. Because of this approximation, the power spectral density of the truncated noise sequence is

$$\tilde{S}_{nT}(\Omega) = \sum_{k=-(N-1)}^{(N-1)} \tilde{R}_n[kT_s]\, e^{-jk\Omega} \approx 2\sigma_n^2 \qquad (7.33)$$

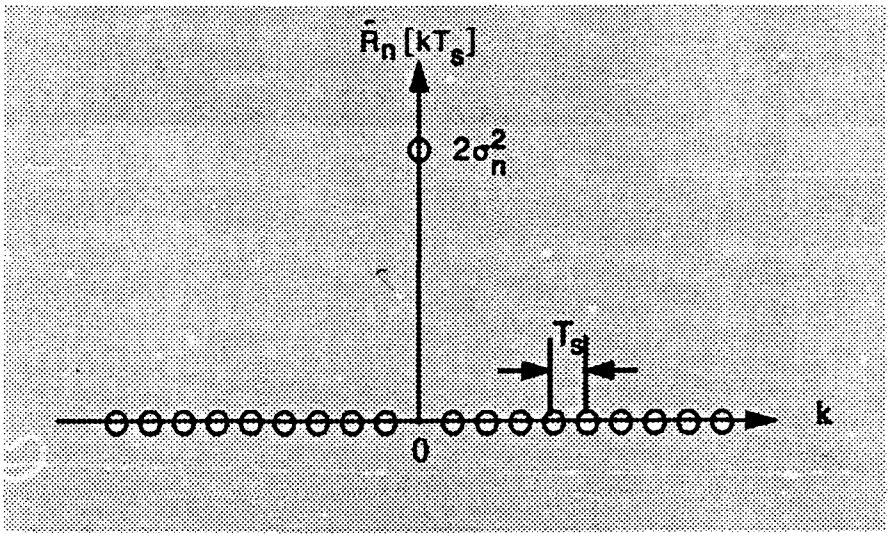

Figure7.7 - Approximate autocorrelation sequence of the sampled thermal noise.

independent of the choice of N. It is concluded that truncation has a negligible effect on the sampled noise spectrum.

7.3.3 Effect of Truncation on the Desired Signal Power Spectral Density

The autocorrelation function of the desired signal complex envelope is given by Eq.(5.16) as

$$\tilde{R}_S(\tau) = 2\sigma_s^2 \cdot e^{j2\pi f_D \tau}. \qquad (7.34)$$

For the sampled signal, the associated correlation sequence is

$$\tilde{R}_S[kT_s] = 2\sigma_s^2 \cdot e^{j2\pi f_D kT_s}. \qquad (7.35)$$

With reference to Eq.(7.15), the power spectral density of the desired signal is

$$\tilde{S}_S(\Omega) = \sum_{k=-\infty}^{\infty} \tilde{R}_S[kT_s]\, e^{-jk\Omega} = 2\sigma_s^2 \cdot \sum_{k=-\infty}^{\infty} e^{j2\pi f_D kT_s} e^{-jk\Omega} \quad . \quad (7.36)$$

For convenience, let

$$\Omega_D = 2\pi f_D T_s \quad . \quad (7.37)$$

The expression for the power spectral density then simplifies to

$$\tilde{S}_S(\Omega) = 2\sigma_s^2 \cdot \sum_{k=-\infty}^{\infty} e^{-jk(\Omega - \Omega_D)} \quad . \quad (7.38)$$

Further simplification is possible by using the Poisson sum formula [6]

$$\sum_{k=-\infty}^{\infty} e^{-jk(\Omega - \Omega_D)} = 2\pi \sum_{k=-\infty}^{\infty} \delta(\Omega - \Omega_D - 2n\pi) \quad (7.39)$$

where $\delta(.)$ denotes the usual Dirac delta function. Use of Eq.(7.39) in Eq.(7.38) results in

$$\tilde{S}_S(\Omega) = 4\pi\sigma_s^2 \sum_{k=-\infty}^{\infty} \delta(\Omega - \Omega_D - 2n\pi) \quad . \quad (7.40)$$

The power spectral density is seen to consist of a periodic impulse train, as shown in Fig.7.8.

The power spectral density of the truncated signal sequence is

$$\tilde{S}_{ST}(\Omega) = 2\sigma_s^2 \cdot \sum_{k=-(N-1)}^{(N-1)} e^{-jk(\Omega - \Omega_D)} \quad . \quad (7.41)$$

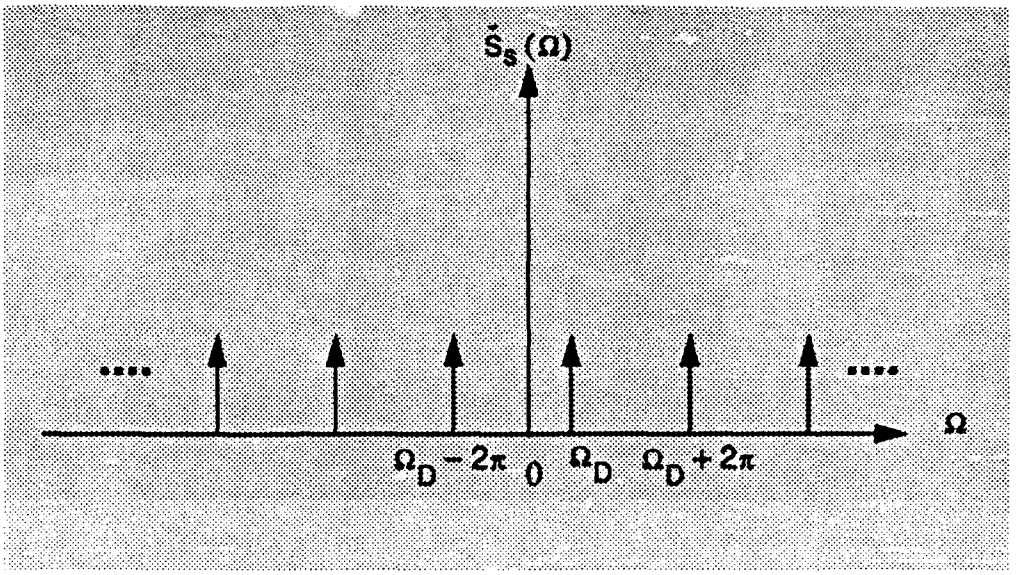

Figure 7.8 - Power spectral density of desired signal.

This is recognized as the sum of a geometric progression which equals

$$\tilde{S}_{ST}(\Omega) = 2\sigma_s^2 \cdot \frac{e^{-j(\Omega-\Omega_D)} e^{-j(N-1)(\Omega-\Omega_D)} - e^{-j(N-1)(\Omega-\Omega_D)}}{e^{-j(\Omega-\Omega_D)} - 1}$$

$$= 2\sigma_s^2 \cdot \frac{e^{-j\left(\frac{\Omega-\Omega_D}{2}\right)}\left(e^{-j(N-\frac{1}{2})(\Omega-\Omega_D)} - e^{j(N-\frac{1}{2})(\Omega-\Omega_D)}\right)}{e^{-j\left(\frac{\Omega-\Omega_D}{2}\right)}\left(e^{-j\left(\frac{\Omega-\Omega_D}{2}\right)} - e^{j\left(\frac{\Omega-\Omega_D}{2}\right)}\right)}$$

$$= 2\sigma_s^2 \cdot \frac{\sin\left[\frac{2N-1}{2}(\Omega-\Omega_D)\right]}{\sin\left[\frac{1}{2}(\Omega-\Omega_D)\right]} \; . \qquad (7.42)$$

The zeros of the numerator occur when

$$\frac{2N-1}{2}(\Omega-\Omega_D) = k\pi$$

or

$$\Omega = \Omega_D + \frac{2k\pi}{2N-1} \qquad ; k = 0,\pm1,\pm2,..... \tag{7.43}$$

while the zeros of the denominator occur when

$$\frac{1}{2}(\Omega - \Omega_D) = l\pi$$

or

$$\Omega = \Omega_D + 2l\pi \qquad ; l = 0, 1, 2,..... \ . \tag{7.44}$$

The maxima of $\tilde{S}_{sT}(\Omega)$ occur when the numerator and denominator are zero simultaneously. This results when

$$\frac{2k\pi}{2N-1} = 2l\pi$$

or

$$k = l(2N-1) \ . \tag{7.45}$$

Consequently, the maxima of $\tilde{S}_{sT}(\Omega)$ occur for

$$\Omega = \Omega_D + 2l\pi \qquad ; l = 0,\pm1,\pm2,..... \tag{7.46}$$

At the maxima,

$$\begin{aligned} \tilde{S}_{sT}(\Omega_D + 2l\pi) &= 2\sigma_s^2 \cdot \frac{\sin[(2N-1)l\pi]}{\sin[l\pi]} \\ &= 2\sigma_s^2 \cdot (2N-1) \ . \end{aligned} \tag{7.47}$$

The power spectral density of the truncated signal sequence is sketched in Fig.7.9. Due to truncation, negative side lobes are seen to exist about the main lobes. These can be eliminated by windowing the data. However, this is not included here because the time-domain analysis of the previous chapters does not involve windowing. In addition, even with negative side lobes, the area under the signal power spectral density equals the average signal power as evaluated in the time domain.

Neverthless, it is instructive to examine how the choice of N affects the shape of the signal power spectral density. With reference to Eq.(7.42), side lobe maxima closely coincide with peaks in the numerator due to the relatively flat shape of the denominator as a function of Ω. Peaks of the numerator result when

$$\frac{2N-1}{2}(\Omega-\Omega_D) = (2k+1)\frac{\pi}{2}$$

or

$$(\Omega-\Omega_D) = \frac{(2k+1)\pi}{2N-1} \quad ; k = 0,\pm1,\pm2,\ldots\ldots. \tag{7.48}$$

For this value of $(\Omega-\Omega_D)$, the argument of the sine function in the denominator is

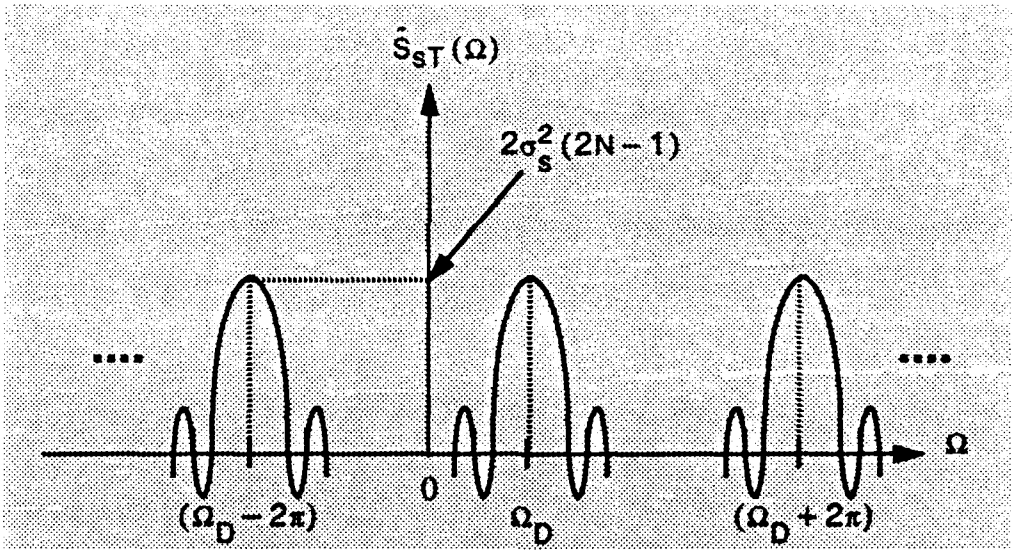

Figure 7.9 - Power spectral density of the truncated signal sequence.

$$\frac{1}{2}(\Omega-\Omega_D) = \frac{2k+1}{2}\frac{\pi}{2N-1}. \tag{7.49}$$

Letting k=1, the amplitude of the first side lobe is

$$A_1 = \frac{2\sigma_s^2}{\left|\sin\left(\frac{3}{2}\frac{\pi}{2N-1}\right)\right|}. \tag{7.50}$$

The ratio of A_1 to the amplitude of the main lobe is

$$r = \frac{A_1}{2\sigma_s^2(2N-1)} = \frac{1}{(2N-1)\left|\sin\left(\frac{3}{2}\frac{\pi}{2N-1}\right)\right|} \quad . \tag{7.51}$$

A plot of r as a function of N is shown in Fig. 7.10. For N ≥5, note that r approaches its asymptotic value of

$$\frac{2(2N-1)}{(2N-1)3\pi} = \frac{2}{3\pi} = 0.212 \quad . \tag{7.52}$$

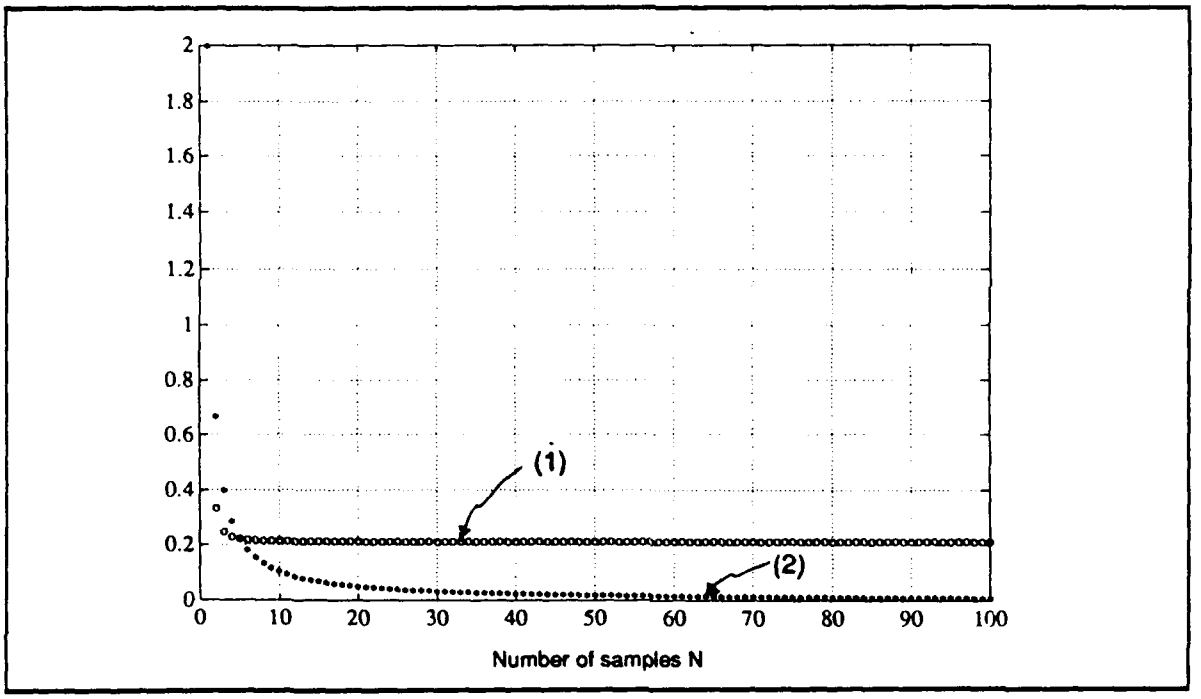

Figure 7.10 - Plots, as a function of N, of 1) Ratio of first side lobe amplitude to that of the main lobe and 2) width of the main lobe.

The width of the main lobe at Ω_D is defined to be the frequency spacing between the two zeros of the power spectral density located at

$$\Omega_1 = \Omega_D - \frac{2\pi}{2N-1} \quad \text{and} \quad \Omega_2 = \Omega_D + \frac{2\pi}{2N-1} \quad .$$

Thus, the main lobe width is given by

$$\Omega_2 - \Omega_1 = \frac{4\pi}{2N-1} \quad . \tag{7.53}$$

Fig.7.10 shows a plot of

$$\frac{\Omega_2 - \Omega_1}{2\pi} = \frac{2}{2N-1} \tag{7.54}$$

as a function of N. Observe that the width approaches zero as N becomes large. For N=15,

$$\frac{\Omega_2 - \Omega_1}{2\pi} = 0.069 \quad . \tag{7.55}$$

The plots in Fig.7.10 are expanded in Fig.7.11 for $1 \leq N \leq 20$.

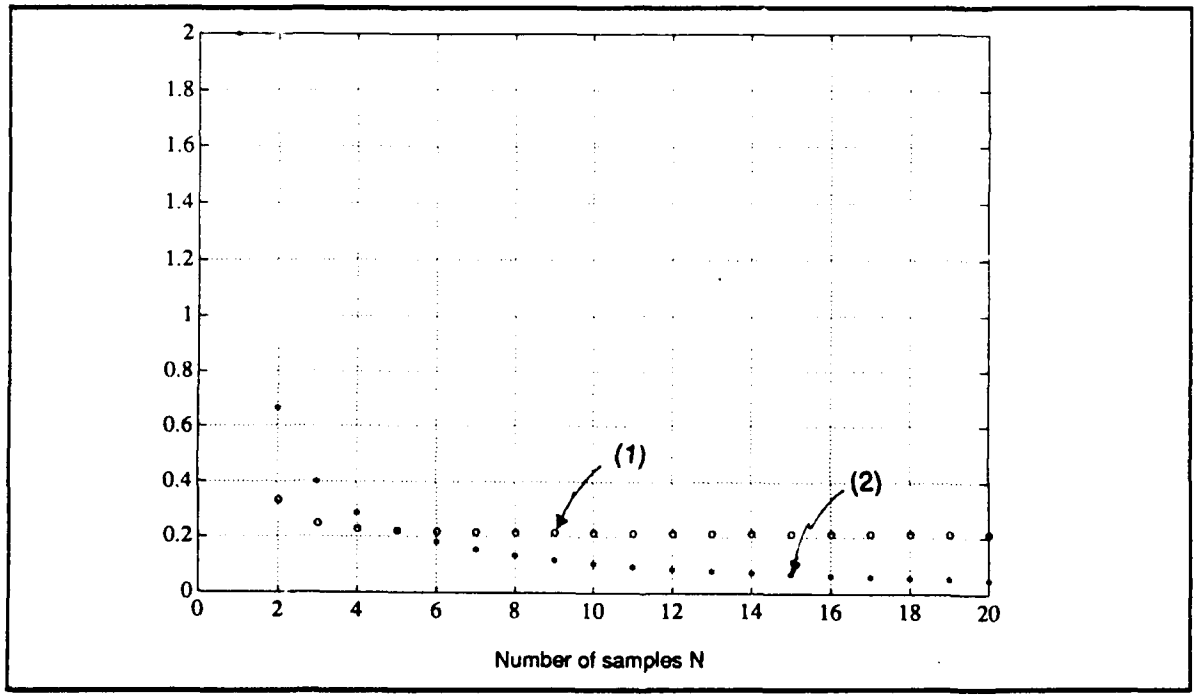

Figure 7.11 - Expanded plots, as a function of N, of 1) Ratio of first side lobe amplitude to that of the main lobe and 2) width of the main lobe.

Plots of the signal power spectral density for N=5,10,15,50 and Ω_D=0 are presented in Figures 7.12 - 7.15, respectively.

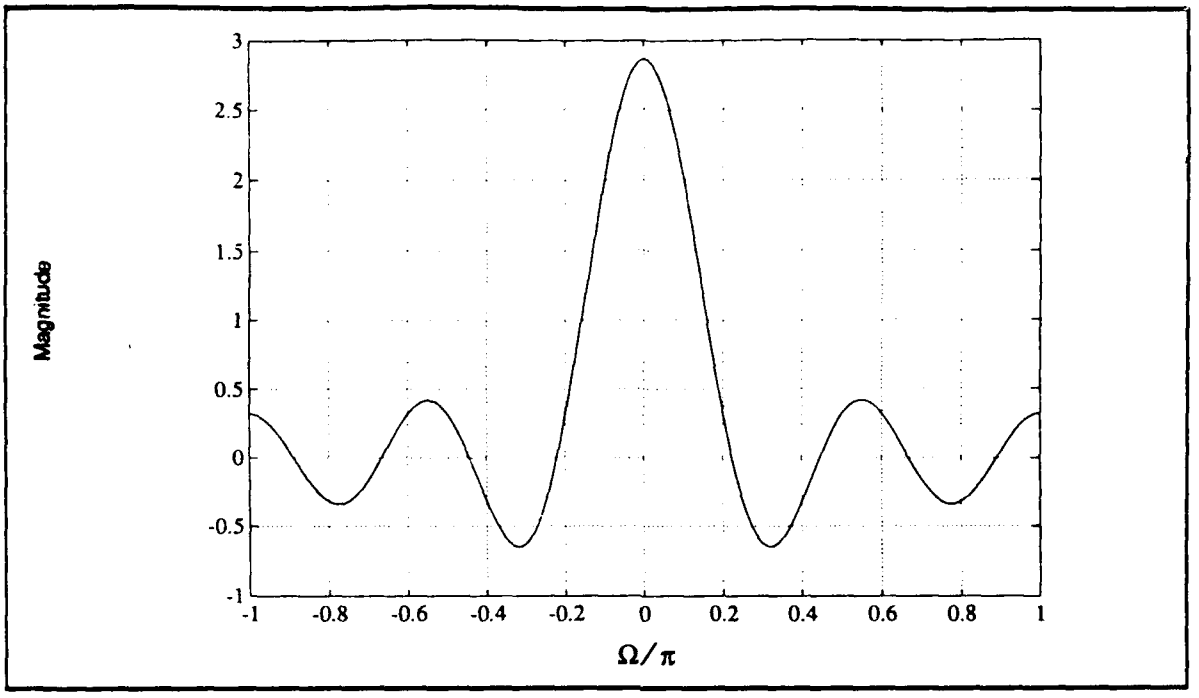

Figure 7.12 - Discrete signal power spectral density for N=5 and Ω_D=0.

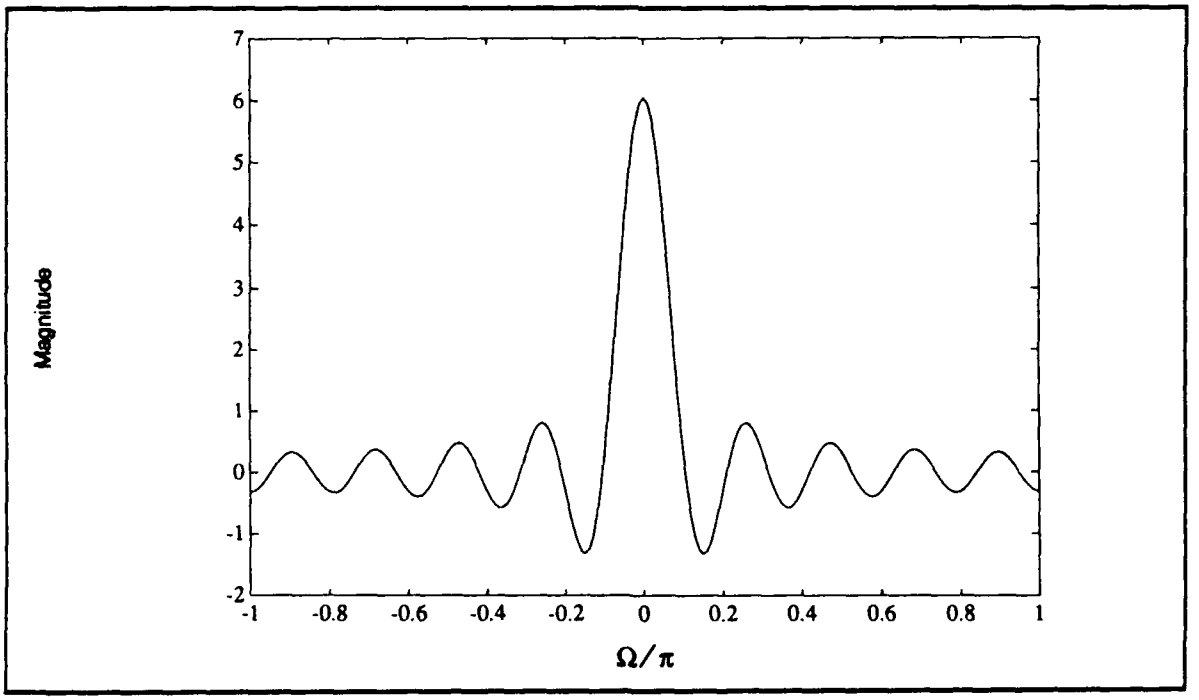

Figure 7.13 - Discrete signal power spectral density for N=10 and Ω_D=0.

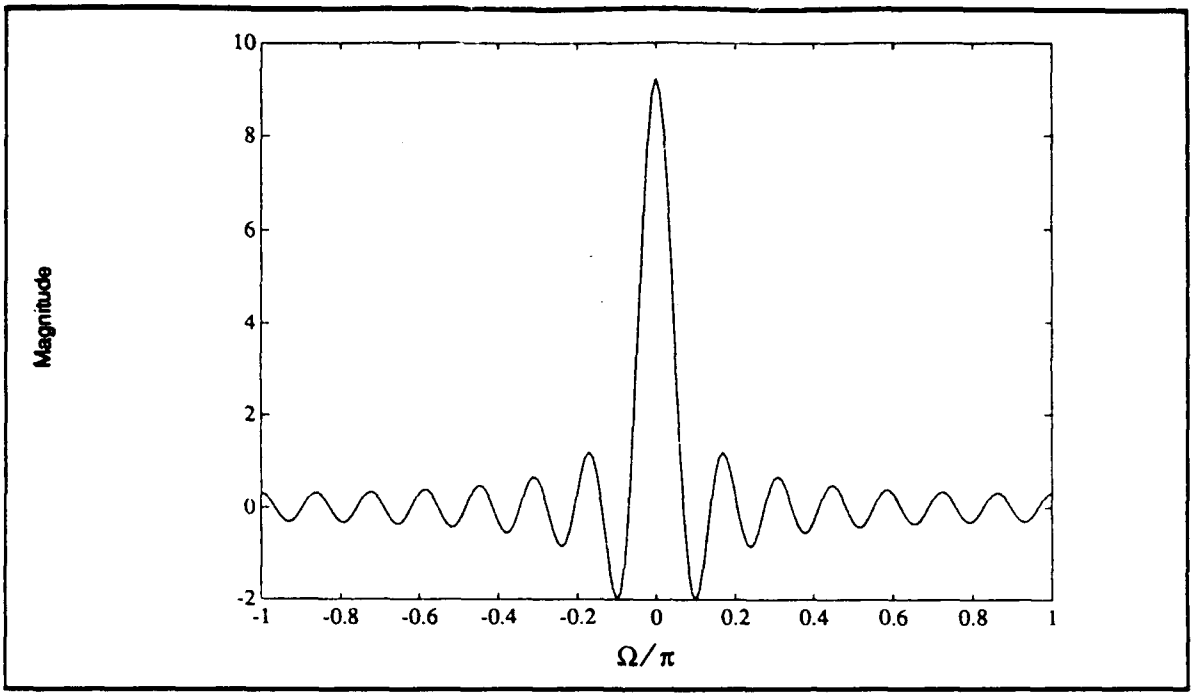

Figure 7.14 - Discrete signal power spectral density for N=15 and Ω_D=0.

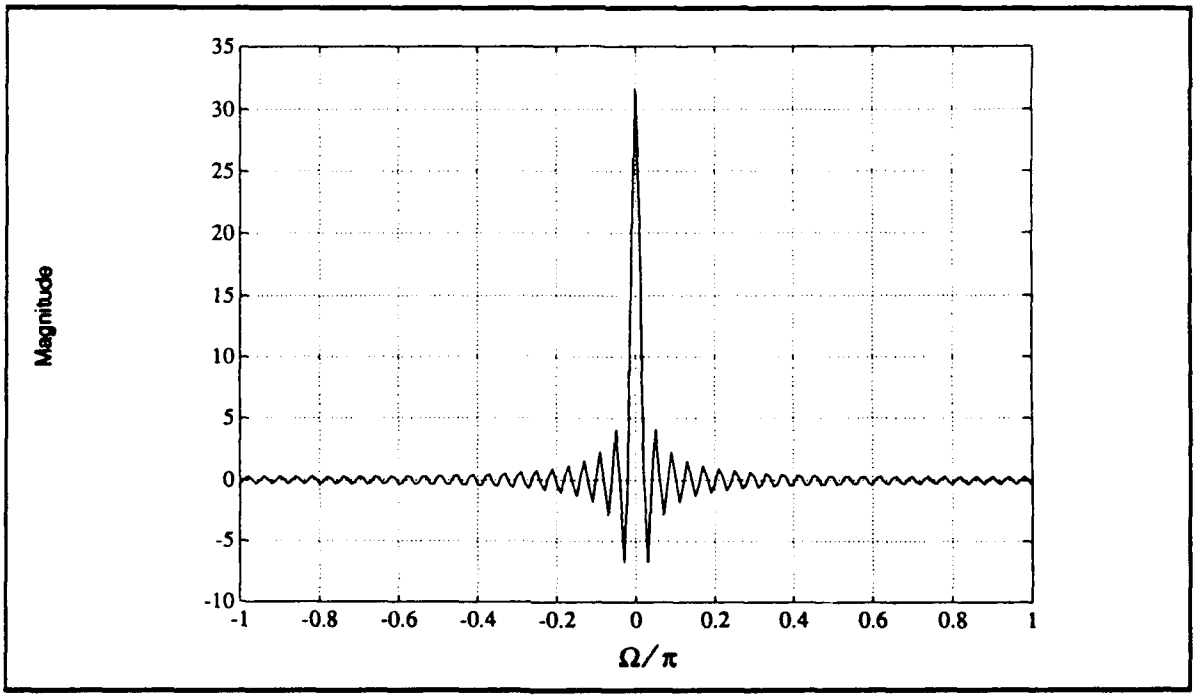

Figure 7.15 - Discrete signal power spectral density for N=50 and Ω_D=0.

7.4 Power Spectral Densities at the Output of the Nonlinearity

As explained in section 6.2, each element of the correlation matrix of the signal at the nonlinearity output consists of (signal x signal) cross terms, (signal x disturbance) cross terms and (disturbance x disturbance) cross terms. By separating out the (signal x signal) cross terms, it is possible to express the correlation matrix as

$$M^{NL} = M_s^{NL} + M_d^{NL} \tag{7.56}$$

where M_s^{NL} is the signal correlation matrix. The disturbance correlation matrix, M_d^{NL}, contains the (signal x disturbance) cross terms plus the (disturbance x disturbance) cross terms and is obtained by substracting M_s^{NL} from M^{NL}.

From Eq.(6.29), the uv^{th} element of M_s^{NL} is given by

$$(M_s^{NL})_{uv} = G^2\sigma_g^2 \sum_{k=0}^{\infty} b_k \cdot \frac{C_k^{2k+1}}{2^{2k+1}} \cdot \left[\frac{1/(2\sigma_1^2)}{1+\alpha^2}\right]^{2k+1} (2\sigma_s^2)^{2k+1} \cdot e^{j2\pi f_D (v-u) T_s} \quad . \tag{7.57}$$

This element corresponds to a lag of $(v-u)T_s$ seconds. As a result, the power spectral density of the desired signal at the output of the nonlinearity can be obtained from

$$\tilde{S}_{sT}^{NL}(\Omega) = \sum_{u=N}^{2} (M_s^{NL})_{u1} e^{-j(1-u)\Omega} + \sum_{v=1}^{N} (M_s^{NL})_{1v} e^{-j(v-1)\Omega} \quad . \tag{7.58}$$

The summation over u involves elements from the first column of M_s^{NL}, incorporating the lags extending from $-(N-1)T_s$ to $-T_s$, while the summation over v involves elements from the first row of M_s^{NL}, incorporating the lags from 0 to $(N-1)T_s$.

The shape of the power spectral density of the desired signal, except for a gain factor, is little affected by the nonlinearity. This is illustrated in Figure 7.16 for the case where

$N=15$, $L=10$, $\sigma_g=5$, $\alpha=0.4975$, $\sigma_n=0.1$, $\sigma_c=5$, $\rho_c=0.9$, $\sigma_s=1.0$, $f_D/f_s=0.5$

and $f_s=1/T_s$ is the pulse repitition frequency of the transmitted signal.

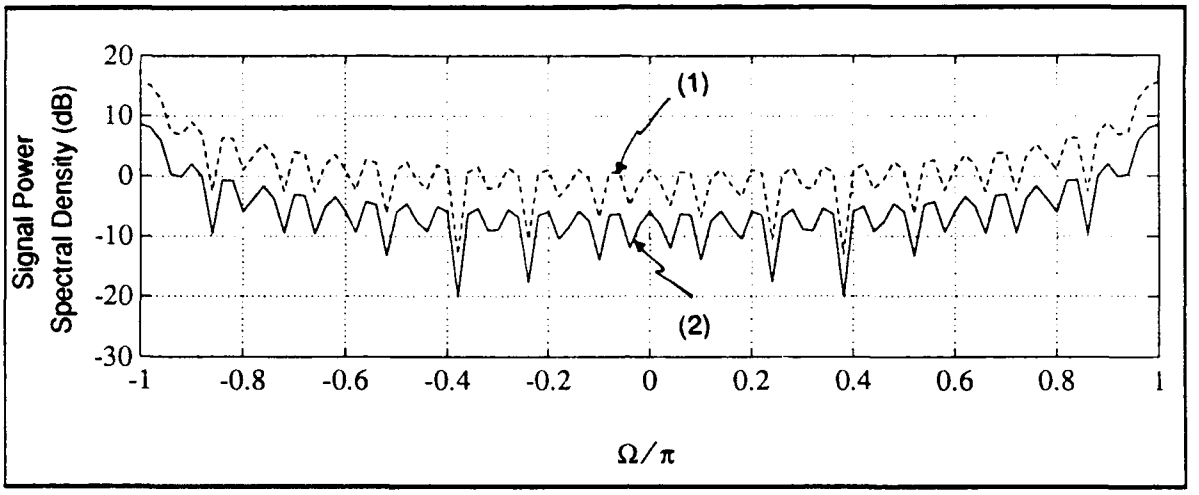

Figure 7.16 - Power spectral densities of the signal at the input of the transversal filter when RF amplifier is: (1) linear, (2) nonlinear.

Because the desired signal power spectral density takes on negative values due to truncation of the autocorrelation sequence, $10\text{Log}_{10}\left|\tilde{S}_{sT}(\Omega)\right|$ and $10\text{Log}_{10}\left|\tilde{S}^{NL}_{sT}(\Omega)\right|$ are plotted in Fig.7.16. Observe that the output power spectral density is identical to the input power spectral density except for an offset of approximately -7 dB. This result is readily explained. Eq.(7.57) can be rewritten as

$$(M_s^{NL})_{uv} = \frac{\sigma_g^2/\sigma_1^2}{1+\alpha^2}\left[\frac{G^2\sigma_s^2}{2}e^{j2\pi f_D(v-u)T_s}\right]\sum_{k=0}^{\infty} b_k \frac{C_k^{2k+1}}{2^{2k}} \cdot \left[\frac{1}{1+\alpha^2}\right]^{2k} \cdot \left(\frac{\sigma_s^2}{\sigma_1^2}\right)^{2k} \quad (7.59)$$

With reference to Eq.(6.12) and recalling that $\alpha=\sigma_s/\sigma_1$, the above expression becomes

$$(M_s^{NL})_{uv} = \frac{\alpha^2}{1+\alpha^2}(M_s^L)_{uv}\left[1+\sum_{k=1}^{\infty} b_k \frac{C_k^{2k+1}}{2^{2k}}\cdot\left[\frac{1}{1+\alpha^2}\right]^{2k}\cdot\left(\frac{\sigma_s^2}{\sigma_1^2}\right)^{2k}\right] \quad . \tag{7.60}$$

In our work it is assumed that $\sigma_s^2 \ll \sigma_c^2$. Hence, the terms involved in the summation on k are negligible and we obtain

$$(M_s^{NL})_{uv} \approx \frac{\alpha^2}{1+\alpha^2}(M_s^L)_{uv} \quad . \tag{7.61}$$

Consequently, the two spectra are identical except for a multiplicative constant. For the curves shown in Fig.7.16, $\alpha=0.4975$. The -7 dB offset is accounted for by the fact that

$$10\text{Log}_{10}\left(\frac{\alpha^2}{1+\alpha^2}\right)\Bigg|_{\alpha=0.4975} = -7.02\text{dB} \quad . \tag{7.62}$$

From Eqs.(6.40) and (6.29), the uv^{th} element of M_d^{NL} is given by

$$\begin{aligned}(M_d^{NL})_{uv} &= (M^{NL})_{uv} - (M_s^{NL})_{uv} \\ &= \frac{\alpha^2}{1+\alpha^2}(M^{NL})_{uv}\Big|_{\text{normalized}}\end{aligned} \tag{7.63}$$

where

$$(M^{NL})_{uv}\Big|_{\text{normalized}} = G^2 \sum_{k=0}^{\infty} b_k \cdot \frac{C_k^{2k+1}}{2^{2k+2}} \cdot \left[\frac{1/(2\sigma_1^2)}{1+\alpha^2}\right]^{2k} \cdot$$

$$\left[\left|\tilde{R}_1[(v-u)T_s]\right|^{2k}\tilde{R}_1[(v-u)T_s] - (2\sigma_s^2)^{2k+1}\cdot e^{j2\pi f_D(v-u)T_s}\right] \quad . \tag{7.64}$$

Comparison of Eqs. (7.61) and (7.63) reveals that $\alpha^2/(1+\alpha^2)$ is a common multiplicative factor to $(M_s^{NL})_{uv}$ and $(M_d^{NL})_{uv}$. As a result, the signal-to-disturbance ratio given by Eq. (6.39) is independent of this factor.

The power spectral density of the disturbance at the nonlinearity output can be expressed as

$$\tilde{S}_{dT}^{NL}(\Omega) = \sum_{u=N}^{2} (M_d^{NL})_{u1} e^{-j(1-u)\Omega} + \sum_{v=1}^{N} (M_d^{NL})_{1v} e^{-j(v-1)\Omega} \quad . \tag{7.65}$$

As with Eq.(7.58), the summations over u and v incorporate the negative and non-negative lags, respectively.

Both Equations (7.58) and (7.60) contain the common multiplicative factor $\alpha^2/(1+\alpha^2)$. In order to compare the spectra for cases II and III with those for case I, it is convenient to divide the spectra for cases II and III by the factor $\alpha^2/(1+\alpha^2)$. This constrains the spectra for cases II and III at the input to the transversal filter to have identical maxima as those for case I. Thereby, any differences in spectral shape for cases II and III from those of case I are readily observed. This normalization procedure has been carried out in all of the remainig spectral plots. With this normalization, the desired signal spectrum at the input to the transversal filter becomes identical for cases I, II, and III.

For the same nonlinearity as in Fig. 7.16, Figs. 7.17 (a) and (b) show the plot of the power spectral density of the disturbance at the input to the transversal filter before and after normalization, respectively. When normalized, the disturbance spectrum for case II has the same maximum as the disturbance spectrum for case I.

The nonlinearity tends to widen the power spectral density of the disturbance (i.e, clutter plus noise). This is illustrated in Figure 7.17 (b). Because the contributions of the nonlinear terms are small relative to the linear term, the output power spectral density at the maximum, in the vicinity of Ω=0, is little changed

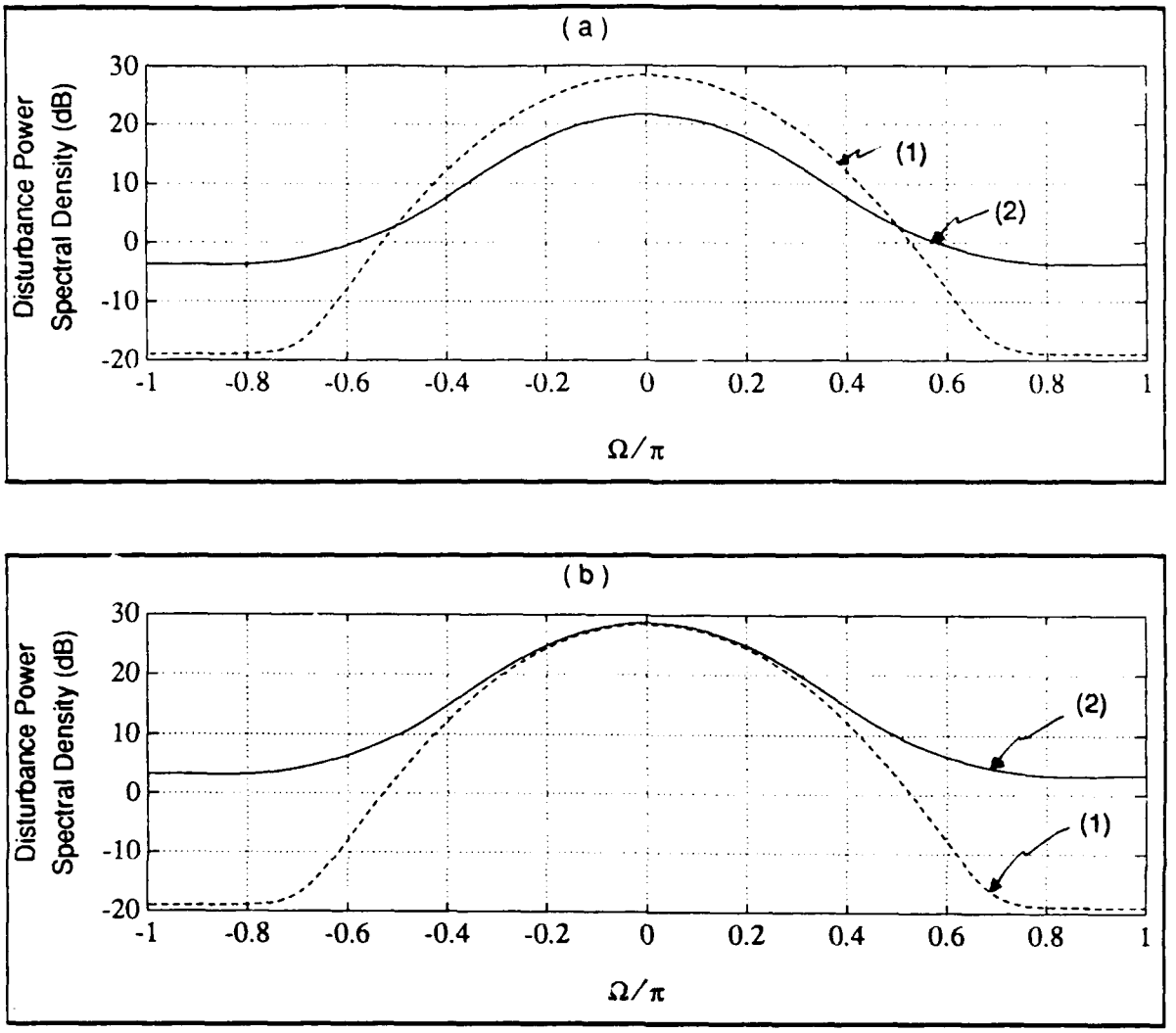

Figure 7.17 - Power spectral densities of the disturbance at the input of the transversal filter when RF amplifier is: (1) linear, (2) nonlinear, (a) unnormalized case, (b) normalized case,

from that at the input. However, at the higher frequencies where the power spectral density is relatively small, the output power spectral density is in excess of 20 dB larger than that at the input.

7.5 Power Spectral Density at the Transversal Filter Output

Let $\tilde{S}_T^{NL}(\Omega)$ denote the power spectral density of the total signal at the out-

put of the nonlinearity (i.e., input to the transversal filter). Because

$$M^{NL} = M_s^{NL} + M_d^{NL}, \tag{7.65}$$

it follows that

$$\tilde{S}_T^{NL}(\Omega) = \tilde{S}_{sT}^{NL}(\Omega) + \tilde{S}_{dT}^{NL}(\Omega) \cdot \tag{7.66}$$

The linear transfer function of the transversal filter is given by Eq.(7.13). Let $\tilde{S}_0(\Omega)$ denote the power spectral density of the transversal filter output. Then

$$\begin{aligned} \tilde{S}_0(\Omega) &= |H_{TF}(\Omega)|^2 \cdot \tilde{S}_T^{NL}(\Omega) \\ &= |H_{TF}(\Omega)|^2 (\tilde{S}_{sT}^{NL}(\Omega) + \tilde{S}_{dT}^{NL}(\Omega)) \cdot \end{aligned} \tag{7.67}$$

The output power spectral density of the desired signal is

$$\tilde{S}_{os}(\Omega) = |H_{TF}(\Omega)|^2 \cdot \tilde{S}_{sT}^{NL}(\Omega) \tag{7.68}$$

whereas the power spectral density of the disturbance is

$$\tilde{S}_{od}(\Omega) = |H_{TF}(\Omega)|^2 \cdot \tilde{S}_{dT}^{NL}(\Omega) \cdot \tag{7.69}$$

To illustrate the effect of filtering by the transversal filter, consider the same case as was used in obtaining the plots of Figs. 7.16 and 7.17. In Fig. 7.18 plots are shown of the signal and disturbance power spectral densities at the filter input plus the magnitude of the filter transfer function optimized to maximize the signal-to-disturbance ratio with the nonlinearity taken into account . The filter output signal and disturbance power spectral densities are shown in Fig. 7.19. Observe that the optimum filter attenuates signals at low frequencies where the disturbance is dominant and passes signals in the frequency band where the signal spectrum is maximum. This results in a maximum value for the signal-to-disturbance ratio.

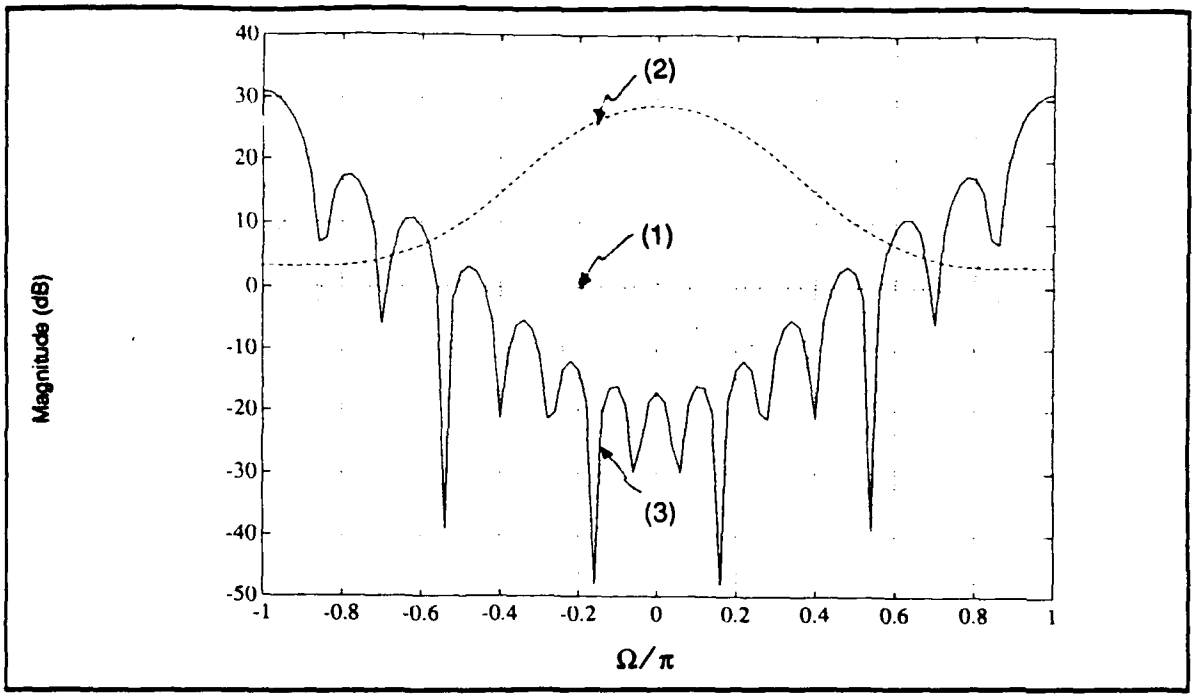

Figure 7.18 - Plots 0f (1) $\tilde{S}_{sT}^{NL}(\Omega)$ *, (2)* $\tilde{S}_{dT}^{NL}(\Omega)$ *, and (3)* $|H_{TF}(\Omega)|$ *.*

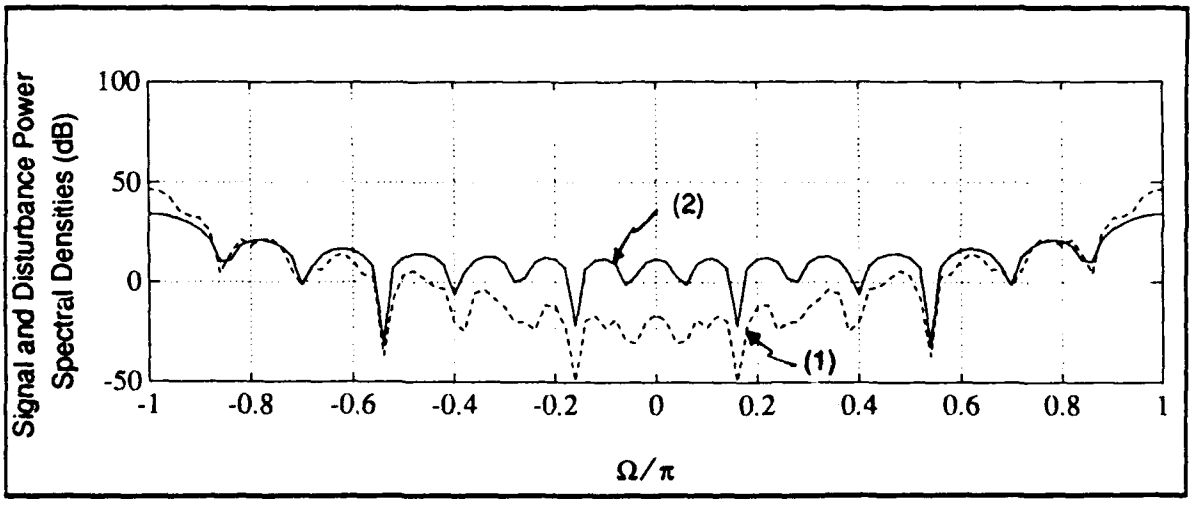

Figure 7.19 - Plots of (1) $\tilde{S}_{0s}(\Omega)$ *and (2)* $\tilde{S}_{0d}(\Omega)$ *.*

Chapter 8

COMPUTER GENERATED RESULTS

In order to assess radar performance degradation caused by the receiver nonlinearity, computer generated results are presented and discussed in this chapter. Both signal and receiver parameters are varied so as to determine how performance is affected. In addition to evaluating signal-to-disturbance ratios at the transversal filter output, signal spectra and transfer functions are plotted where ever they are useful in interpreting results. In terms of the normalized frequency variable

$$\Omega = 2\pi f T_s = 2\pi \frac{f}{f_s}, \tag{8.1}$$

the spectra and transfer functions are periodic with period 2π. Consequently, they need to be plotted only over the interval

$$-\pi \leq \Omega \leq \pi \ . \tag{8.2}$$

Division by π results in the inequality

$$-1 \leq \frac{f}{f_s/2} \leq 1 \ . \tag{8.3}$$

Hence, the end points of the plots correspond to

$$f = \pm \frac{f_s}{2} \ . \tag{8.4}$$

The variable

$$\frac{\Omega}{\pi} = \frac{f}{f_s/2} \tag{8.5}$$

is used in all of the plots.

Three different cases are considered depending upon whether the transversal filter weights apply to

1) an ideal linear receiver (case I),

2) a nonlinear receiver having the same transversal filter as was used with the ideal linear receiver (case II),

3) a nonlinear receiver with the transversal filter modified to account for the receiver nonlinearity (case III).

Unless stated otherwise, a situation where the desired signal is strong relative to the thermal noise but is weak relative to the clutter is studied. In particular, the standard deviations of the signal, clutter, and noise are specified to be

$$\sigma_s = 1, \sigma_c = 10, \sigma_n = 0.1 \, . \tag{8.6}$$

Consequently, the input signal-to-noise ratio is

$$(SNR)_{in} = 20Log_{10}\left(\frac{\sigma_s}{\sigma_n}\right) = 20dB \, , \tag{8.7}$$

the input signal-to-clutter ratio is

$$(SCR)_{in} = 20Log_{10}\left(\frac{\sigma_s}{\sigma_c}\right) = -20dB \, , \tag{8.8}$$

the input noise-to-clutter ratio is

$$(NCR)_{in} = 20Log_{10}\left(\frac{\sigma_n}{\sigma_c}\right) = -40dB \, , \tag{8.9}$$

and the input signal-to-disturbance ratio is

$$(SDR)_{in} = 20Log_{10}\left(\frac{\sigma_s}{\sigma_1}\right) = -20.044dB \tag{8.10}$$

where

$$\sigma_1^2 = \sigma_s^2 + \sigma_c^2 + \sigma_n^2 \ . \tag{8.11}$$

8.1 Computer Generated Results for Case I: The Ideal Linear Receiver

Case I refers to the situation where the radar receiver is modeled as though it is linear with a gain of

$$G = \sqrt{\frac{2}{\pi}} \cdot \frac{L}{\sigma_g} \ . \tag{8.12}$$

Assuming the weights of the transversal filter are chosen to maximize the signal-to-disturbance ratio at the output of the transversal filter, it is shown in Eq.(6.65) that the maximum output signal-to-disturbance ratio is given by

$$(SDR)_I = \frac{G^2\sigma_s^2}{2} \cdot \underline{a}^T (M_d^L)^{-1} \underline{a}^* \tag{8.13}$$

where

$$\underline{a}^T = [a_1 a_2 \ldots\ldots a_N] \ , \tag{8.14}$$

$$a_k = e^{j2\pi f_D (j-i) T_s} \ ; k = 1,2,\ldots\ldots,N \tag{8.15}$$

and the uv^{th} element of the matrix M_d^L is given in Eq.(6.13) as

$$(M_d^L)_{uv} = \frac{G^2}{2}\left[\sigma_c^2 \cdot e^{-\frac{((v-u)T_s)^2}{2\sigma_w^2}} + \sigma_n^2 \cdot \frac{\sin(\pi W (v-u) T_s)}{\pi W (v-u) T_s}\right] \ . \tag{8.16}$$

It follows that each element in $(M_d^L)^{-1}$ is proportional to $2/G^2$. Consequently, $(SDR)_I$, where the subscript I refers to case I, is independent of G and, therefore, is also independent of the choices for L and σ_g.

Dependence of $(SDR)_I$ on the remaining parameters is difficult to ascertain by inspection because of the complexity of the (NxN) matrix $(M_d^L)^{-1}$. Therefore, computer generated results are used in the following subsections to study the effects of these parameters.

8.1.1 Dependence of $(SDR)_I$ on Doppler Frequency

As printed out in chapter 7, the desired signal power spectral density is centered at f_D. Because one period of the spectra spans frequencies in the interval $0 \leq f \leq f_s$, frequencies higher than f_s are folded over into this interval. To avoid ambiguities in the Doppler frequency, it is assumed that

$$0 \leq \frac{f_D}{f_s} \leq 1 \text{ .} \tag{8.17}$$

A plot of $(SDR)_I$ versus f_D/f_s is shown in Fig.8.1 for three different values of

$$\rho_c = e^{-\frac{T_s^2}{2\sigma_w^2}} \text{.} \tag{8.18}$$

When $\rho_c=0$, the clutter power spectral density is white (i.e., constant). Since the noise power spectral density is also white, the total power spectral density of the disturbance is a constant with respect to frequency. Therefore, $(SDR)_I$ is independent of the center frequency of the desired signal spectrum and plots as a constant. Even so, observe that the transversal filter is able to increase the output signal-to-disturbance ratio from approximately -20 dB at its input to approximately -8 dB at its output. This amounts to a processing gain of approximately 12 dB.

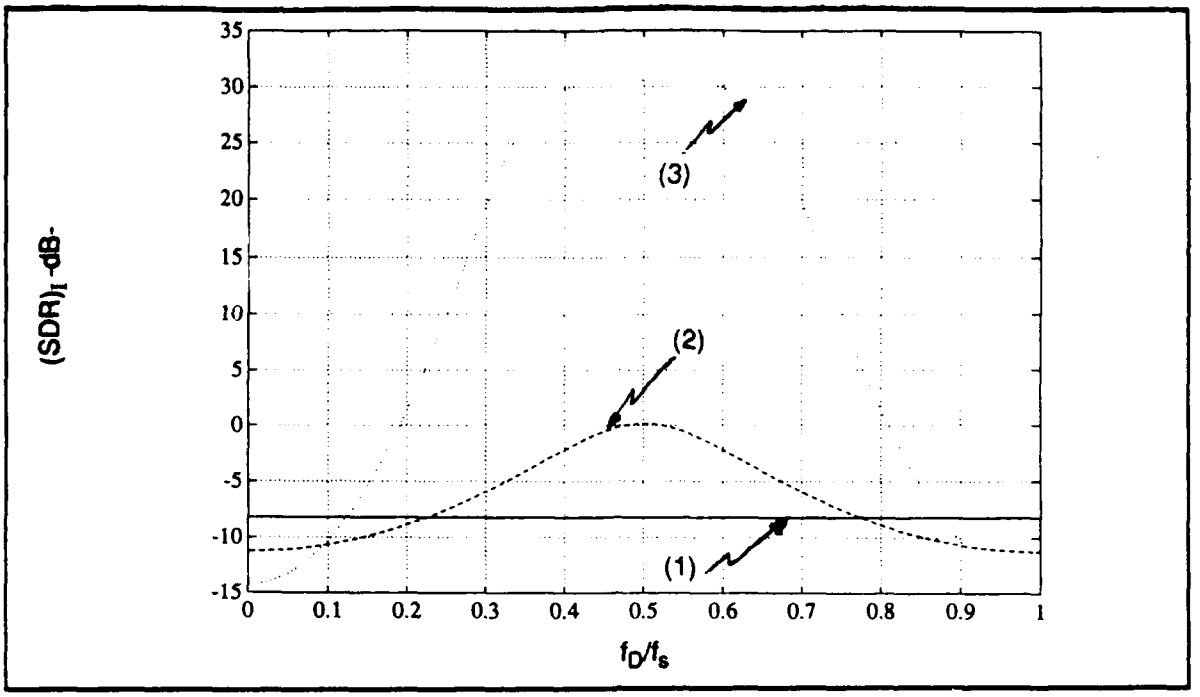

Figure 8.1 - Dependence of $(SDR)_I$ on the Doppler Frequency (1) ρ_c=0, (2) ρ_c=0.5, (3) ρ_c=0.9.

When ρ_c=0.9, the clutter power spectral density is relatively narrow. Because of periodicity in the spectrum, it peaks both at f_D/f_s=0 and f_D/f_s=1. The smallest values of the power spectral density occur in the neighborhood of f_D/f_s=0.5. Consequently, the plot of $(SDR)_I$ is maximum at this value of Doppler frequency. When f_D=0.5f_s, a processing gain in excess of 50 dB is achieved. (Note that the input signal-to-disturbance ratio has been increased from approximately -20 dB to approximately 31 dB).

ρ_c=0.5 corresponds to an intermediate situation. The smallest values of the clutter power spectral density are still in the vicinity of f_D/f_s=0.5 so that the plot of $(SDR)_I$ peaks at this value. However, because the clutter power spectral density is much wider than it was for ρ_c=0.9, the clutter spectrum is significantly larger at f_D=0.5f_s and the processing gain is only approximately 20 dB.

8.1.2 Dependence of $(SDR)_I$ on The Clutter Correlation Parameter

As pointed out in chapter 7, the clutter correlation sequence can be ex-

pressed as

$$\tilde{R}_c[kT_s] = 2\sigma_c^2 \cdot \rho_c^{k^2} \tag{8.19}$$

where ρ_c is given by Eq.(8.18). The clutter samples are said to be highly correlated when $\rho_c \approx 1$ and uncorrelated when $\rho_c = 0$. A plot of the normalized clutter correlation sequence, $(\tilde{R}_c[kT_s])/(2\sigma_c^2)$, is shown in Fig.8.2. The correlation sequence is observed to become wider as the value of ρ_c is increased. As a result, the clutter power spectral density becomes narrower for larger values of ρ_c. A plot of $(SDR)_I$ versus ρ_c is shown in Fig.8.3 for three different values of f_D/f_s.

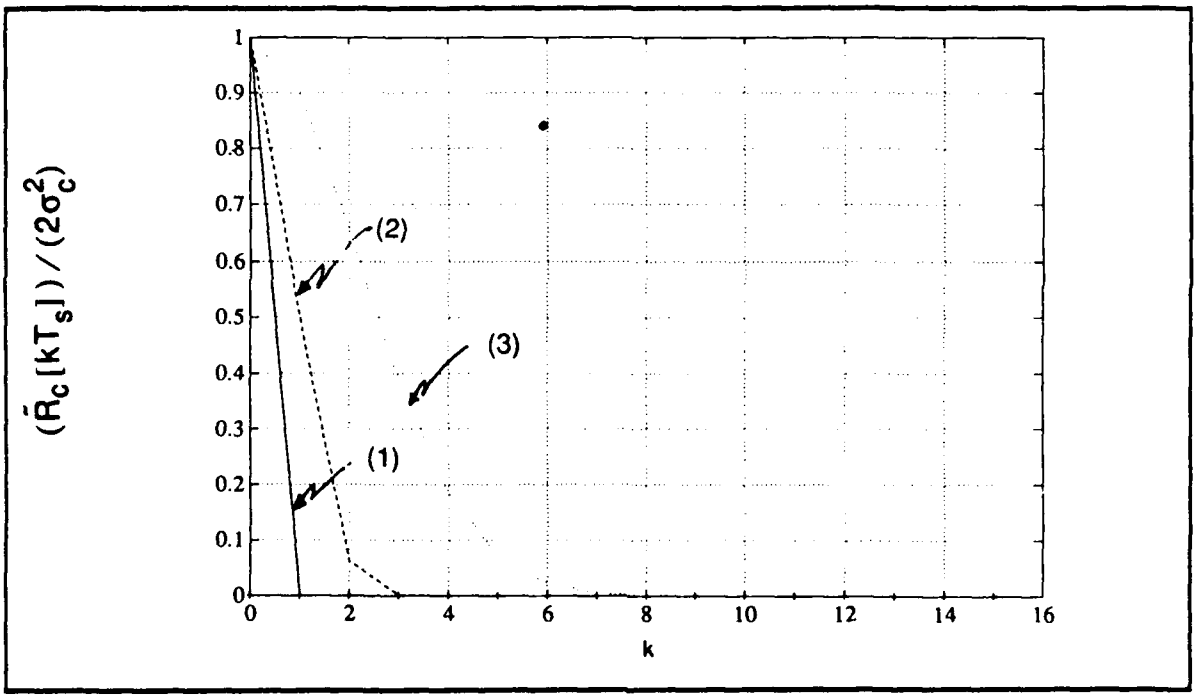

Figure 8.2 - Normalized Clutter Correlation Sequence (1) ρ_c=0, (2) ρ_c=0.5, (3) ρ_c=0.9.

As shown in Fig.8.1, the most favorable positioning of the desired signal spectrum occurs when $f_D = 0.5f_s$. Because the clutter spectrum becomes narrower as ρ_c becomes larger, the signal-to-disturbance ratio increases with increasing values of ρ_c.

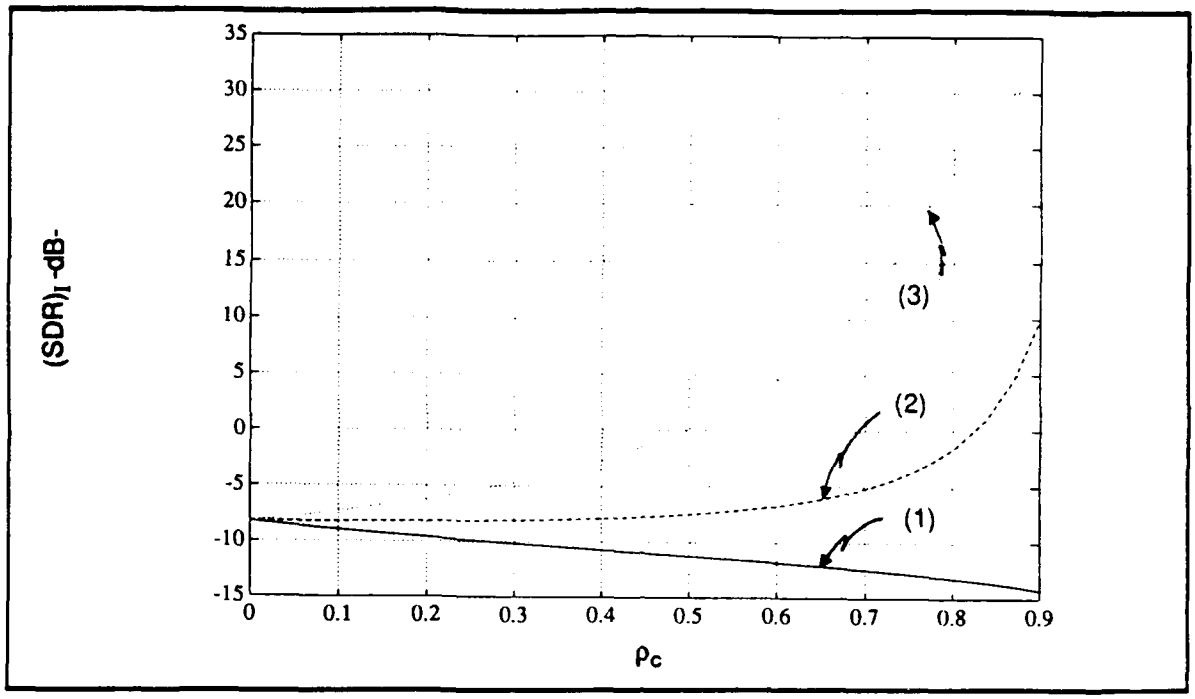

Figure 8.3 - Dependence of $(SDR)_I$ on the Clutter Correlation Parameter
(1) f_D/f_s=0, (2) f_D/f_s=0.25, (3) f_D/f_s=0.5.

Since the clutter spectrum peaks at f=0, the worst case positioning of the desired signal spectrum occurs when f_D=0. The area of the clutter power spectral density remains constant at $2\sigma_c^2$ independent of the value for ρ_c. Therefore, as the clutter spectrum becomes narrower, its maximum value at f=0 becomes larger. As a result, the output signal-to-disturbance ratio decreases as ρ_c increases.

An intermediate situation results when $f_D=0.25f_s$. Because the peak of the desired signal spectrum is offset from that of the clutter spectrum, the output signal-to-disturbance ratio improves as the clutter spectrum narrows. Nevertheless, performance is not as good as when $f_D=0.5f_s$.

For ρ_c=0, the clutter power spectral density is constant. Consequently, the location of the desired signal power spectral density is immaterial and all three curves in Fig.8.3 have identical values at ρ_c=0.

8.1.3 Dependence of $(SDR)_I$ on the Thermal Noise Power Level

From Eq.(7.29), the correlation sequence of the thermal noise is

$$\tilde{R}_n[kT_s] = 2\sigma_n^2 \cdot \frac{\sin(\pi W k T_s)}{\pi W k T_s} \quad . \tag{8.20}$$

As explained in Chapter 7, this can be approximated by

$$\tilde{R}_n[kT_s] \approx \begin{cases} 2\sigma_n^2 & ; k=0 \\ 0 & ; k \neq 0 \end{cases} \quad . \tag{8.21}$$

As a result, the thermal noise power spectral density is approximately constant. Throughout this work, it is assumed that the total clutter power is much larger than the total thermal noise power. Consequently, as σ_n is varied over the interval

$$0.1 \leq \sigma_n \leq 1 \, , \tag{8.22}$$

σ_c is fixed at $\sigma_c=10$.

Because the clutter power spectral density is Gaussian shaped while the noise power spectral density is constant, it is possible for the thermal noise to be significant when the desired signal spectrum is positioned at the minimum of the clutter power spectral density. This is illustrated in Fig.8.4 where $\rho_c=0.9$ and $f_D=0.5f_s$. The power spectral densities at the input to the transversal filter are shown in parts (a) and (b) of the figure while the output power spectral densities

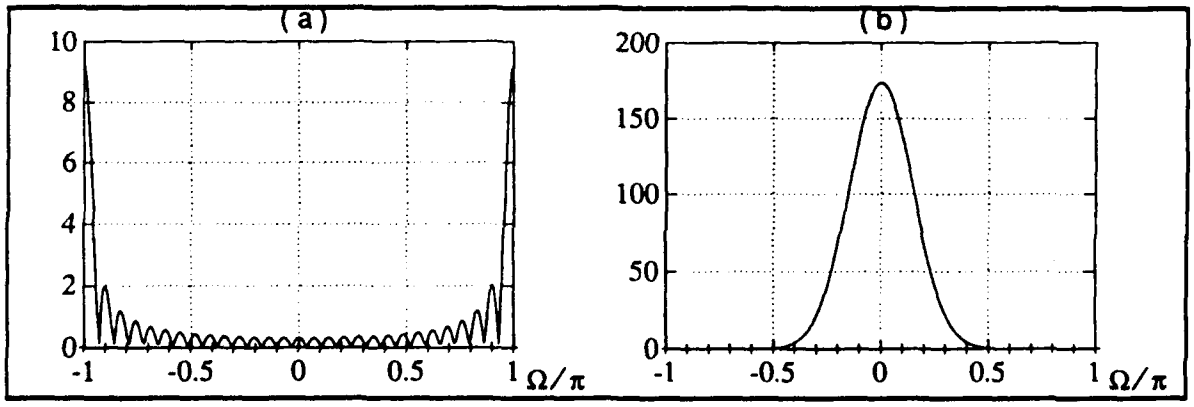

Figure 8.4 - (Caption appears on next page).

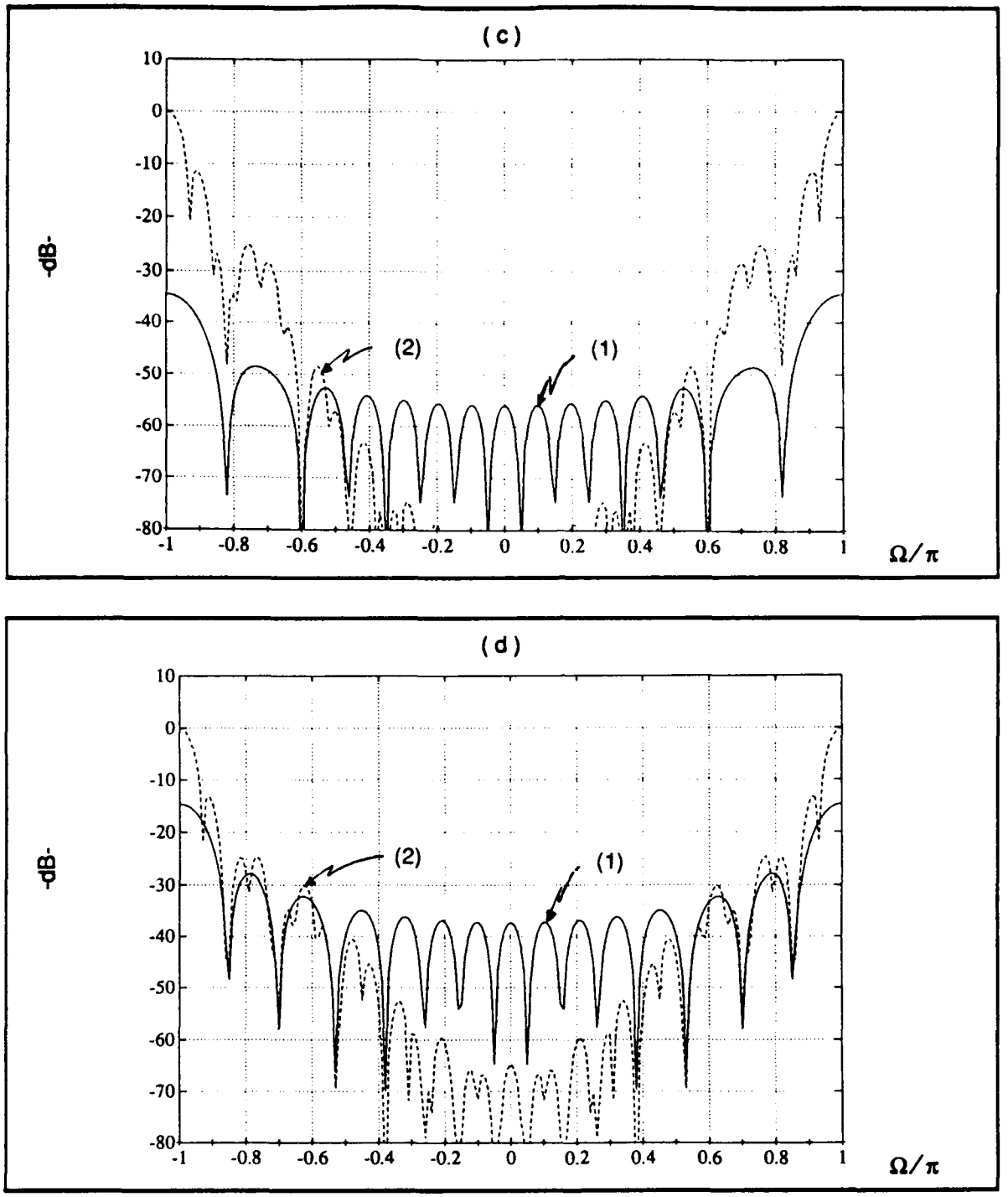

Figure 8.4 - a) Power spectral density of desired signal at input to the transversal filter (f_D=0.5f_s), b) power spectral density of clutter at input to the transversal filter (ρ_c=0.9), c) power spectral densities at output of transversal filter for σ_n=0.1: (1) clutter plus noise, (2) desired signal, (d) power spectral densities at output of transversal filter for σ_n=1: (1) clutter plus noise, (2) desired signal.

are shown in parts (c) and (d) for the noise-to-clutter ratio equal to -40dB and -20 dB, respectively. Note that the transversal filter is successful in removing most of the low-frequency clutter power. However, the increase in thermal noise power of 20dB does result in an increase of the noise floor by approximately 20dB at the transversal filter output. For σ_n=0.1, $(SDR)_I$=30.6dB while $(SDR)_I$=11.4dB for σ_n=1. Hence, the 20dB increase in thermal noise power results in a degradation of 19.2dB in the output signal-to-disturbance ratio.

On the other hand, when the desired signal spectrum is positioned at the peak of the clutter power spectral density, the 20dB increase in thermal noise power has negligible effect. This is illustrated in Fig.8.5 where, as in Fig.8.4, ρ_c=0.9 but now f_D=0. Observe that the output power spectral densities in part (d) are little changed from those in part (c). For σ_n=0.1, $(SDR)_I$=-14.2dB while $(SDR)_I$=-14.5dB for σ_n=1. Thus, the 20dB increase in thermal noise power results in only a 0.3dB decrease of the output signal-to-disturbance ratio.

Analogous to the results of Fig.8.5, when f_D=0, the 20dB increase in thermal noise power has negligible effect when the clutter power spectral density is white. This is illustrated in Fig.8.6 where ρ_c=0 and f_D=0.25f_s. As in Fig.8.5, the output power spectral densities in part (d) are little changed from those in part (c). For σ_n=0.1, $(SDR)_I$=-8.2dB while $(SDR)_I$=-8.3dB for σ_n=1. Here, the 20dB increase in thermal noise power results in only a 0.1dB decrease of the output signal-to-disturbance ratio.

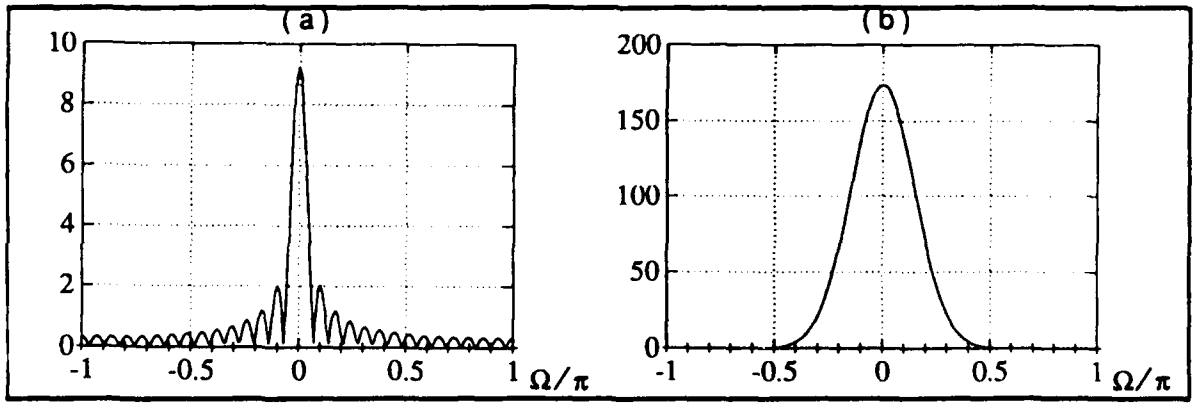

Figure 8.5 - (Caption appears on next page).

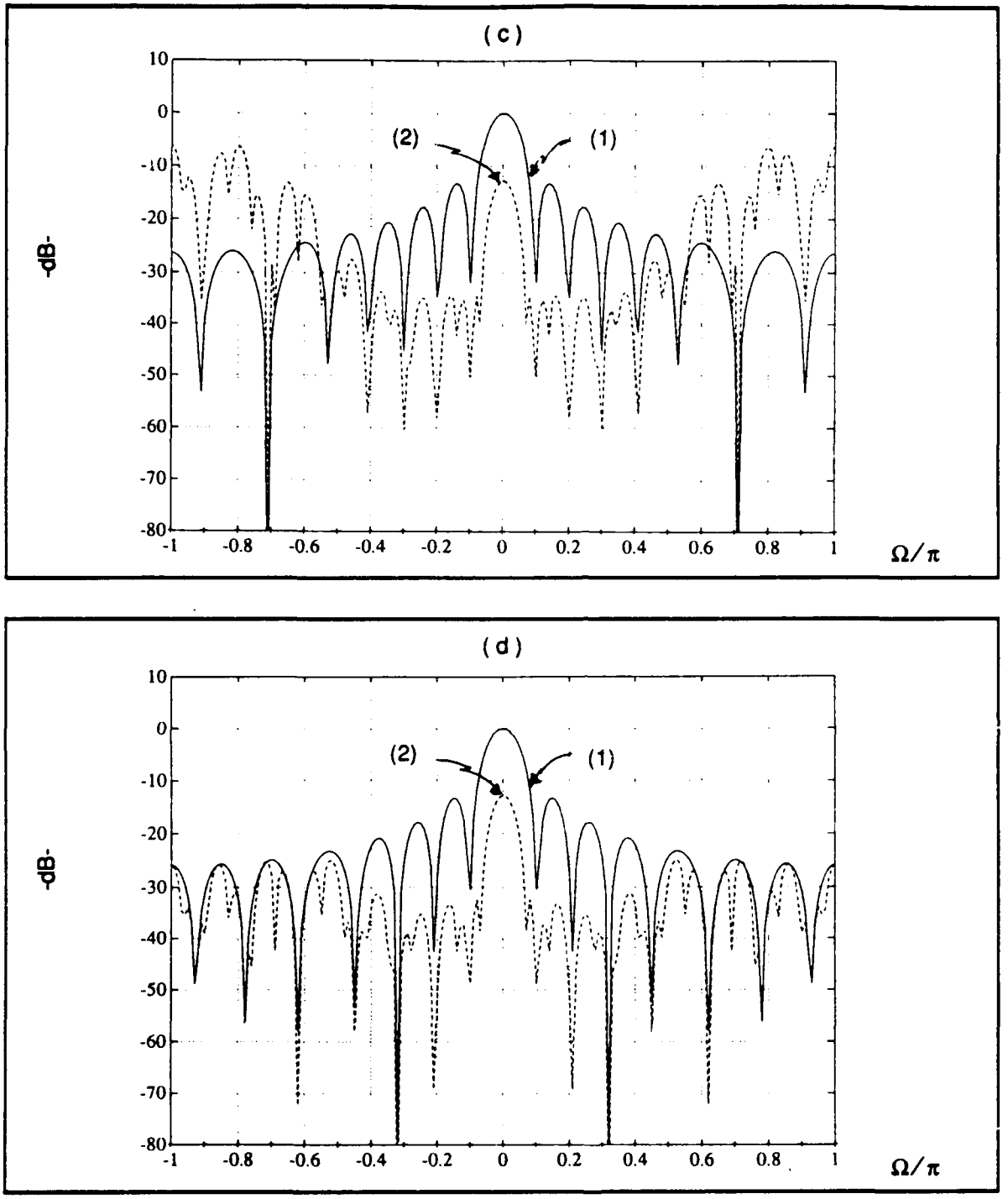

Figure 8.5 a) Power spectral density of desired signal at input to the transversal filter (f_D=0.5f_s), b) power spectral density of clutter at input to the transversal filter (ρ_c=0.9), c) power spectral densities at output of transversal filter for σ_n=0.1: (1) clutter plus noise, (2) desired signal, (d) power spectral densities at output of transversal filter for σ_n=1: (1) clutter plus noise, (2) desired signal.

Plots of $(SDR)_I$ versus the input noise-to-clutter ratio, as defined in Eq.(8.9), are shown in Fig.8.7. In part (a), $f_D=0.5f_s$. For highly correlated samples ($\rho_c=0.9$), where the clutter power spectral density is relatively narrow, the output signal-to-disturbance ratio falls off linearly in dB as the thermal noise power is increased. Specifically, a 20 dB increase in $(NCR)_{in}$ results in approximately a 20 dB decrease of $(SDR)_I$. For moderately correlated ($\rho_c=0.5$) and uncorrelated ($\rho_c=0$) clutter, where the clutter power spectral density is wider, the signal-to-disturbance ratio remains constant as σ_n is increased. However, $(SDR)_I$ is approximately 8 dB larger at $\rho_c=0.5$ than it is at $\rho_c=0$. In part (b) of the figure, $f_D=0.25fs$. For $\rho_c=0.9$,the decrease in $(SDR)_I$ is approximately 3.5 dB,

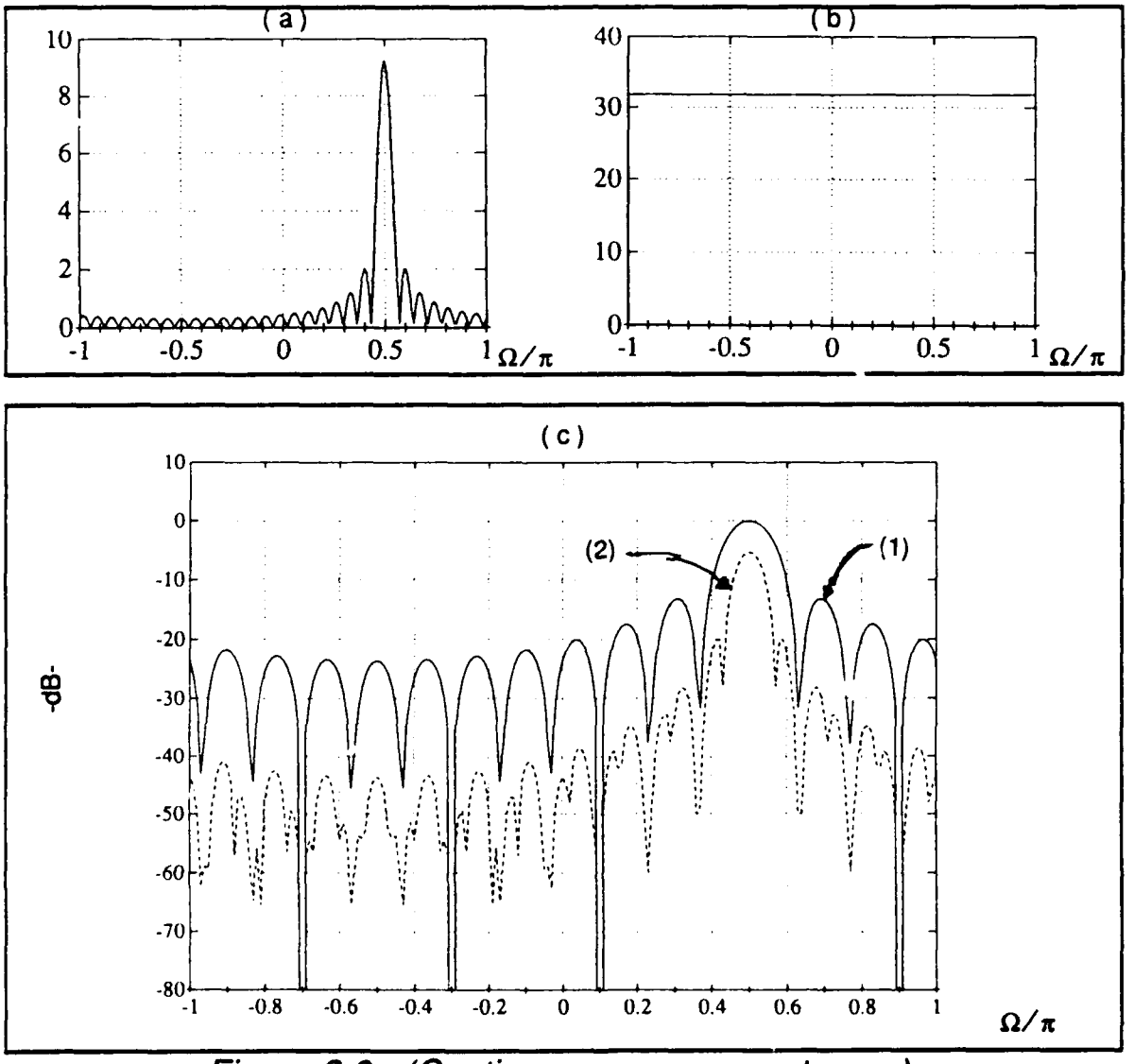

Figure 8.6 - (Caption appears on next page).

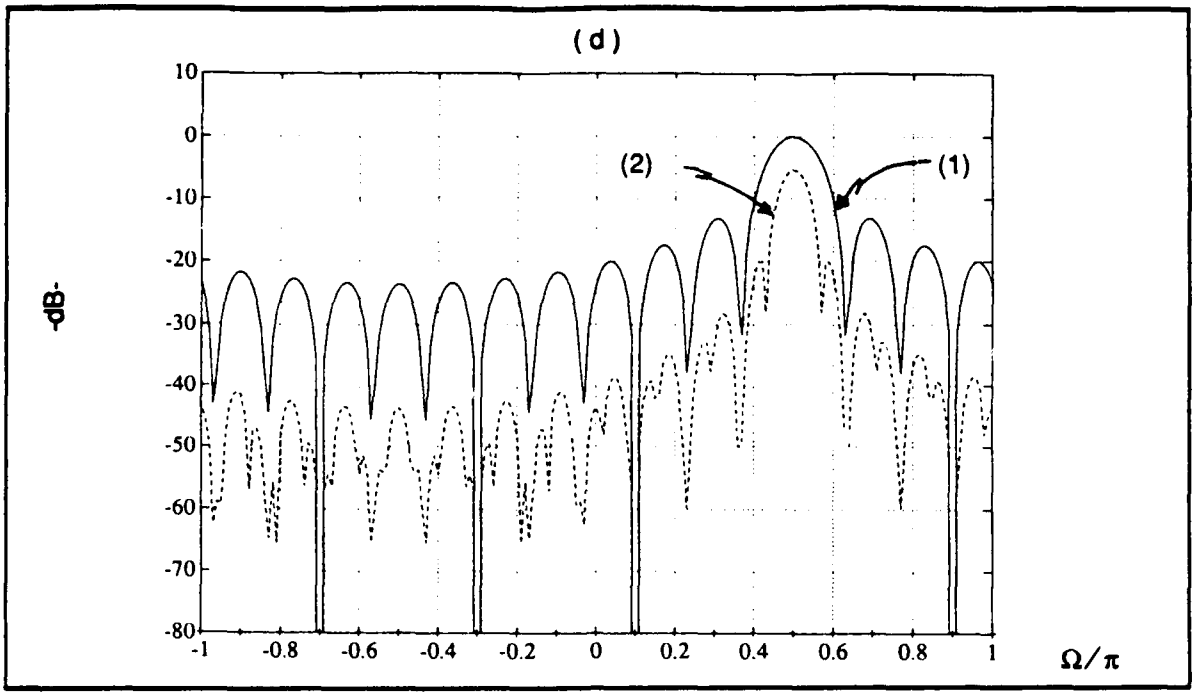

Figure 8.6 a) Power spectral density of desired signal at input to the transversal filter (f_D=0.25f_s), b) power spectral density of clutter at input to the transversal filter (ρ_c=0), c) power spectral densities at output of transversal filter for σ_n=0.1: (1) clutter plus noise, (2) desired signal, (d) power spectral densities at output of transversal filter for σ_n=1: (1) clutter plus noise, (2) desired signal.

considerably less than it was for f_D=0.5 fs. Also, the constant output signal-to-disturbance ratio at ρ_c=0.5 is only approximately 1 dB larger than the value for ρ_c=0. In part (c) of the figure, f_D=0. Thus, the clutter and desired signal power spectral densities both peak at f=0. For ρ_c=0.9, $(SDR)_I$ is relatively insensitive to the increase in thermal noise power (note the expanded vertical scale) because the disturbance is dominated by the clutter in the vicinity of f=0. As in parts (a) and (b), the curves are constant for ρ_c=0.5 and ρ_c=0. However, in contrast to parts (a) and (b), the output signal-to-disturbance ratio decreases with increasing values of ρ_c. As explained previously, this is due to the fact that the peak value of the clutter power spectral density increases at f=0 with increasing values of ρ_c because the

area under the density remains constant as the spectrum becomes narrower.

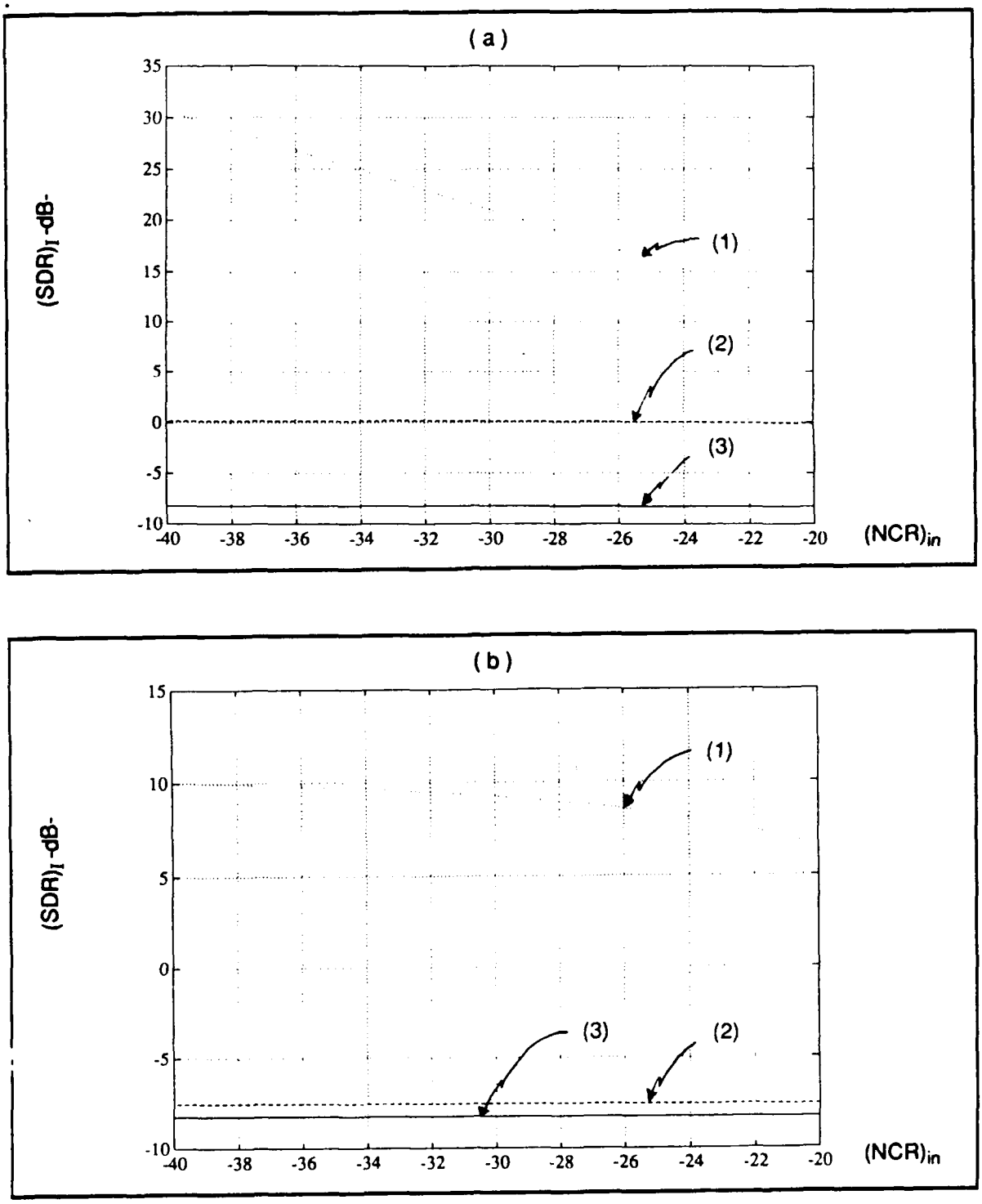

Figure 8.7 - (Caption appears on next page).

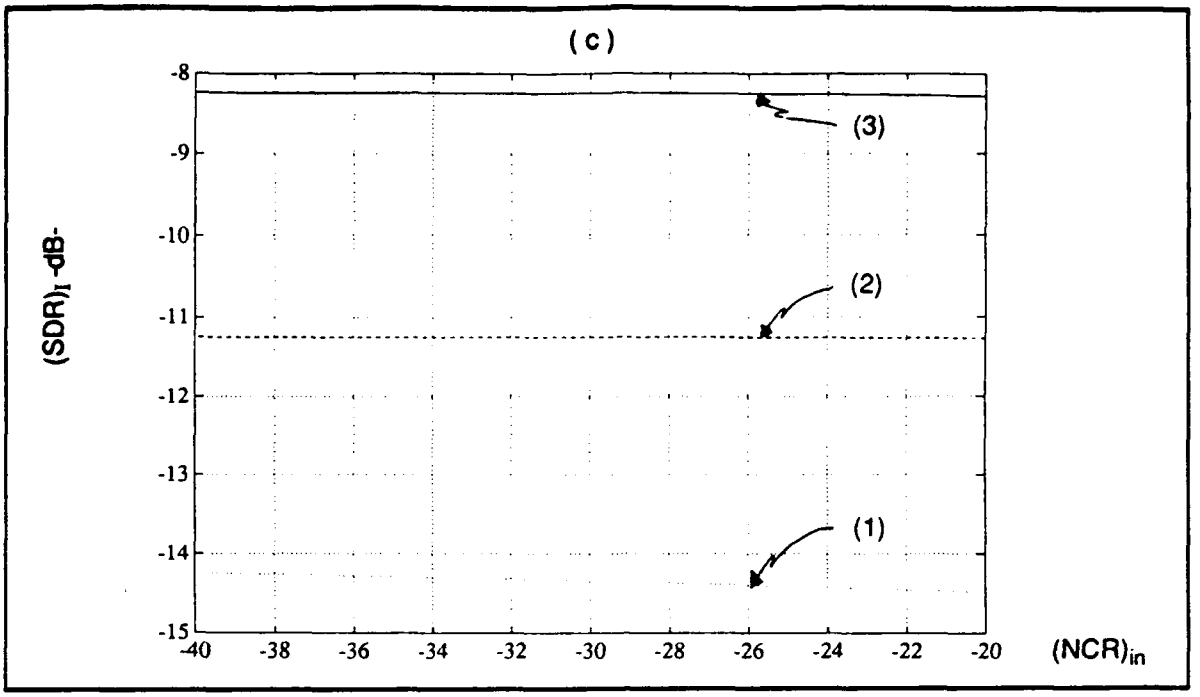

Figure 8.7 - Dependence of $(SDR)_I$ on Thermal Noise Power Level: (1) ρ_c=0.9, (2) ρ_c=0.5, (3) ρ_c=0 (a) f_D/f_s=0.5, (b) f_D/f_s=0.25, (c) f_D/f_s=0.

8.1.4 Dependence of $(SDR)_I$ on the Clutter Power Level

In this section σ_c is varied over the interval

$$10 \le \sigma_c \le 100 \tag{8.23}$$

while σ_s and σ_n are held fixed at σ_s=1 and σ_n=0.1. Therefore, the input signal-to-clutter ratio and input noise-to-clutter ratio, as defined by Eqs. (8.8) and (8.9), vary according to

$$-40\text{dB} \le (SCR)_{in} \le -20\text{dB} \tag{8.24}$$

and

$$-60\text{dB} \le (NCR)_{in} \le -40\text{dB}\ . \tag{8.25}$$

Dependence of $(SDR)_I$ on the clutter power level is illustrated in Fig.8.8. In

part (a) of the figure, $f_D=0.5f_s$. For $\rho_c=0.9$, the clutter power spectral density is sufficiently narrow, such that the thermal noise dominates the disturbance at $f=0.5f_s$. Consequently, the output signal-to-disturbance ratio is relatively insensitive to variations in the clutter power. However, for the remaining cases considered in parts (a), (b), and (c), the clutter dominates the disturbance in the frequency inter-

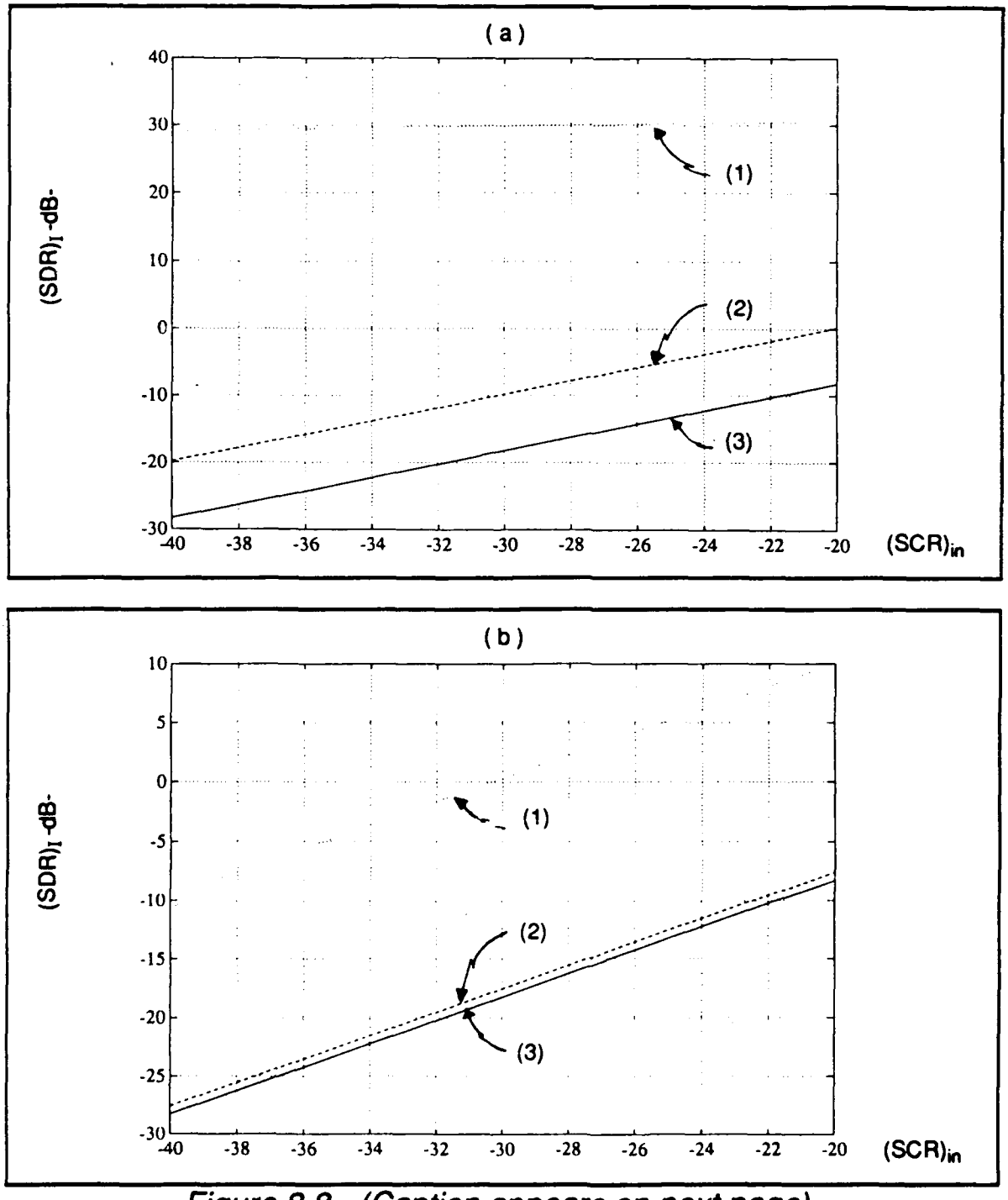

Figure 8.8 - (Caption appears on next page).

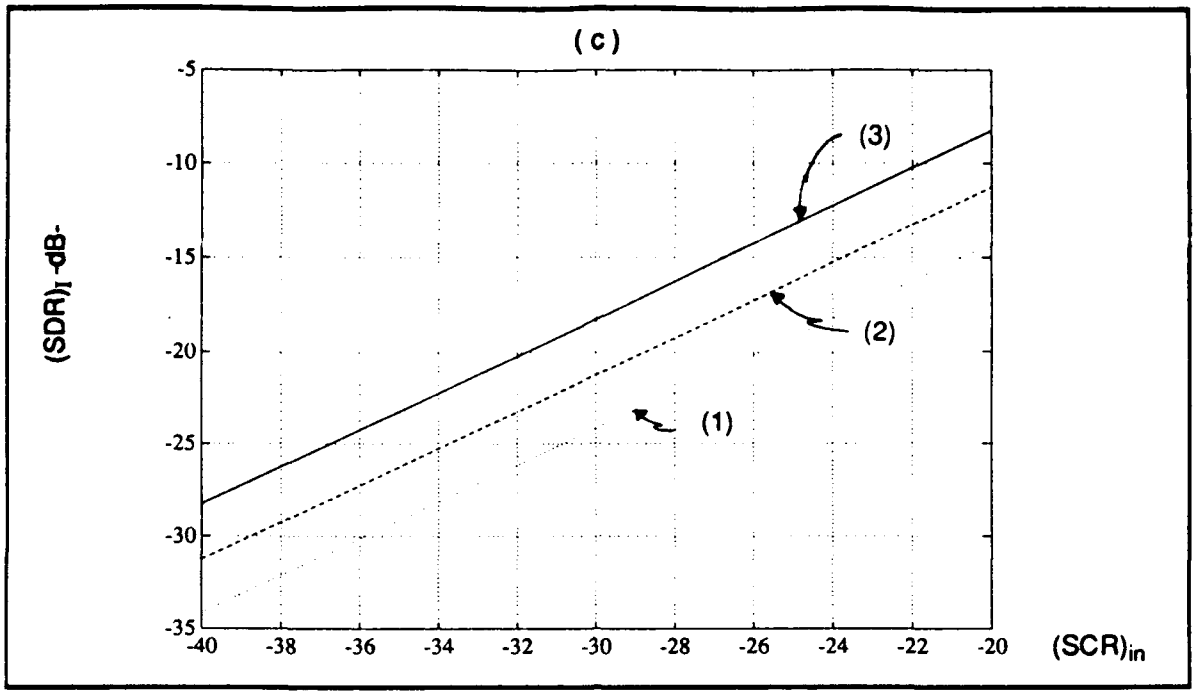

Figure 8.8 - Dependence of $(SDR)_I$ on the Clutter Power Level: (σ_s=1, σ_n=0.1): (1) ρ_c=0.9, (2) ρ_c=0.5, (3) ρ_c=0 (a) f_D/f_s=0.5, (b) f_D/f_s=0.25, (c) f_D/f_s=0.

val where the major part of the desired signal power is located. As a result, the curves plot as straight lines with slopes such that a 20 dB increase in the input signal-to-clutter ratio is accompanied by approximately a 20 dB increase in the output signal-to-disturbance ratio. This is reasonable because $(SDR)_I$ is given by Eq.(8.13) where the uvth element of the matrix M_d^L is given by Eq.(8.16). For those frequencies where the clutter power is much larger then the thermal noise power, the matrix $(M_d^L)^{-1}$ is inversely proportional to σ_c^2.

8.1.5 Dependence of $(SDR)_I$ on the Number of Samples, N.

It is expected that the output signal-to-disturbance ratio should increase with an increase in the number of samples processed. This is shown to be the case in Fig. 8.9 for f_D/f_s=0.5, 0.25 ,0 and ρ_c=0.9, 0.5, 0.

The improvement is due to two factors: 1) the power in the desired signal becomes more concentrated in the frequency interval centered at f_D, and 2) the

number of degrees of freedom of the transversal filter is equal to N. The input power spectral densities for N=15 and N=35 are shown in Fig. 8.10. Note that the clutter plus noise power spectral density remains unchanged whereas the power spectral density of the desired signal has a narrower central lobe with its peak

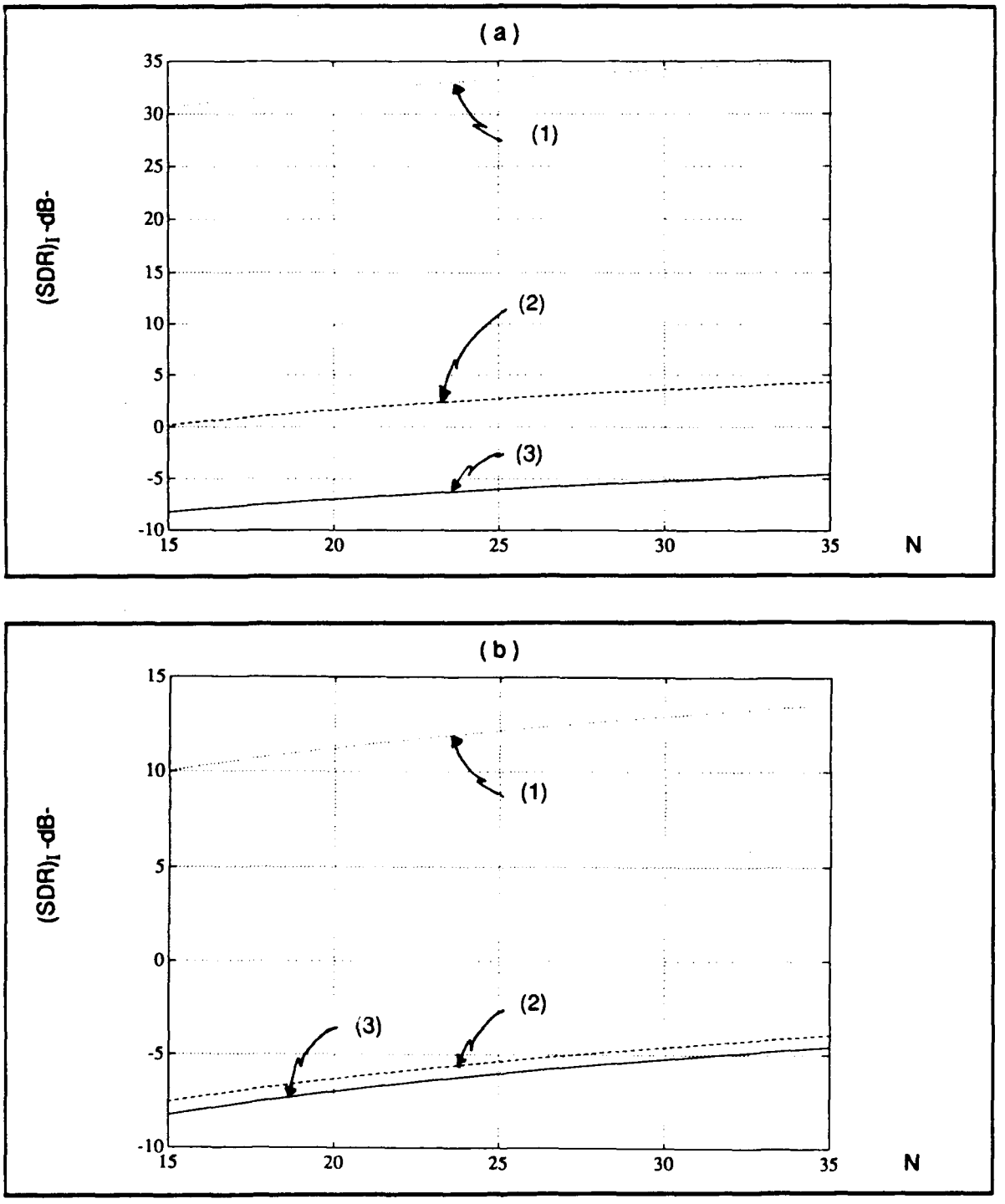

Figure 8.9 - (Caption appears on next page).

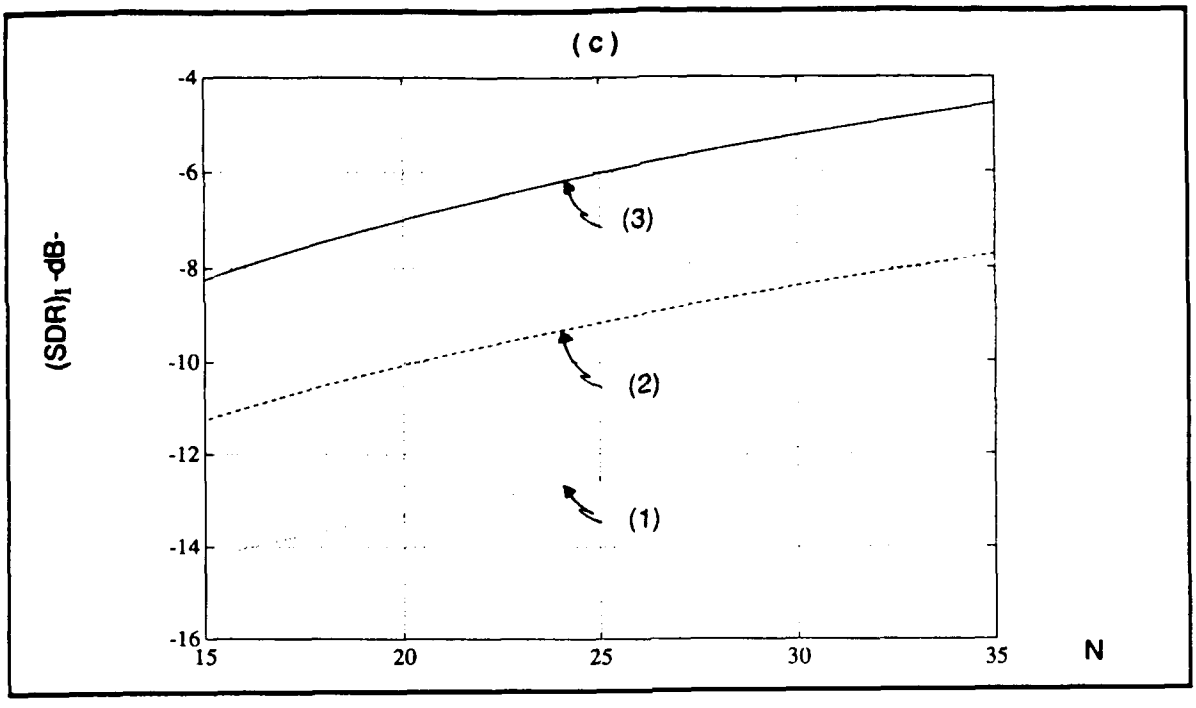

Figure 8.9 - Dependence of $(SDR)_I$ on the Number of Samples: (1) ρ_c=0.9, (2) ρ_c=0.5, (3) ρ_c=0 (a) f_D/f_s=0.5, (b) f_D/f_s=0.25, (c) f_D/f_s=0.

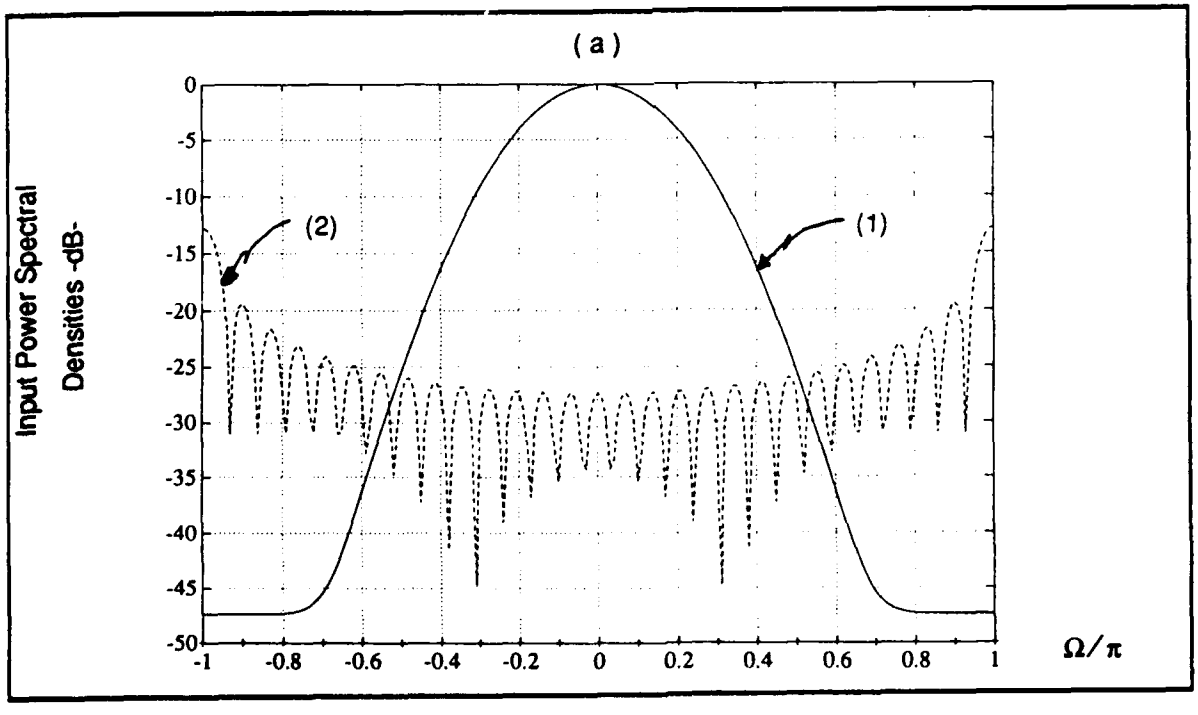

Figure 8.10 - (Caption appears on next page).

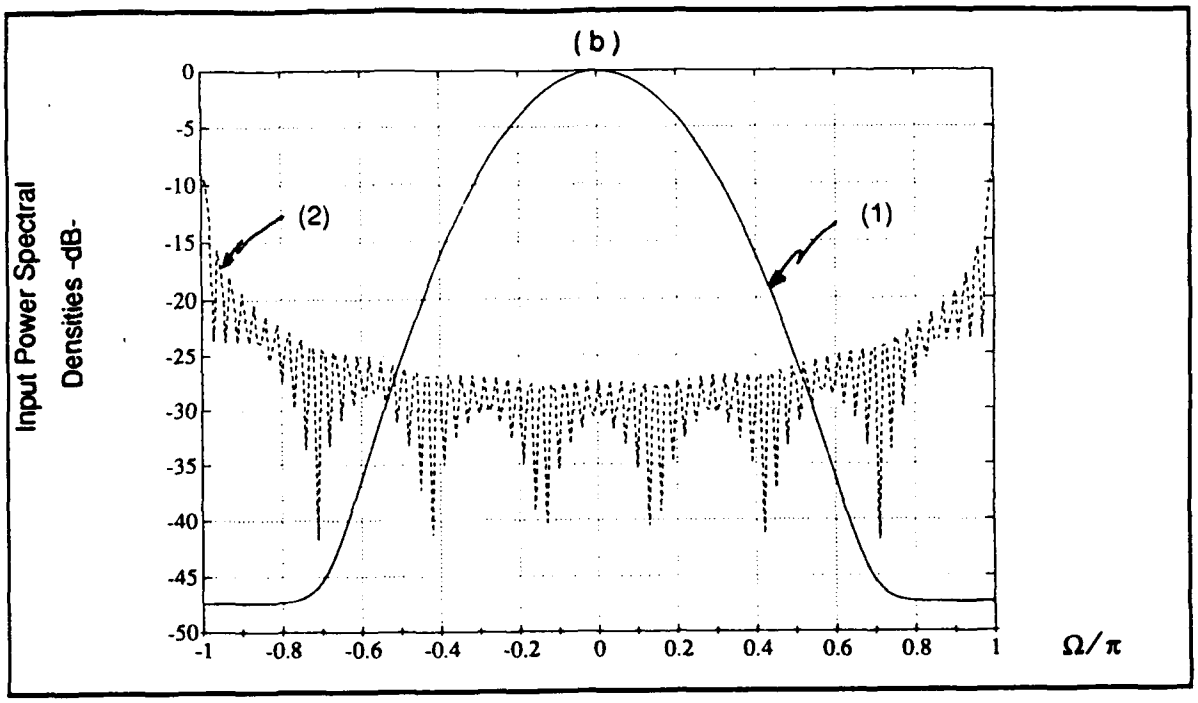

Figure 8.10 - Input Power Spectral Densities: (1) clutter plus noise, (2) desired signal (a) N=15, (b) N=35.

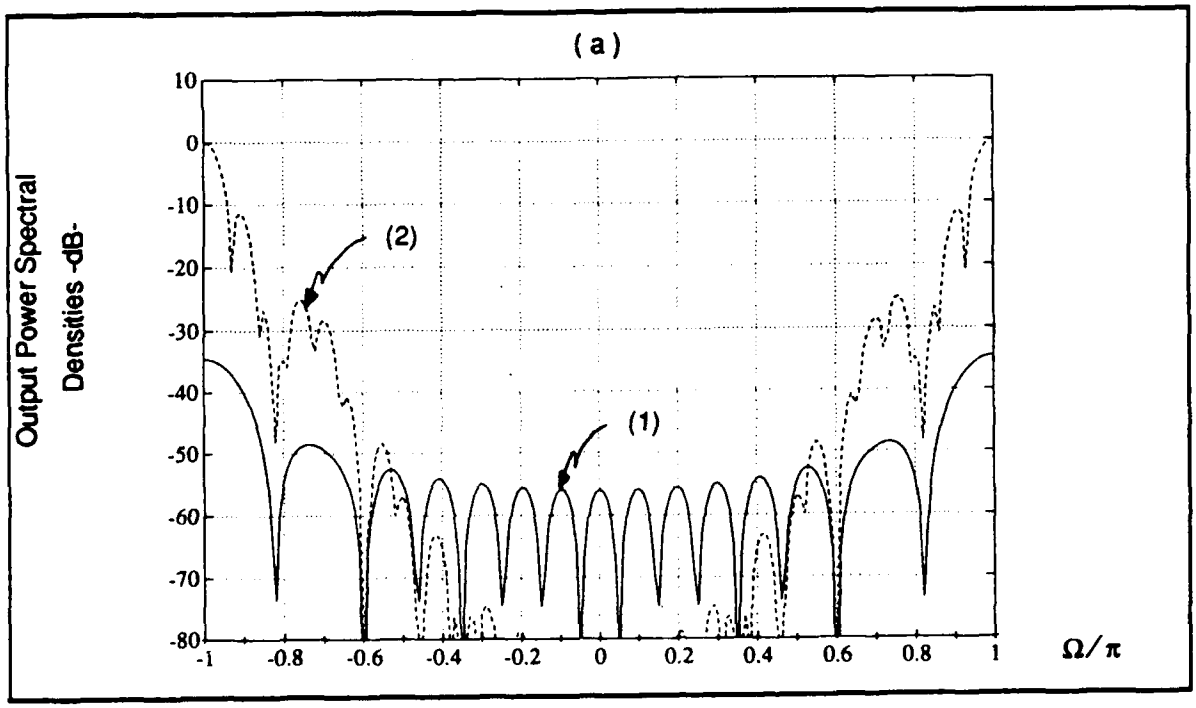

Figure 8.11 - (Caption appears on next page).

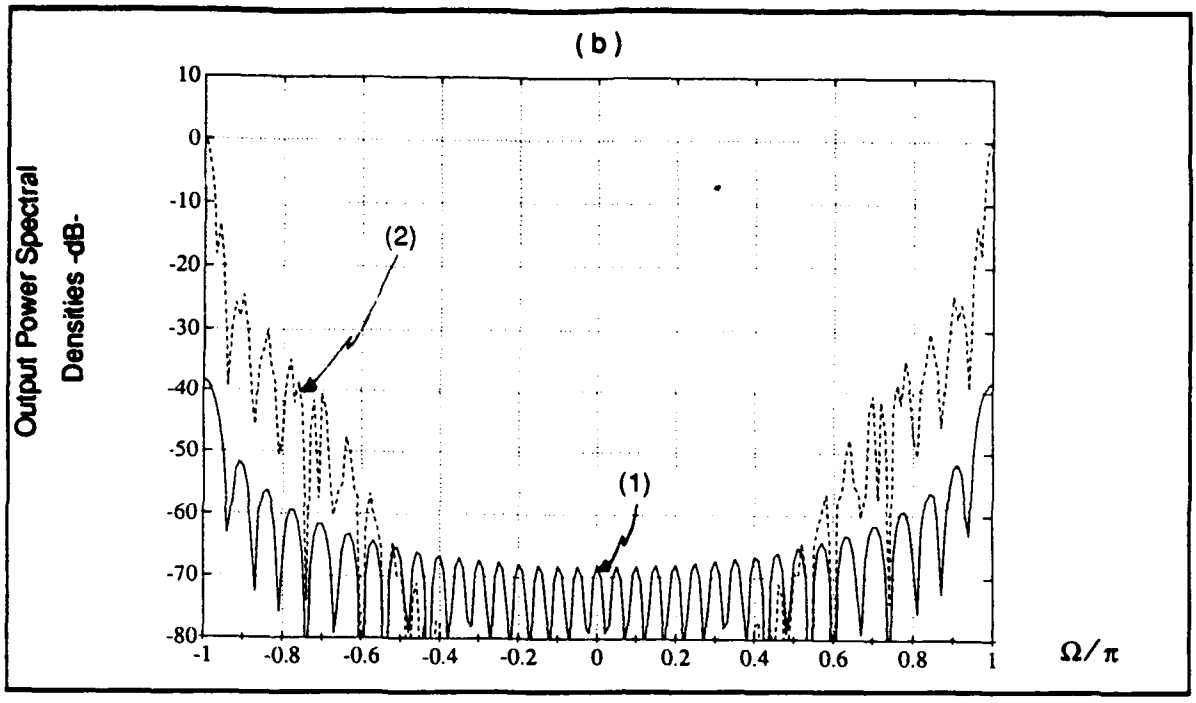

Figure 8.11 - Output Power Spectral Densities: (1) clutter plus noise, (2) desired signal (a) N=15, (b) N=35.

value having increased by approximately 3 dB. The corresponding output power spectral densities are shown in Fig. 8.11. The increased degrees of freedom of the transversal filter result in spectra having finer grain where the clutter plus noise density has been reduced approximately 10dB in the vicinity of f=0 and 3 dB in the vicinity of $f=0.5f_s$.

8.2 Computer Generated Results for Case II: The Nonlinear Receiver with the Same Transversal Filter as in Case I

Case II refers to the situation where the radar receiver is nonlinear. Nevertheless, the transversal filter designed for the ideal linear receiver is used to improve the output signal-to-disturbance ratio. This case can arise when either the design engineer is unaware of the nonlinearity or does not choose to take it into account.

From Eq.(6.67) the output signal-to-disturbance ratio is given by

$$(SDR)_{II} = \frac{\underline{\tilde{w}}^H M_s^{NL} \underline{\tilde{w}}}{\underline{\tilde{w}}^H M_d^{NL} \underline{\tilde{w}}} \qquad (8.26)$$

where the transversal filter weight vector is determined according to Eq.(6.63) as

$$\underline{\tilde{w}} = k \cdot (M_d^L)^{-1} \underline{a}^* \quad . \qquad (8.27)$$

In Eq.(8.27) k is an arbitrary constant and $\underline{a}$ is defined by Eqs.(8.14) and (8.15). For simplicity, k is set equal to unity. M_d^L is the (NxN) matrix whose uv^{th} element is given by Eq.(8.16). The uv^{th} element of the (NxN) matrix M_s^{NL} is given by Eq.(6.29) as

$$(M_s^{NL})_{uv} = G^2 \sigma_g^2 \sum_{k=0}^{\infty} b_k \cdot \frac{C_k^{2k+1}}{2^{2k+1}} \cdot \left[\frac{1/(2\sigma_1^2)}{1+\alpha^2} \right]^{2k+1}$$

$$(2\sigma_s^2)^{2k+1} \cdot e^{j2\pi f_D (v-u) T_s} \quad . \qquad (8.28)$$

Finally, the uv^{th} element of the (NxN) matrix M_d^{NL} is given by Eqs. (6.34) and (6.40) as

$$(M_d^{NL})_{uv} = (M^{NL})_{uv} - (M_s^{NL})_{uv} \qquad (8.29)$$

where

$$(M^{NL})_{uv} = G^2 \sigma_g^2 \sum_{k=0}^{\infty} b_k \cdot \frac{C_k^{2k+1}}{2^{2k+1}} \cdot \left[\frac{1/(2\sigma_1^2)}{1+\alpha^2} \right]^{2k+1}$$

$$\cdot \left| \tilde{R}_1 [(v-u) T_s] \right|^{2k} \cdot \tilde{R}_1 [(v-u) T_s] \qquad (8.30)$$

and, from Eq.(6.25),

$$\tilde{R}_1((v-u)T_s) = 2\left[\sigma_s^2 \cdot e^{j2\pi f_D((v-u)T_s)} + \sigma_c^2 \cdot e^{-\frac{((v-u)T_s)^2}{2\sigma_w^2}} \cdot \sigma_n^2 \cdot \frac{\sin(\pi W((v-u)T_s))}{\pi W((v-u)T_s)}\right]. \quad (8.31)$$

In Chapter 6 it is shown that suitable approximations to the infinite summations in Eqs. (8.28) and (8.30) can be achieved by summing over the first 12 terms.

By substitution of Eq.(8.27) into Eq.(8.26), the expression for the output signal-to-disturbance ratio becomes

$$(SDR)_{II} = \frac{\underline{a}^T (M_d^L)^{-1} M_s^{NL} (M_d^L)^{-1} \underline{a}^*}{\underline{a}^T (M_d^L)^{-1} M_d^{NL} (M_d^L)^{-1} \underline{a}^*}. \quad (8.32)$$

Because all matrices are proportional to G^2, $(SDR)_{II}$ is independent of G. From Eq.(8.12), it follows that the output signal-to-disturbance ratio is independent of the saturation level, L, of the nonlinearity.

8.2.1 Dependence of $(SDR)_{II}$ on the Clutter Correlation Parameter

As pointed out in Chapter 7, when the clutter is much larger than the signal, the nonlinearity tends to broaden the clutter power spectral density without significantly changing the shape of the desired signal. This is illustrated in Fig.8.12 for the situation where

$$\sigma_s=1,\ \sigma_c=10,\ \sigma_n=0.1,\ \sigma_g=5\ ,\ \alpha=\sigma_g/\sigma_1=0.4975.$$

Since the standard deviation of the total input signal is approximately twice the linear range of the nonlinearity, the input-output characteristic of the nonlinearity is

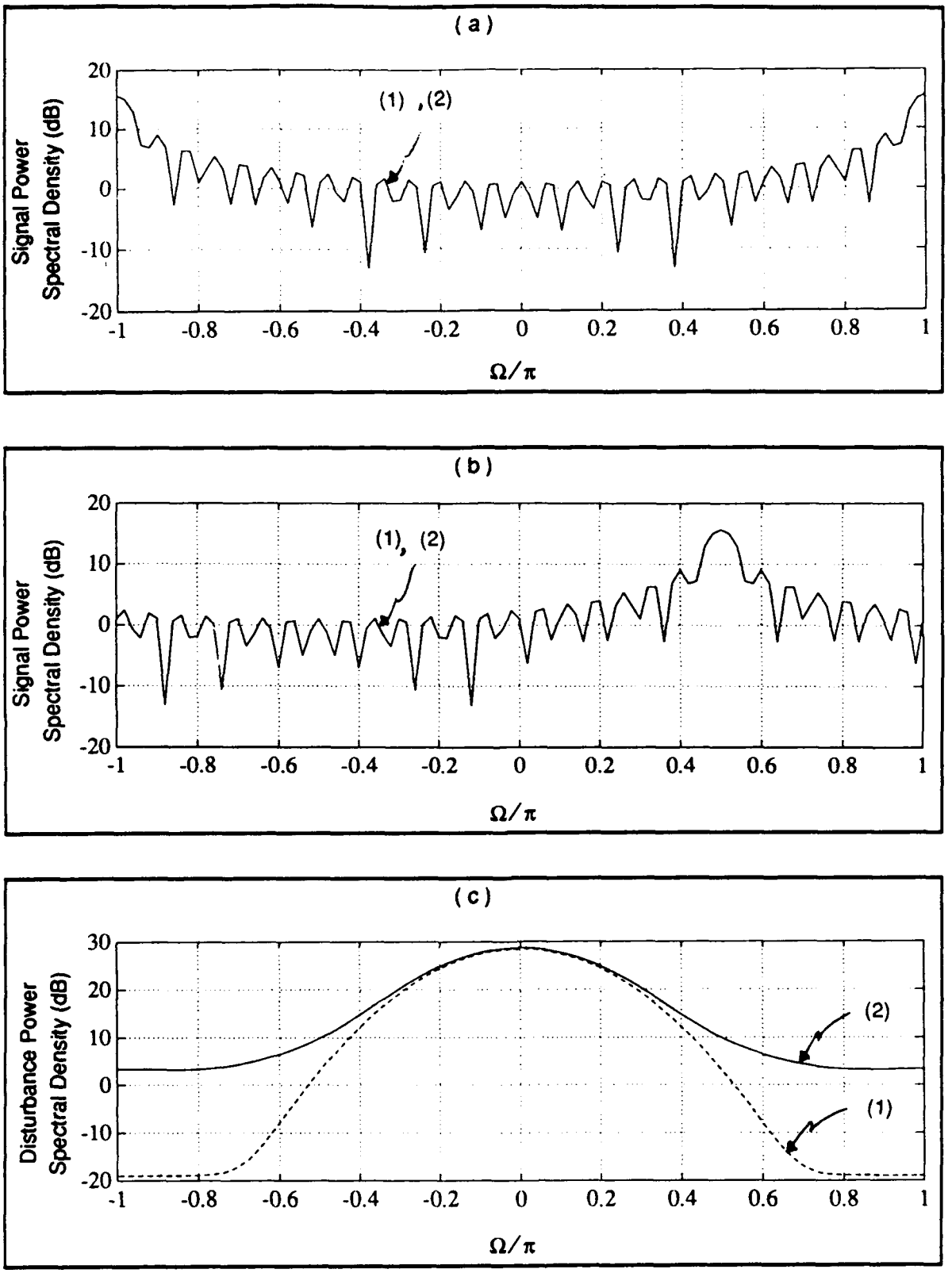

Figure 8.12 - (Caption appears on next page).

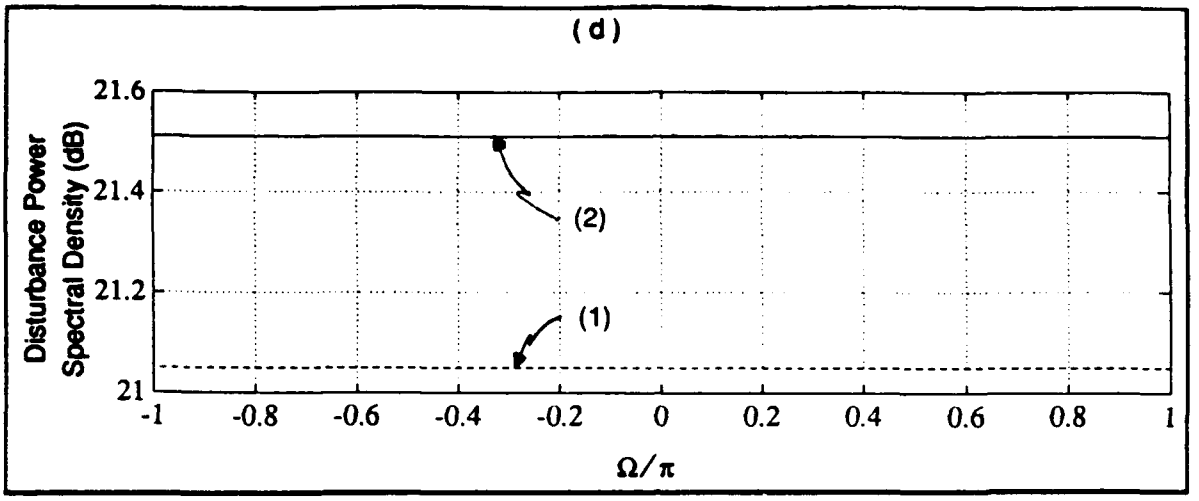

Figure 8.12 - Power Spectral Densities at Nonlinear Output (σ_s=1, σ_q=5, α=0.4975):(1) case I ,(2) case II (a) Desired signal (f_D/f_s=0.5), (b) Desired signal (f_D/f_s=0.25), (c) clutter plus noise (ρ_c=0.9), (d) clutter plus noise (ρ_c=0).

being driven into its nonlinear region. However, note that the desired signal is small enough such that, by itself, it would operate entirely in the linear region of the nonlinearity. In part (a) where $f_D=0.5f_s$ and in part (b) where $f_D=0.25f_s$, the shape of the power spectral density of the desired signal at the nonlinearity output is seen to be unchanged. This is due to the relatively small desired signal level. In part (c), where ρ_c=0.9, the power spectral density of the clutter plus noise at the nonlinearity output is observed to be noticeably wider due to the nonlinearity. Because the nonlinear terms in Eq.(8.30) are much smaller than the linear term, the most noticeable increase in the spectral level occurs at high frequencies where the disturbance power spectral density is small. At $f=f_s$, the increase is approximately 22 dB whereas at f=0, it is on the order of a few tenths of a dB . In part (d), where ρ_c=0 and the disturbance power spectral density is a constant both at the input and output of the nonlinearity, the increase in spectral level is seen to be around 0.4 dB.

Dependence of the output signal-to-disturbance ratio on the clutter correlation parameter, ρ_c, is shown for both case I and case II in Fig.8.13. In part (a) of the figure, $f_D=0.5f_s$. Here the desired signal spectrum is located at the minimum

value of the clutter plus noise power spectral density. Consistent with the increased levels of the disturbance seen in Fig.8.12, the nonlinearity causes a 22 dB loss of the output signal-to-disturbance ratio for ρ_c=0.9 and an approximate 0.4 dB loss for ρ_c=0. This is to be expected since the transfer function of the transversal filter is the same for both cases I and II. In Fig.8.13 (b), where $f_D=0.25f_s$, the losses are approximately 10 dB for ρ_c=0.9 and 0.4 dB for ρ_c=0. The 10 dB loss is consistent with the increase in disturbance level shown in Fig.8.12 (c) at Ω/π=0.5 (i.e.; $f=0.25f_s$). In Fig.8.13 (c), f_D=0. The decrease in $(SDR)_{II}$ for increasing values of ρ_c follows the same trend observed in the linear case. However, the loss of approximately 2.2 dB for ρ_c=0.9 is larger than the 0.4 dB loss predicted at f=0 in Fig.8.12 (c). Note that

$$(SDR)_I > (SDR)_{II} \tag{8.33}$$

for all values of ρ_c in Figs. 8.13 (a), (b), and (c). This is reasonable since the shape of the power spectral density of the desired signal has been unaffected by the nonlinearity while the width of the disturbance power spectral density has been increased.

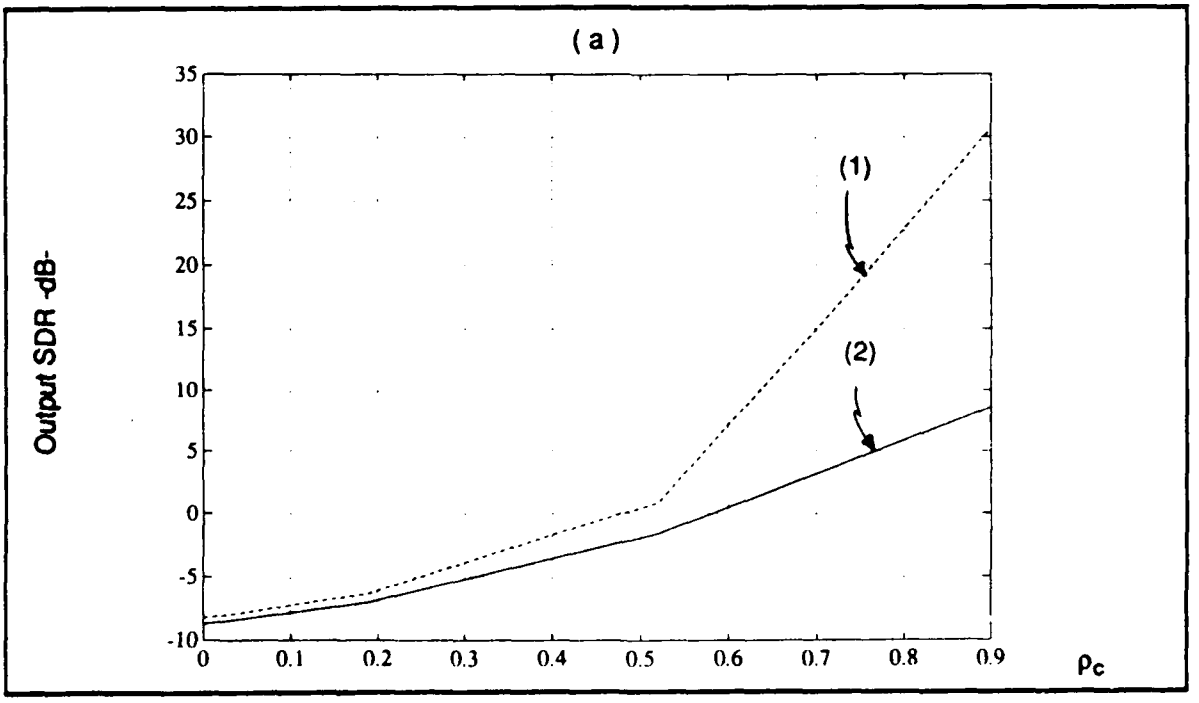

Figure 8.13 - (Caption appears on next page).

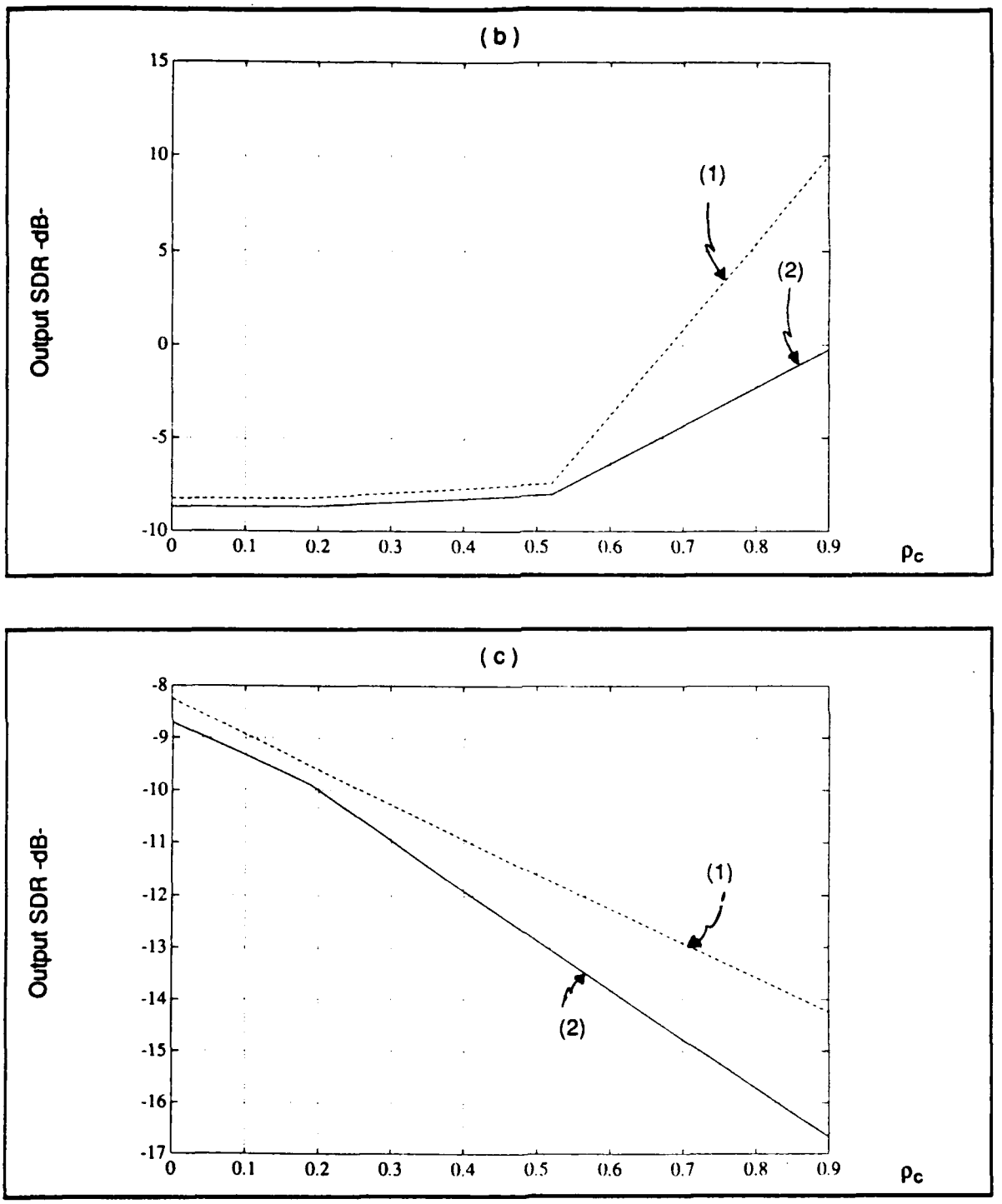

Figure 8.13 - Dependence of $(SDR)_{II}$ on the Clutter Correlation Parameter (σ_s=1, σ_d=5, α=0.4975): (1) $(SDR)_I$ -dB-, (2) $(SDR)_{II}$ -dB- a) f_D/f_s=0.5, b) f_D/f_s=0.25, c) f_D/f_s=0.

8.2.2 Dependence of $(SDR)_{\Pi}$ on $\alpha=\sigma_g/\sigma_1$

Recall that σ_g is a measure of the linear range of the nonlinearity whereas σ_1 represents the r.m.s. value of the total input signal. Consequently, the larger is the value of α, the more linear is the behavior of the nonlinearity. As α increases, it is expected that the output signal-to-disturbance ratio for Case II will approach that of Case I. This is verified in Fig.8.14 where α is varied by changing σ_g from 5 to 50 while all signal levels are held fixed. In Fig.8.14 (a), where $f_D=0.5f_s$ and $\rho_c=0.9$, the system is seen to behave linearly for $\alpha\geq 5$. For all of the other cases considered in the figure, linearity is approached for $\alpha\geq 3$. Also, the inequality in Eq.(8.33) is satisfied for each case.

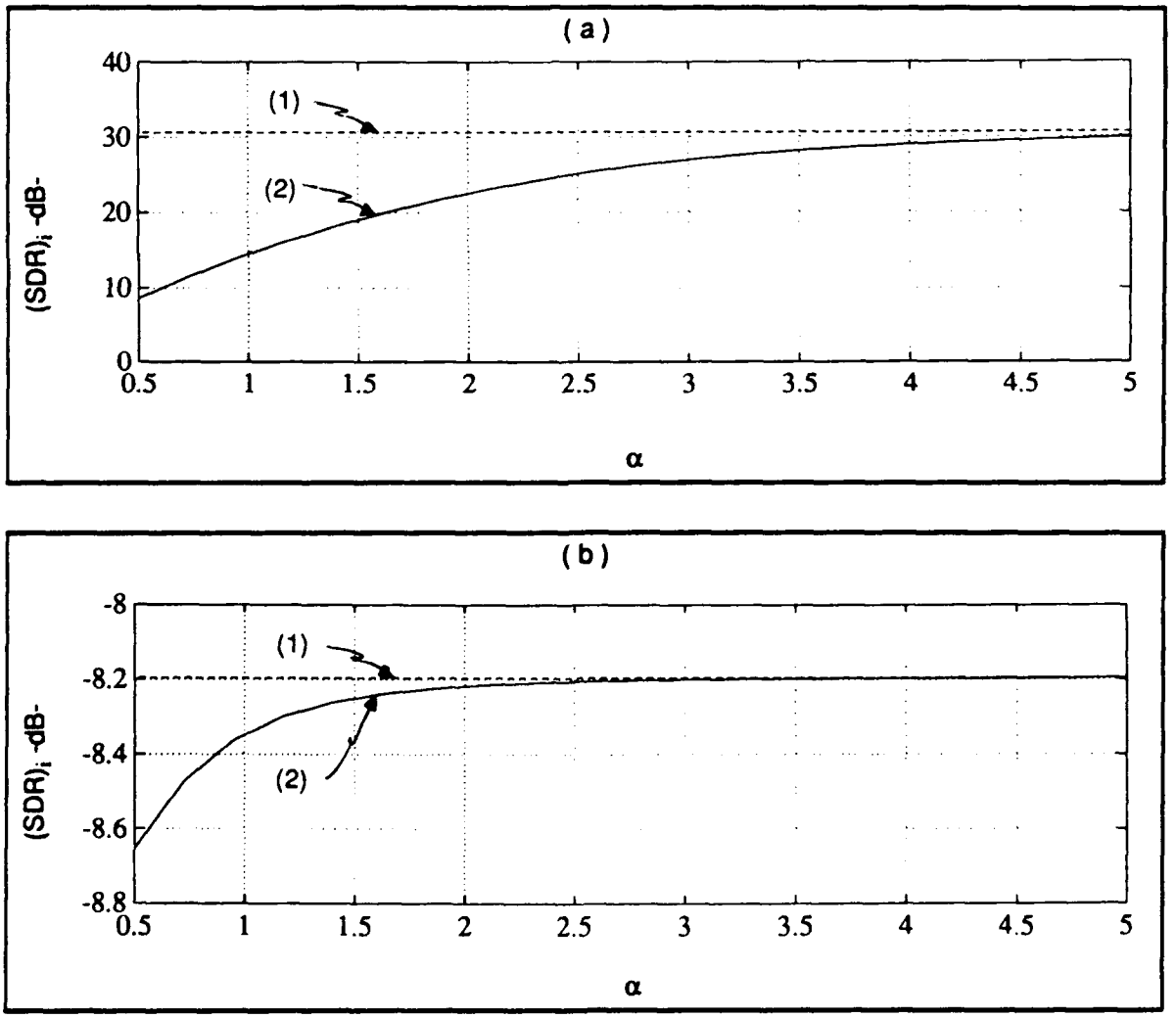

Figure 8.14 - (Caption appears on page 128).

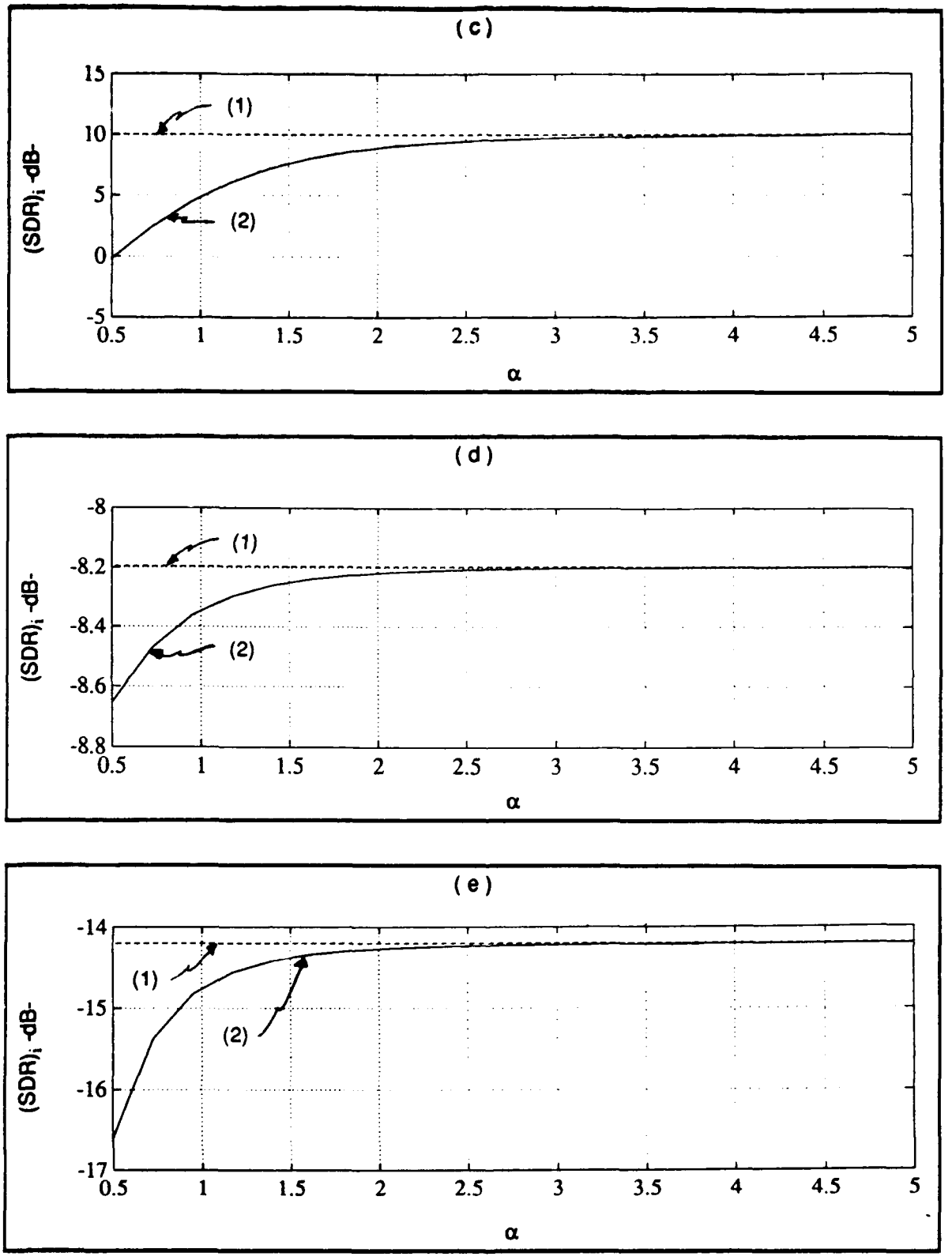

Figure 8.14 - (Caption appears on next page).

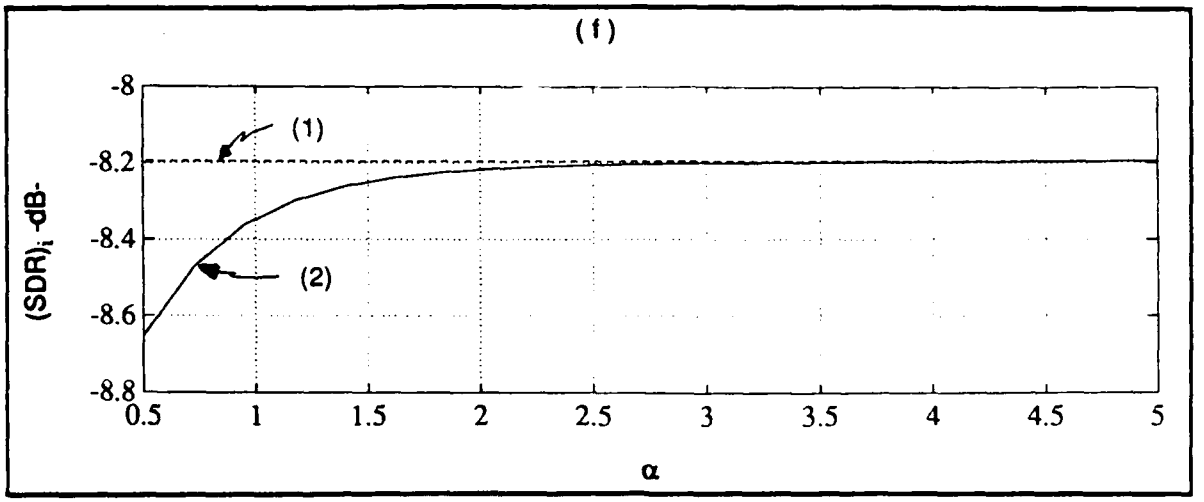

Figure 8.14 - Dependence of $(SDR)_{II}$ on $\alpha=\sigma_g/\sigma_1$: (1) $(SDR)_I$ -dB-, (2) $(SDR)_{II}$ -dB- a) $f_D/f_s=0.5$, $\rho_c=0.9$, b) $f_D/f_s=0.5$, $\rho_c=0$ c) $f_D/f_s=0.25$, $\rho_c=0.9$, (d) $f_D/f_s=0.25$, $\rho_c=0$, e) $f_D/f_s=0$, $\rho_c=0.9$, f) $f_D/f_s=0$, $\rho_c=0$.

8.2.3 Dependence of $(SDR)_{II}$ on the Thermal Noise Power Level

As in section 8.1.3, it is assumed that the total clutter power is always much larger than the total thermal noise power. Consequently, σ_c is held fixed at $\sigma_c=10$ while σ_n is varied over the interval

$$0.1 \le \sigma_n \le 1 \, . \tag{8.34}$$

Plots of $(SDR)_{II}$ versus the input noise-to-clutter ratio, as defined in Eq.(8.9), are shown in Fig.8.15. To provide a basis for comparison, curves of $(SDR)_I$ for the

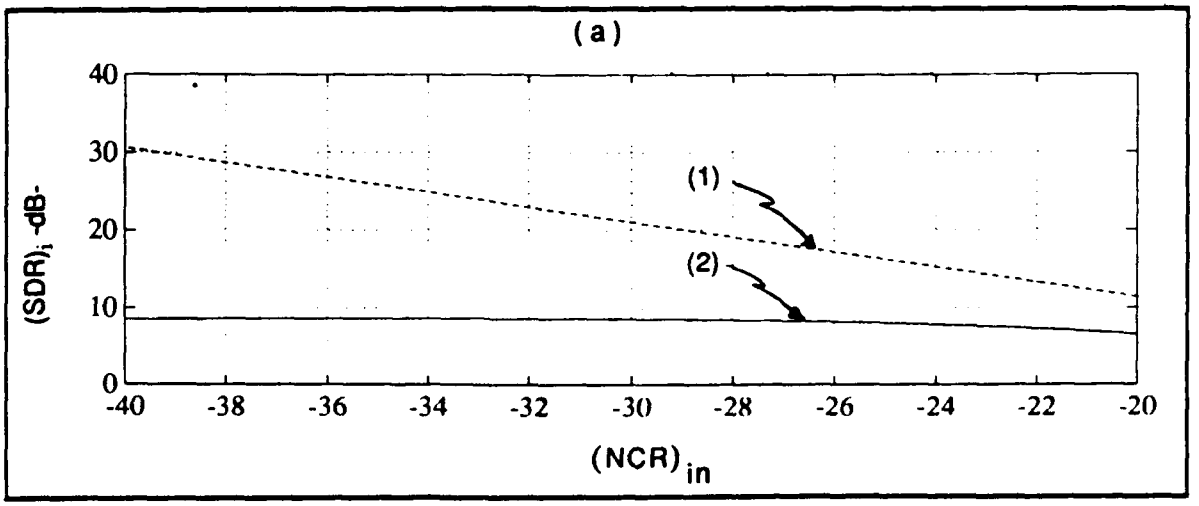

Figure 8.15 - (Caption appears on page 130).

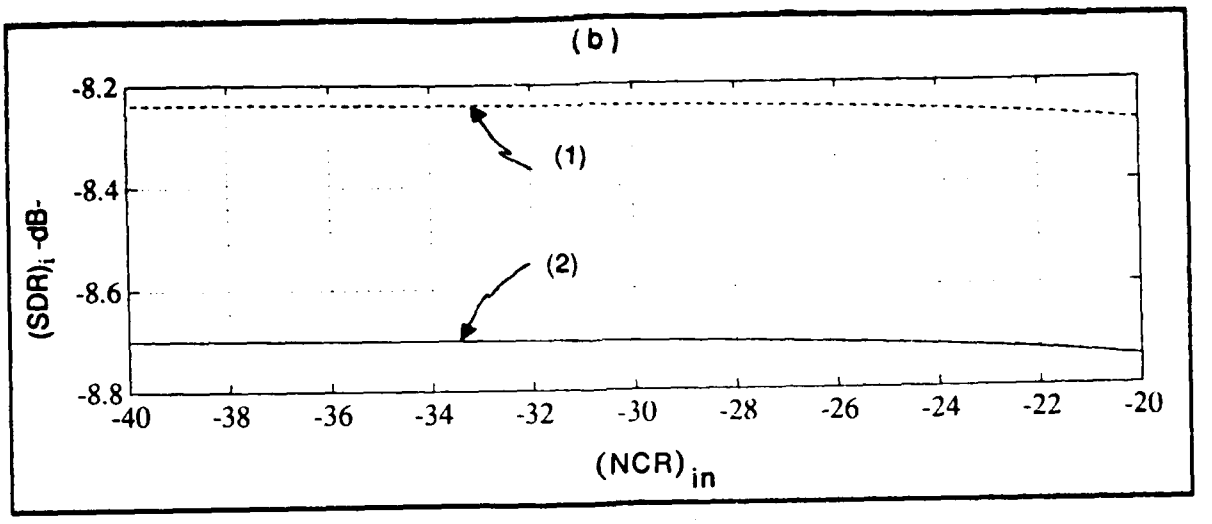

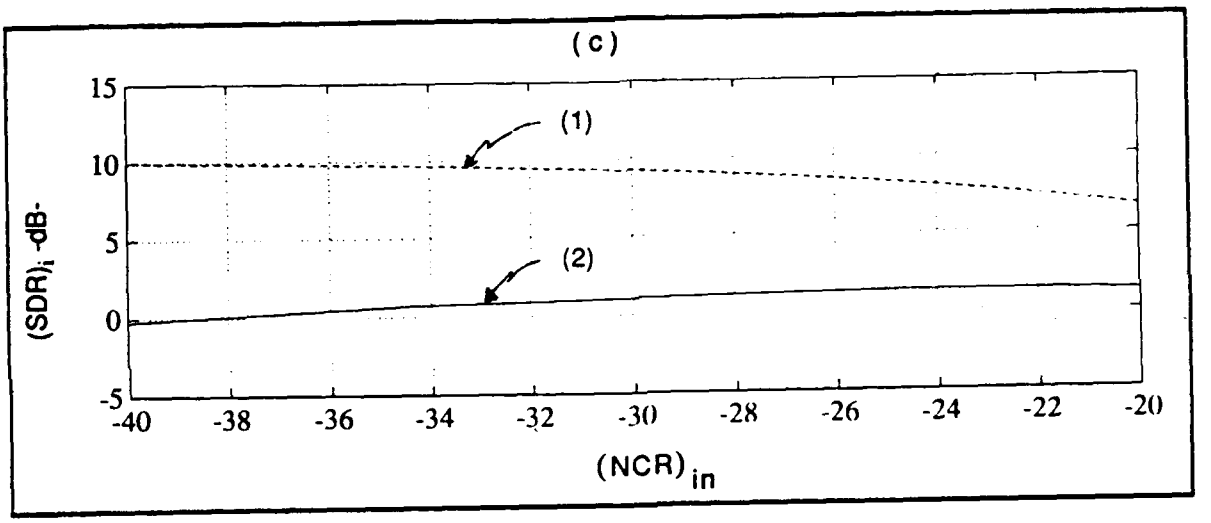

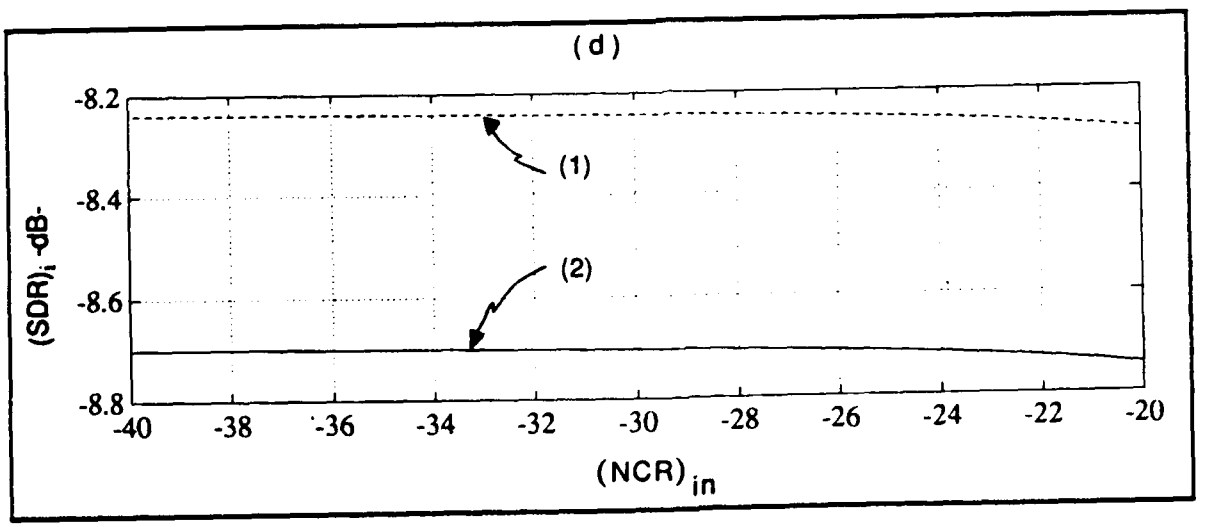

Figure 8.15 - (Caption appears on next page).

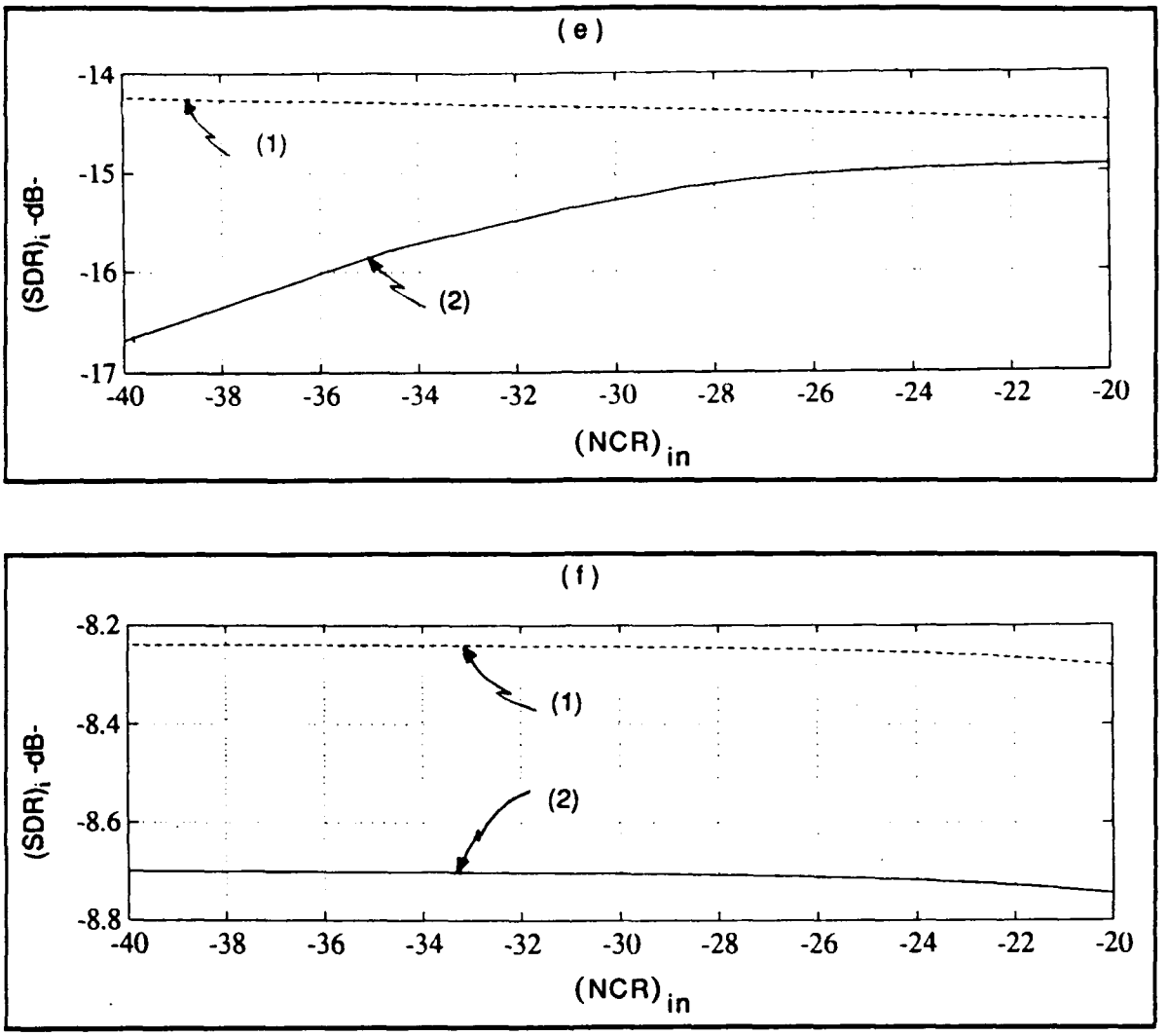

Figure 8.15 - Dependence of $(SDR)_{II}$ on the Thermal Noise Power Level(α=0.4975): (1) $(SDR)_I$ -dB-, (2) $(SDR)_{II}$ -dB- a) f_D/f_s=0.5, ρ_c=0.9, b) f_D/f_s=0.5, ρ_c=0 c) f_D/f_s=0.25, ρ_c=0.9, (d) f_D/f_s=0.25, ρ_c=0, e) f_D/f_s=0, ρ_c=0.9, f) f_D/f_s=0, ρ_c=0.

linear case are also shown. Because of the broadening of the clutter power spectral density by the nonlinearity, the output signal-to-disturbance ratio is less sensitive to an increase in the thermal noise power than was the case for the linear receiver. This is seen in Figs.8,15 (a) and (c). In some cases, the output signal-to-disturbance ratio actually increases with an increase in thermal noise power, as seen in Figs.8.15 (c) and (e). This latter behavior can be understood by examining Fig.8.16 which shows some of the input spectra and the corresponding transfer

functions related to the plot of Fig.8.15 (e). The power spectral density of the desired signal is shown in Fig.8.16 (a) . The clutter plus noise power spectral densities for σ_n=0.1 and σ_n=1 are shown in Fig.8.16 (b) and (d), respectively. Finally, the squared magnitudes of the transversal filter transfer functions for σ_n=0.1 and σ_n=1 are shown in Figs.8.16 (c) and (e), respectively. When σ_n=0.1, the transversal filter tries to maximize the output signal-to-disturbance ratio by passing frequencies limited to the range

$$0.53f_s \leq |f| \leq f_s \tag{8.35}$$

even though the main lobe of the desired signal is centered at f_D=0. When σ_n=1, the tails of the clutter plus noise power spectral density have been increased by approximately 6 dB. The transversal filter is now able to maximize the output signal-to-disturbance ratio by passing frequencies over the entire frequency range given by

$$0 \leq |f| \leq f_s \text{ .} \tag{8.36}$$

This results in a larger value for $(SDR)_{II}$ when σ_n=1 than when σ_n=0.1.

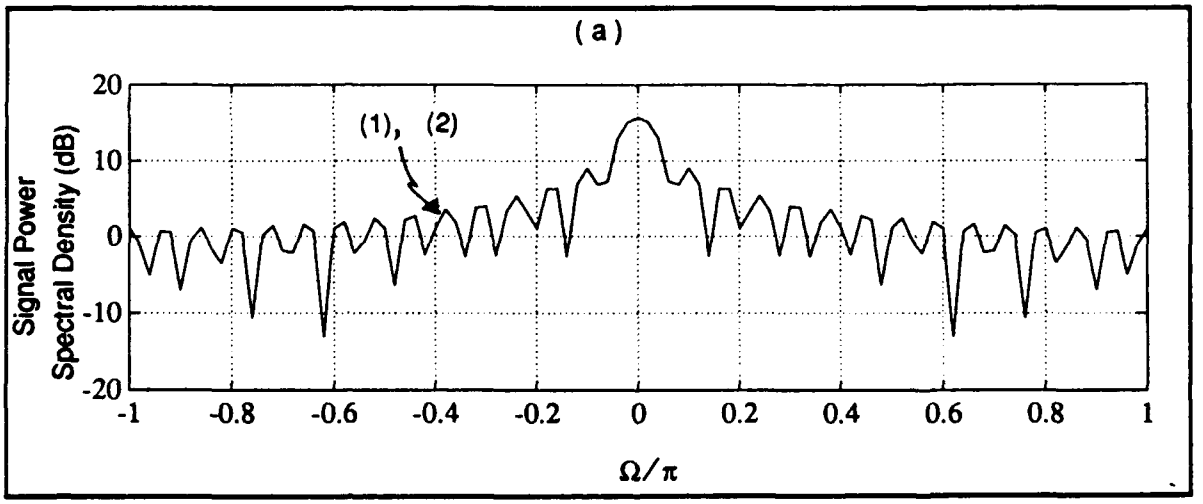

Figure 8.16 - (Caption appears on page 133).

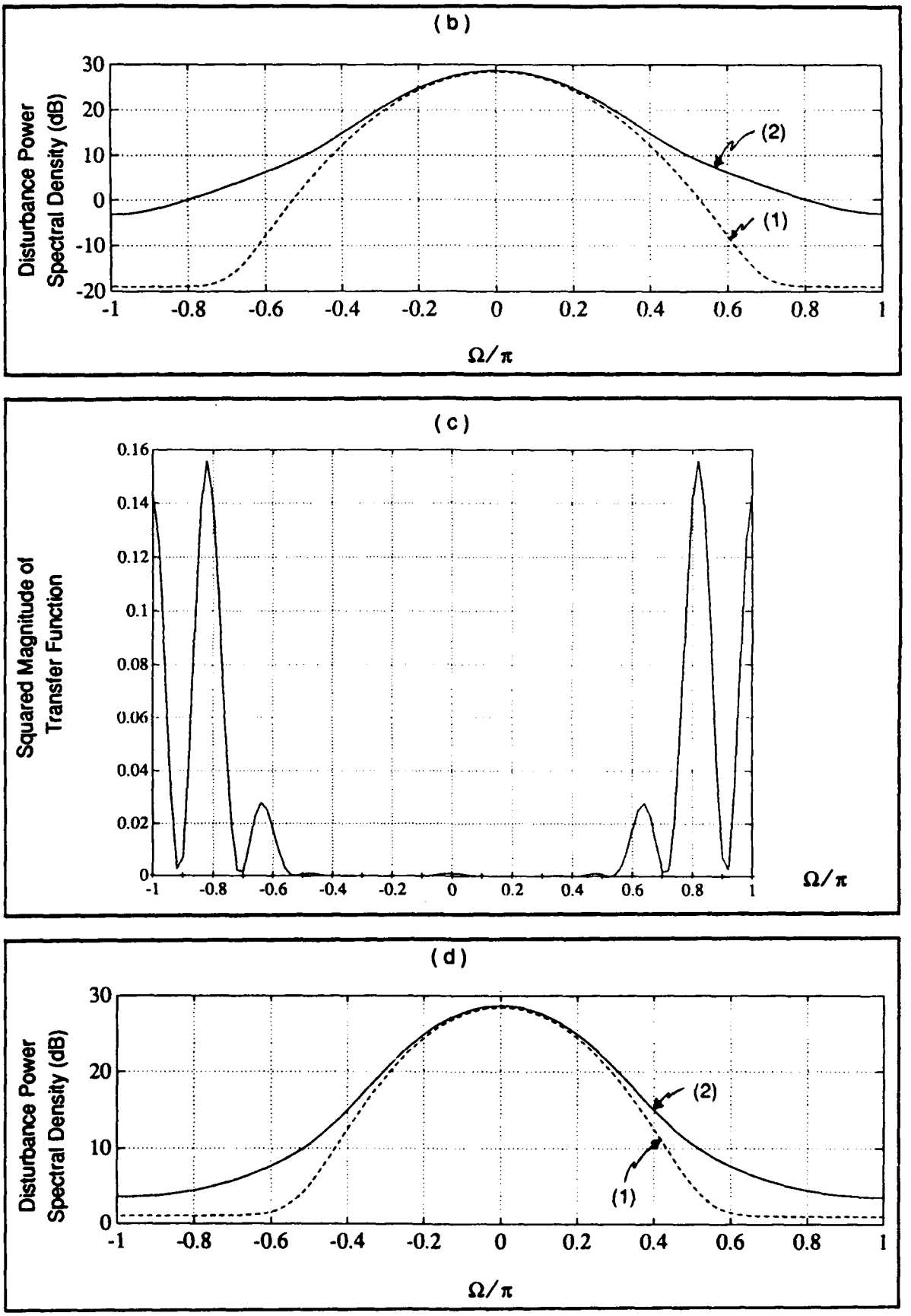
(b)
Disturbance Power Spectral Density (dB)
30
20
10
0
-10
-20
-1
-0.8
-0.6
-0.4
-0.2
0
0.2
0.4
0.6
0.8
1
(2)
(1)
Ω/π
(c)
Squared Magnitude of Transfer Function
0.16
0.14
0.12
0.1
0.08
0.06
0.04
0.02
0
Ω/π
(d)
Disturbance Power Spectral Density (dB)
(2)
(1)
Ω/π

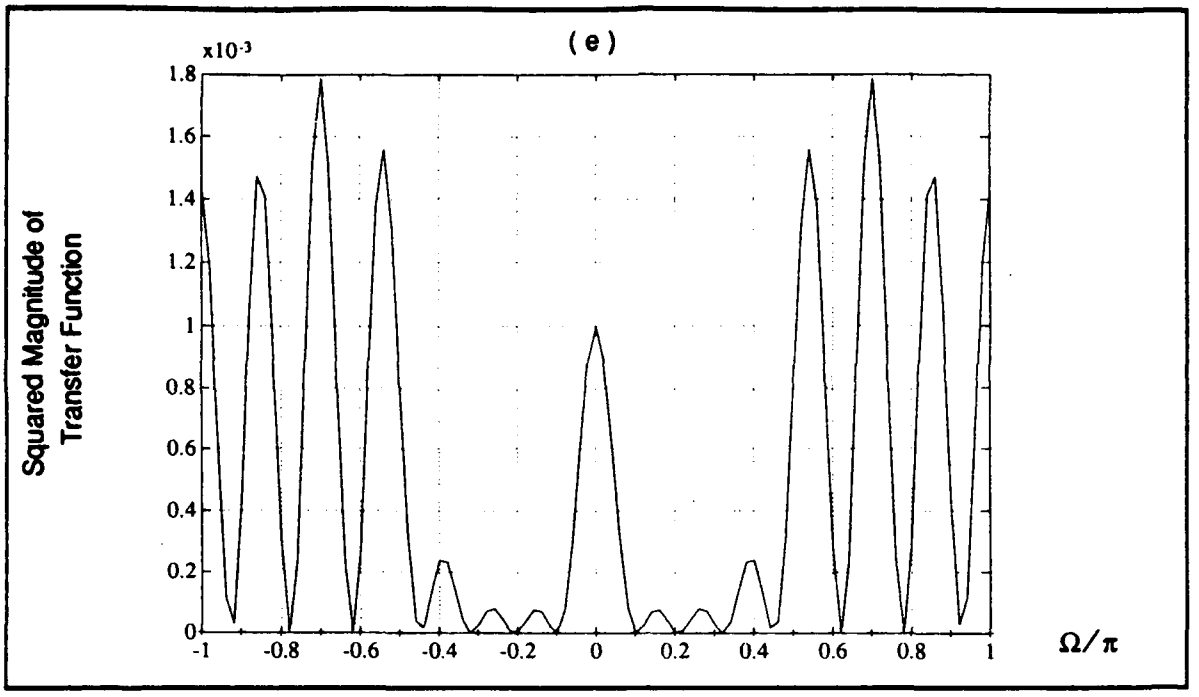

Figure 8.16 - Input spectra and transfer functions related to Fig.8.15(e): (a) power spectral density of the desired signal, (b) clutter plus noise power spectral density when σ_n=0.1, (c) squared magnitude of transfer function when σ_n=0.1, (d) clutter plus noise power spectral density when σ_n=1, (e) squared magnitude of transfer function when σ_n=1
(1) case I, (2) case II.

8.2.4 Dependence of $(SDR)_{II}$ on the Clutter Power Level

As in section 8.1.4, σ_c is varied over the interval

$$10 \le \sigma_c \le 100$$

while σ_s and σ_n are held fixed at σ_s=1 and σ_n=0.1. Dependence of $(SDR)_{II}$ on the clutter power level is illustrated in Fig.8.17. To provide a basis for comparison, curves of $(SDR)_I$ for the linear case are also shown. As expected, when the clutter dominates the disturbance in the frequency region about f_D, the curves decrease significantly as the total clutter power increases by 20 dB. As σ_c varies from 10 to 100, α varies from 0.4975 to 0.05. Thus, the nonlinearity is

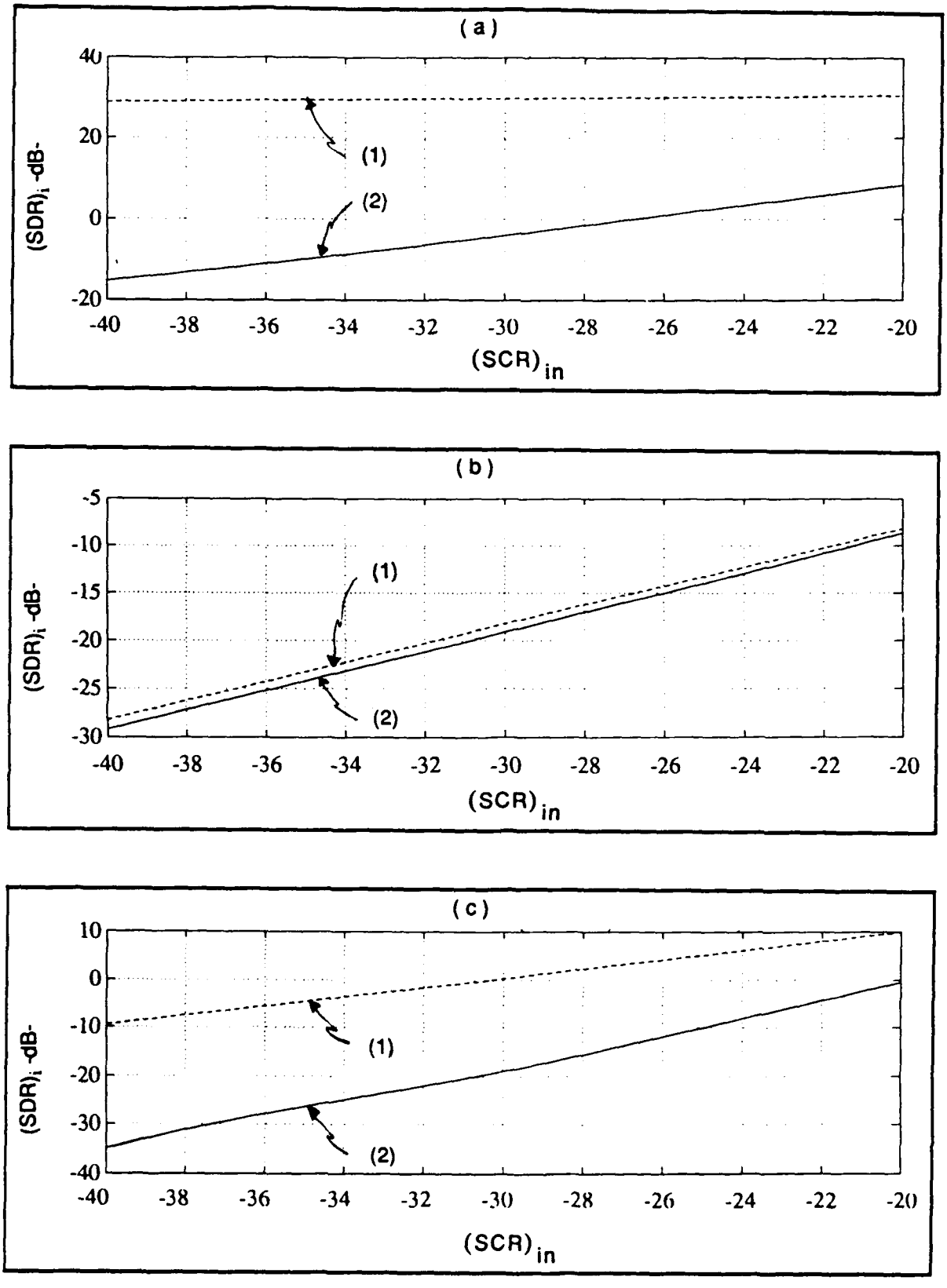

Figure 8.17 - (Caption appears on next page).

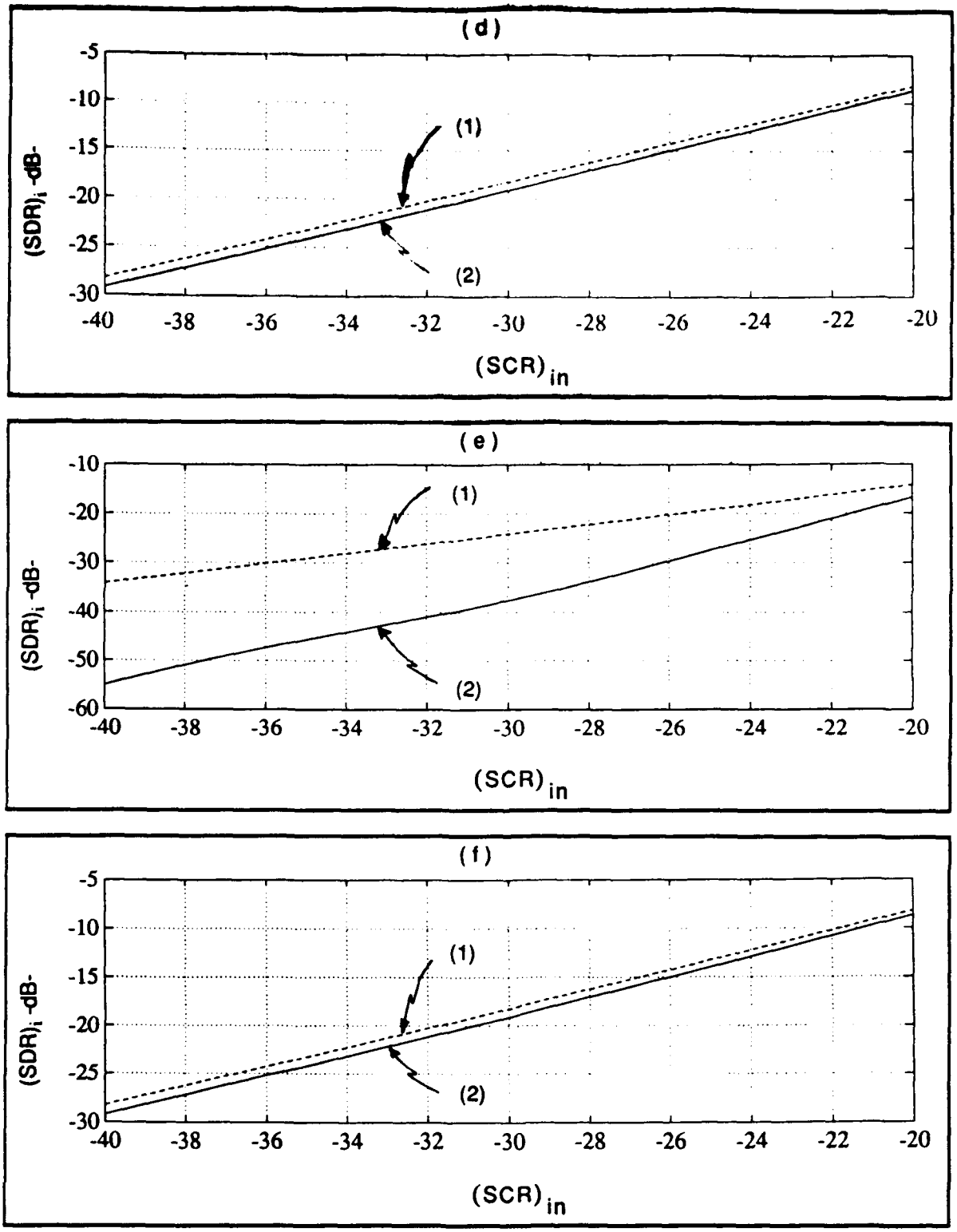

Figure 8.17 - Dependence of $(SDR)_{II}$ on the Clutter Power Level ($0.05 \le \alpha \le 0.4975$): (1) $(SDR)_I$ -dB-, (2) $(SDR)_{II}$ -dB- a) $f_D/f_S=0.5$, $\rho_C=0.9$, b) $f_D/f_S=0.5$, $\rho_C=0$ c) $f_D/f_S=0.25$, $\rho_C=0.9$, (d) $f_D/f_S=0.25$, $\rho_C=0$, e) $f_D/f_S=0$, $\rho_C=0.9$, f) $f_D/f_S=0$, $\rho_C=0$.

driven harder as the clutter power is increased. This, in turn, results in increased spreading of the clutter power spectral density. Consequently, compared to the linear receiver, the degradation in output signal-to-disturbance ratio is greater for the nonlinear receiver (see Figs.8.17 (a), (c), and (e) where ρ_c=0.9). This effect is not seen in Figs.8.17(b), (d), and (f) where ρ_c=0 and the disturbance power spectral density is white.

8.2.5 Dependence of $(SDR)_{II}$ on the Doppler Frequency

A plot of $(SDR)_{II}$ versus f_D/f_s is shown in Fig.8.18 for ρ_c=0.9 and ρ_c=0. To provide a basis for comparison, curves of $(SDR)_I$ for the linear case are also shown. When ρ_c=0.9 both $(SDR)_I$ and $(SDR)_{II}$ peak at f_D/f_s=0.5. This corresponds to the situation where the desired signal spectrum is positioned at the minimum of the clutter power spectral density. When ρ_c=0, the clutter plus noise power spectral density is white. Hence, the output signal-to-disturbance ratios are independent of f_D/f_s. In all cases note that the nonlinearity results in

$$(SDR)_I > (SDR)_{II} \cdot \tag{8.37}$$

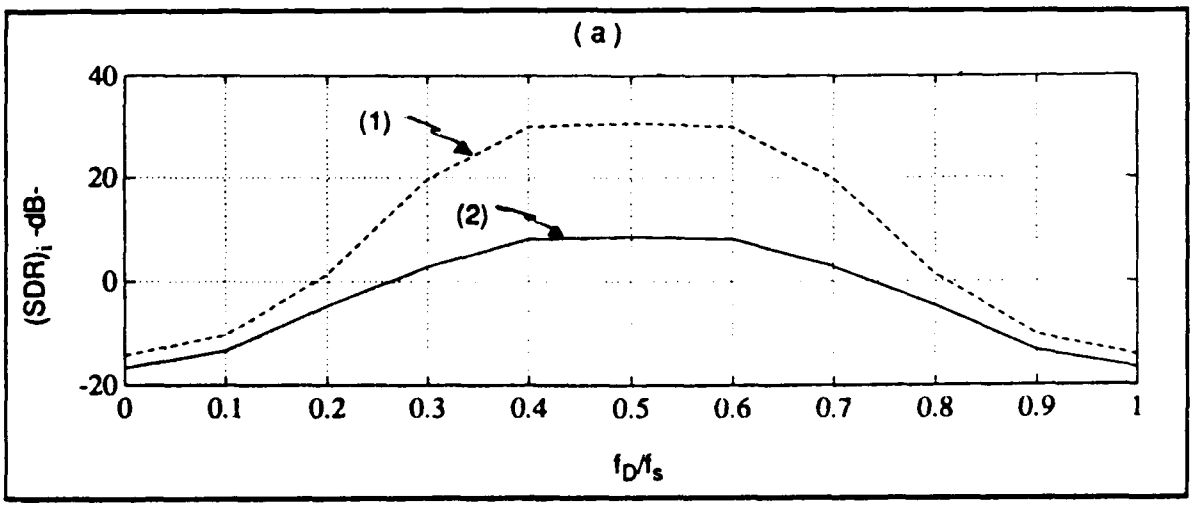

Figure 8.18 - (Caption appears on next page).

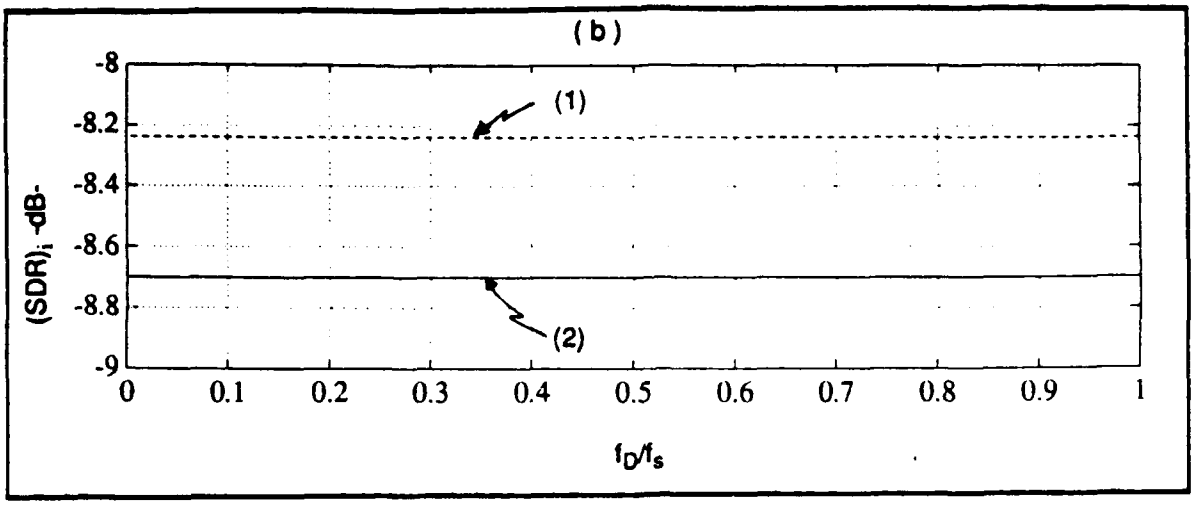

Figure 8.18 - Dependence of $(SDR)_{II}$ on the Doppler Frequency (α=0.4975): (1) $(SDR)_I$ -dB-, (2) $(SDR)_{II}$ -dB- a) ρ_c=0.9, b) ρ_c=0.

8.2.6 Dependence 0f $(SDR)_{II}$ on the Number of Samples, N

The dependence of $(SDR)_{II}$ on the number of samples, N, is shown in Fig.8.19 for f_D/f_s=0.5, 0.25, 0 and ρ_c=0.9,0. Plots for $(SDR)_I$ are also included as a basis for comparison. As expected, the output signal-to-disturbance ratios increase with an increase in the number of samples processed. The amount of improvement for the nonlinear receiver approximately equals that of the linear recei-

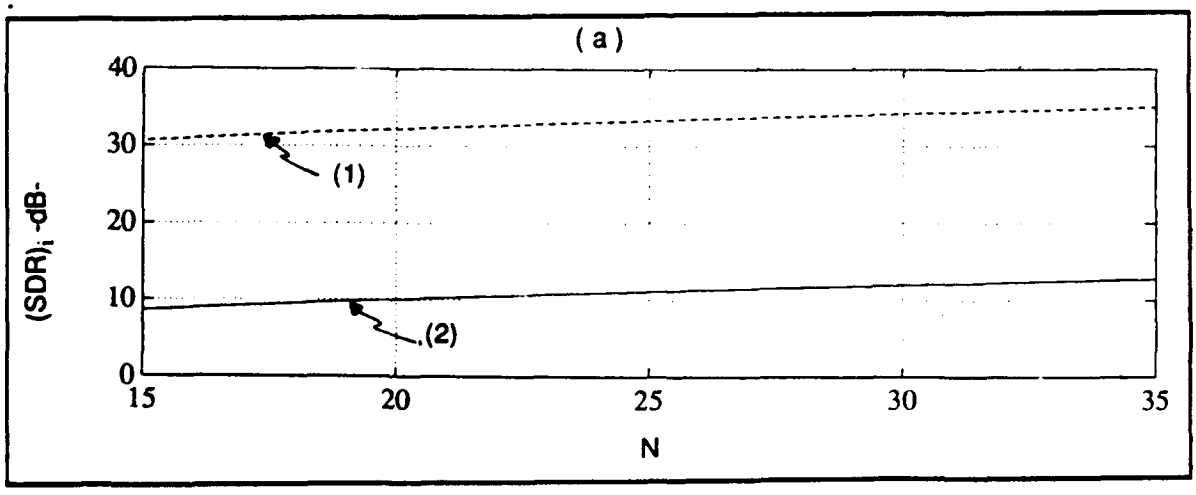

Figure 8.19 - (Caption appears on page 139).

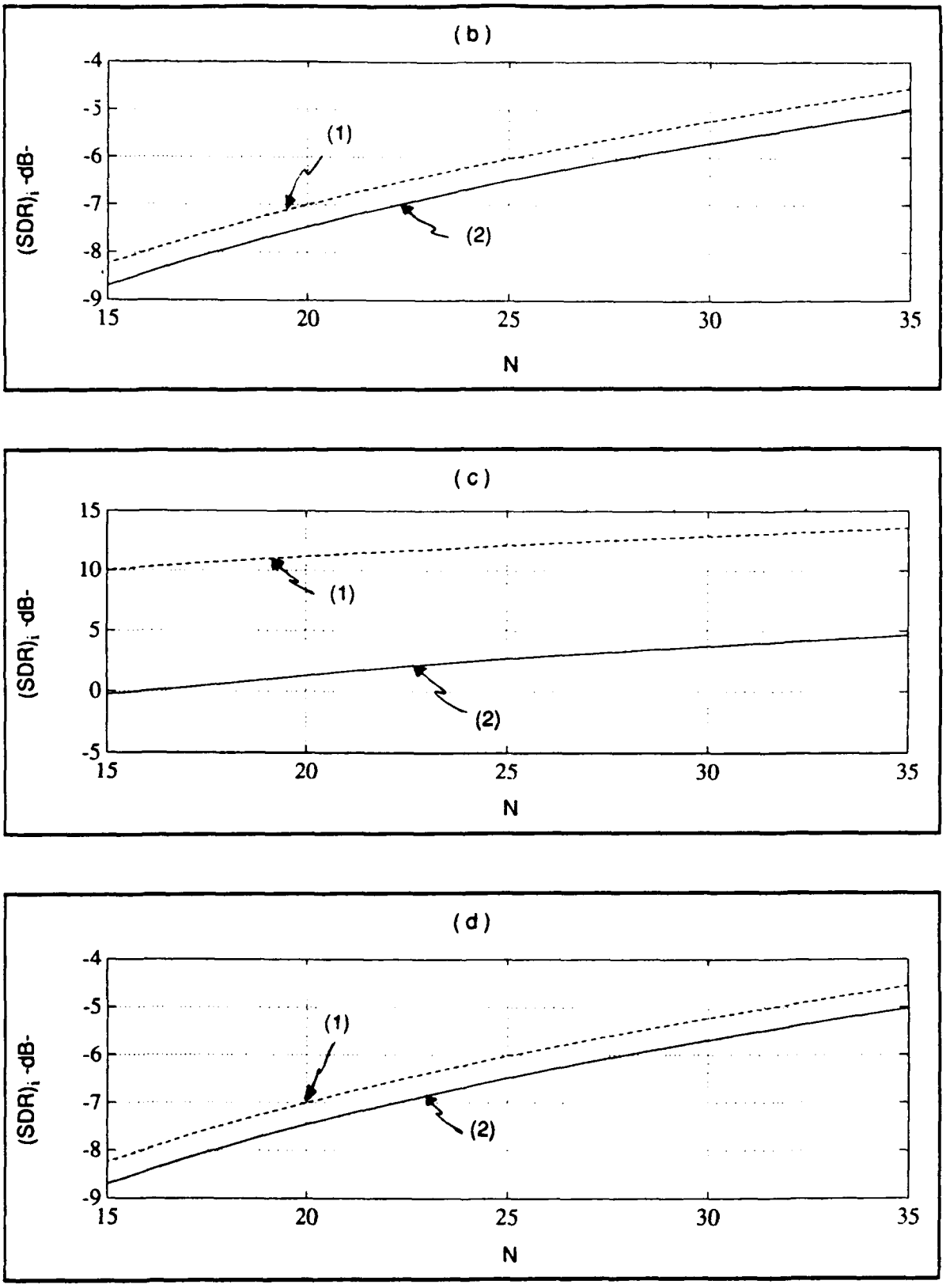

Figure 8.19 - (Caption appears on next page).

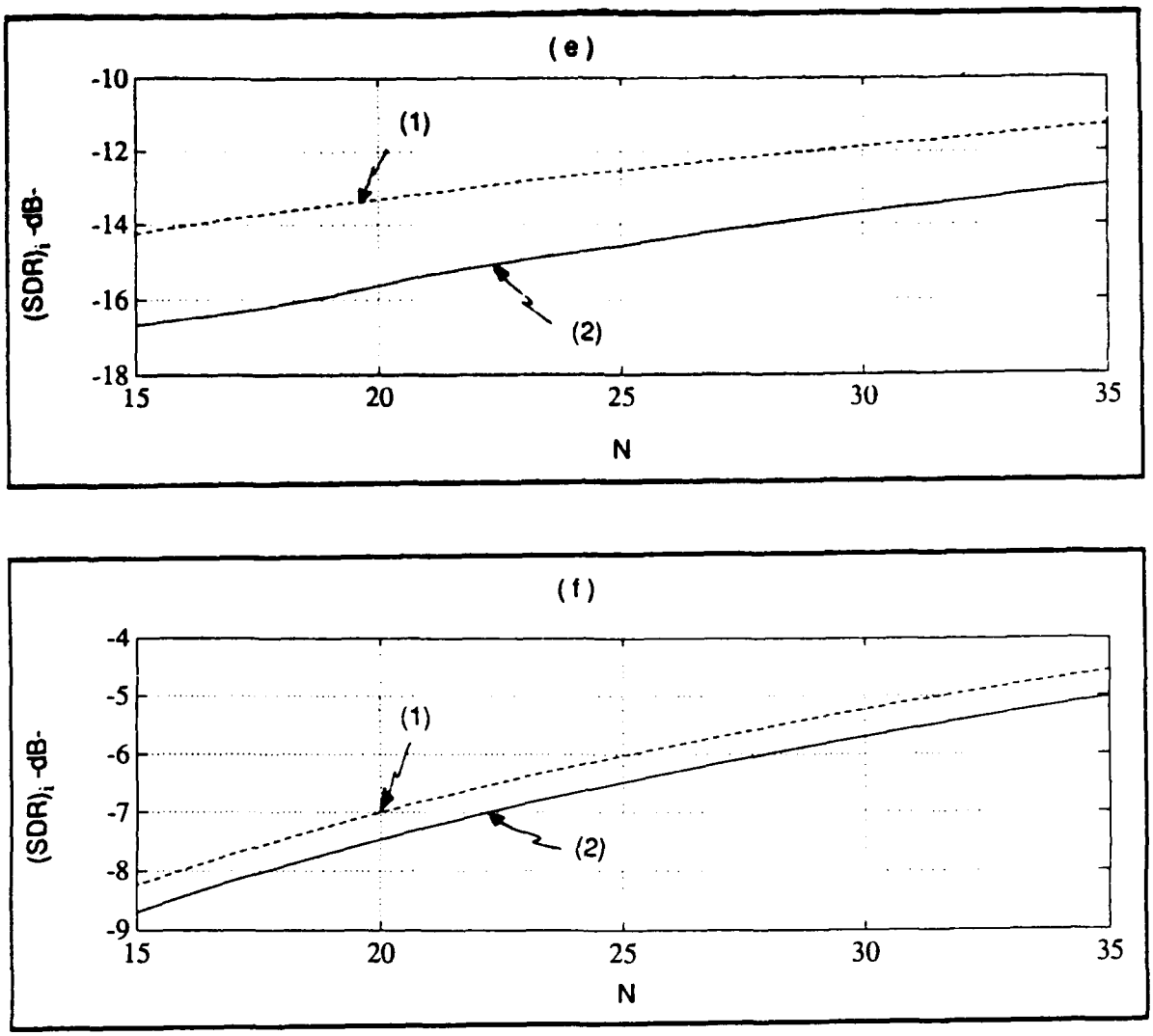

Figure 8.19 - Dependence of $(SDR)_{II}$ on the Number of Samples (α=0.4975): (1) $(SDR)_I$ -dB-, (2) $(SDR)_{II}$ -dB- a) f_D/f_s=0.5, ρ_c=0.9, b) f_D/f_s=0.5, ρ_c=0 c) f_D/f_s=0.25, ρ_c=0.9, (d) f_D/f_s=0.25, ρ_c=0, e) f_D/f_s=0, ρ_c=0.9, f) f_D/f_s=0, ρ_c=0.

ver. As explained in section 8.1.5, the improvement is due to 1) the power spectral density of the desired signal becoming more concentrated about f_D and 2) the degrees of freedom of the transversal filter increasing with N.

8.3 Computer Generated Results for Case III: Nonlinear Receiver with the Transversal Filter optimized to Account for the Receiver Nonlinearity

Case III refers to the situation where the radar receiver is nonlinear and the

transversal filter is optimized to account for the receiver nonlinearity so as maximize the output signal-to-disturbance ratio.

From Eq.(6.68) the output signal-to-disturbance ratio is given by

$$(SDR)_{III} = \frac{\underline{\tilde{w}}^H M_s^{NL} \underline{\tilde{w}}}{\underline{\tilde{w}}^H M_d^{NL} \underline{\tilde{w}}} \tag{8.38}$$

where the transversal filter weight vector is determined according to Eq.(6.74) as

$$\underline{\tilde{w}} = k \cdot (M_d^{NL})^{-1} \underline{a}^* \ . \tag{8.39}$$

In Eq.(8.39) k is an arbitrary constant and $\underline{a}$ is defined by Eqs.(8.14) and (8.15). For simplicity, k is set equal to unity. M_s^{NL} is the (NxN) matrix whose uv^{th} element is given by Eq.(8.28). The uvth element of the (NxN) matrix M_d^{NL} is given by Eq.(8.30). These elements are expressed as infinite series. Once again, suitable approximations are obtained by summing over the first 12 terms in the series.

From Eqs.(6.70) and (6.75), the expression for the output signal-to-disturbance ratio can be simplified to

$$(SDR)_{III} = A \cdot \underline{a}^T (M_d^L)^{-1} \underline{a}^* \tag{8.40}$$

where

$$A = G^2 \sigma_g^2 \sum_{k=0}^{\infty} b_k \cdot \frac{C_k^{2k+1}}{2^{2k+1}} \cdot \left[\frac{1/(2\sigma_1^2)}{1+\alpha^2} \right]^{2k+1} (2\sigma_s^2)^{2k+1} \ . \tag{8.41}$$

Because $(M_d^{NL})^{-1}$ is inversely proportional to G^2 whereas A is proportional to G^2, $(SDR)_{III}$ is independent of G. From Eq.(8.12), it follows that the output signal-to-

disturbance ratio is independent of L, the saturation level of the nonlinearity.

8.3.1 Dependence of $(SDR)_{III}$ on the Clutter Correlation Parameter

Dependence of the output signal-to-disturbance ratio on the clutter correlation parameter, ρ_c, is shown in Fig.8.20 for cases I, II, III. In part (a), where $f_D=0.5f_s$, case III shows negligible improvement over case II for $0\leq\rho_c\leq0.6$. Thereafter, the improvement increases with increasing values of ρ_c. However, at $\rho_c=0.9$, the improvement is only around 1 dB. In parts (b) and (c), where $f_D/f_s=0.25$ and 0, respectively, case III provides a noticeable improvement over case II for $\rho_c\geq0.53$ which increases to approximately 2 dB at $\rho_c=0.9$. It is concluded that the more correlated is the clutter, the better is case III able to outperform case II. To put it another way, the narrower is the shape of the clutter power spectral density, the more distorted is the spectrum by the nonlinearity and the more that can be done by shaping the transfer function of the transversal filter to maximize the output signal-to disturbance ratio.

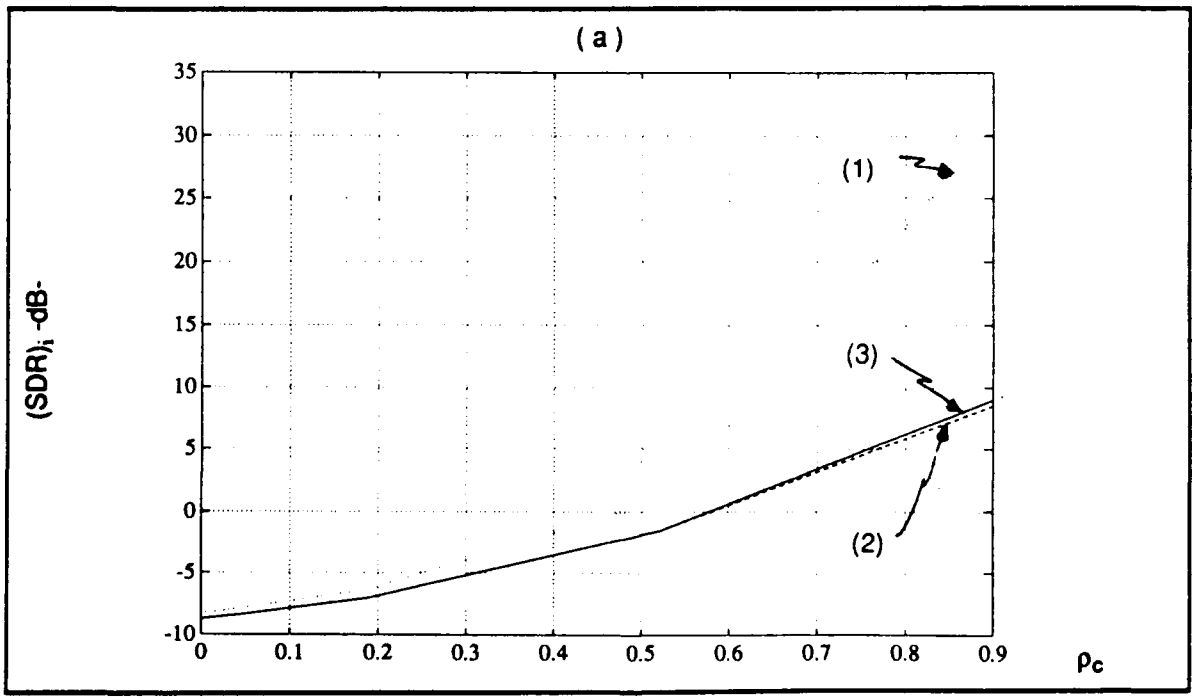

Figure 8.20 - (Caption appears on next page).

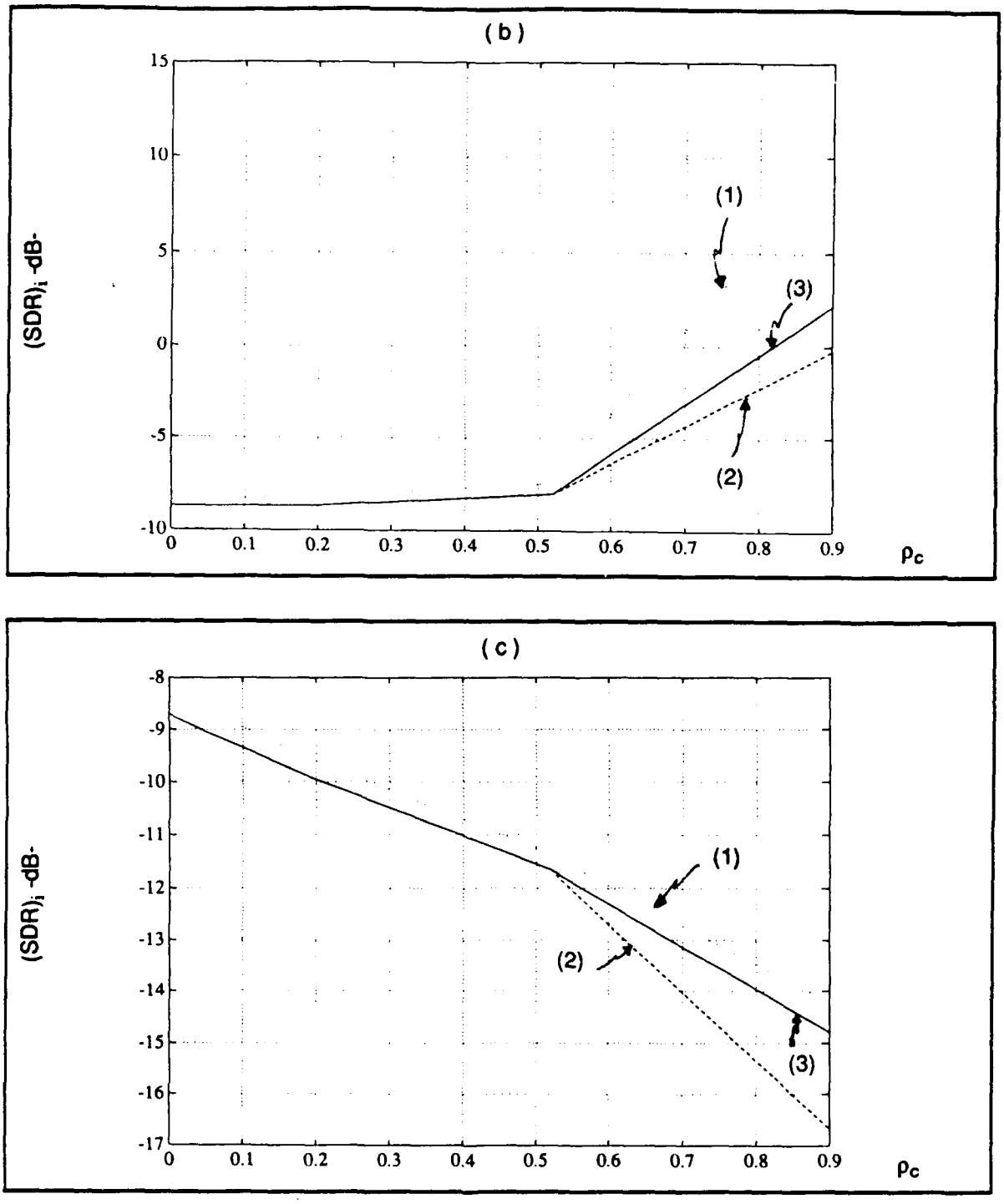

Figure 8.20 - Dependence of Output Signal-to-Disturbance Ratios on the Clutter Correlation Parameter (σ_s=1, σ_q=5, α=0.4975): (1) $(SDR)_I$ -dB-, (2) $(SDR)_{II}$ -dB-, (3) $(SDR)_{III}$ -dB- a) f_D/f_s=0.5, b) f_D/f_s=0.25, c) f_D/f_s=0.

8.3.2 Dependence of $(SDR)_{III}$ on $\alpha=\sigma_g/\sigma_1$

As explained in section 8.2.2, the larger is the value of α, the more linear is the behavior of the nonlinearity. Dependence of the output signal-to-disturbance ratio on α is shown in Fig.8.21 for cases I, II, and III. The simulation was carried out by allowing σ_g to vary in the interval $5 \leq \sigma_g \leq 50$ while all signal levels were held constant. As suggested by the results presented in Fig.8.20, there is little difference between cases II and III when $\rho_c=0$. For $\rho_c=0.9$, case III is better able to outperform case II as the nonlinearity is driven harder. Consistent with Fig.8.20, the improvement for $\rho_c=0.9$ and $\alpha=0.5$ is approximately 1 dB for $f_D=0.5f_s$ and approximately 2 dB for $f_D=0.25f_s$ and 0.

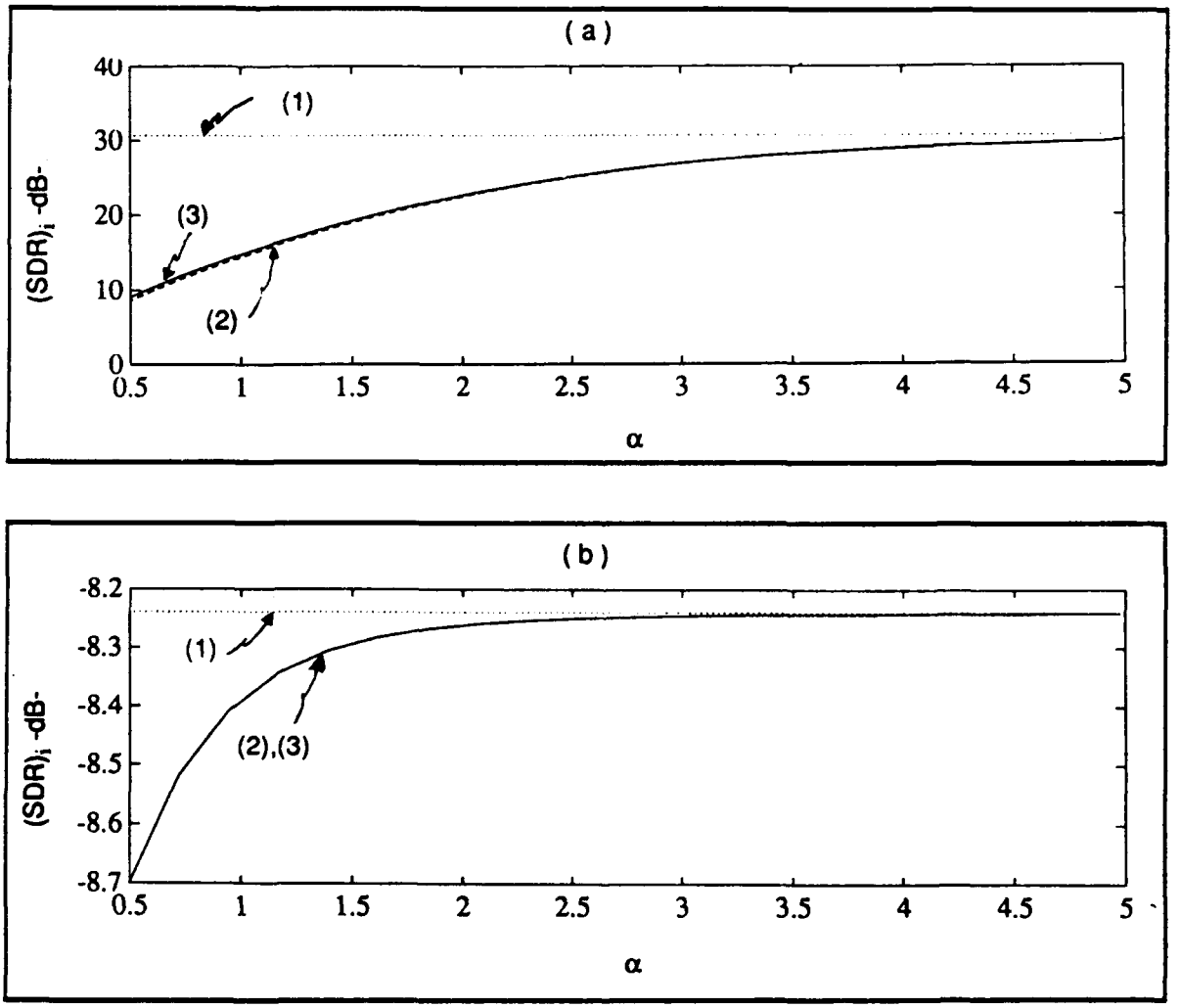

Figure 8.21 - (Caption appears on page 145).

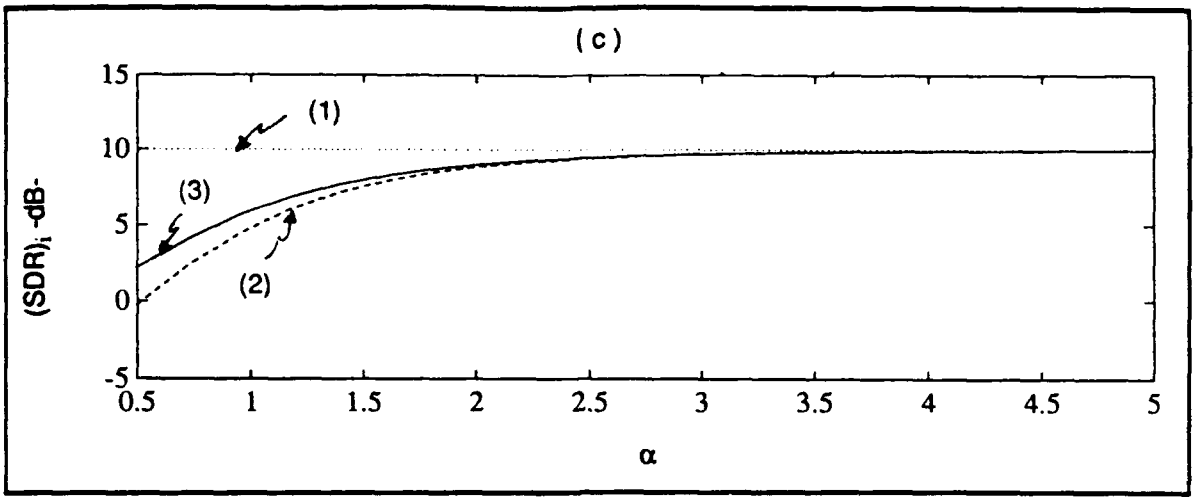

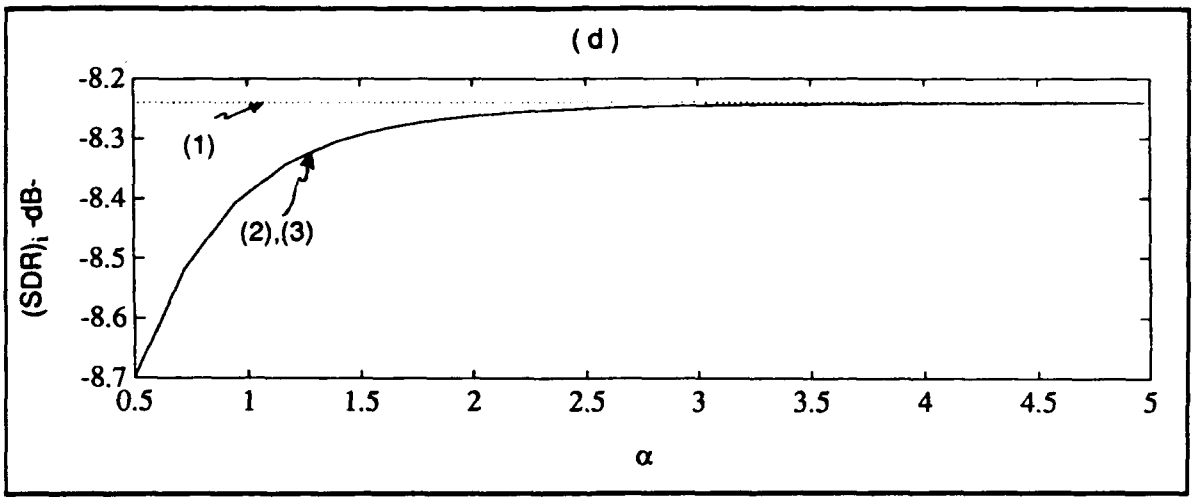

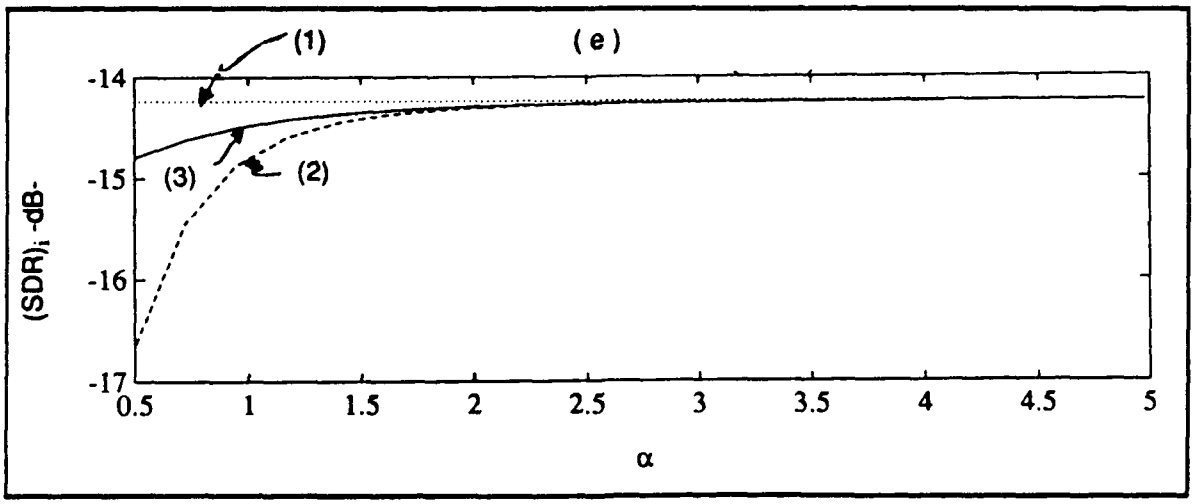

Figure 8.21 - (Caption appears on next page).

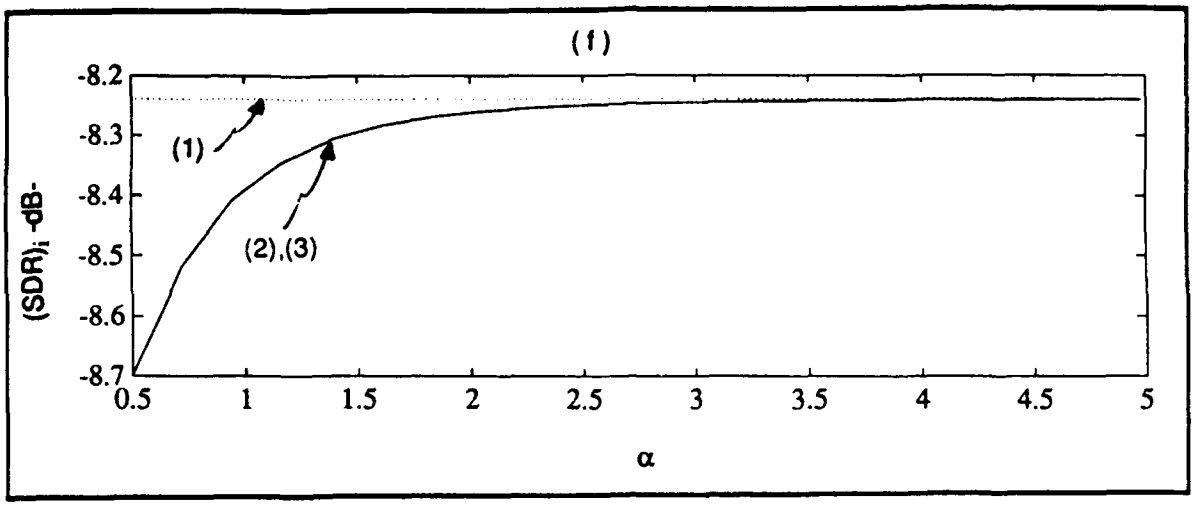

Figure 8.21 - Dependence of $(SDR)_{III}$ on $\alpha=\sigma_g/\sigma_I$: (1) $(SDR)_I$ -dB-, (2) $(SDR)_{II}$ -dB-, (3) $(SDR)_{III}$ -dB- a) $f_D/f_s=0.5$, $\rho_c=0.9$, b) $f_D/f_s=0.5$, $\rho_c=0$ c) $f_D/f_s=0.25$, $\rho_c=0.9$, (d) $f_D/f_s=0.25$, $\rho_c=0$, e) $f_D/f_s=0$, $\rho_c=0.9$, f) $f_D/f_s=0$, $\rho_c=0$.

8.3.3 Dependence of $(SDR)_{III}$ on the Thermal Noise Power Level

As in sections 8.1.3 and 8.2.3, it is assumed that the total clutter power is always much larger than the total thermal noise power. Consequently, σ_c is held fixed at $\sigma_c=10$ while σ_n is varied over the interval

$$0.1 \le \sigma_n \le 1 \,. \tag{8.42}$$

Plots of $(SDR)_i$ versus the input noise-to-clutter ratio, as defined in Eq.(8.9), are plotted in Fig.8.22 for i=I, II, III. Once again, there is little difference between cases II and III for $\rho_c=0$. However, for $\rho_c=0.9$, case III performs better than case II as the thermal noise power is reduced. Reduction of the thermal noise power results in the clutter plus noise power spectral density becoming less flat in the tails of the spectrum. The plots in Figs.8.22 (c) and (e) suggest that the transversal filter transfer function, optimized for case III, is able to take advantage of this change in spectral shape.

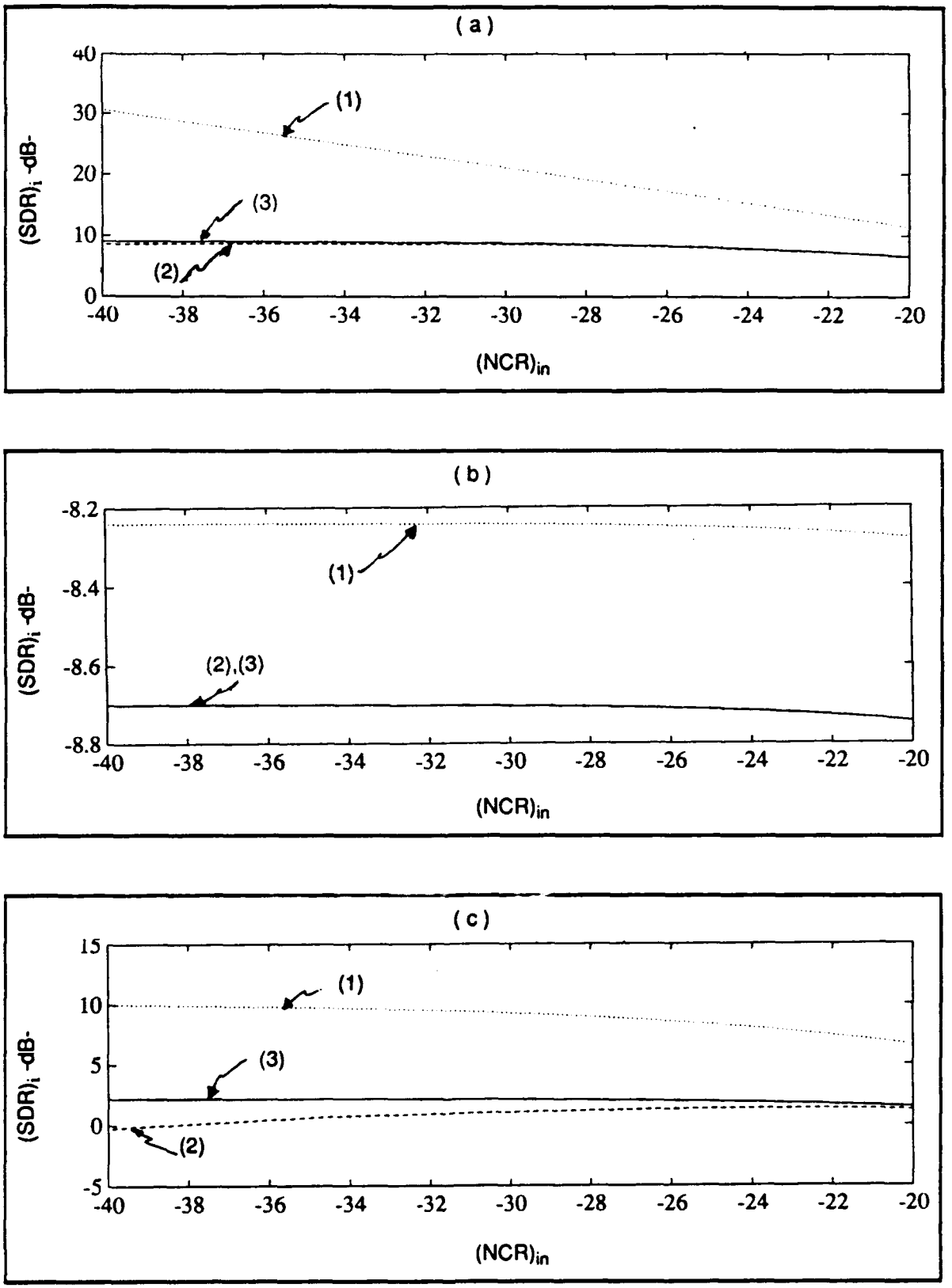

Figure 8.22 - (Caption appears on next page).

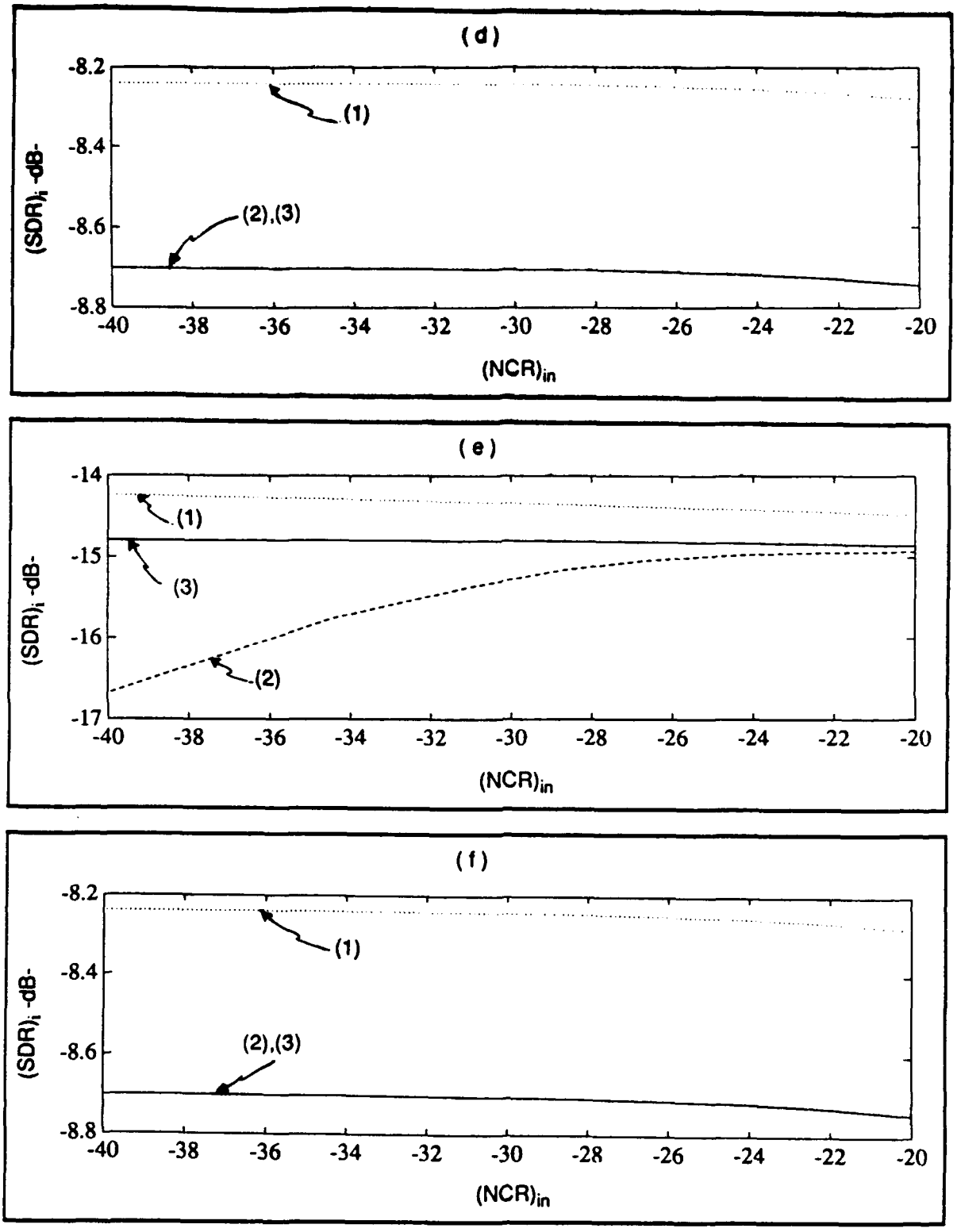

Figure 8.22 - Dependence of $(SDR)_{III}$ on theThermal Noise Power Level (α=0.4975): (1) $(SDR)_I$ -dB-, (2) $(SDR)_{II}$ -dB-, (3) $(SDR)_{III}$ -dB-, a) f_D/f_s=0.5, ρ_c=0.9, b) f_D/f_s=0.5, ρ_c=0 c) f_D/f_s=0.25, ρ_c=0.9, (d) f_D/f_s=0.25, ρ_c=0, e) f_D/f_s=0, ρ_c=0.9, f) f_D/f_s=0, ρ_c=0.

8.3.4 Dependence of $(SDR)_{III}$ on the Clutter Power Level

As in sections 8.1.4 and 8.2.4, σ_s and σ_n are held constant at $\sigma_s=1$ and $\sigma_n=0.1$ while σ_c is varied over the interval

$$10 \le \sigma_c \le 100 \ . \tag{8.43}$$

Dependence of $(SDR)_i$ on the clutter power level is plotted in Fig.8.23 for i=I, II, and III. Once again, case III does not differ from case II for $\rho_c=0$ due to the flat nature of the clutter power spectral density. The nonlinearity is driven harder as σ_c is increased. This results in greater distortion of the clutter power spectral density when $\rho_c=0.9$. Since the transversal filter for case III is optimized to this distortion

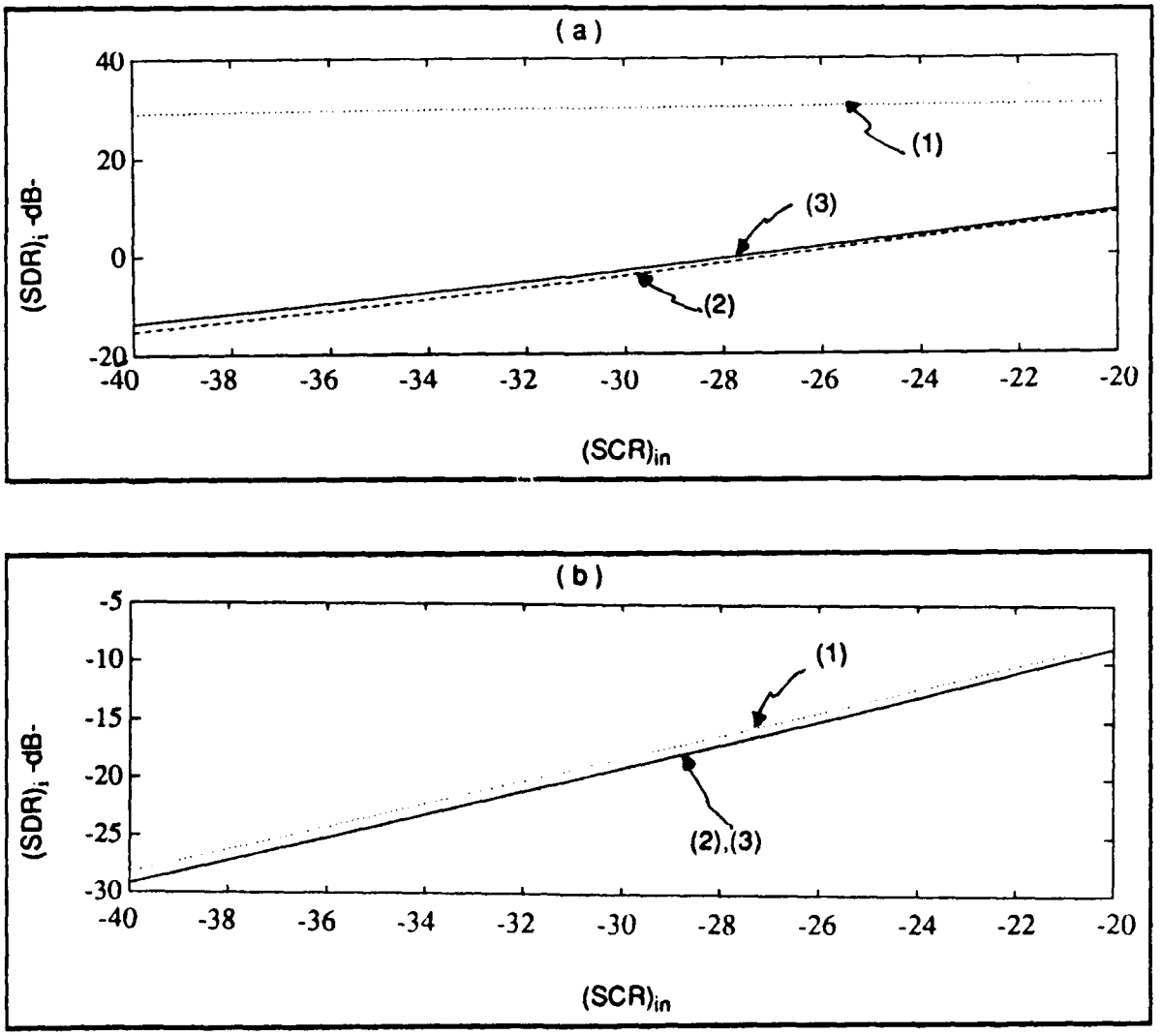

Figure 8.23 - (Caption appears on page 150).

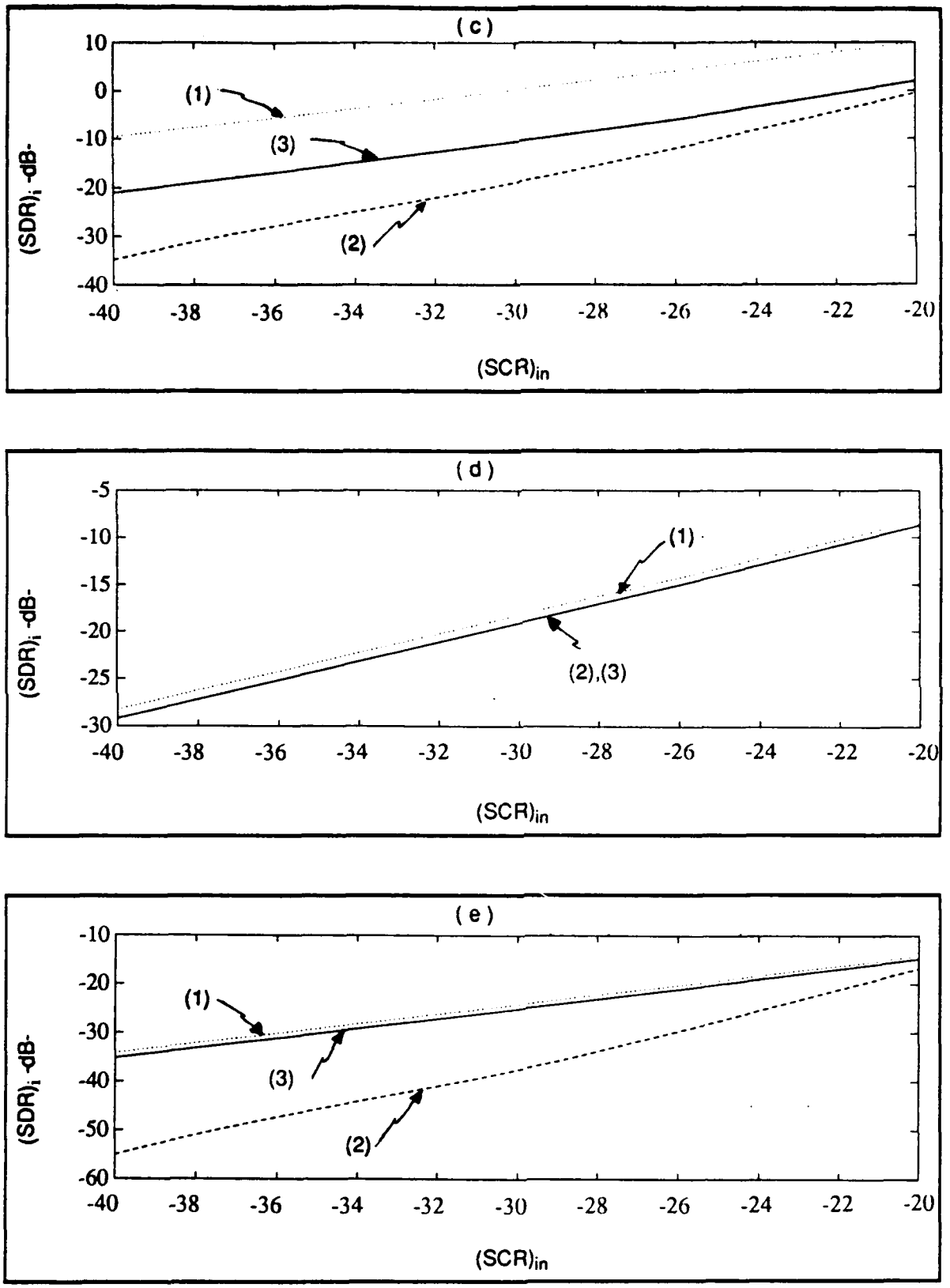

Figure 8.23 - (Caption appears on next page).

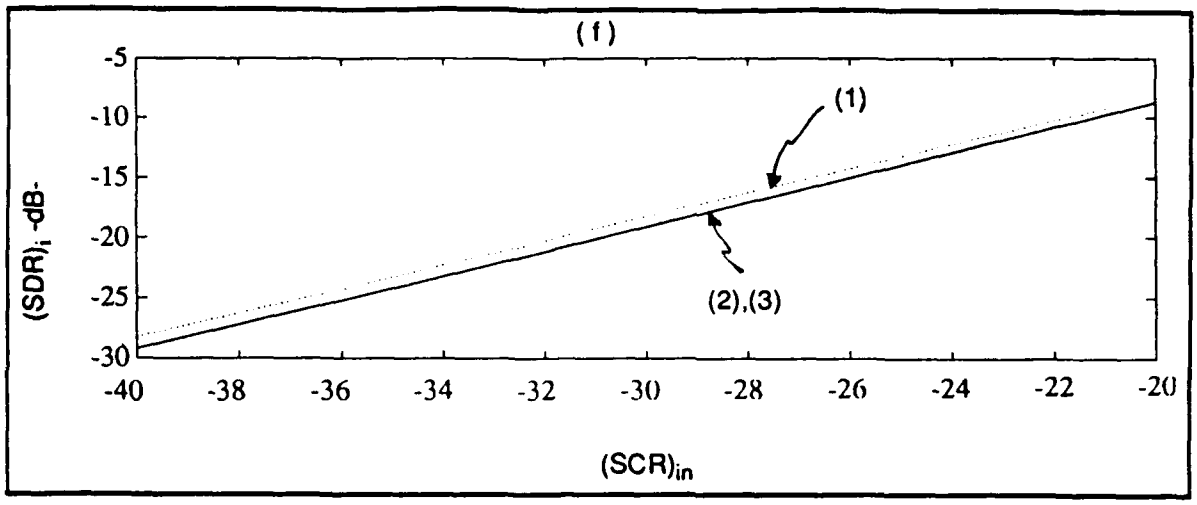

Figure 8.23 - Dependence of $(SDR)_{III}$ on the Clutter Power Level ($0.05 \le \alpha \le 0.4975$): (1) $(SDR)_I$ -dB-, (2) $(SDR)_{II}$ -dB-, (3) $(SDR)_{III}$ -dB-, a) $f_D/f_s=0.5$, $\rho_c=0.9$, b) $f_D/f_s=0.5$, $\rho_c=0$ c) $f_D/f_s=0.25$, $\rho_c=0.9$, (d) $f_D/f_s=0.25$, $\rho_c=0$, e) $f_D/f_s=0$, $\rho_c=0.9$, f) $f_D/f_s=0$, $\rho_c=0$.

whereas it is designed on the basis of a linear receiver for case II, the output signal-to-disturbance ratio is much larger for case III than for case II (see Figs.8.23 (c) and (e)).

8.3.5 Dependence of $(SDR)_{III}$ on the Doppler Frequency

Plots of $(SDR)_i$ versus f_D/f_s are shown in Fig.8.24 for i=I, II, and III. The cases of $\rho_c=0.9$ and $\rho_c=0$ are considered. When $\rho_c=0.9$, all three curves of $(SDR)_i$ have their maxima at $f_D=0.5f_s$. This corresponds to the situation where the desired signal spectrum is positioned at the minimum of the clutter power spectral density. When $\rho_c=0$, the output signal-to-disturbance ratios are independent of f_D/f_s due to the flat nature of the disturbance power spectral density. As would be expected, note that

$$(SDR)_I > (SDR)_{III} \ge (SDR)_{II} \bullet \qquad (8.44)$$

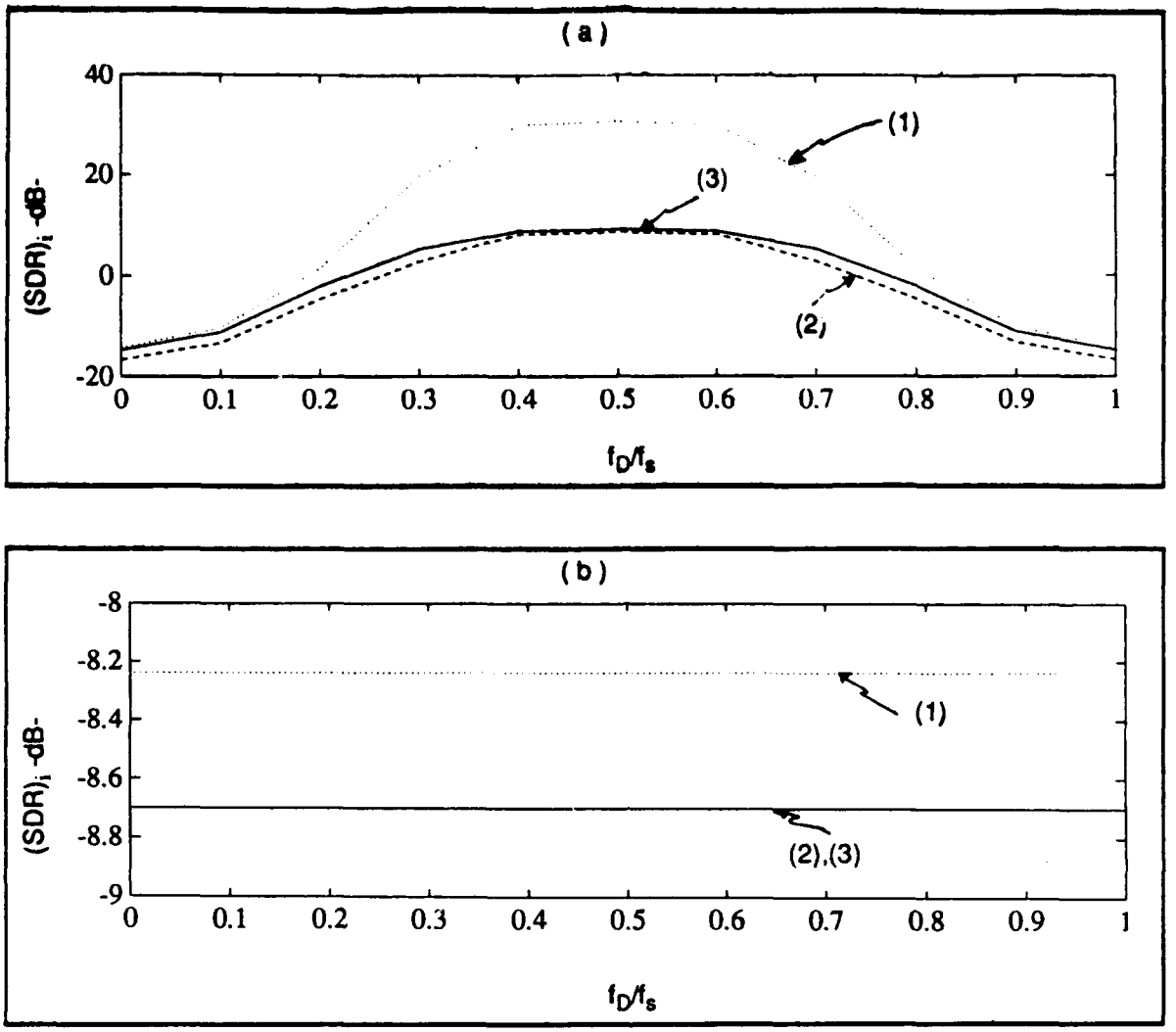

Figure 8.24 - Dependence of $(SDR)_{III}$ on the Doppler Frequency (α=0.4975): (1) $(SDR)_I$ -dB-, (2) $(SDR)_{II}$ -dB-, (3) $(SDR)_{III}$ -dB- a) ρ_c=0.9, b) ρ_c=0.

8.3.6 Dependence 0f $(SDR)_{III}$ on the Number of Samples, N

Plots of $(SDR)_i$, for i=I, II, and III, are shown in Fig.8.25 for f_D/f_s=0.5, 0.25, 0 and ρ_c=0.9, 0. Once again, the output signal-to-disturbance ratios increase with an increase in the number of samples processed. The amount of improvement is approximately the same for cases I, II, and III. As explained in section 8.1.5, the improvement is due to 1) the power spectral density of the desired signal becoming more concentrated about f_D and 2) the increase in the degrees of freedom of the transversal filter as N is increased.

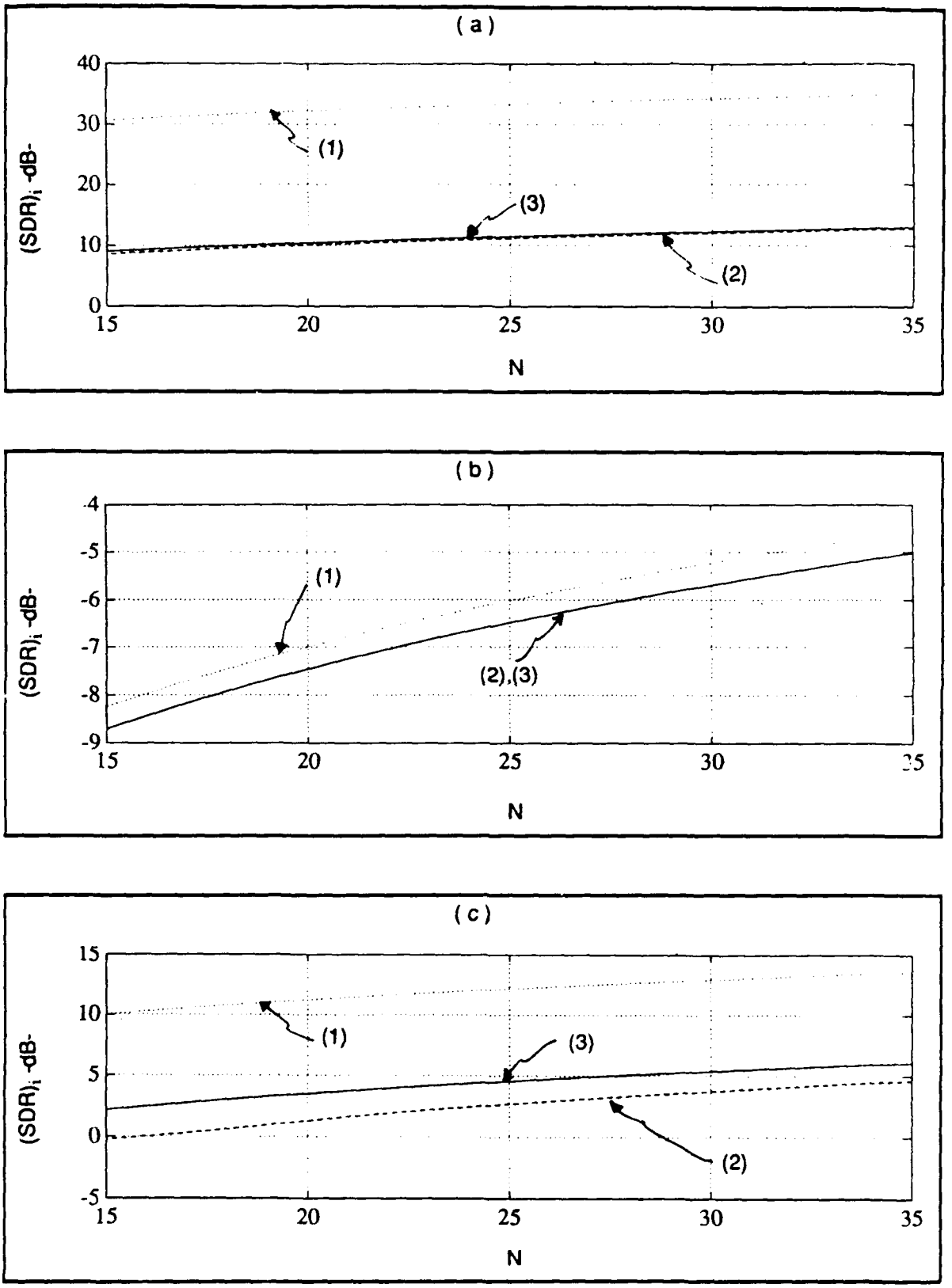

Figure 8.25 - (Caption appears on next page).

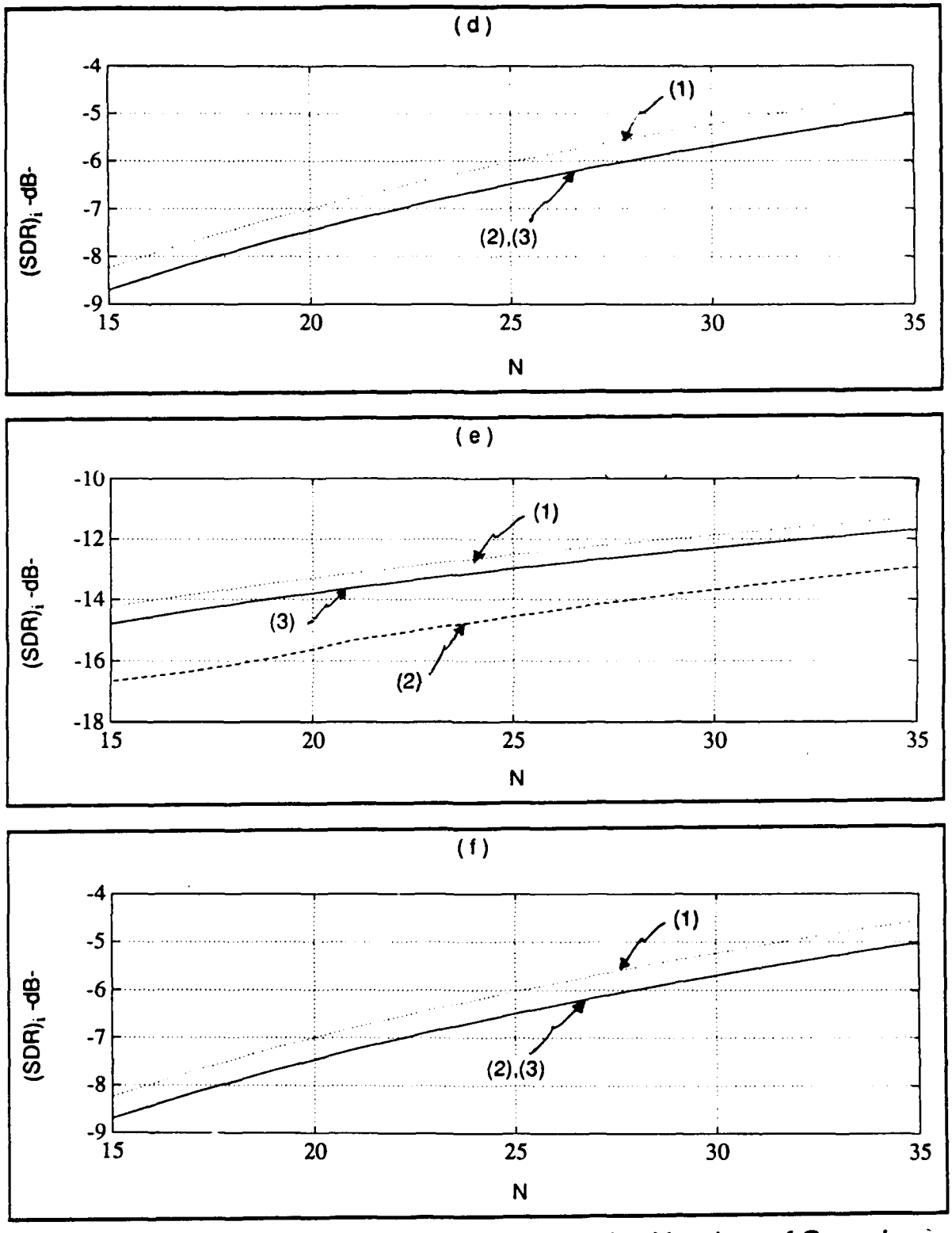

Figure 8.25 - Dependence of $(SDR)_{III}$ on the Number of Samples (α=0.4975): (1) $(SDR)_I$ -dB-, (2) $(SDR)_{II}$ -dB-, (3) $(SDR)_{III}$ -dB- a) f_D/f_S=0.5, ρ_C=0.9, b) f_D/f_S=0.5, ρ_C=0 c) f_D/f_S=0.25, ρ_C=0.9, (d) f_D/f_S=0.25, ρ_C=0, e) f_D/f_S=0, ρ_C=0.9, f) f_D/f_S=0, ρ_C=0.

8.4 Comparison of Cases I, II, and III

Recall that $(SDR)_{in}$ denotes the signal-to-disturbance ratio at the receiver input while $(SDR)_i$, where i=I, II, and III, denotes the signal-to-disturbance ratio at the transversal filter output. Since the signal-to-disturbance ratios are expressed in dB, the processing gain for Case i, i=I, II, and III, is defined to be

$$(PG)_i = (SDR)_i - (SDR)_{in} . \tag{8.45}$$

As seen in the previous sections, the nonlinearity causes a reduction in $(SDR)_i$ for cases II and III when compared to case I. For i=II, III, let this loss be denoted by

$$(NLL)_i = (SDR)_I - (SDR)_i . \tag{8.46}$$

Finally, by tailoring the weights of the transversal filter to account for the nonlinearity, case III outperforms case II. The amount by which $(SDR)_{III}$ exceeds $(SDR)_{II}$ is denoted by

$$\begin{aligned} J &= (SDR)_{III} - (SDR)_{II} \\ &= (NLL)_{II} - (NLL)_{III} . \end{aligned} \tag{8.47}$$

Letting ρ_c=0.9, N=15, σ_g=5, σ_n=0.1, σ_s=1.0 and using the numerical values given in Eqs.(8.6)-(8.10), results were obtained for the pairs (α=0.5, σ_c=10) and (α=0.05, σ_c=100). These are tabulated in Tables 8.1 and 8.2, respectively. Note that both Tables apply to the same nonlinearity. However, the nonlinearity for Table 8.2 is driven 20dB harder than that of Table 8.1. Because of the relatively narrow power spectral density, the maximum processing gain is seen to occur for f_D/f_s=0.5. The loss in SDR caused by the nonlinearity is maximum for f_D/f_s=0.5 and decreases as f_D/f_s approaches zero. As would be expected, $(NLL)_i$ is much larger for α=0.05 than for α=0.5. With respect to the Tables,

$$0.39\,(dB) \le J \le 2.49\,(dB) \tag{8.48}$$

for α=0.5 whereas

$$1.56\ (\text{dB}) \leq J \leq 19.92\ (\text{dB}) \qquad (8.49)$$

for α=0.05. The improvement of case III over case II tends to be larger for smaller values of the signal-to-disturbance ratio at the transversal filter output.

f_D/f_s		0.5	0.4	0.3	0.2	0.1	0
$(SDR)_{in}$	-dB-	-20.04	-20.04	-20.04	-20.04	-20.04	-20.04
$(SDR)_I$	-dB-	30.63	29.92	19.67	1.42	-10.3	-14.24
$(SDR)_{II}$	-dB-	8.56	8.14	2.85	-4.66	-13.31	-16.68
$(SDR)_{III}$	-dB-	8.95	8.65	5.16	-2.17	-11.25	-14.88
$(PG)_I$	-dB-	50.67	49.96	39.71	21.46	9.74	5.8
$(PG)_{II}$	-dB-	28.6	28.18	22.89	15.38	6.73	3.36
$(PG)_{III}$	-dB-	28.99	28.69	25.2	17.87	8.79	5.16
$(NLL)_{II}$	-dB-	22.07	21.78	16.82	6.08	3.01	2.44
$(NLL)_{III}$	-dB-	21.68	21.27	14.51	3.59	0.95	0.64
J	-dB-	0.39	0.51	2.31	2.49	2.06	1.8

Table 8.1
Relative Performance of cases I, II, and III when α=0.5.

In this work we have emphasized the situation where the signal is much larger than the noise but is much smaller than the clutter. Some general conclusions

f_D/f_s		0.5	0.4	0.3	0.2	0.1	0
$(SDR)_{in}$	-dB-	-40.00	-40.00	-40.00	-40.00	-40.00	-40.00
$(SDR)_{I}$	-dB-	29.00	22.49	1.06	-18.32	-30.15	-34.12
$(SDR)_{II}$	-dB-	-15.27	-18.86	-28.41	-41.87	-51.79	-55.05
$(SDR)_{III}$	-dB-	-13.71	-15.16	-18.41	-24.26	-31.87	-35.25
$(PG)_{I}$	-dB-	69.00	62.49	41.06	21.68	9.85	5.88
$(PG)_{II}$	-dB-	24.73	21.14	11.59	-1.87	-11.79	-15.05
$(PG)_{III}$	-dB-	26.29	24.84	21.59	15.74	8.13	4.75
$(NLL)_{II}$	-dB-	44.27	41.35	29.47	23.55	21.64	20.93
$(NLL)_{III}$	-dB-	42.71	37.65	19.47	5.94	1.72	1.13
J	-dB-	1.56	3.7	10.00	17.61	19.92	19.80

Table 8.2
Relative Performance of cases I, II, and III when α=0.05.

that can be drawn from the numerical results presented in this Chapter are given below:

1) The nonlinearity can cause a significant reduction in the processing gain of the transversal filter.

2) The signal-to-disturbance ratios for the three cases satisfy the inequality

$$(SDR)_I > (SDR)_{III} \geq (SDR)_{II} \cdot \qquad (8.50)$$

3) The nonlinearity tends to broaden the clutter power spectral density. However, a white spectrum at the input of the nonlinearity remains white at its output.

4) $(SDR)_i$, where i=I, II, and III, is maximized when the peak of the target signal spectrum is positioned at the minimum of the clutter spectrum.

5) When the peak of the target signal spectrum is offset from the peak of the clutter spectrum, $(SDR)_i$, where i=I, II, and III, tends to increase as the clutter correlation is increased due to the narrowing of the clutter spectrum.

6) The clutter model constrains the area of the clutter power spectral density to remain constant at $2\sigma_c^2$ as the clutter correlation is varied. Consequently, the clutter spectral peak at f=0 becomes larger as ρ_c increases and the spectrum becomes narrower. Therefore, when the peak of the target signal spectrum is centered at f=0, $(SDR)_i$, where i=I, II, and III, tends to decrease with increasing values of ρ_c.

7) For $\rho_c=0$, the clutter is white and the total power spectral density of the disturbance is a constant. Hence, $(SDR)_i$, where i=I, II, and III, is independent of the Doppler shift, f_D.

8) Because the shape of the clutter power spectral density is modeled as Gaussian, the tails fall off exponentially. Thus, even though the average clutter power is much larger than the average noise power, the noise power can limit performance when the peak of the target signal spectrum is positioned in the tails of the clutter spectrum. Then an increase in the noise power can cause a significant reduction in the output signal-to-disturbance ratio. However, when the target signal spectrum is positioned such that the clutter limits performance, a moderate increase in the average noise power has negligible effect on the output signal-to-disturbance ratio.

9) When the peak of the target signal is positioned in the tails of the clutter spectrum and the clutter spectrum is relatively narrow, a modest increase in the clutter power does not affect $(SDR)_i$, where i=I, II, and III. However, when the target signal spectrum is positioned such that the clutter is dominant over the noise,

$(SDR)_i$ decreases as the clutter power is increased.

10) As the number of samples, N, grows, the output signal-to-disturbance ratio increases because (i) the power in the target signal becomes more concentrated in the frequency interval centered at f_D and (ii) the degrees of freedom of the transversal filter increase.

11) As α increases, the system becomes more linear and the performance of case II approaches that of case I.

12) Because of the widening by the nonlinearity of the clutter power spectral density, the output signal-to-disturbance ratio becomes less sensitive to an increase in the average noise power. However, as explained in section 8.2.3, the output signal-to disturbance ratio can increase with an increase in noise power.

13) When the clutter is white, the decrease in output signal-to-disturbance ratio is identical for cases I and II as the average clutter power is increased. However, when the clutter is not white, the degradation is greater for case II than for case I.

14) Case III is better able to outperform case II when the clutter is more correlated (i.e., the clutter spectrum is narrower) because the nonlinearity causes a greater distortion in the clutter spectrum. Cases II and III perform the same when the clutter is white.

15) When the clutter is not white, case III performs increasingly better relative to case II as the nonlinearity is driven harder.

16) For a narrow clutter power spectral density, case III performs increasingly better relative to case II as the average noise power is reduced.

17) As can be seen from Fig.4.4, the output of the nonlinearity is decidedly nonGaussian when $\alpha \leq 1$. Yet, the Gaussian receiver is surprisingly robust with respect to the signal-to-disturbance ratio at the output of the transversal filter, especially when $\alpha=1$.

18) When the receiver is nonlinear, use of the transversal filter optimized for the linear receiver can result in $(SDR)_{II}$ being smaller than $(SDR)_{in}$, as shown in Table 8.2.

Appendix A

Derivation of Equation (4.3)

In general, the received signal $r_1(t)$ will be a modulated signal with carrier frequency f_c. The quadrature components of $r_1(t)$ are given by

$$r_{1c}(t) = [r_1(t) \cdot \cos(2\pi f_c t)]_{ILP} \tag{A.1}$$

and

$$r_{1s}(t) = [r_1(t) \cdot \sin(2\pi f_c t)]_{ILP} \tag{A.2}$$

where $[.]_{ILP}$ denotes the operation of passing the argument through an ideal low pass filter. The received signal can then be expressed as

$$\begin{aligned} r_1(t) &= r_{1c}(t)\cos(2\pi f_c t) - r_{1s}(t)\sin(2\pi f_c t) \\ &= \mathrm{Re}\{[r_{1c}(t) + j r_{1s}(t)]\, e^{j2\pi f_c t}\} \quad . \end{aligned} \tag{A.3}$$

However, from Eq.(3.4), $r_1(t)$ is related to its complex envelope according to the relation

$$r_1(t) = \mathrm{Re}\{\tilde{r}_1(t) \cdot e^{j2\pi f_c t}\} \quad . \tag{A.4}$$

Comparison of Eqs.(A.3) and (A.4) reveals that

$$\tilde{r}_1(t) = r_{1c}(t) + j r_{1s}(t) \quad . \tag{A.5}$$

Use of Eqs.(A.1) and (A.2) in Eq.(A.5) results in

$$\tilde{r}_1(t) = \{r_1(t) \cdot e^{j2\pi f_c t}\}_{ILP} \quad . \tag{A.6}$$

This operation is depicted in Fig.A.1 where $g_{ILP}(t)$ denotes the impulse response of the ideal low pass filter whose transfer function is shown in Fig.A.2. The band

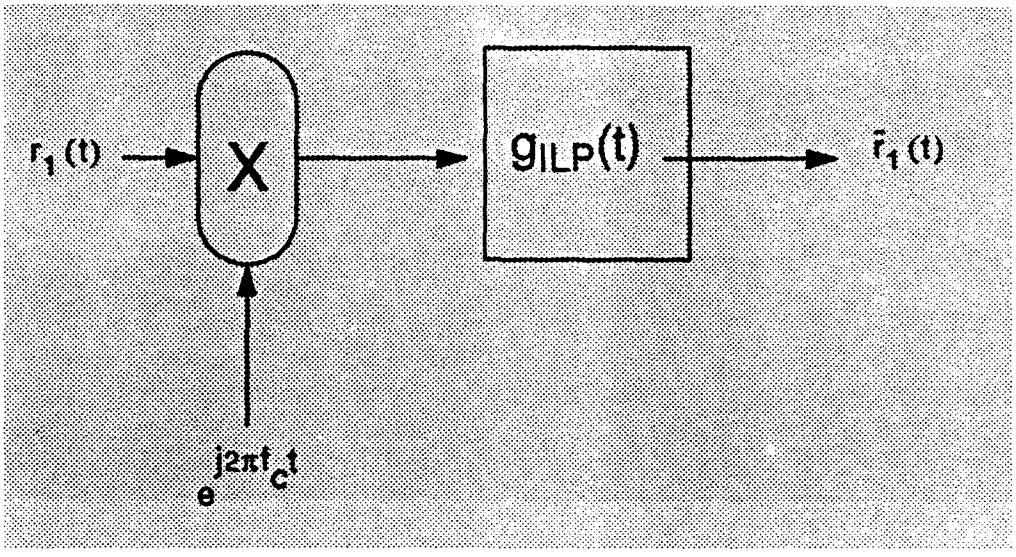

Figure A.1 - Generation of $\tilde{r}_1(t)$ from $r_1(t)$.

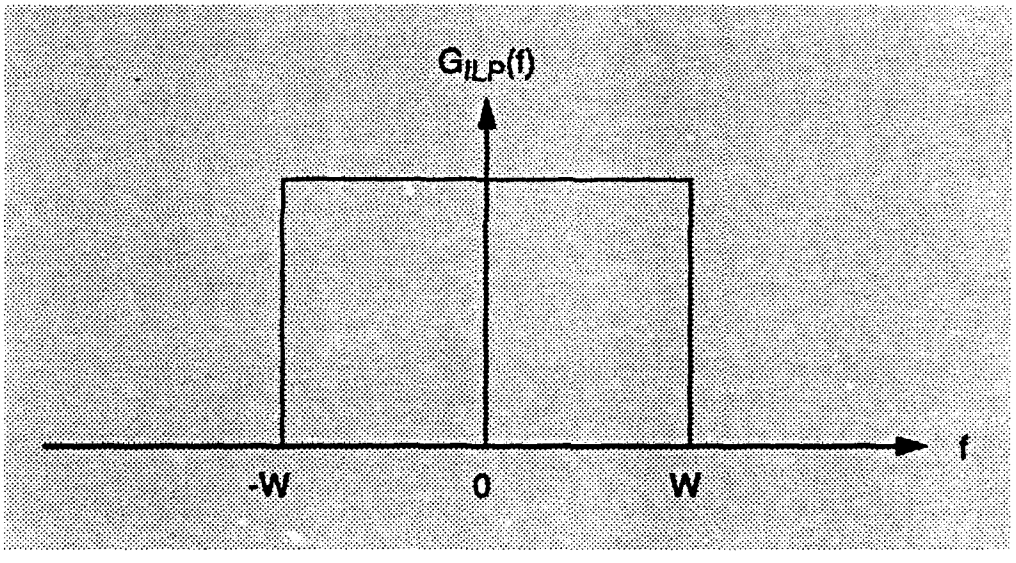

Figure A.2 - Transfer Function of Ideal Low Pass Filter.

width W is chosen equal to half the bandwidth of $r_1(t)$.

From Fig.A.1, it is obvious that the complex envelope is determined by the convolution of $r_1(t)e^{j2\pi f_c t}$ with $g_{ILP}(t)$. It follows that

$$\tilde{r}_1(t) = \int_{-\infty}^{\infty} r_1(x) \cdot e^{j2\pi f_c x} \cdot g_{ILP}(t-x)\,dx \quad . \qquad (A.7)$$

As a result

$$E[\tilde{r}_1(t_1)\tilde{r}_1(t_2)] = E\left[\int_{-\infty}^{\infty} r_1(x_1)\cdot e^{j2\pi f_c x_1}\cdot g_{ILP}(t_1-x_1)\,dx_1 \cdot \int_{-\infty}^{\infty} r_1(x_2)\cdot e^{j2\pi f_c x_2}\cdot g_{ILP}(t_2-x_2)\,dx_2\right]$$

$$= \int_{-\infty}^{\infty}\int_{-\infty}^{\infty} E[r_1(x_1)\cdot r_1(x_2)]\, e^{j2\pi f_c(x_1+x_2)} \cdot g_{ILP}(t_1-x_1)\cdot g_{ILP}(t_2-x_2)\,dx_1dx_2 \quad . \quad (A.8)$$

Assuming the received waveform from a given range cell is stationary, the auto-correlation function has the property that

$$R_1(x_1,x_2) = E[r_1(x_1)\cdot r_1(x_2)] = R_1(x_1-x_2) \quad . \quad (A.9)$$

Hence, Eq.(A.8) becomes

$$E[\tilde{r}_1(t_1)\tilde{r}_1(t_2)] = \int_{-\infty}^{\infty}\int_{-\infty}^{\infty} R_1(x_1-x_2)\, e^{j2\pi f_c(x_1+x_2)} \cdot g_{ILP}(t_1-x_1) \cdot g_{ILP}(t_2-x_2)\,dx_1dx_2 \quad . \quad (A.10)$$

In terms of the power spectral density of $r_1(t)$, which is denoted by $S_1(f)$, the auto-correlation function can be expressed as

$$R_1(x_1-x_2) = \int_{-\infty}^{\infty} S_1(f)\cdot e^{j2\pi f(x_1-x_2)}\,df \quad . \quad (A.11)$$

Substitution of Eq.(A.11) into Eq.(A.10) yields

$$E[\tilde{r}_1(t_1)\tilde{r}_1(t_2)] = \int_{-\infty}^{\infty}\int_{-\infty}^{\infty}\int_{-\infty}^{\infty} S_1(f)\cdot e^{j2\pi f(x_1-x_2)}\cdot e^{j2\pi f_c(x_1+x_2)} \cdot g_{ILP}(t_1-x_1)\cdot g_{ILP}(t_2-x_2)\,dx_1dx_2df$$

$$= \int_{-\infty}^{\infty} S_1(f) \left\{ \int_{-\infty}^{\infty} g_{ILP}(t_1 - x_1) \cdot e^{j2\pi x_1 (f+f_c)} dx_1 \right.$$

$$\left. \cdot \int_{-\infty}^{\infty} g_{ILP}(t_2 - x_2) \cdot e^{-j2\pi x_2 (f-f_c)} dx_2 \right\} df$$

$$= \int_{-\infty}^{\infty} S_1(f) \left\{ \int_{-\infty}^{\infty} g_{ILP}(v_1) \cdot e^{-j2\pi v_1 (f+f_c)} dv_1 \right.$$

$$\left. \cdot \int_{-\infty}^{\infty} g_{ILP}(v_2) \cdot e^{j2\pi v_2 (f-f_c)} dv_2 \right\} e^{j2\pi t_1 (f+f_c) - j2\pi t_2 (f-f_c)} df \quad . \quad (A.12)$$

However,

$$G_{ILP}(f) = \int_{-\infty}^{\infty} g_{ILP}(t) \cdot e^{-j2\pi ft} dt \quad . \quad (A.13)$$

Use of Eq.(A.13) in Eq.(A.12) yields

$$E[\tilde{r}_1(t_1)\tilde{r}_1(t_2)] = \int_{-\infty}^{\infty} S_1(f) \cdot G_{ILP}(f+f_c) \cdot G_{ILP}^{*}(f-f_c)$$

$$\cdot e^{j2\pi t_1 (f+f_c) - j2\pi t_2 (f-f_c)} df \quad . \quad (A.14)$$

Assuming the modulation of $r_1(t)$ to vary slowly relative to variations of the carrier, $f_c >> W$. It follows that the transfer functions $G_{ILP}(f+f_c)$ and $G_{ILP}^{*}(f-f_c)$ will not overlap in frequency. Thus,

$$G_{ILP}(f+f_c) \cdot G_{ILP}^{*}(f-f_c) = 0 \quad . \quad (A.15)$$

Consequently, the integrand in Eq.(A.14) is zero and

$$E[\tilde{r}_1(t_1)\tilde{r}_1(t_2)] = 0 \quad . \tag{A.16}$$

When $t_1 = t$ and $t_2 = t-\tau$, this result becomes

$$E[\tilde{r}_1(t)\tilde{r}_1(t-\tau)] = 0 \quad . \tag{A.17}$$

Appendix B

Derivation of Equations (4.56) and (4.57)

Recall from Eq.(3.30) that

$$\tilde{r}_2\Big|_{f_c} = \frac{2L}{\sqrt{2\pi\sigma_g^2}} \cdot \left[1 + \sum_{k=1}^{\infty} \left(\frac{-1}{\sigma_g^2} \right)^k \cdot \frac{C_k^{2k+1}}{2^{2k}} \cdot \frac{(2k-1)!!}{(2k+1)!} \cdot \left|\tilde{r}_1\right|^{2k} \right] \cdot \tilde{r}_1 \quad . \quad \text{(B.1)}$$

To simplify this expression, let

$$G = \frac{2L}{\sqrt{2\pi\sigma_g^2}} \quad \text{(B.2)}$$

and

$$A_k = \left(\frac{-1}{\sigma_g^2} \right)^k \cdot \frac{C_k^{2k+1}}{2^{2k}} \cdot \frac{(2k-1)!!}{(2k+1)!} \quad . \quad \text{(B.3)}$$

Eq.(B.1) then becomes

$$\tilde{r}_2\Big|_{f_c} = G \cdot \left[\tilde{r}_1 + \sum_{k=1}^{\infty} A_k \cdot \left|\tilde{r}_1\right|^{2k} \cdot \tilde{r}_1 \right]. \quad \text{(B.4)}$$

As seen in Eq.(4.55), the relation for $R_3(t,\tau)$ involves $E\left[\tilde{r}_2(t)\Big|_{f_c} \tilde{r}_2(t-\tau)\Big|_{f_c} \right]$ and $E\left[\tilde{r}_2(t)\Big|_{f_c} \tilde{r}_2^{\,*}(t-\tau)\Big|_{f_c} \right]$. The evaluation of these two expectations is considered in this appendix.

We first consider

$$E\left[\tilde{r}_2(t)\Big|_{f_c} \tilde{r}_2(t-\tau)\Big|_{f_c} \right] = G^2 E\left\{ \left[\tilde{r}_1(t) + \sum_{k=1}^{\infty} A_k \cdot \left|\tilde{r}_1(t)\right|^{2k} \cdot \tilde{r}_1(t) \right] \right.$$

$$\left. \cdot \left[\tilde{r}_1(t-\tau) + \sum_{p=1}^{\infty} A_p \cdot \left|\tilde{r}_1(t-\tau)\right|^{2p} \cdot \tilde{r}_1(t-\tau) \right] \right\}$$

$$= G^2 E\Bigg[\tilde{r}_1(t)\tilde{r}_1(t-\tau) + \sum_{p=1}^{\infty} A_p \cdot \tilde{r}_1(t) \cdot [\tilde{r}_1(t-\tau)]^{2p+1} \cdot [\tilde{r}_1^{\,*}(t-\tau)]^{2p}$$

$$+ \sum_{k=1}^{\infty} A_k \cdot [\tilde{r}_1(t)]^{2k+1} \cdot [\tilde{r}_1^{\,*}(t)]^{2k} \cdot \tilde{r}_1(t-\tau)$$

$$+ \sum_{k=1}^{\infty}\sum_{p=1}^{\infty} A_k A_p \cdot [\tilde{r}_1(t)]^{2k+1} \cdot [\tilde{r}_1^{\,*}(t)]^{2k} \cdot [\tilde{r}_1(t-\tau)]^{2p+1}$$

$$\cdot [\tilde{r}_1^{\,*}(t-\tau)]^{2p}\Bigg] \,. \qquad \text{(B.5)}$$

Interchanging the order of summation and expectation, we obtain

$$E\left[\tilde{r}_2(t)\Big|_{f_c}\tilde{r}_2(t-\tau)\Big|_{f_c}\right] = G^2 E[\tilde{r}_1(t)\tilde{r}_1(t-\tau)]$$

$$+ G^2 \sum_{p=1}^{\infty} A_p E\{\tilde{r}_1(t) \cdot [\tilde{r}_1(t-\tau)]^{2p+1} \cdot [\tilde{r}_1^{\,*}(t-\tau)]^{2p}\}$$

$$+ G^2 \sum_{k=1}^{\infty} A_k E\left[[\tilde{r}_1(t)]^{2k+1} \cdot [\tilde{r}_1^{\,*}(t)]^{2k} \cdot \tilde{r}_1(t-\tau)\right]$$

$$+ G^2 \sum_{k=1}^{\infty}\sum_{p=1}^{\infty} A_k A_p E\Big[[\tilde{r}_1(t)]^{2k+1} \cdot [\tilde{r}_1^{\,*}(t)]^{2k} \cdot [\tilde{r}_1(t-\tau)]^{2p+1}$$

$$\cdot [\tilde{r}_1^{\,*}(t-\tau)]^{2p}\Big] \,. \qquad \text{(B.6)}$$

From Eq.(A.17)

$$E[\tilde{r}_1(t)\tilde{r}_1(t-\tau)] = 0 \,. \qquad \text{(B.7)}$$

Hence, the first term on the right hand side of Eq.(B.6) is zero.

To proceed further, recall that $\tilde{r}_1(t)$ is modeled as a zero mean stationary complex Gaussian random process. If $z_1, z_2, \ldots\ldots, z_{2m}$ denote 2m jointly Gaussian random variables, it is known [7] that

$$E[z_1 z_2 \ldots\ldots z_{2m}] = \sum_{\substack{\text{all} \\ \text{pairs}}} \left(\prod_{j \neq k}^{m} E[z_j z_k] \right) . \tag{B.8}$$

Each term in the summation of Eq.(B.8) contains the product of m pair wise expectations where each of the 2m random variables appears once and only once. The number of terms in the summation equals the number of different ways 2m different variables $z_1, z_2, \ldots\ldots, z_{2m}$ can be chosen in pairs, which is $(2m)!/(2^m m!)$. For example, when m = 2, the summation in Eq.(B.8) consists of three terms as given by

$$E[z_1 z_2 z_3 z_4] = E[z_1 z_2] E[z_3 z_4] + E[z_1 z_3] E[z_2 z_4] + E[z_1 z_4] E[z_2 z_3] . \tag{B.9}$$

Now examine $E\{\tilde{r}_1(t) [\tilde{r}_1(t-\tau)]^{2p+1} [\tilde{r}_1^*(t-\tau)]^{2p}\}$. This expectation involves the product of (4p+2) jointly Gaussian random variables. Consequently, a typical term in Eq.(B.8) consists of a product of (2p+1) pair wise expectations. To avoid a zero result, it is necessary that at least one of these terms not have $E[\tilde{r}_1(t) \cdot \tilde{r}_1(t-\tau)]$ as a factor. However, this is not possible. The term with the fewest number of factors of the form $E[\tilde{r}_1(t) \cdot \tilde{r}_1(t-\tau)]$ arises when $\tilde{r}_1(t-\tau)$ is paired with $\tilde{r}_1^*(t-\tau)$ a total of 2p times and $\tilde{r}_1(t)$ is paired with $\tilde{r}_1(t-\tau)$ once. All other terms in the summation of Eq.(B.8) have factors in which $\tilde{r}_1(t)$ is paired with $\tilde{r}_1(t-\tau)$ more than once. It follows that

$$E\{\tilde{r}_1(t)\,[\tilde{r}_1(t-\tau)]^{2p+1}\,[\tilde{r}_1^{\,*}(t-\tau)]^{2p}\} = 0 \quad . \tag{B.10}$$

Eq.(B.7) is valid for all values of τ, including $\tau = 0$. Hence,

$$E[\tilde{r}_1(t)\,\tilde{r}_1(t)] = E[\tilde{r}_1(t-\tau)\,\tilde{r}_1(t-\tau)] = 0 \quad . \tag{B.11}$$

Noting Eq.(B.11) and using similar reasoning as above, it is concluded that

$$E\{[\tilde{r}_1(t)]^{2k+1}\,[\tilde{r}_1^{\,*}(t)]^{2k}\,\tilde{r}_1(t-\tau)\} = 0 \tag{B.12}$$

and

$$E\{[\tilde{r}_1(t)]^{2k+1}\,[\tilde{r}_1^{\,*}(t)]^{2k}\,[\tilde{r}_1(t-\tau)]^{2p+1}\,[\tilde{r}_1^{\,*}(t-\tau)]^{2p}\} = 0 \quad . \tag{B.13}$$

Substitution of these results into Eq.(B.6) yields the conclusion that

$$E\left[\tilde{r}_2(t)\Big|_{f_c}\,\tilde{r}_2(t-\tau)\Big|_{f_c}\right] = 0 \quad . \tag{B.14}$$

We next consider $E\left[\tilde{r}_2(t)\Big|_{f_c}\,\tilde{r}_2^{\,*}(t-\tau)\Big|_{f_c}\right]$. From Eq.(B.4) it follows that

$$E\left[\tilde{r}_2(t)\Big|_{f_c}\,\tilde{r}_2^{\,*}(t-\tau)\Big|_{f_c}\right] = G^2 E\left\{\left[\tilde{r}_1(t) + \sum_{k=1}^{\infty} A_k \cdot |\tilde{r}_1(t)|^{2k} \cdot \tilde{r}_1(t)\right]\right.$$

$$\left.\cdot\left[\tilde{r}_1^{\,*}(t-\tau) + \sum_{p=1}^{\infty} A_p \cdot |\tilde{r}_1(t-\tau)|^{2p} \cdot \tilde{r}_1^{\,*}(t-\tau)\right]\right\}$$

$$= G^2 E[\tilde{r}_1(t)\tilde{r}_1^*(t-\tau)]$$

$$+ G^2 \sum_{p=1}^{\infty} A_p E\{\tilde{r}_1(t)\cdot[\tilde{r}_1^*(t-\tau)]^{2p+1}\cdot[\tilde{r}_1(t-\tau)]^{2p}\}$$

$$+ G^2 \sum_{k=1}^{\infty} A_k E\left[[\tilde{r}_1(t)]^{2k+1}\cdot[\tilde{r}_1^*(t)]^{2k}\cdot\tilde{r}_1^*(t-\tau)\right]$$

$$+ G^2 \sum_{k=1}^{\infty}\sum_{p=1}^{\infty} A_k A_p E\left[[\tilde{r}_1(t)]^{2k+1}\cdot[\tilde{r}_1^*(t)]^{2k}\cdot[\tilde{r}_1^*(t-\tau)]^{2p+1}\right.$$

$$\left.\cdot\,[\tilde{r}_1(t-\tau)]^{2p}\right] . \qquad \text{(B.15)}$$

Each expectation can be expanded as a sum of products of pair wise expectations as given by Eq.(B.8). In each summation it is readily seen that there exists at least one term that is nonzero. The nonzero terms involves factors of the form

$$\begin{aligned}
\tilde{R}_1(0) &= E[\tilde{r}_1(t)\tilde{r}_1^*(t)] \\
\tilde{R}_1(\tau) &= E[\tilde{r}_1(t)\tilde{r}_1^*(t-\tau)] \\
\tilde{R}_1^*(0) &= E[\tilde{r}_1^*(t-\tau)\tilde{r}_1(t-\tau)] \\
\tilde{R}_1^*(\tau) &= E[\tilde{r}_1^*(t)\tilde{r}_1(t-\tau)] .
\end{aligned} \qquad \text{(B.16)}$$

From this and assuming stationarity of $\tilde{r}_1(t)$, it is readily concluded that the autocorrelation $E\left[\tilde{r}_2(t)\Big|_{f_c}\tilde{r}_2^*(t-\tau)\Big|_{f_c}\right]$ is a function of τ alone.

REFERENCES

[1] Brennan, L. E. and Reed, I. S., "Theory of Adaptive Radar," IEEE Trans. Aerospace and Electronic Systems, vol AES-9, No.2, pp. 237-252, March 1973.

[2] Reed, I. S., Mallett, J. D., and Brennan, L. E., "Rapid Convergence Rate in Adaptive Arrays," IEEE Trans. Aerospace and Electronic Systems, vol AES-10, No.6, pp. 853-863, November 1974.

[3] Skolnick, M. I., Introduction to Radar Systems, Mc Graw-Hill Book Co., New York, 1980.

[4] H. L. Van Trees, Detection, Estimation and Modulation Theory, Part III, John Wiley & Sons, Inc., New York, 1971, p.241.

[5] Baum, R. F., "The Correlation Function of Smoothly Limited Gaussian Noise," IRE Trans. Information Theory, vol IT-3, pp. 193-197, September 1957.

[6] Papoulis, A., Signal Analysis, Mc Graw-Hill Book Company, 1977, p. 24.

[7] Middleton, D., An Introduction to Statistical Communication Theory, Mc Graw-Hill Book Co., 1960, p. 343.

[8] Alan V. Oppenheim, Ronald W. Schafer,Digital Signal Processing, PRENTICE-HALL INTERNATIONAL, INC., Englewood Cliffs, 1988, p.21.

BIOGRAPHY

NAME	Mohamed Adel SLAMANI
DATE AND PLACE OF BIRTH	January 19, 1963, Algiers, Algeria.
ELEMENTARY SCHOOL	Ecole Volta, Algiers, Algeria. Graduate 1974.
PRE HIGH SCHOOL	C.E.M. Capitaine Mennani, Algiers, Algeria. Graduate 1978.
HIGH SCHOOL	Lycee Emir Abdelkader, Algiers, Algeria. Graduate 1981.
College	Ecole Nationale Polytechnique, Algiers, Algeria. Graduate 1986.
GRADUATE WORK	Syracuse University, Research Assistant.

MISSION

OF

ROME LABORATORY

Rome Laboratory plans and executes an interdisciplinary program in research, development, test, and technology transition in support of Air Force Command, Control, Communications and Intelligence (C^3I) activities for all Air Force platforms. It also executes selected acquisition programs in several areas of expertise. Technical and engineering support within areas of competence is provided to ESD Program Offices (POs) and other ESD elements to perform effective acquisition of C^3I systems. In addition, Rome Laboratory's technology supports other AFSC Product Divisions, the Air Force user community, and other DOD and non-DOD agencies. Rome Laboratory maintains technical competence and research programs in areas including, but not limited to, communications, command and control, battle management, intelligence information processing, computational sciences and software producibility, wide area surveillance/sensors, signal processing, solid state sciences, photonics, electromagnetic technology, superconductivity, and electronic reliability/maintainability and testability.